

Haakon Jørlo Haugerud

# Analysis on the extent of water inflow in the tunnel system of SmiSto Hydropower Project in Nordland

An assessment of engineering geological factors influencing groundwater inflow and grout consumption

Master's thesis in Geotechnology  
Supervisor: Krishna Kanta Panthi  
January 2020

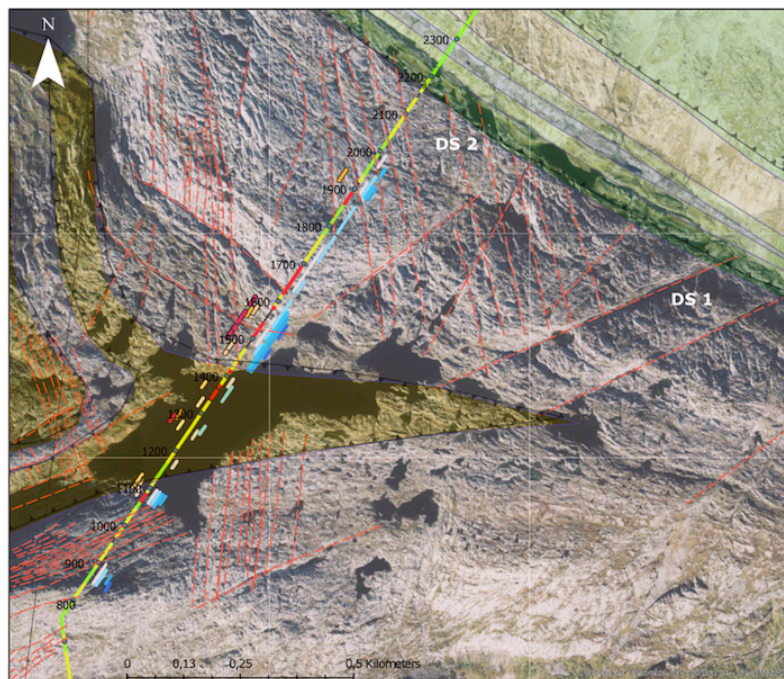


Image from the ArcGIS Pro Model of SmiSto. Map data from Kartverket.



Haakon Jørlo Haugerud

# **Analysis on the extent of water inflow in the tunnel system of SmiSto Hydropower Project in Nordland**

An assessment of engineering geological factors  
influencing groundwater inflow and grout  
consumption

Master's thesis in Geotechnology  
Supervisor: Krishna Kanta Panthi  
January 2020

Norwegian University of Science and Technology  
Faculty of Engineering  
Department of Geoscience and Petroleum







Your ref.: MS/N36T53/IGP/HJHKKP

Date: 19.08.2019

**TGB4930 INGGEOL/BERGMEK - MSc thesis  
for  
Eng. geo. student Haakon Jørlo Haugerud**

## **Analysis on the extent of water inflow in the tunnel system of SmiSto Hydropower Project in Norland**

### **Background**

SmiSto scheme has two hydropower system consisting Smibelg and Storåvatn hydropower projects, each located at the opposite side of Gjervalen fjord in Rødøy and Lurøy municipality in Nordland. These projects have an installed capacity of 33 and 25 MW, respectively and are at the stage of construction completion. Both projects are high head hydropower schemes with considerable storage capacity without constructing any big dams. The water is discharged to these two hydropower stations using in total 27 km long headrace pressure tunnels and shafts. The owner of the projects is SmiSto Kraft AS, a consortium of Salten Kraftsamband (SKS) and Hegeland Kraft (HK). The EPC contract module is used for the development of the scheme where Hæhre is the main contractor and Multiconsult works as Engineer. Due to considerable water inflow occurred during excavation of tunnels extensive pre-injection grouting is carried out to control the inflow.

### **MSc thesis task**

The candidate has written project work where he has evaluated structural geological condition that influenced the inflow along the headrace tunnel system of SmiSto hydropower scheme and collected data and information for the MSc thesis. This master thesis is the extension of his project work and therefore the candidate will focus his MSc thesis with following tasks:

- Literature review on the hydrogeological, engineering geological and mechanical properties of the rock mass. Discuss inflow and leakage assessment methodologies used for rock tunnels.
- Review principles and important factors regarding the grouting process, and briefly discuss the principal of pre- and post-injection grouting. Review grouting requirements for headrace tunnels compared to other infrastructure tunnels, such as road and railway tunnels.

- Gather and systematize information about rock mass quality, water inflow conditions and rock mass grouting and present in a geographic model.
- Discuss the conditions related to water inflow along certain segments of the tunnel system and link these to the engineering geological conditions prevailing in the project area.
- Assess potential inflow magnitude using empirical and semi-analytical methods.
- Assess the grout consumption in relation with the rock mass quality and evaluate on which of the main rock mass parameters are significant regarding grout consumption.
- Conclude the work with recommendations.

### **Relevant computer software packages**

Candidate shall use *roc-science* and *ArcGis* packages and other relevant computer software.

### **Background information for the study**

- Relevant information about the project such as reports, maps, information and data received from the supervisors and collected by the candidate.
- The information provided by the professor about rock engineering and hydropower.
- Scientific papers and books related to international tunnelling cases.
- Literatures in rock engineering, rock support principles, rock mechanics and tunnelling.

### **Cooperating partner**

Multiconsult is a cooperating partner and Ms. Magni Vestad from the Multiconsult is a contact person and co-supervisor of this project work.

The MSc thesis work is to start on August 19, 2019 and to be completed by January 13, 2020.

The Norwegian University of Science and Technology (NTNU)  
Department of Geoscience and Petroleum

August 19, 2019



Dr. Krishna K. Panthi  
Professor of geological engineering, main supervisor

---

# Abstract

The SmiSto hydro power project, situated near the Gjervalen fjord in Nordland, is a recent initiative in the Norwegian hydro power industry. During excavation of the tunnel systems, considerable problems related to groundwater inflow and rock mass grouting have been encountered.

Groundwater inflow and the need for grouting the rock mass are not new issues in tunneling. Inrushes of water can have a negative effect on the environment outside of the tunnel. The working conditions can also become very unpleasant for the workers inside the underground structure. The final consequences can be significant delays in project completion and cost-overruns, which can trouble owners, contractors and consultants involved in the project.

This thesis analyzes the engineering geological conditions in the SmiSto hydro power project which, from experience, are considered to potentially influence both the inflow of groundwater and the consumption of rock mass grout. The study also includes a statistical comparison between parameters regarding the rock mass conditions and the groundwater inflows. A semi-analytical approach was used to estimate groundwater inflows and compare these to the actual water inflow quantities. A multivariate linear regression model was also developed to assess if parameters regarding the rock mass conditions could give a satisfactory model for predicting the grout consumption. Further, a geographic model has been developed with ESRI's ArcGIS Pro, where gathered data related to rock mass quality, groundwater inflows and grout consumption have been presented.

The analysis reveals resemblances between the character of the water-conducting joints in the SmiSto project and discontinuities related to pinnate fissures associated with high hydraulic conductivity observed in other tunneling projects. The statistical analyses indicate a weak relationship between parameters related to the rock mass quality by the Q-system and the groundwater inflow quantities. Of the analyzed parameters, a higher groundwater inflow seems to be associated with higher rock cover above the tunnel level. The applied semi-analytical approach generally overestimates the groundwater inflow amounts. In certain areas, the estimated quantities correspond fairly well with the actual inflow rates. The developed multivariate linear regression model does not seem to give a good fit to the data set regarding the consumption of rock mass grout. Other statistical methods may be more appropriate for analysing the relationship between the rock mass parameters and the grout take. It is assumed that an improved model could have been developed by including other parameters relevant for the grout consumption, which were not included in this analysis.





---

# Sammendrag

SmiSto vannkraftprosjekt, som bygges ut ved Gjervalenfjorden i Nordland, er et nytt bidrag til vannkraftindustrien i Norge. Ved drivingen av tunnelsystemene har det vært betydelige problemer knyttet til innlekkasje av vann og behov for berginjeksjon.

Vanninnlekkasjer og berginjeksjon er velkjente problemstillinger i tunnelindustrien. Innlekkasje av vann kan ha negative konsekvenser på miljøet utenfor tunnelen. For tunnelarbeidere kan forholdene inne i tunnelen også bli meget utfordrende. Problemene kan føre til at prosjektet ikke blir ferdigstilt innen planlagt tid, og en kan få omfattende budsjettoverskridelser. De nevnte forhold vil gi hodebry for både eiere, de utførende og konsulenter i prosjektet.

Denne masteroppgaven analyserer ingeniørgeologiske forhold i SmiSto-prosjektet som, fra erfaring, antas å ha påvirkning på både potensial for vanninnlekkasje og injeksjonsforbruk. Arbeidet omfatter også en statistisk sammenligning mellom parametere knyttet til bergmasseforholdene og de opplevde vannlekkasjene. En semi-analytisk tilnærming er blitt brukt for å estimere vannlekkasjene i enkelte områder av tunnelsystemene. Resultatene er deretter blitt sammenlignet med de faktiske innlekkasjene i prosjektet. En multipl lineær regresjon er også blitt utviklet for å undersøke om bergmasseparametere for et gitt område i tunnelen kan gi en prognose for injeksjonsforbruket. Resultater av bergmassekvalitet, sonderboring og injeksjon i prosjektet er også blitt fremstilt in en geografisk modell ved bruk av ESRI's ArcGIS Pro.

De undersøkte forhold viser likhetstrekk mellom kjennetegn ved de vannførende sprekkene i prosjektet og diskontinuiteter knyttet til fjærsprekker som er kjent for å ha en høy ledningsevne av vann i andre tunnelprosjekter. Resultater fra den statiske analysen antyder en svak kobling mellom parametere knyttet til bergmassens kvalitet ved Q-systemet og opplevde vannmengder under tunneldriving. Det synes å være en tendens til at vanninnlekkasjene øker med bergoverdekning. Estimering av vanninnlekkasjer med en semi-analytisk metode viser en generell overvurdering av lekkasjemengdene. En multipl lineær regresjon synes ikke å gi en modell av tilfredsstillende kvalitet for å vurdere injeksjonsforbruk, basert på datasettet som er blitt brukt. Andre statistiske metoder kan gi modeller av bedre kvalitet for sammenligning mellom bergmasseparametere og injeksjonsforbruket. Parametere som ikke er blitt inkludert i modellen, men som kan å ha påvirkning på forbruket av injeksjon, antas å kunne gi bedre presisjon dersom de ble tatt med.



---

# Preface

This thesis concludes the Master's Degree Program, Geotechnology, at the Norwegian University of Science and Technology (NTNU) which I have attended from 2014 to the fall of 2019. This paper is a continuation of my project work which I started in the spring of 2019 and is written in collaboration with Multiconsult.

I wish to express my gratitude to my supervisor, Professor Krishna Kanta Panthi, for rewarding discussions and guidance throughout my study. His ability to share many years of experience in the field of engineering geology and rock mechanics has been essential for my thesis. Further, I would like to thank my co-supervisor, Magni Larsen Vestad, for valuable information regarding the project and creditable advice for my work. I am also grateful to her, and other employees in Multiconsult for the possibility to visit the SmiSto project site twice during the work with this paper. I am also thankful to Oddbjørn Aasen for sending me relevant literature regarding groundwater inflow in tunnels and rock mass grouting.

Other parties involved in the SmiSto projects have also been of great help. I would like to thank engineers in Zenith for access to project BIM files in Gemini Terrain 14. I also wish to thank Ernst Ove Johansen in Hæhre for continuously answering my questions related to the grouting procedures used in the project.

I am grateful to the peers from Geotechnology 2014 for four great years in Trondheim. The friendly and open learning environment with enthusiastic students has really been important for me. John Anders Flø Gustad deserves credit for the proofreading of this document. I would also like to thank colleagues in Geotechnology 2015 with whom I have had the pleasure to finish my studies during the fall of 2019.

Finally, I wish to thank my family and close friends for continuous support during my studies.

Haakon Jørlo Haugerud  
Trondheim, January 2020

---

# Table of Contents

<b>Abstract</b>	<b>i</b>
<b>Sammendrag</b>	<b>iii</b>
<b>Preface</b>	<b>v</b>
<b>Table of Contents</b>	<b>xi</b>
<b>List of Tables</b>	<b>xiv</b>
<b>List of Figures</b>	<b>xviii</b>
<b>Abbreviations</b>	<b>xix</b>
<b>1 Introduction</b>	<b>1</b>
1.1 Background . . . . .	1
1.2 Objectives and scope . . . . .	2
1.3 Methodology . . . . .	3
1.4 Limitations . . . . .	3
<b>2 Properties of the rock mass</b>	<b>5</b>
2.1 Intact rock . . . . .	5
2.1.1 Composition . . . . .	5
2.1.2 Mechanical properties . . . . .	5
2.2 Properties of the rock mass . . . . .	6
2.2.1 Discontinuities . . . . .	6
2.2.2 Rock mass strength . . . . .	8
2.3 Rock mass classification systems . . . . .	8

---

2.3.1	Rock Quality Designation (RQD)	9
2.3.2	Q-system	9
2.3.3	Other rock mass classification systems	10
<b>3</b>	<b>Water in the rock mass</b>	<b>13</b>
3.1	Introduction	13
3.2	Consequences of water inflow	14
3.2.1	Environmental	14
3.2.2	Internal environment in the structure	15
3.3	Theoretical background of fluid flow in the rock mass	15
3.3.1	Groundwater flow in a 2D discontinuity	15
3.4	Geological parameters controlling groundwater inflow in tunnels	16
3.4.1	Fault zones	16
3.4.2	Dykes	17
3.4.3	Joint characteristics	18
3.4.4	Stress situation	19
3.5	Prediction of groundwater inflow in rock tunnels	20
3.5.1	Geologic background	21
3.5.2	Probe drilling	21
3.5.3	Tunnel Seismic Prediction	21
3.6	Approaches for assessing groundwater inflow potential	21
3.6.1	Empirical approaches	22
3.6.2	Analytical and semi-analytical approaches	22
<b>4</b>	<b>Rock mass grouting</b>	<b>27</b>
4.1	Use of grouting in underground construction	27
4.2	Components and principles of rock mass grouting	27
4.2.1	Methodology of grouting	28
4.2.2	Grout materials	29
4.2.3	Pressure	31
4.3	Grouting requirements	32
4.3.1	Road and railway tunnels	32
4.3.2	Water way tunnels	34
4.4	Factors influencing grout consumption	35
4.4.1	Tunnel type and size	35
4.4.2	Rock mass conditions	35

---

---

<b>5</b>	<b>The SmiSto hydro power project</b>	<b>39</b>
5.1	Introduction . . . . .	39
5.2	Regional geology . . . . .	40
5.3	Geological and engineering geological conditions . . . . .	41
5.3.1	Topography . . . . .	41
5.3.2	Rock types . . . . .	42
5.3.3	Weakness zones and large-scale discontinuities . . . . .	43
5.3.4	Hydrogeological conditions and water sources . . . . .	45
5.3.5	Rock stress conditions . . . . .	45
5.3.6	Stress measurements . . . . .	46
5.4	Expected conditions in the pre-liminary phase . . . . .	48
5.4.1	Rock mass quality . . . . .	48
5.4.2	Groundwater inflow . . . . .	50
5.4.3	Grout consumption . . . . .	51
5.5	Conditions encountered during project construction . . . . .	51
5.5.1	Rock mass conditions . . . . .	51
5.5.2	Groundwater inflow . . . . .	53
5.5.3	Rock mass grouting . . . . .	54
5.6	Methodology of grouting and water inflow measurement . . . . .	55
<b>6</b>	<b>Methodology</b>	<b>57</b>
6.1	Data gathering . . . . .	57
6.2	Data systematization . . . . .	57
6.2.1	Probe drilling results . . . . .	58
6.2.2	Rock mass grouting . . . . .	59
6.2.3	Tunnel mapping . . . . .	60
6.3	ArcGIS Pro . . . . .	61
6.4	Statistical analysis . . . . .	62
6.4.1	Semi-analytical approach for estimating specific leakage . . . . .	63
6.4.2	Multiple linear regression (MLR) model . . . . .	63
<b>7</b>	<b>Analysis of tunnel segments</b>	<b>67</b>
7.1	Introduction . . . . .	67
7.2	Tunnel segment A . . . . .	68
7.2.1	Introduction . . . . .	68
7.2.2	Conditions on the surface . . . . .	69
7.2.3	Conditions in the tunnel . . . . .	74
7.2.4	Rock mass grouting . . . . .	77

---

---

7.2.5	Discussion . . . . .	78
7.3	Tunnel segment B . . . . .	81
7.3.1	Introduction . . . . .	81
7.3.2	Conditions on the surface . . . . .	81
7.3.3	Conditions in the tunnel . . . . .	83
7.3.4	Rock mass grouting . . . . .	88
7.3.5	Discussion . . . . .	89
<b>8</b>	<b>Statistical analysis</b>	<b>91</b>
8.1	Groundwater inflow . . . . .	91
8.1.1	Overview of the results . . . . .	91
8.1.2	Statistical analysis . . . . .	96
8.1.3	Comparison of water inflow quantities and rock mass parameters . . . . .	98
8.2	Rock mass grouting - Multiple Linear Regression (MLR) . . . . .	98
8.2.1	Description of the data set . . . . .	99
8.2.2	Stepwise regression analysis . . . . .	102
<b>9</b>	<b>Discussion</b>	<b>105</b>
9.1	Analysis in areas of interest . . . . .	105
9.1.1	Groundwater inflow . . . . .	105
9.1.2	Rock mass grouting . . . . .	106
9.2	Statistical analysis . . . . .	107
9.2.1	Groundwater inflow . . . . .	107
9.2.2	MLR model of grout take and rock mass parameters . . . . .	110
<b>10</b>	<b>Conclusions and recommendations</b>	<b>113</b>
10.1	Conclusions . . . . .	113
10.2	Recommendations for further work/research . . . . .	114
	<b>Bibliography</b>	<b>115</b>
	<b>Appendices</b>	<b>121</b>
<b>A</b>	<b>The Q-system (NGI, 2015)</b>	<b>123</b>
<b>B</b>	<b>Typical documentation</b>	<b>133</b>
B.1	Probe drilling results . . . . .	134
B.2	Engineering geological mapping . . . . .	135
B.3	Rock mass grouting . . . . .	136

---



---

<b>C</b>	<b>SmiSto - ArcGIS Pro model</b>	<b>137</b>
C.1	Legend . . . . .	138
C.2	SmiSto overview . . . . .	139
C.3	Smibelg HPP . . . . .	141
C.4	Storåvatn HPP . . . . .	150
<b>D</b>	<b>Longitudinal profiles</b>	<b>163</b>
D.1	Longitudinal, geologic profiles from Chapter 7 . . . . .	164
D.2	Longitudinal profiles Storåvatn main head race tunnel . . . . .	167
<b>E</b>	<b>Python scripts for data processing</b>	<b>171</b>
E.1	Standard formatting names . . . . .	172
E.2	Identify standard formatted columns in Excel . . . . .	174
E.3	Assign Q-values to bore holes . . . . .	176
E.4	Processing of strike and dip results . . . . .	179
E.5	Overburden calculation . . . . .	181
E.6	Export maximum inflow in probe drilling round to new Excel file . . . . .	183
E.7	Semi-analytical water leakage analysis with approach proposed by Panthi (2006)	186
E.8	Multivariate linear regression in Python . . . . .	189



# List of Tables

2.1	RQD-classification. From Deere (1966), cited in Nilsen and Palmström (2000).	9
4.1	Suggestions to water inflow requirements for T 8.5 tunnels, from Klüver and Kveen (2004).	33
5.1	Key data of the SmiSto hydro power project (Aasen and Lunde, 2017).	39
5.2	Explanation of the rock mass classification used in the pre-liminary phase of the project (Lunde and Lie, 2013).	49
5.3	Expected grout consumption in the SmiSto project. The total grout take is equally distributed among the two hydro power plants.	51
5.4	Percentages of Q-values below certain upper limits regarding quality for the main head race tunnel of Smibelg. Based on NGI (2015).	52
5.5	Percentages of Q-value below certain upper quality limits for the Storåvatn head race tunnel. Based on NGI (2015).	53
5.6	Detailed overview of the results from Figure 5.13. The cement consumptions are in tonnes.	55
6.1	Division of rock mass quality categories. The division is based on NGI (2015).	61
7.1	Overview of the analysis areas.	67
7.2	Summary of discontinuity sets observed on surface imagery for Storåvatn branch tunnel.	70
7.3	Table showing the approximate orientations of the foliation and JS <sub>A</sub> 1.	75
7.4	Joint sets present in tunnel segment B.	85
8.1	Overview of highest category in the analyzed tunnel sections.	93

---

8.2	Covariates and the response variable in the model. The Q-value is dependent on the other RMG-parameters and was therefore not included. . . . .	99
8.3	Models in stepwise regression using backward elimination of covariates. . . . .	103
8.4	Results for the coefficients of covariates in the model with standard error and 95% confidence interval. . . . .	103

# List of Figures

2.1	Illustration of the different scales of discontinuities (Palmström, 1995). . . . .	7
2.2	Rock mass strength and dependence on the load direction compared to the orientation of discontinuity planes. From Hudson and Harrison (2000). . . . .	8
3.1	The hydrologic cycle. Modified after Nilsen and Palmström (2000). . . . .	14
3.2	Water flow through a cylinder with parameters in Darcy's law. Modified after Gustafson (2009). . . . .	16
3.3	Illustration of a typical fracture pattern in a fault zone. Modified after Braathen and Gabrielsen (2000). . . . .	17
3.4	Theory of large fault zones and permeable pinnate fissures. The arrows indicate the stress situation and relative movement near the fault zones. Modified after (Selmer-Olsen, 1981). . . . .	18
3.5	Change in hydraulic conductivity towards depth for five locations in pre-Cambrian rocks in Sweden (Carlsson and Olsson, 1977). . . . .	20
3.6	Illustration of parameters and principles used for estimating water inflow to a tunnel using analytical approaches. . . . .	23
3.7	Illustration for how the depth parameter ( $D$ ) is calculated in Equation 3.7. . . . .	24
4.1	Example of a modern grouting rig (Hognestad et al., 2011). . . . .	28
4.2	Illustration of the pre-groutig process. Modified after Gustafson (2009). . . . .	29
4.3	Principle of post-excavation grouting. Based on Gustafson (2009). . . . .	30
4.4	Photo by L. Erikstad of Puttjern above the Romeriksporten railway tunnel. Puttjern was a water source to the high inflows in the tunnel, and the water table consequently got drained (Kveen and Lindstrøm, 2005). . . . .	33
4.5	Bedrock gneiss in Ås, Norway. This rock mass is an example of class B in the categorization by Klüver and Kveen (2004). . . . .	36

---

4.6	Illustration of the influence between orientation of similarly spaced discontinuities and groutability. One can see that more discontinuities are perforated in the uppermost situation. . . . .	37
5.1	Overview map of Smibelg and Storåvatn hydro power plants and the tunnel systems (Haugerud, 2019). . . . .	40
5.2	Main tectonic units near the Gjervalen fjord. Modified after Qvale et al. (2012). . . . .	41
5.3	Geologic map of the Smibelg tunnel system, including water sources (Haugerud, 2019). . . . .	42
5.4	Geologic map of the tunnel system of Storåvatn, with water sources on the surface (Haugerud, 2019). . . . .	43
5.5	Aerial photograph of LD 1 and LD 2 for a location near Sendselva on the southern side of the Gjervalen fjord. . . . .	44
5.6	Indications on the regional horizontal rock stress conditions based on previous stress measurements. Modified after Myrvang (2001). . . . .	45
5.7	Results from hydraulic jacking tests with chainage numbers in the Smibelg head race tunnel. The overburden is roughly sketched. . . . .	47
5.8	Safety factor from hydraulic jacking tests related to cone placement in the main head race tunnel of Storåvatn. Overburden is roughly sketched. Results from SINTEF (2016). . . . .	48
5.9	Anticipated rock mass quality in the Smibelg HPP. . . . .	49
5.10	Anticipated rock mass quality in the Storåvatn HPP. . . . .	50
5.11	Histogram of rock mass quality (Q-value) between chainage 0+000 m and 8+300 m for the head race tunnel of Smibelg. . . . .	52
5.12	Histogram of rock mass quality (Q-value) between chainage 0+000 m and 7+200 m for the Storåvatn main head race tunnel. . . . .	53
5.13	Distribution of the consumption for the different cement types used during construction of the SmiSto hydro power project. For explanation of the cement types, see Appendix E.1. . . . .	55
6.1	Water inflow categories based on quantitative estimates and qualitative comments. . . . .	58
6.2	A probe drill hole crossing multiple chainage intervals ( $Q_1 \neq Q_2 \neq Q_3$ ). Illustrating the problem of selecting Q-values for the probe drill hole results. . . . .	59
6.3	Division of pre-grouting rounds in categories based on total grout consumption. . . . .	60
6.4	Ortophoto illustrating the rock mass quality, groundwater inflow and rock mass grouting categories. The photo shows the conditions between chainage 1+600 m to around 1+700 m of the Storåvatn main head race tunnel. See change numbers for image scale. . . . .	62

---

---

7.1	The analysis areas shown in an ortophoto with elevation lines. The contour interval is 50 m on the map. . . . .	68
7.2	Topographic map of the Storåvatn branch tunnel with water inflow and grouting categories. Contour interval = 50 m. . . . .	69
7.3	Aerial photograph of the Storåvatn branch tunnel with overview of rock mass grouting and water inflow in probe drilling rounds. The image also shows distribution of rock mass quality (Q-values) along the tunnel. . . . .	71
7.4	Aerial photograph of the weakness zone crossing the branch tunnel to Storåvatn lake. See chainage numbers for scale. . . . .	72
7.5	Geological profile sketch along the Storåvatn branch tunnel. The blue dashed line indicates a rough sketch of the groundwater table level based on water sources on the surface and an assumption of a high groundwater table. An enlarged image of the geologic profile is included in Appendix D.1. Made with Autodesk's Civil 3D. . . . .	73
7.6	Stereonet contour plot with interpreted joint set and foliation. Chainage interval of Storåvatn branch tunnel: 0+000 m to 1+000 m. Made with Dips by Rocscience. . . . .	74
7.7	Safety factor estimated from hydraulic jacking results for Storåvatn branch tunnel. Overburden is roughly sketched. Results from SINTEF (2016). . . . .	76
7.8	Distribution of different cement types along the branch tunnel to Storåvatn lake. For explanation of the cement types in Figure 7.8, see Appendix E.1. . . . .	77
7.9	Sketch of a possible situation at Storåvatn where the maximum principal stress is oriented nearly in-plane to the main joint set within the rock massif for some locations. This presupposes the assumption that topographic effects control the stress orientations near the tunnel. Red lines indicates the joint system, the black line indicates the tunnel and the orange crosses the directions of $\sigma_1$ and $\sigma_3$ . . . . .	79
7.10	Geological map showing the main head race tunnel of Storåvatn with distribution of Q-values. . . . .	82
7.11	Distribution of water inflow categories and estimates in tunnel segment B. The circles denote quantitative estimates and the crosses categories of the encountered groundwater inflows. . . . .	83
7.12	Aerial photograph with the section for analysis (chainage 1+200 m to 1+650 m). For legend regarding the rock types, see Figure 7.10. . . . .	84
7.13	Contour stereonet for the distribution of joints in tunnel segment B. . . . .	85
7.14	Longitudinal, geologic profile of tunnel segment B. Symbology is similar to that of Figure 7.5. Joint sets observed in the tunnel with water inflows are shown for plan view illustration of the tunnel. An enlarged image of this figure is found in Appendix D.1. Made with Autodesk's Civil 3D. . . . .	87

---

---

7.15	Distribution of different cement types in tunnel segment B. For explanation of the cement types, see Appendix E.1. Cement consumptions are in kg. . . . .	88
8.1	Distribution of water inflow categories from the four analyzed tunnels. In total, n = 293 data points are included. . . . .	92
8.2	The average and standard deviation of critical parameters . . . . .	94
8.3	The average and standard deviation of critical parameters . . . . .	95
8.4	The average and standard deviation of critical parameters . . . . .	97
8.5	Distribution of estimated and actual inflow rates in probe drilling holes along the tunnel face locations in the Storåvatn main head race tunnel. . . . .	99
8.6	Distribution and box plot of the response variable ( $\bar{C}_{tot}$ ) in $\frac{kg}{m}$ . . . . .	100
8.7	The average and standard deviation of critical parameters . . . . .	101
8.8	Distribution of the normalized residuals after log-transforming the response variable ( $\bar{C}_{tot}$ ). . . . .	102



---

# Abbreviations

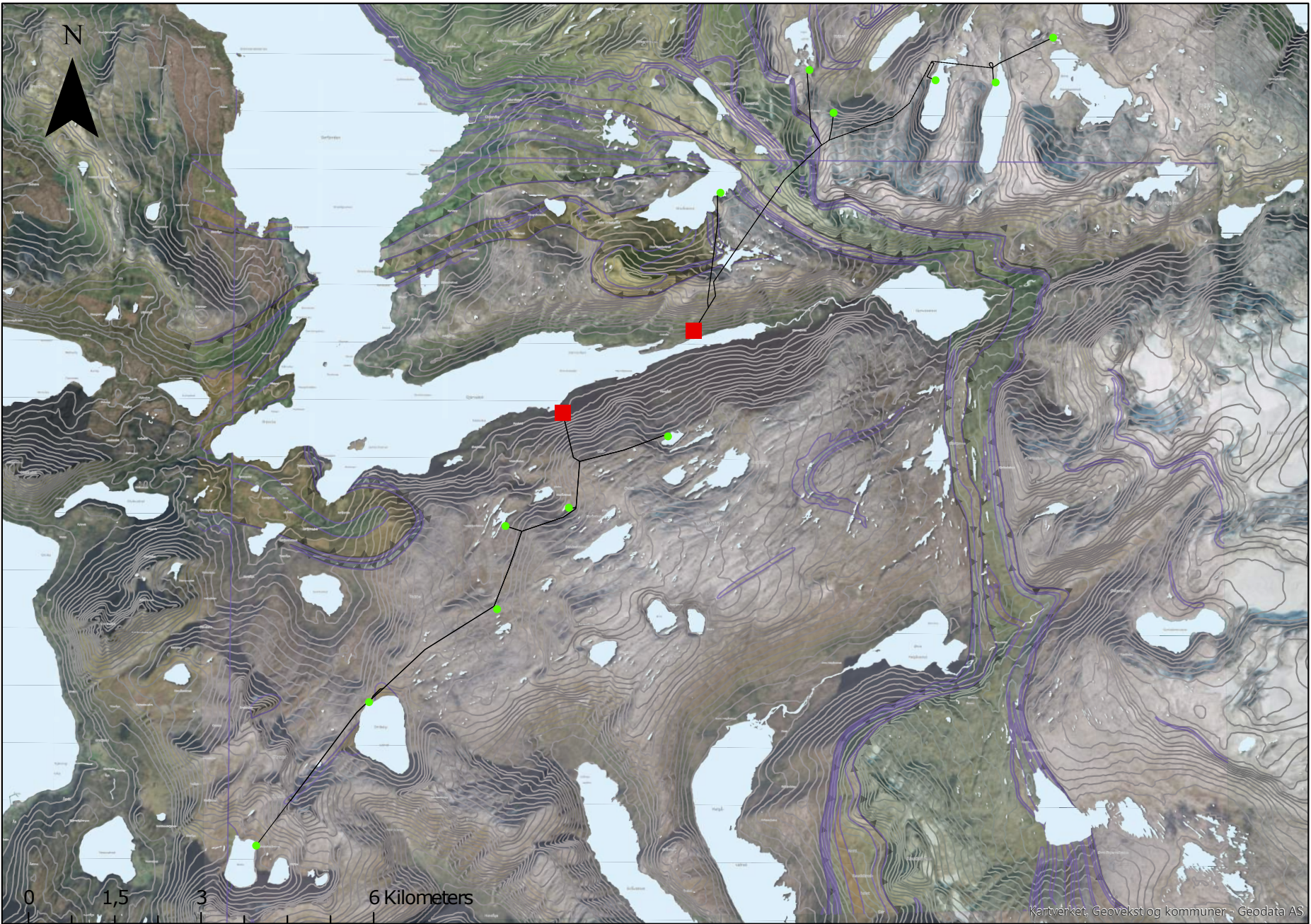
SmiSto HPP = Smibelg and Storåvatn hydro power project  
PD = Probe drilling  
RMG = Rock mass grouting

k = Permeability  
K = Hydraulic conductivity  
 $\sigma_1$  = Major principal stress  
 $\sigma_2$  = Intermediate principal stress  
 $\sigma_3$  = Minor principal stress

LD 1 = Large-scale discontinuity system 1, near Smibelg HPP  
LD 2 = Large-scale discontinuity system 2, near Smibelg HPP  
DS 1 = Large-scale discontinuity system 1, near Storåvatn HPP  
DS 2 = Large-scale discontinuity system 2, near Storåvatn HPP  
DS 3 = Large-scale discontinuity system 3, near Storåvatn HPP

$Q_{75}$  = 75 % quartile  
 $Q_{25}$  = 25 % quartile  
 $IQR_{75}$  = Interquartile range





N



0 1,5 3 6 Kilometers



# Introduction

## 1.1 Background

Inflow of groundwater can cause significant difficulties for an underground project constructed in rock. Tunnels for different purposes are common underground structures where this can occur. The encountered inflows can be associated with both high pressures and water amounts. In the Gotthard Piora pilot, in Switzerland, water pressures corresponding to 900 m water column was encountered. In the Abou tunnel in Japan, water ingress of up to 3000 l/sec were reported (Fu et. al. cited in BASF (2011)). These are extreme cases, but smaller inrushes of water can also cause severe problems. Nilsen and Palmström (2000) have summarized some of the common negative consequences related to inrushes of groundwater:

- Unpleasant environment of the workers inside the tunnel.
- Drill and blast operations can become considerably more challenging to perform.
- The roadway in the tunnel can be damaged, and in some cases completely washed out.
- The groundwater table can be lowered due to drainage of the water source. This can cause soft sediments above the tunnel to settle. Buildings can suffer damage because of the settlements (Karlsruud, 2001).
- Difficulties can also be related to the freezing of the water.

The final consequences can be extensive delays and budget overrun for the project. In the worst case, there can be casualties related to the construction, and the underground structure might be lost (Panthi, 2006). Today, there are numerous examples where inflow of groundwater has caused significant delays and cost overrun in Norwegian and international projects (Selmer-Olsen, 1981, Zarei et al., 2011).

When groundwater inflow in a tunnel occurs, the water must be tackled by either pumping it and letting it drain out of the tunnel or perform grouting to seal the water-conducting voids in the rock mass (BASF, 2011). Pre-grouting at the tunnel face is a technique that has undergone many advances in recent decades and is extensively used in undergrounds projects today (Hognestad et al., 2011). This is more preferable compared to grouting behind the tunnel face by post-excavation grouting. Though some recommendations have been developed from years of experience, universal guidelines that ensure a satisfactory grouting result do not exist.

To prevent the unfavorable situations described above, a variety of authors have contributed for assessing the leakage potential in a pre-liminary phase of a project. Experienced-based approaches are generally used, but analytical and numerical approximations are available today. Some empirical considerations are described by Selmer-Olsen (1981) and Klüver and Kveen (2004). El Tani has summarized some important developments in analytical solutions, and has developed an exact analytical solution for water inflow (El Tani, 2003). Hassani et al. (2016) gives an example of groundwater inflow estimation with a numerical method.

During excavation of a tunnel, probe drilling with several drill holes is important to detect water-bearing formations ahead of the tunnel face. Several exploration holes should be drilled systematically in areas where larger water inflows can pose a risk. Other exploration techniques, e.g. geophysical methods exist, but are not commonly used.

Despite continuous improvements of the methodologies, unexpected inflow of groundwater is still a considerable problem in hard rock tunneling today.

## 1.2 Objectives and scope

This thesis is a continuation of the project work by the author. While the project work mainly regarded a study of the Smibelg HPP, this thesis has focused on the conditions in Storåvatn HPP. The reader is referred to Haugerud (2019) for more information on the results.

The scope and objectives of the study can be summarized as follows:

- Theoretical review of the hydrogeological, engineering geological and mechanical properties of the rock mass. Review of methodologies for leakage estimation and inflow estimation in rock tunnels.
- Review of factors relevant for the grouting process with a brief discussion of pre- and post-excavation grouting. Review of grouting requirements for different rock tunnels.

- Review of the engineering geological conditions prevailing in the project area of SmiSto.
- Data gathering and systematization of information regarding rock mass grouting, water inflow and rock mass conditions.
- Application of empirical and semi-analytical methods to assess potential inflow magnitudes.
- Evaluation of the grout consumption based on information of rock mass quality, and investigation of which parameters are significant for the grout take.
- Conclusion of the work with recommendations.

## 1.3 Methodology

The methodology used in this master thesis can be divided in the following:

1. Review of relevant literature.
2. Collection and systematization of results from probe drilling, rock mass grouting and tunnel mapping. The methodologies used for this part is explained further in Chapter 6.
3. Analyzing the data:
  - Analysis of groundwater inflow and rock mass grouting in areas of interest using empirical methods.
  - Statistical analysis of the gathered data.
4. Evaluating and assessing the results.

## 1.4 Limitations

The main limitations to the statistical analysis are related to assigning one Q-value for results of water inflow and rock mass grouting. There are several situations where both the pre-grouting and probe drilling rounds cross segments assigned with different rock mass quality. Further, the Q-system developed by NGI is mainly intended for evaluating the rock mass with respect to stability and the need for support and reinforcement. Other rock mass classification systems might be more suitable for comparing the water inflows and grout takes with the rock mass conditions.

The author has generally relied on hand-written documents of the performed rock mass grouting, probe drilling and tunnel mapping in the tunnels. Consequently, there will be a risk of misinterpreting the data. The author has had the ability to visit the project site at two occasions and

mapped some areas of the tunnel himself. However, certain areas of the tunnels have not been available for inspection during the project site visits. Further, it seems likely that the documentation received by the author related to rock mass grouting is incomplete. This particularly regards one of the analyzed tunnel segments in the branch tunnel to Storåvatn, discussed in Chapter 7.



# Properties of the rock mass

The rock mass is a particular material used for construction purposes. Unlike other materials used in construction its properties can show a high variability. Its condition also depends on processes that have formed the material for millions, or even billions of years. A brief review of some characteristics relevant for the rock mass will be given in the following chapter.

## 2.1 Intact rock

According to Hudson and Harrison (2000) the definition of intact rock in engineering terms is a rock without significant fractures. However, discontinuities on a microscopic scale exist also in an intact rock sample.

### 2.1.1 Composition

Rocks are naturally occurring and consists of one or more minerals dependent on the the formation of the respective rock. The size of the mineral grains, the shape, fabric and the material that holds them together depends on processes from the formation of the rock and up till its present state (Nelson, 2012).

### 2.1.2 Mechanical properties

Since aggregates of minerals makes up the rock, its mechanical properties are dependent on the characteristics of these constituents. The strength of intact rock can be tested with different test methodologies and are valuable to assess the mechanical behavior of the respective rock. To determine mechanical properties of the rock such as stiffness by  $E$ -modulus, poisson's ratio ( $\nu$ ) and uniaxial compressive strength (UCS), the uniaxial compressive test is a commonly used

method. A triaxial test can be used to apply a confining pressure to the specimen. Other, simpler methods exist for testing the mechanical properties (Hudson and Harrison, 2000).

## 2.2 Properties of the rock mass

The rock mass is "rock penetrated by discontinuities". The properties of the rock mass is consequently dependent on the two main constituents of the material, namely the properties of the rock type and the properties of the discontinuities (Nilsen and Palmström, 2000).

### 2.2.1 Discontinuities

In rock engineering, a discontinuity denotes any separation in the rock where the tensile strength is zero (Hudson and Harrison, 2000). Discontinuities can be categorized dependent on their respective scale:

- Regional pattern by larger weakness zones or faults.
- Second order blocks formed by singularities (small weakness zones or seams).
- Third order blocks formed by normal joints.
- Small joints that appear as bedding or schistosity patterns are considered the smallest pattern of interest for engineering purposes.
- Microcracks in the rock. These discontinuities are often considered a property of the intact rock.

(Nilsen and Palmström, 2000).

The two main groups of discontinuities are joints and weakness zones. Figure 2.1 lists different discontinuities and their respective scale.

#### Joints

According to ISRM (1975) cited in Palmström (1995), a joint is a discontinuity of natural origin along where it has been no visible displacement. Joints can be related to tectonic forces, exfoliation or bedding of the rock. Other joint types also exist.

The characteristics of the joints are relevant for the properties of the discontinuities. Some of the characteristics are mentioned in the following.

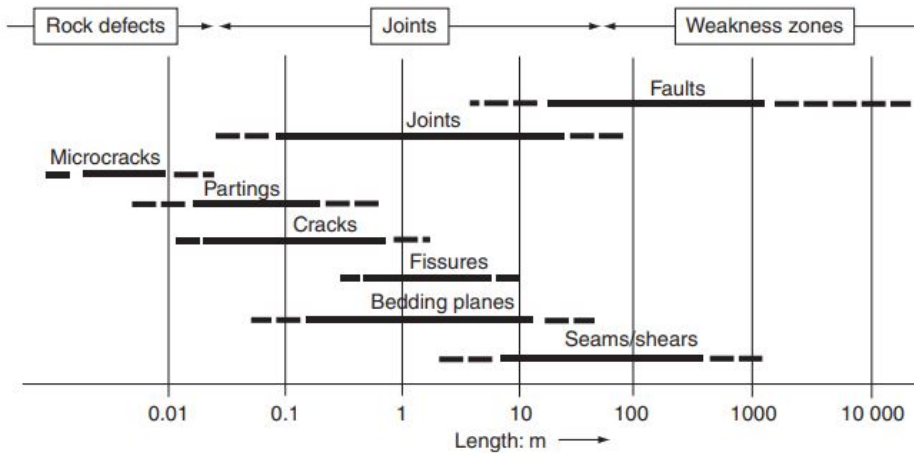


**Figure 2.1:** Illustration of the different scales of discontinuities (Palmström, 1995).

*Persistence* is the areal extent of the joint plane and can be estimated by observing the discontinuities on the surface. *Aperture* is the maximum distance between joint walls. The *character* of the joint surface can influence the frictional properties of the joint. The surface can be stained, fresh, weathered or coated. Joint *filling* consists of material from country rocks and can have a variety of minerals. Swelling material can also be present in the joints (Palmström, 1995).

### Weakness zones and faults

A weakness zone is an area of the rock mass with significantly reduced mechanical properties than the adjacent rock mass. Faults, shears/shear zones, thrust zones and weak mineral layers are examples of weakness zones. The type of weakness zones can be categorized in two main groups; those formed from tectonic events, and those consisting of weak materials that originate from other processes (Nilsen and Palmström, 2000).

Faults and fault zones are a result of a series of ruptures in geologic time. These zones can be divided in shear fault zones and tension fault zones. Shear fault zones are crushed and consist of a number of intersecting joints. The middle part of such a zone may be entirely altered to clay or only show some indications of weathering. The size of these faults can range from a few centimeters to many meters. Tension faults are related to stress-relief and often contain a filling of soft material in the discontinuity. The filling material can consist of both swelling and non-swelling minerals. Feather and pinnate fissures are types of tension faults (Nilsen and Palmström, 2000).

## 2.2.2 Rock mass strength

The strength of the rock mass depends highly on the properties of the discontinuities. If the loading direction is parallel or perpendicular to the discontinuity planes, it will have no effect on the sample strength. However, if the discontinuity plane is inclined at an angle  $45^\circ + \frac{\phi}{2}$ , a significant reduction in the strength will occur (Hudson and Harrison, 2000). This situation is illustrated in Figure 2.2. The Mohr-Coloumb criterion is used for this theory regarding a single plane of weakness.

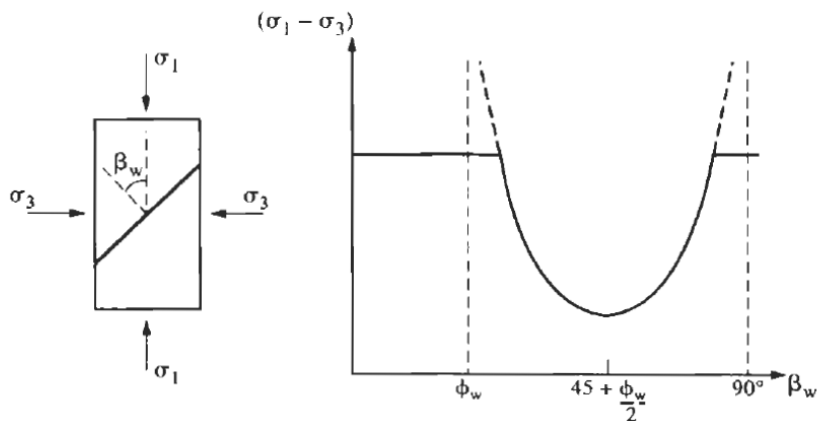


**Figure 2.2:** Rock mass strength and dependence on the load direction compared to the orientation of discontinuity planes. From Hudson and Harrison (2000).

In a situation with multiple discontinuities having different orientations, the rock mass will be weakened in more than one direction.

The Mohr-Coloumb criterion mentioned above expresses a linear relationship between shear and normal rock stress. The criterion will not be discussed further, but rather mentioned as a commonly used criterion for evaluating the rock mass strength. Other criteria such as the Hoek-Brown empirical strength criterion is commonly used in mechanical analyses of the rock mass today.

## 2.3 Rock mass classification systems

When investigation of the rock mass is undertaken it is often relevant to group or classify the findings. The most suitable classification system will depend both on the type of rock mass and the problem at hand. Rock mass classification systems can serve with a general purpose to describe the geological and technical properties of the rock mass, or they can be used to a

more specific purpose to e.g. determine appropriate drill and blast method or the support and reinforcement of a tunnel (Nilsen, 2016).

### 2.3.1 Rock Quality Designation (RQD)

Rock quality designation is used to characterize the degree of jointing in a borehole core. It is a simple and rapid method to execute. The RQD-value is determined by estimating the percentage of rock core pieces longer than 0.1 m to the total length of the core. The method has several limitations due to its simplicity and the small volume of rock that is considered in the classification (Nilsen and Palmström, 2000). Table 2.1 shows the division of rock quality from RQD.

**Table 2.1:** *RQD-classification. From Deere (1966), cited in Nilsen and Palmström (2000).*

Term	RQD
Very poor	<25
Poor	25-50
Fair	50-75
Good	75-90
Excellent	90-100

### 2.3.2 Q-system

The Q-system is classification system for rock masses with respect to stability of tunnels and underground constructions. It can be applied both for rock mass on the surface and underground. The classification system was developed by NGI between 1971 and 1974, and has since been revised with the improvements in tunneling technology (NGI, 2015). Tables and diagrams of the Q system are attached in Appendix A.

The Q system consists of six parameters;

- Rock quality designation, *RQD*
- Number of joint sets,  $J_n$
- Roughness of the most unfavourable joint or discontinuity,  $J_r$
- Degree of alteration or filling along the weakest joint,  $J_a$
- Water inflow,  $J_w$
- Stress reduction factor, *SRF*

The Q-value is then given by the following formula:

$$Q = \frac{RQD}{J_n} \cdot \frac{J_r}{J_a} \cdot \frac{J_w}{SRF} \quad (2.1)$$

The first quotient can be considered an estimate of the block size. The second quotient can be regarded as an indicator of the inter-block shear strength and the third quotient as the "active stresses".

### **Application to rock support and reinforcement**

The Q-system can be applied as a guidance to rock support and rock reinforcement by using the Q-value, the safety level of the underground structure, and the dimensions of the structure. The Excavation Support Ratio (ESR) is used to express the safety requirements of the underground space. A low ESR-value indicates a high safety requirement. The demand for rock support and reinforcement will generally increase with increasing dimensions of the underground space. (NGI, 2015). Appendix A shows recommended support and reinforcement diagrams given rock mass quality, ESR and the dimension of the structure dimension.

### **Limitations**

The Q-system is based on a number of reference cases mainly in hard and fractured rock. In cases of weak rocks with few or no fractures, the rock mass classification system can be less adequate (NGI, 2015). Palmstrom and Broch (2006) emphasized the approximation from which the system was based, which in itself is related to a high degree of uncertainty. Further, the values are chosen subjectively based on the interpretation and experience by the person.

### **2.3.3 Other rock mass classification systems**

There are other rock mass classification systems available at use. These will be mentioned and explained briefly in the following.

#### **Geological strength index (GSI)**

The geological strength index can be used to estimate the reduction in rock mass strength for different geological conditions by field investigations. Two main parameters determine the GSI-value; the structure of the rock mass and surface conditions of the discontinuities. The first parameter depends on the number of discontinuities in the rock and the foliation (if any). The second parameter denotes the condition of the joints with respect to roughness and alteration (Nilsen and Palmström, 2000). GSI is a popular rock mass classification system since it can be used to determine parameters in the Hoek-Brown failure criterion (Nilsen, 2016).

### **Rock Mass Rating (RMR)**

The rock mass rating is applied by dividing a tunnel route in a number of sections where the change in geological conditions are relatively small. For each section, a rock mass rating is assigned by determining six parameters;

1. Uniaxial compressive strength (UCS) of intact rock material
2. Rock quality designation
3. Spacing of the discontinuities
4. Condition of the discontinuities
5. Groundwater conditions
6. Orientation of the discontinuities

Based on estimates of each parameter a rock mass rating ranging from 0 to 100 is assigned to the rock mass (Nilsen and Palmström, 2000).





# Water in the rock mass

Inflow of groundwater in tunnels and other underground structures can result in challenging working conditions within the structure, but can also have negative effects on the environment outside. This chapter reviews established comprehensions of the groundwater's behavior in the rock mass and its significance in underground projects.

## 3.1 Introduction

Water has a natural place in the rock mass, and takes part in the hydrologic cycle, See Figure 3.1.

The location of the groundwater table can vary between different rock types, but can also show fluctuations with time. Factors that control the infiltration of water to the ground are summarized below.

- The amount of precipitation.
- The size of the catchment area.
- The evaporation in the area.
- Amount of precipitation that run-off on the surface.

When the water infiltrates the ground, parameters regarding the flow properties become relevant. These are mainly connected to the properties of the discontinuities in the rock. The conductivity of the joints and the connection between them are also relevant. Other factors that control the behavior of the groundwater when it has infiltrated the ground are the reservoir capacity and the presence of other water sources (Davik et al., 2002).

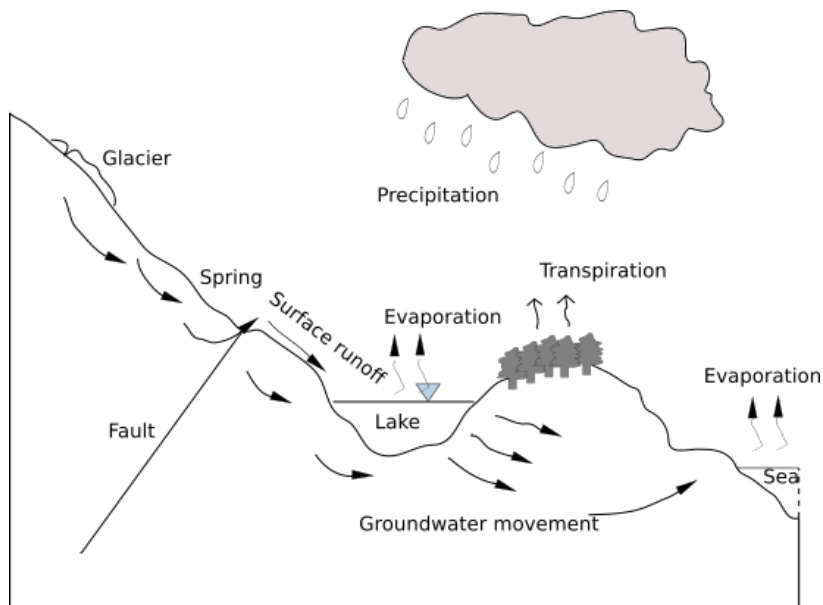


**Figure 3.1:** *The hydrologic cycle. Modified after Nilsen and Palmström (2000).*

A majority of the underground structures constructed in rock will be located beneath the groundwater table. In the planning phase of an underground project it is therefore of great importance that one at an early stage evaluates what problems the groundwater might cause. This must be assessed both for the construction phase, and after completion of the project. Inrushes of groundwater in underground projects are well-known from the past, and continue to cause challenges in projects today (Nilsen, 2016).

## 3.2 Consequences of water inflow

### 3.2.1 Environmental

Groundwater inflow in a tunnel that has discontinuities communicating from the rock to overlying, saturated soil, will cause a reduction of the groundwater level. This will again reduce the pore pressures in the soil, increasing the effective stresses. A consolidation process can occur, causing significant settlements in soils with an abundance of clayey material (Davik et al., 2002).

### 3.2.2 Internal environment in the structure

Inflow of water in an underground construction reduces the quality of the working conditions for the personnel inside the structure. In the case of a tunnel, the process of drill and blast can become very challenging when high water inflows and water pressures are encountered. Damages to the roadway can occur and pumping the water out of the tunnel can also be a challenge (Selmer-Olsen, 1981). Due to the unfavorable inflows, the efficiency of the tunneling process can be reduced considerably. High water pressures will also influence the stress situation around the tunnel, giving additional stress on the tunnel surface, tunnel face and on the support structure. This can, in turn, affect the overall stability of the tunnel (Gong et al., 2018).

## 3.3 Theoretical background of fluid flow in the rock mass

The flow of groundwater in the rock occurs principally in the discontinuities of the rock. This is unlike the flow of groundwater in soils, which takes place in the interconnected pores (Gustafson, 2009).

The flow of groundwater in both rock masses and soils is commonly considered to be laminar. Darcy's law presupposes laminar flow of a fluid, and is extensively used for calculations regarding flow of groundwater in porous media (see Equation 3.1).

$$Q = K \cdot A \cdot \frac{\Delta h}{\Delta l} \quad (3.1)$$

Which states that the flow through a porous media ( $Q$ ) is proportional to the hydraulic gradient ( $i = \frac{\Delta h}{\Delta l}$ ). Figure 3.2 gives an illustration of flow through a cylinder and the parameters in Darcy's law.

### 3.3.1 Groundwater flow in a 2D discontinuity

In reality, the discontinuities in the rock mass can be considered as two-dimensional structures and consequently planar structures (Gustafson, 2009). The flow rate in a joint will depend on the width or aperture of the joint. For a set of planar discontinuities parallel to each other, Louis proposed a relation between the hydraulic conductivity ( $k$ ) and the opening ( $e$ ) and spacing ( $S$ ) of the joints, see Equation 3.2 (Nilsen and Palmström, 2000).

$$k = \frac{g \cdot e^3}{12\nu \cdot S} \quad (3.2)$$

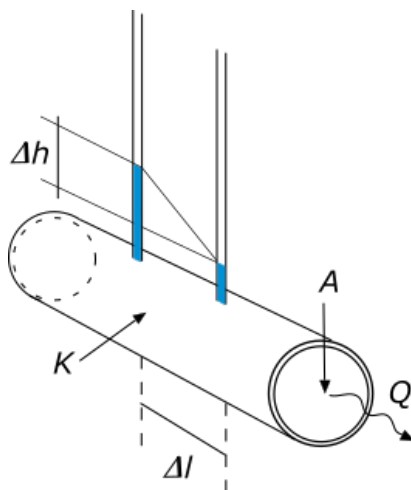


**Figure 3.2:** Water flow through a cylinder with parameters in Darcy's law. Modified after Gustafson (2009).

From this equation it is evident that an increase in the aperture by a factor of two will increase the hydraulic conductivity by a factor of eight. The nature of discontinuities will seldom be perfectly planar and can contain fillings of clay or other fine material. This can cause the flow of groundwater in a rock mass to be limited to channels rather than "discontinuity planes". The assumptions from which Darcy's law and Louis's equation are formed, may in some cases not be valid. However, they are useful to understand the parameters affecting groundwater flow in the rock mass (Nilsen and Palmström, 2000).

### 3.4 Geological parameters controlling groundwater inflow in tunnels

This section presents common comprehensions today, regarding which geological parameters that are assumed to influence the groundwater flow into underground excavations in rock. The aspects that are introduced are related to empirical approaches available for assessing the potential for groundwater inflow (see Section 3.6.1).

#### 3.4.1 Fault zones

In addition to represent a challenge with respect to increased fracture density and poor rock stability, fault zones are generally considered as a geologic structure that could also increase the risk of groundwater inflow into a tunnel (Ganerød et al., 2008). Figure 3.3 shows an example of the typical fracture pattern in a fault zone.

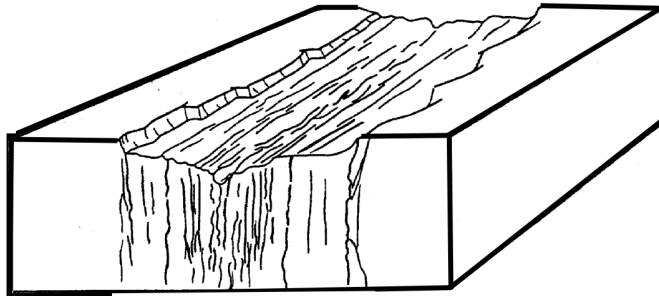


**Figure 3.3:** *Illustration of a typical fracture pattern in a fault zone. Modified after Braathen and Gabrielsen (2000).*

From investigations in the Semnan tunnel in Iran, Zarei et al. (2011) concluded that discontinuities with a steep dip had the greatest potential for causing water inflow into the tunnel. These joints were mainly related to strike-slip faults. Discontinuities associated with normal faults and thrust faults usually had a shallower dip. This observation is similar to that of Rolf Selmer-Olsen almost 40 years ago. Selmer-Olsen studied issues related to groundwater inflow during excavation for eleven underground hydro power plants in Norway. From the work he observed that they had a tendency to be oriented in mean angles to nearby tectonic faults (see Figure 3.4). Further, they almost exclusively were observed with a steep dip. His hypothesis consisted of that recent in-situ rock stresses and differences in shear strength caused particularly low stresses in mean angles to the faults. This could have reactivated "pinnate fissures" in the rock mass, which are characterized by great persistence and potentially large capacity of conducting groundwater. The rock type was typically rocks with high strength and a rigid mechanical properties. The phenomenon was common in areas where the fault zone changed direction or character (Selmer-Olsen, 1981).

### 3.4.2 Dykes

Dykes can either act as barriers or conduits of groundwater flow (Singhal, 2010). The density of the fracture systems and the hydraulic gradient determine their properties related to the flow of groundwater. In cases where a dyke does not allow much water to flow through it, groundwater pressure will build up on either side of the geological feature (Babiker and Gudmundsson, 2004). Løset (1981) studied a sewer tunnel in Oslo and noted that the eruptive dykes in the Oslo region can be more fractured than the surrounding rock. When such dykes are lithified, they will contract because the material is cooled, and open discontinuities might develop due to the

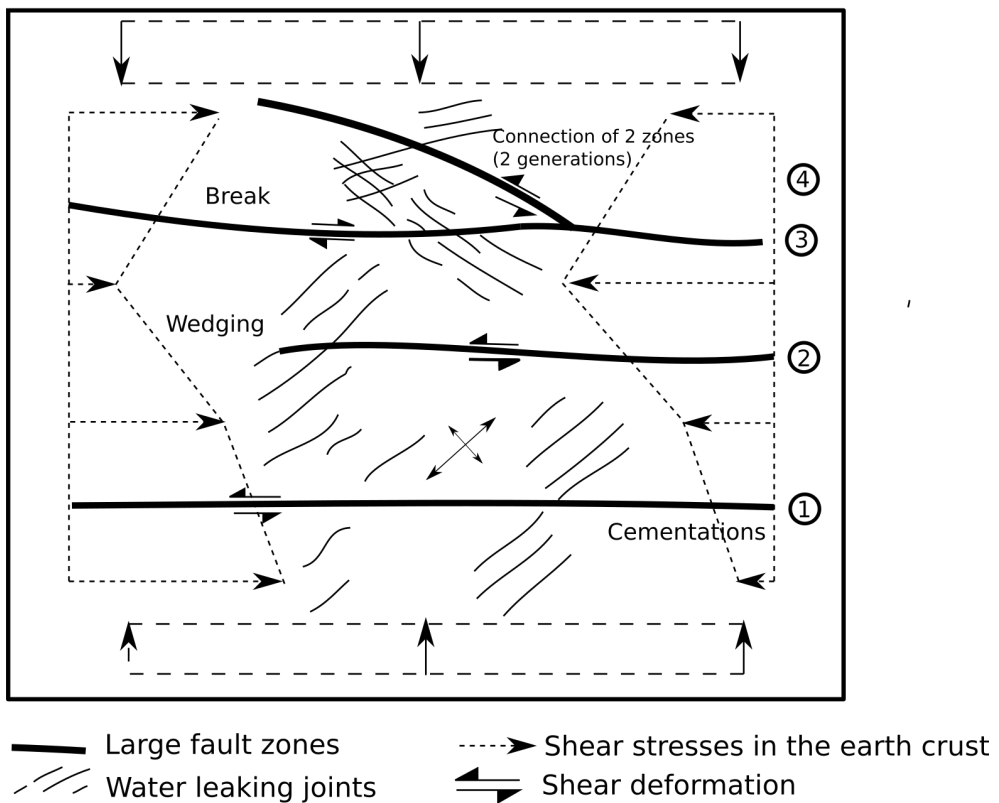


**Figure 3.4:** Theory of large fault zones and permeable pinnate fissures. The arrows indicate the stress situation and relative movement near the fault zones. Modified after (Selmer-Olsen, 1981).

induced tension forces. From the investigations, there seemed to be a clear relationship between the occurrences of groundwater inflow and locations of the eruptive dykes.

### 3.4.3 Joint characteristics

Joints and discontinuities having a large *persistence and aperture*, can be expected to pose a risk of leading water to an excavated tunnel. Some joint characteristics which are considered to influence the hydraulic conductivity are discussed below.

Joints and discontinuities will generally always have some degree of *asperity*. Asperities reduces the fluid flow in discontinuities and causes the fluid to flow in channels where the resistance to flow is smaller (Holmøy, 2008, Singhal, 2010). However, higher roughness of joints can give a decrease in permeability when there is an increase in the stresses normal to the joint plane.

*Infillings and coatings of discontinuities* in the rock mass will reduce the potential for fluid flow. Such material can partly or completely fill the void space. Depending on the grain size and mineralogy, different infill materials will have different permeability (Holmøy, 2008).

Greater *joint density* can in some cases indicate a higher hydraulic conductivity. Bore hole results from an investigation in Sweden showed that the correlation is generally low. In fractured zones with a higher joint density, the probability that some of them can be water-leading will generally increase (Gustafson, 2009). Singhal (2010) argues that joint spacing has a profound influence on the permeability and groundwater flow in the rock mass.

### 3.4.4 Stress situation

Since the rock stresses generally increases with increasing overburden, the aperture of joints towards depth will tend to decrease. The spacing between the joints can also increase. This will again cause a lower hydraulic conductivity of the joints located at great depths in the rock mass (Gustafson, 2009, Nilsen and Palmström, 2000). Figure 3.5 shows the estimated hydraulic conductivity with depth at test locations in Sweden by Carlsson and Olsson (1977).

Fractures parallel to the maximum stress direction tend to be more open, while the perpendicular oriented fractures will normally be more closed and water-conductive (Singhal, 2010). This observation has been confirmed from experiments. Pratt et al. (1977) performed tests on a 3 meter block of granite. The results showed that the flow rate doubled with an increase of 12 MPa having the stress direction parallel to the joint plane. An increase in the stress perpendicular to the joint plane with 3 MPa, reduced the flow rate with four times the initial value.

A general form to express the relationship between the depth and permeability has been proposed by Black (1987):

$$k = a \cdot z^{-b} \quad (3.3)$$

Carlsson and Olsson (1977) used results from water loss measurements at five locations in Sweden to estimate a relationship between hydraulic conductivity and depth.

$$K = 10^{-(1.6 \cdot \log z + 4)} \quad (3.4)$$

Where  $z$  is the depth in meters and  $K$  is the hydraulic conductivity in  $\frac{m}{s}$ . The results are graphed in the figure above.

The decrease in permeability with depth is often not systematic. This can be observed in cases of greater rock overburden (>50 m). There can also be large variations in permeability of the

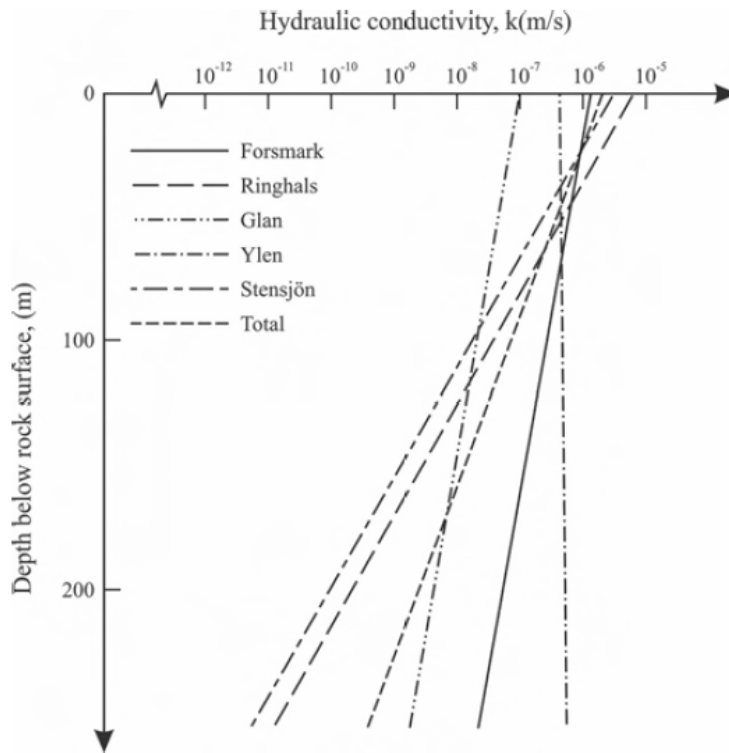


**Figure 3.5:** Change in hydraulic conductivity towards depth for five locations in pre-Cambrian rocks in Sweden (Carlsson and Olsson, 1977).

rock mass at similar depths below the ground surface. Differences in rock mass stiffness can cause local variations in the rock stresses which, in turn, can affect the hydraulic conductivity. At depths of above 1000 m, appreciable hydraulic conductivity has been measured in rock masses. The applicability of empirical relationships between hydraulic conductivity and depth can consequently be limited (Singhal, 2010).

### 3.5 Prediction of groundwater inflow in rock tunnels

Estimating and predicting groundwater inflow for rock tunnels in Norway has mainly been based on knowledge about the geological conditions in the area. That is, information about rock types, weakness zones, faults and knowledge from similar projects nearby. However, the data that can be collected for use in such an approach often leads to limited knowledge on how to use the information to give reliable predictions of groundwater inflow. The geological, hydro-geological and hydraulic factors show dependencies on each other. Investigation costs are often relatively expensive, and this can limit the amount of information available (Holmøy, 2008).



### 3.5.1 Geologic background

An understanding of the geologic history in the area of interest is key for understanding the hydro-geologic properties that dominate. An important aspect to consider is how each rock type relates to each another, and how they have affected one another during their formation. In the late phase of the rock formation, plastic deformations gradually shift to brittle. Large deformation zones are formed in this phase that can be reactivated by subsequent active tectonic phases. Some discontinuities will be hydraulic active, and others will be inactive with respect to groundwater flow (Gustafson, 2009).

### 3.5.2 Probe drilling

Probe drilling is a common approach used in tunneling to investigate conditions ahead of the tunnel face. Normal drill lengths are between 20 to 30 m, but can be both shorter or longer. Parameters such as weaker zones in the rock, groundwater occurrences and penetration rates are typically logged.

### 3.5.3 Tunnel Seismic Prediction

Thomas et al. (2016) has indicated that results from tunnel seismic prediction (TSP) can be used to predict water-bearing formations ahead of the tunnel face. This investigation method is executed by recording the full wave-field of reflected P and S-waves up to 150 meters ahead of the tunnel face location. The method is limited for prediction of water bearing zones, but since S-waves do not travel in fluids, variations in Poisson's ratio ( $\nu$ ) can give some indications on the hydrogeologic conditions ahead of the tunnel face, see Equation 3.5.

$$\nu = \frac{V_p^2 - 2V_s^2}{2(V_p^2 - V_s^2)} \quad (3.5)$$

Where  $V_s$  and  $V_p$  is the velocity of the shear and pressure wave, respectively. From Equation 3.5 a shear wave velocity of zero would give  $\nu = 0.5$ . The possibility of detecting water formations ahead of the tunnel face with this method will depend on quality of the seismic response, as well as the experience of the person interpreting the results.

## 3.6 Approaches for assessing groundwater inflow potential

For predicting groundwater inflow in rock tunnels, four approaches are mainly used:

- Empirical approaches
- Semi-analytical approaches

- Analytical approaches
- Numerical approaches

Numerical approaches available for use today will not be reviewed. However, these methods can be of great use to provide estimates regarding groundwater flow in complex situations. Software applying numerical methods have experienced a significant improvement in recent years.

### **3.6.1 Empirical approaches**

Empirical approaches are most common for prediction of groundwater inflow in underground projects in Norway today. Experience from previous projects with similar geological conditions form the basis for the assessments. However, situations arise where the rock mass conditions can be different from those encountered in underground projects located close to the relevant area (Holmøy, 2008). Zarei et al. (2011) argue that assessment of high local groundwater inflow in rock tunnels based on geological features is a more reliable method than analytical and other empirical estimations.

Geologic structures and factors known to be associated with higher water inflow potential, i.e. fault zones, dykes, topography and rock types with open discontinuities (see Section 3.4), are commonly the conditions looked for in an experience-based method to assess inflow potential and the need for grouting. Klüver (2000) suggested an approach by dividing the rock mass in four classes: A, B, C and D. The classes were chosen mainly based on the potential for water inflow and the grouting strategy that should be used. Rohr-Torp (1994) studied the correlation between post-glacial uplift rate and water yield in well tests. The results showed a strong correlation supporting existing theories that post-glacial uplift has reactivated old fracture systems and probably also generated new discontinuities. Consequently, in areas with higher uplift rates, a higher hydraulic conductivity might be expected.

### **3.6.2 Analytical and semi-analytical approaches**

#### **Analytical approaches**

Simple closed-form analytical solutions for predicting groundwater inflow in a rock tunnel exist only given certain assumptions. The aquifer is often assumed to be semi-infinite, isotropic and homogeneous. Further, the rock mass below the groundwater table is assumed to be fully saturated. It is also assumed that the groundwater level suffers no draw-down due to drainage into the tunnel. These simplifications are seldom realistic, but the solutions can be used for making rough estimations of the groundwater inflow. Figure 3.6 illustrates the typical case considered when estimating groundwater inflow into a tunnel with analytical approaches.

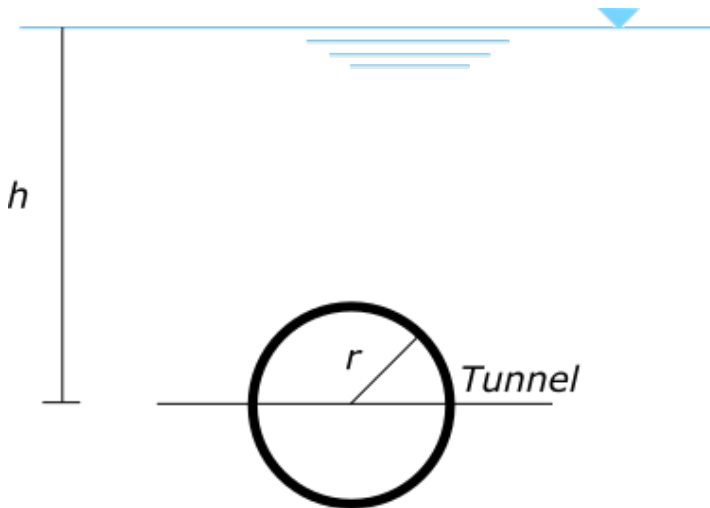


**Figure 3.6:** *Illustration of parameters and principles used for estimating water inflow to a tunnel using analytical approaches.*

A variety of analytical approaches have been developed, considering both a constant level of the groundwater table and a reduction in the groundwater level due to drainage. Muskat (1937) introduced an equation for the water inflow later transformed by Goodman et al. (1965). A similar equation was proposed in the work of Karlsrud (2001). An exact solution for the conditions described above was developed by El Tani (2003). The equation presupposed a total head equal to the elevation head. Other approaches considering a constant groundwater table have also been derived, see for instance Kolymbas and Wagner (2007).

A constant groundwater level tends to overestimate the water inflow into a tunnel. This is because a reduction in the groundwater level will reduce the pore pressure which in turn increases the effective normal stresses in the joints near the tunnel. This will decrease the hydraulic conductivity of the rock mass. Moon and Fernandez (2010) used the distinct element method to assess the effect of groundwater level draw-down on the tunnel inflow.

Since the analytical solutions are dependent on simplifying assumptions in order to estimate groundwater inflow into a tunnel, the results often vary in quality. The rock mass is generally an anisotropic and in-homogeneous medium that shows different hydraulic properties in different directions. To account for such variations in the analytical solutions, will be a difficult task. Further, the analytical approximations to groundwater inflow in a tunnel can highly overestimate the actual groundwater inflow experienced. This can particularly be seen in discontinuous rock mass having a high anisotropy (Hadi and Homayoon, 2017).

### Semi-analytical methods

Panthi (2006) analyzed extensive amounts of data from the Khimti headrace tunnel in Nepal. The aim was to investigate the possible outflow of water from the tunnel and the need for grouting. The methodology of the measurements consisted of pumping water in exploratory drill holes ahead of the tunnel face with 1.5 times the prospective operating pressure in the tunnel. The flux of water in the drill holes were then estimated and compared to rock mass parameters incorporated in the Q system and the hydrostatic head at the respective tunnel location ( $h_{static}$ ). It was observed a strong correlation to the flow rate with a combination between  $J_n$ ,  $J_r$ ,  $J_a$  and  $h_{static}$  (see Equation 3.6).

$$q_t = f_a \cdot h_{static} \cdot \frac{J_n \cdot J_r}{J_a} \quad (3.6)$$

Where  $f_a$  in  $\frac{l}{min}$  per  $m^2$  is a parameter related to the discontinuities' water-conducting properties. According to Panthi and Nilsen (2010) this factor will vary depending on the conditions of the discontinuities with respect to the material infilling. Panthi and Basnet (2019) introduced an approximation to the  $f_a$  value, shown in Equation 3.7.

$$f_a = \frac{J_p}{D \cdot J_s} \quad (3.7)$$

The  $J_p$  is a parameter related to the persistence of the joint. According to Panthi (2010) this parameter has a maximum value of 25 m.  $J_s$  denotes the joint spacing observed in the tunnel. Figure 3.7 shows how the depth parameter ( $D$ ) is estimated. The leakage ( $q_t$ ) is the ratio be-

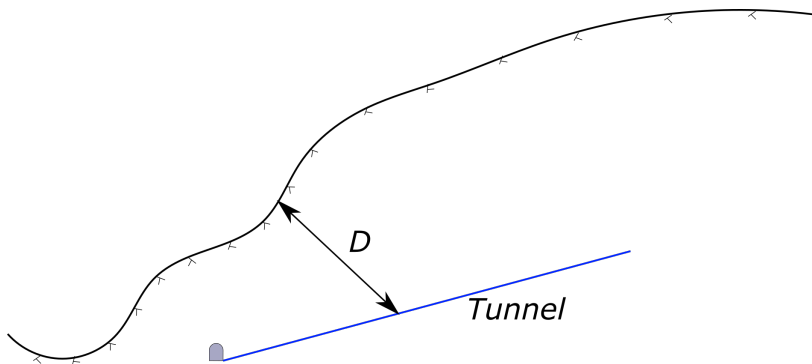


**Figure 3.7:** Illustration for how the depth parameter ( $D$ ) is calculated in Equation 3.7.

tween the flux of water and the length of the respective bore hole and has units [ $\frac{l}{min}$  per m].

The equation supports comprehensions that parameters related to discontinuities influence the potential for groundwater inflow. A higher value of  $J_a$  indicates that the joints are altered and

may have material-infillings. This can prevent water flow if the material within the joint has a low permeability. As commented in Chapter 2,  $J_n$  is a parameter related to the number of joint sets. A higher value could give increased potential for water inflow in the tunnel. Further, pressure differences are driving forces for groundwater inflow and it is reasonable that this parameter has a positive influence on the flux of groundwater.



# Rock mass grouting

This chapter discusses theories and practices in rock mass grouting. The topics will mainly be explained based on the common practice in Norway. Rafi and Stille (2014) describes the objective of rock mass grouting to "fill existing fractures with the lowest amount of grout and in the shortest time without causing any damage".

## 4.1 Use of grouting in underground construction

Rock mass grouting has been a central part of Norwegian tunnelling. A high groundwater level in the rock mass is typical for the Norwegian conditions and pose a risk of water inflows in underground constructions. A natural gradient towards the tunnel regarding water flow may in some cases be favorable for unlined underground facilities. However, intrushes of groundwater in a tunnel will reduce the groundwater table and can cause considerable challenges in a project (Hognestad et al., 2011).

## 4.2 Components and principles of rock mass grouting

Grouting of the rock mass can utilize a variety of components and can be executed differently. This section reviews the principle of pre- and post-excavation grouting and explains some common materials used in the grouting process. Figure 4.1 shows a modern grouting rig.



**Figure 4.1:** Example of a modern grouting rig (Hognestad et al., 2011).

### 4.2.1 Methodology of grouting

The decision on whether to grout or not is usually determined from water loss, or permeability measurements ahead of the tunnel face. If the groundwater inflows are above the acceptable level for the specific underground structure, rock mass grouting should be carried out (Nilsen, 2016).

After it has been decided to grout the rock mass, the grouting procedure will be executed by drilling bore holes in the rock mass. It is generally recommended that the holes in the invert of the underground structure are grouted first. This is due to that the holes located at a lower level might be challenging to grout at a later stage. Later, packers are inserted in the bore holes before the grouting commences. Based on information of the rock mass conditions, the grout material is chosen (Hognestad et al., 2011).

#### Pre-excavation grouting

Pre-grouting is carried out by drilling a curtain of bore holes in front of the tunnel face. Usually one bore hole is grouted at a time. By injecting fine material in the bore holes, a low-permeable zone around the tunnel face is achieved (Gustafson, 2009). Figure 4.2 gives an illustration of the principle of pre-grouting.

By selecting an adequate grouting pressure and particle size of the grout material, one accomplishes to penetrate a distance,  $I$ , in the discontinuities such that the distance between each bore



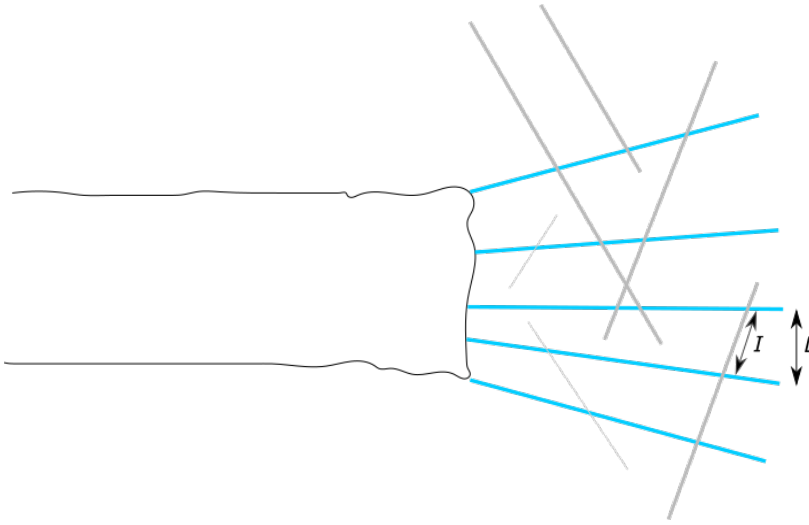


**Figure 4.2:** Illustration of the pre-grouting process. Modified after Gustafson (2009).

hole,  $L$ , is filled with grout. This can be challenging to accomplish for a number of reasons. Some of these regard the grout material being used, and this will be more discussed in Section 4.2.

### Post-excavation grouting

Post-grouting is the process of grouting a section of an underground structure, usually a tunnel, behind the face location. It is advantageous that the grout holes in post-grouting is oriented in the opposite direction of the pre-grouting holes (Hognestad et al., 2011). Figure 4.3 illustrates the principle of post-excavation grouting.

It is often more challenging to achieve a satisfactory result by post-grouting than pre-grouting. This has been experienced in a number of tunneling projects (Nilsen, 2016, Panthi, 2013). In the Romeriksporten tunnel in Norway, post-excavation grouting was used to seal the rock mass in a 2.2 km long section. The grouting works took more than one year to complete which caused increased costs, delay and negative attention to the project (Holmøy, 2008).

## 4.2.2 Grout materials

### Industry cement

The Norwegian Public Road Administration's (NPRA) process code 025 defines standard grout cement where the 95 % of the grains are greater than than  $25 \mu m$  ( $D_{95} > 25 \mu m$ ). This type of cement has many areas of use and has not been intended specifically for use in rock mass grout-

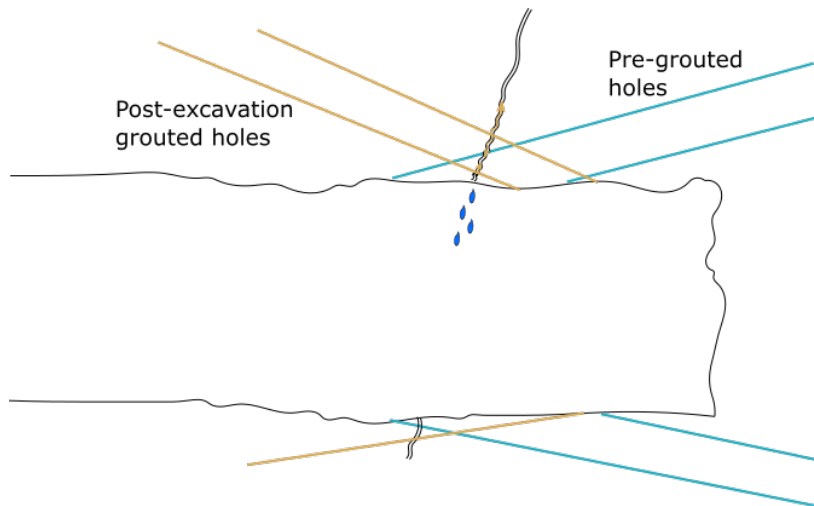


**Figure 4.3:** Principle of post-excitation grouting. Based on Gustafson (2009).

ing (Hognestad et al., 2010). The use of industry cement will usually be sufficient to achieve a satisfactory grouting result in typical Norwegian rock mass conditions. This presupposes that the applied grouting strategy is adapted to the conditions.

### **Micro cement**

Micro cements are ordinary cements where the cement particles are crushed to smaller sizes. A cement is categorized as a micro cement if  $D_{95} < 20 \mu\text{m}$ . The cement type is used particularly to grout discontinuities with smaller aperture. A specific surface area makes the cement more chemically active and can make the mixing process more challenging (Hognestad et al., 2011).

### **Water/cement ratio**

A high water/cement (w/c) ratio gives improved flow properties to the grout mix. It is important to adjust the w/c-ratio to the rock mass conditions, since an un-adapted water/cement ratio can have several negative effects:

- Reduced quality on hardened grout.
- Prolonged time for grout hardening and an increased grouting time.
- Low pressure build-up in nearby rock mass because of transport of grout further away from the contour of the underground structure. This implies a reduced grouting effect close to the tunnel.
- Unnecessary large consumption of grout.

- Increased risk of jacking the rock mass.

The discontinuities in the rock is generally water-filled. This implies that when the void spaces are filled, some water will mix and some of the water will be displaced by the grout. Grout with a lower w/c-ratio can be more diluted before a reduction in the grout quality is experienced (Klüver and Kveen, 2004).

### **Superplasticisers**

Superplasticisers or dispersants are used in most grout mixes. The additive reduces the electrical bonds causing the cement particles to lump. This results in a finer mix that has better penetrability properties. A normal amounts of dispersants in a grout mix is around 1.5 % to 2 % of the cement weight (Hognestad et al., 2011).

### **Accelerators**

An accelerator is a solution that is added to the grout mix to control the setting time of the grout. The accelerator is normally added to the grout mix through a nozzle when grout is pumped in the drill hole.

This substance may be valuable when the required pressure-buildup in a grout hole is not reached. By shortening the setting time of the grout, the accelerator is useful when there are migrating leaks in and behind the working face, and in cases of large grout consumption (Hognestad et al., 2011).

### **Water**

The water quality is important for the grout mix to behave as expected. Common practice today is that the water used in grouting is recycled water, i.e. cleaned operating water. The recycled water can give an increased setting time of the grout, especially in cases where the water contains a high concentration of salts. Recycled water can have a higher salt concentration due to the waste material from explosives (Hognestad et al., 2011).

### **4.2.3 Pressure**

The grout result in the discontinuities of the rock mass depends on the applied grout pressure. In order to achieve grout spread in fractures, the grout pressure must exceed the pressure of the groundwater. If the grout pressure is too high, fractures might dilate. This can cause an uncontrolled spread of the grout, permanent deformations of the rock mass and a reduced sealing effect (Hognestad et al., 2011, Stille, 2015).

In Norway, maximum grout pressures are normally in the range of 80 to 100 bar nearly independent of the rock overburden. Davik et al. (2002) argue that one should adjust to a lower w/c-ratio to control the pumped amount in cases of low rock cover.

### **4.3 Grouting requirements**

The water inflow criteria and the need for rock mass grouting should be adapted the given tunnel project. For a tunnel constructed in remote areas with no strict requirements on groundwater influence or a dry internal environment, the inflow criteria will be governed by the pumping capacity and practical limitations associated with the excavation process. The effect of leakage to the work safety in the tunnel should also be assessed.

For a tunnel constructed in an urban area, the maximum inflow requirement can be as low as 2-4 liters per minute per 100 meter tunnel. This strict requirement is due to the potential influence the tunneling works can have on the groundwater level. A draw-down of the groundwater table can give a range of negative consequences on the surroundings (Hognestad et al., 2011).

Substantial water inflow amounts was encountered in the Romeriksporten railway tunnel. Figure 4.4 shows a photo of a water source above the tunnel which was drained due to the inflows in the tunnel. This incident, among other projects, initiated a new research and development project where several participants from the Norwegian tunneling industry contributed. Kveen and Lindstrøm (2005) called attention to that the acceptable amount of water inflow into a tunnel in a given area can be determined from studying local factors. Factors such as the water balance in nature, hydraulic conductivity of the rock mass, potential for soil settlement, vulnerability of the vegetation and the performed grouting procedures were considered to be of significance.

Blindheim and Øvstedal (n.d.) argued that the budget, time schedule and the contract form should take into account the potential need for grouting. Hognestad et al. (2011) underlined that unless the surroundings demand particular requirements regarding water inflow, the extent of the grouting works should be based on safety and life cycle costs. To grout a tunnel so that there would be no need for water shielding after construction would be associated with significant costs.

#### **4.3.1 Road and railway tunnels**

Factors for determining the inflow criteria in a tunnel, mentioned in Section 4.3, are relevant for both road and railway tunnels. The sections below regard some typical inflow requirements that have been developed from previous projects, and what measures are taken to secure a "dry"



**Figure 4.4:** Photo by L. Erikstad of Puttjern above the Romeriksporten railway tunnel. Puttjern was a water source to the high inflows in the tunnel, and the water table consequently got drained (Kveen and Lindstrøm, 2005).

climate inside the tunnel.

### Road tunnels

Few drivers would appreciate having water dripping from the roof while driving in a road tunnel. The above-mentioned factors in Section 4.3 also apply regarding the inflow criteria for these tunnels. Consequently, allowable inflow amounts for a road tunnel constructed in an urban area is likely to have different requirements than a tunnel planned in a rural area. In handbook N500, SVV (2016) states that measures must be taken to secure road tunnels against water, and that there should be no leakage water within the tunnel's traffic space. Water that infiltrates the tunnel should be conducted around the tunnel lining and be lead in the tunnel's drainage network. Klüver and Kveen (2004) divide the inflow requirements in the following classes for T 8.5 road tunnels (8.5 m tunnel width):

**Table 4.1:** Suggestions to water inflow requirements for T 8.5 tunnels, from Klüver and Kveen (2004).

Class	Maximum allowable inflow [l/min per 100 m tunnel]
Extremely strict	1 - 3
Strict	3 - 7
Moderate	7 - 15
Small requirements	Above 15

### **Subsea tunnels**

Norway have constructed and are still constructing a number of subsea road tunnels. For road tunnels located below the sea, the supply of water that can infiltrate is practically unlimited. Regarding inflow requirements, Blindheim and Øvstedal (n.d.) argued that there was no specific requirement for the allowable inflow. However, a normal acceptable permanent inflow can be in the order of 20-30 l/min per 100 m tunnel (Blindheim and Øvstedal, n.d. Nilsen, 2016). For the Frøya subsea tunnel, grouting was initiated if the inflow in a bore hole was greater than 5 l/min or greater than 3-5 l/min in more than one bore hole (Lien et al., 2000).

### **Railway tunnels**

Similar to road tunnels, the water inflow requirements will be adapted the specific railway tunnel with respect to the conditions mentioned in Section 4.3. To prevent impacts on the environment, the inflow criteria for different projects can be similar to those presented in Table 4.1.

The technical legislation of Bane NOR states that the water-protecting installation must be able to avoid water from dripping or flowing on to the other railway technical installations (Bane NOR, 2019).

## **4.3.2 Water way tunnels**

Tunnels conveying water are commonly used in Norway. Generally, these types of tunnels are built in more remotely located areas, so that the inflow requirements are typically less strict than for road and railway tunnels. Similar to other tunnel structures, the possible environmental consequences must be considered when tunnels for water-conveying purposes are constructed (Hognestad et al., 2011).

### **Head race tunnels**

For head race tunnels, the rock may have to withstand high water pressures after the tunnel system has been filled. Water can dissipate from the tunnel through open joints and discontinuities. In light of the water pressures that the rock mass must withstand, one must consider leakage from the tunnel system and compare grouting costs with expenses related to the lost production (Davik et al., 2002). On the other hand, if the groundwater pressure exceeds the internal water pressure of the tunnel, there will be a pressure gradient towards the tunnel. This can be constructive for the production of electricity in the hydro power plant. The extent of grouting must therefore minimize the risk that water flows out of the tunnel during operation. Simultaneously, there is no need for the tunnel to have very strict water inflow requirements, unless there is a clear threat to the surrounding environment.

## **4.4 Factors influencing grout consumption**

This section reviews some factors that can influence the grout take in the rock mass. Some parameters related to the grouting process and grout material were mentioned in the foregoing sections and will therefore not be focused.

### **4.4.1 Tunnel type and size**

The size of the tunnel will have a direct influence to how much grout that may be required in cases of water inflow. When the cross-section of tunnel increases, so will the volume of the rock mass that potentially requires grouting. This should not be considered as a rule, since several other properties control the final grout take. According to Klüver and Kveen (2004) a tunnel of width 8.5 m and a w/c-ratio of 0.75 will have an expected grout take in the order of 340 kg to 1750 kg per meter tunnel.

### **4.4.2 Rock mass conditions**

#### **Rock mass classes**

Four rock mass types presented by Klüver and Kveen (2004) were mentioned in Section 3.6.1. These rock mass classes are briefly described in the following.

Rock mass type A is characterized by having open discontinuities without significant amounts of infilling material. The hydraulic conductivity is generally high and the rock mass type is considered to normally be easy to grout. The water/cement ratio should in this case be low to prevent unwanted spread of the grout. Industry cement is considered to be the most adequate cement material for this type of rock mass.

Rock mass type B has joints with some presence of infilling material (often clay). This can facilitate flow in more permeable channels in the rock mass, typical in pre-Cambrian gneisses and other metamorphic rock types. Achieving a good grout result in this type of rock mass is considered fairly easy. Since the infilling condition of the joints can vary, there is a higher need for adapting the grout strategy to the local rock mass conditions. It is recommended to start with a w/c-ratio in the order of 1.2 to 0.9 and gradually reduce this ratio until the desired pressure of around 80 to 100 bar is reached. Industry cement and micro cement are usually suitable cement types. Figure 4.5 shows an example of rock mass type B.

Rock mass type C denotes plastic rocks characterized with a high degree of joint infillings and low aperture. This rock mass is typically difficult to grout and has a low conductivity. Minor inflows can occur, often in connection with weaker zones in the rock mass. Micro-cements and

micro-silica are recommended as grout materials for this rock mass type. To maintain good flow properties, the w/c-ratio should be reduced carefully during pressure build-up.

Rock mass type D indicates different types of rock mass influenced by tectonic processes or rocks with karst which have resulted in particularly open fractures or open voids in the rock mass. In this case, there are no specific recommendations as to which grout materials that should be used. In extreme cases of water inflow, coarser cements have been used with aggregates adapted to the aperture of the void spaces.



**Figure 4.5:** *Bedrock gneiss in Ås, Norway. This rock mass is an example of class B in the categorization by Klüver and Kveen (2004).*

### **Orientation of discontinuities**

The orientation of discontinuities can affect the groutability of the rock mass and the grout consumption. When executing grouting of the rock, it is essential that the bore holes intersect the discontinuities. In cases where the bore hole is oriented in large angles to the discontinuities in the rock, the orientation can be considered favorable. If the drilled holes for grouting are about parallel to the discontinuities, one can risk that very few discontinuities are perforated and the groutability can consequently be low. The grouting is likely to have a low effect in this situation. Figure 4.6 gives an illustration of two cases. One with discontinuities in larger angles to bore holes, and another with discontinuities in sharper angles to the drill holes.



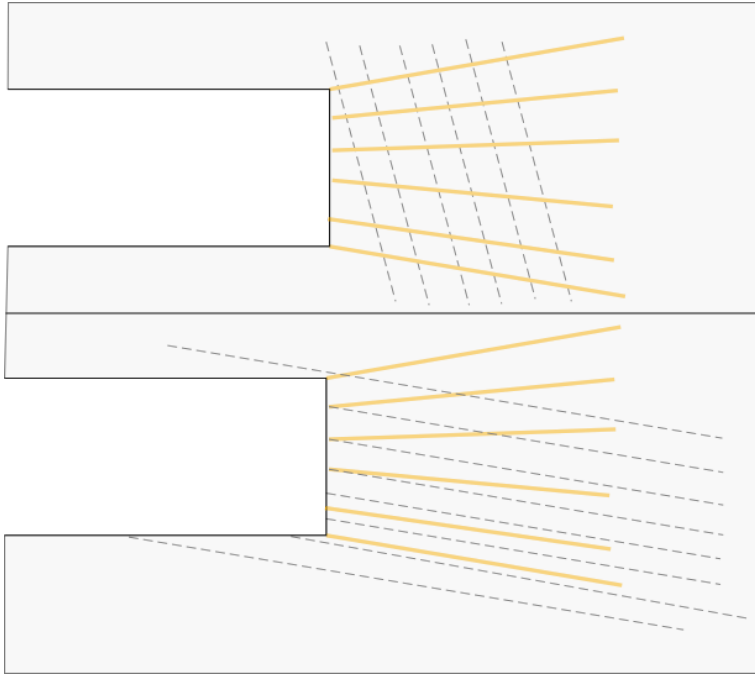


**Figure 4.6:** Illustration of the influence between orientation of similarly spaced discontinuities and groutability. One can see that more discontinuities are perforated in the uppermost situation.

### Statistical studies

Nia et al. (2016) studied the relationship between grout take and parameters such as rock mass quality (Q-value), grout pressure and joint aperture for a double-curvature dam in Iran. Multiple linear regression was used in the analysis, and a log-transformation of the response variable achieved fulfillment of the normality criterion of the residuals. From the studies, Nia et al. (2016) found that the joint aperture and applied grout pressure influenced the grout take the most, by increasing the consumption. A decrease in the Q-value gave a small decrease in the grout consumption, but had a much smaller impact on the grout take than the other parameters. Studies by Changyong et al. (2014) have however indicated that caution should be made when using log-transformation in such statistical analyses. They argue that applying such a transformation to the response variable, will in some cases not give any improvement to the model diagnostics.

Strømsvik (2019) found a significant negative correlation between grout consumption and Q-values for 91 grout rounds in different Norwegian tunneling projects.  $J_n$ ,  $RQD$ ,  $J_r$ ,  $J_w$  and  $SRF$  did not affect the grout take considerably and was omitted in the model.  $J_a$  had a significant positive correlation to the grout consumption.



# The SmiSto hydro power project

## 5.1 Introduction

The SmiSto hydro power project is a recent initiative in the Norwegian hydro power industry and consists of Smibelg and Storåvatn hydro power plants. It is the largest hydro power project to be developed in Norway since 2004. The owners of the project are Salten Kraftsamband and Helgeland Kraft each holding 50 % of the shares. Hæhre is the contractor in an EPC contract, and Multiconsult is the consulting company in the project (Brekhus, 2015).

The hydro power plants are located near the Gjervalen fjord in Lurøy and Rødøy municipality in Nordland. Each hydro power plant is located on opposite sides of the fjord; Storåvatn HPP on the northern side and Smibelg HPP on the southern side. Both projects are high-head hydro power schemes with large storage capacity without the use of large dams. In total, 27 km of tunnel will be constructed and the project is in the phase of construction completion (Multiconsult, n.d.). Table 5.1 gives some key data of the project after completion.

**Table 5.1:** Key data of the SmiSto hydro power project (Aasen and Lunde, 2017).

Parameter	Smibelg	Storåvatn 1 Turbine	Storåvatn 2 Turbine
Turbine output	33 MW	8 MW	28 MW
Dim. Discharge	7.5 m <sup>3</sup> /s	2.0 m <sup>3</sup> /s	5.0 m <sup>3</sup> /s
Head	504 m	452 m	618 m
Power generation	120 GWh	24.2 GWh	66.3 GWh
Total inflow	78.9 mill. m <sup>3</sup>	22.1 mill. m <sup>3</sup>	45.5 mill. m <sup>3</sup>
Reservoir capacity*	35.4 %	79.6 %	53.5 %

\*) degree of reservoir regulation compared with unregulated yearly flow

An overview map of the hydro power plants is shown in Figure 5.1.

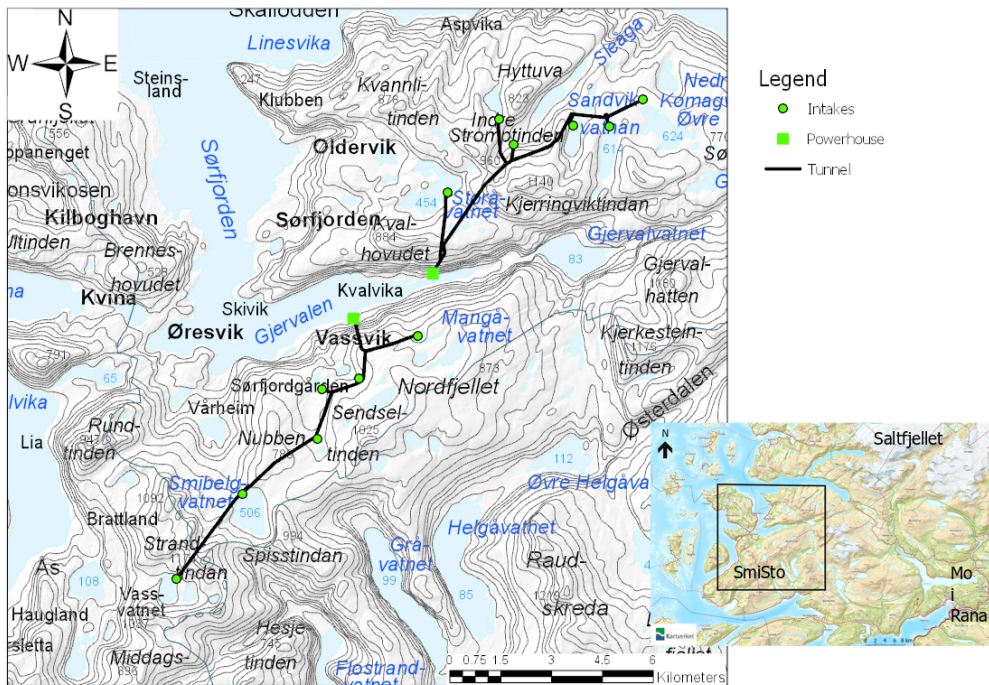


**Figure 5.1:** Overview map of Smibelg and Storåvatn hydro power plants and the tunnel systems (Haugerud, 2019).

## 5.2 Regional geology

During the formation of the Caledonian mountain chain, some 450 Ma ago, younger rocks were overthrust the eastern Baltic bedrock. The rocks that were overthrust from the west are mainly sedimentary rocks, while a major part of the Baltic bedrock consists of pre-Cambrian gneiss. The continental collision caused folding and deformations of rocks within both continental plates. The geologic layers that were overthrust the autochtone bedrock have been divided in four: lower, middle, upper and uppermost allochtone (Fossen et al., 2013). Rock types near SmiSto take part of the uppermost allochtone and the pre-Cambrian bedrock.

Figure 5.2 shows a simplified geological map with the main tectonic units in the project area. Locations of the hydro power plants are marked in red. The main tectonic units near the Gjer-

valen fjord are the Helgeland and Rödingsfjället nappe complex.

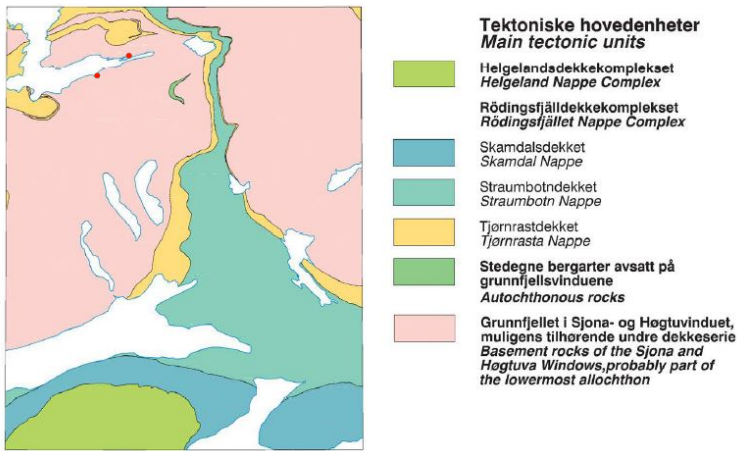


**Figure 5.2:** Main tectonic units near the Gjervalen fjord. Modified after Qvale et al. (2012).

Straumbotn and Tjörnраста nappes within Rödingsfjället nappe complex are located the closest to the project area. The rocks in the Straumbotn and Tjörnраста nappe are mainly mica schists and gneissic rocks of varying composition. The rocks are considered to be of Neoproterozoic to Cambro-Silurian age (Qvale et al., 2012). The Storåvatn tunnel system crosses these units at certain locations, while the Smibelg tunnel system is generally located in the pre-Cambrian gneiss.

The area has been subjected to a number of tectonic events with thrusting and overthrusting of the gneiss and younger, metamorphosed sedimentary rocks. This makes the geologic history in the area complex (Aasen and Lunde, 2017).

## 5.3 Geological and engineering geological conditions

Information presented in this section is mainly based on information from geological maps by NGU and preliminary studies for the SmiSto project by Lunde and Lie (2013).

### 5.3.1 Topography

The landscape in the project area is dominated by sharp ridges, steep hillsides and high mountain peaks. To a large extent, these land forms are assumed to be formed from glacial activity and erosion. A major part of the surface near the project has rock exposed on the surface. Some talus and moraine material is occasionally found above the bedrock (Lunde and Lie, 2013).

### 5.3.2 Rock types

#### *Smibelg*

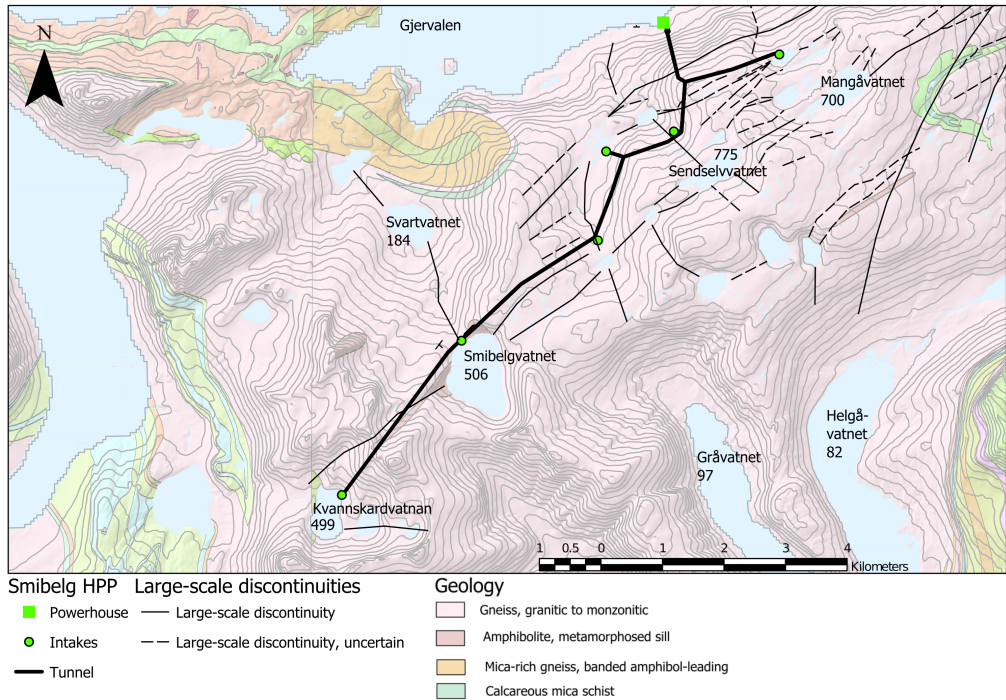


**Figure 5.3:** Geologic map of the Smibelg tunnel system, including water sources (Haugerud, 2019).

Smibelg HPP is mainly located in pre-Cambrian gneiss, granitic to monzonitic in composition (NGU, n.d.). This is a rock type known for its generally high stiffness and strength. Studies by Qvale et al. (2012) indicate that the foliation of the gneiss has a varying dip direction on the southern side of Gjervalen. The dip of the foliation is generally gentle  $\sim 30^\circ$ . Results from tunnel mapping indicates a layer of amphibolite from chainage 6+000 m to around 6+600 m in the main head race tunnel. Geologic mapping on the surface indicates sills of amphibolite near this area.

#### *Storåvatn*

There is a greater variation in rock types near the Storåvatn HPP, than near Smibelg HPP. The tectonic units and the pre-Cambrian gneiss are separated by thrust zones. According to bedrock maps from NGU, it is expected that both the main head race tunnel and Storåvatn branch tunnel

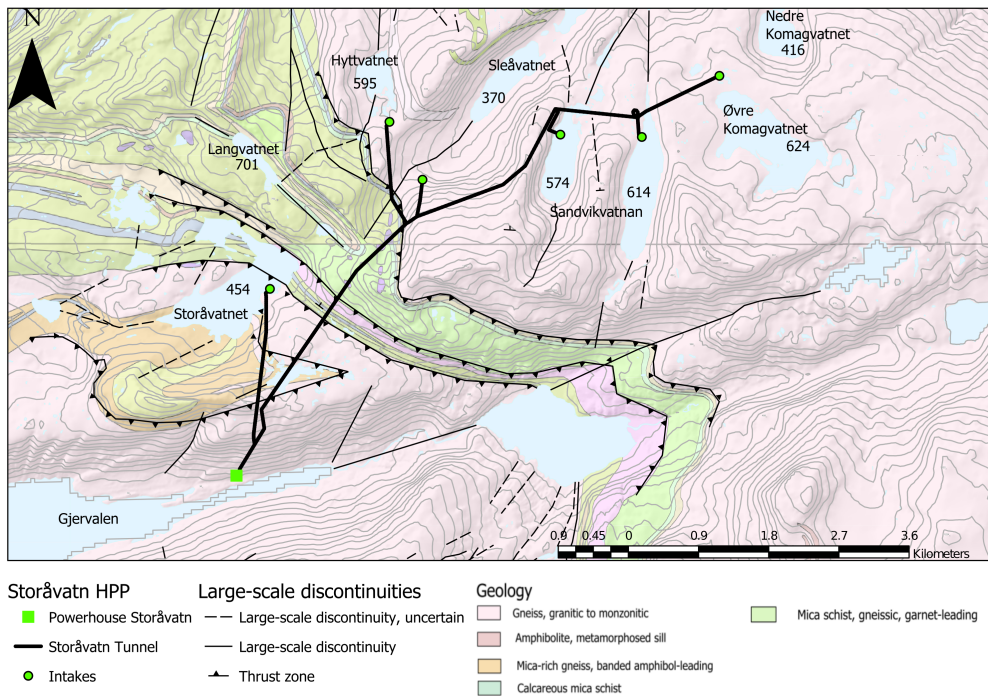


**Figure 5.4:** Geologic map of the tunnel system of Storåvatn, with water sources on the surface (Haugerud, 2019).

will pass in the pre-Cambrian gneiss near the hydro power station. The branch tunnel to Storåvatn is then expected to cross a layer of mica-rich gneiss separated from the monzonitic gneiss by a thrust boundary. For the main head race tunnel of Storåvatn, it is anticipated that the tunnel will intersect the Tjörnrastra and Straumbotn nappe complex. The rocks in these tectonic units consist of gneissic mica schist, calcite marble and tonalitic gneiss.

### 5.3.3 Weakness zones and large-scale discontinuities

As commented in Section 5.3.2, the pre-Cambrian gneiss and the metamorphosed, sedimentary rocks are separated by thrust zones. At these locations, rocks have experienced shearing and deformation. Weak rock conditions with higher degree of fracturing is expected in these areas. Moreover, the Gjervalen fjord is expected to follow a major weakness zone.

#### *Smibelg*

From aerial and topographic maps, there seem to be two orientations of major scale discontinuities on the surface near the Smibelg tunnel system. The first system of large-scale discontinu-

ities, hereafter denoted LD 1, has orientation NE-SW. This orientation follows the foliation of the gneiss in the area (Lunde and Lie, 2013). A relatively straight path in the variable topography indicates that the discontinuities are likely to have a steep dip. Another discontinuity system, hereafter referred to as LD 2, can occasionally be observed on the surface south of Gjervalen. It has orientation near perpendicular to LD 1, i.e. NW-SE, but is less pronounced on the surface. Its appearance indicates that also these discontinuities have a steep dip. Figure 5.5 shows an excerpt from a location near Sendselva illustrating LD 1 and LD 2.

### *Storåvatn*

Foliation and schistosity with orientation N-S to NW-SE and mean dip towards the north dominates in the schistose rocks and the upper cover of gneiss. These discontinuities can be observed on aerial photographs.

Aerial photographs near the Storåvatn tunnel system indicate that there is a large-scale discontinuity system with orientation NE-SW. This joint system is similar to LD 1, but has an orientation more towards N-S. Hereafter it is denoted as DS 3. The large-scale discontinuities located closer to Storåvatn HPP will be more discussed in Chapter 7.

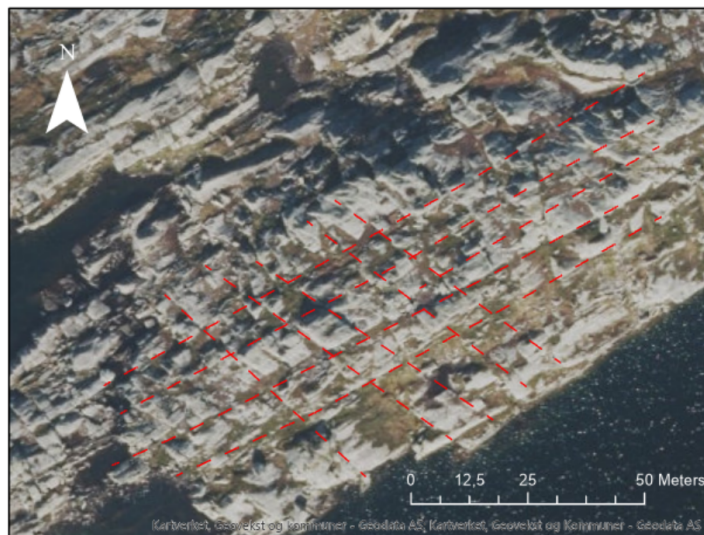


**Figure 5.5:** Aerial photograph of LD 1 and LD 2 for a location near Sendselva on the southern side of the Gjervalen fjord.



### 5.3.4 Hydrogeological conditions and water sources

There are a number of water sources located at higher elevations in the project area. The level of the groundwater table is generally uncertain. Water sources on the surface has been used to get an impression of these conditions. Based on a high precipitation in the area and relatively large water sources at high elevations, the water table is assumed to be located close to the topographical surface.

### 5.3.5 Rock stress conditions

Arne Myrvang presented a number of horizontal rock stress measurements in Norway with a geographic map, see Figure 5.6. Previous stress measurements indicate variable rock stress directions in the Cambrian-Silurian rock types south of Bodø. A general characteristic of the regional horizontal rock stress directions in Norway is that they tend to be oriented depending on the orientation of the mid-ocean-ridge (MOR). In the northern parts of Norway, the MOR is N-S oriented.

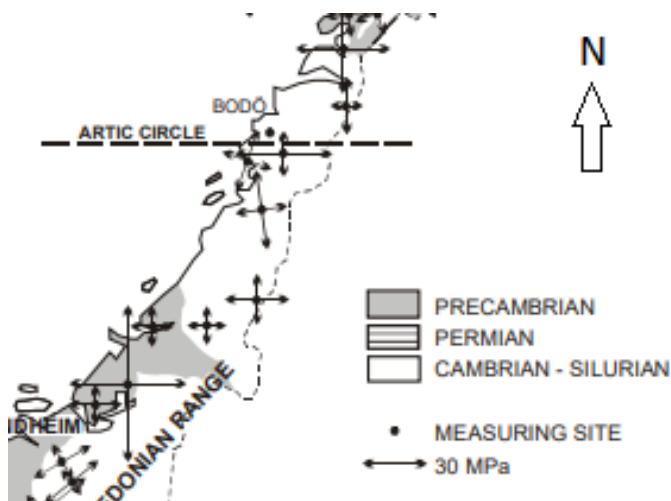


**Figure 5.6:** Indications on the regional horizontal rock stress conditions based on previous stress measurements. Modified after Myrvang (2001).

The project area is dominated by steep hillsides and high mountainous ridges. The local rock stress conditions are consequently expected to be controlled by topographic effects. Further, it is believed that the strongest earthquake north of the Alps in historical times, occurred on the Lurøy island in 1819. The earthquake was of magnitude M5.8, and was felt throughout Scandinavia. Lindholm (2019) observed that the isochrones from deglaciation have the most intense

gradient in seismically active areas. That is, in areas where the Holocene glacial retreat has been the slowest. These are areas where the last glaciers in Norway still exist after episodes of progression and regression. Further, the areas are associated with an intense earthquake activity. Conrad Lindholm argued that areas with high elevation and with partial glaciation could have been subjected to small isostatic adjustments which has kept local faults and fractures alive until today.

Geological investigations have revealed that rocks with high and low stiffness are present interchangeably. Further, the degree of fracturing of the rock mass can be seen to show considerable variation between locations on the surface. Differences in rock mass stiffness must therefore be expected, as must local variations in rock stresses. Due to local differences in the mechanical properties of the rock mass, the rock stresses can build up to unanticipated high levels in competent rock near areas of weaker rock layers. Similarly, in the weaker rocks, local reduction of the stresses can be observed.

These conditions have been evaluated in the initial phase of the hydro power project, and is an important factor to investigate for unlined hydro power tunnels with high internal water pressures. For determining suitable locations of transition between lined and unlined tunnel, stress measurements have been conducted. These will be presented and compared to rock overburden estimates below.

### 5.3.6 Stress measurements

Stress measurements by hydraulic jacking has been conducted both at Storåvatn and Smibelg HPP in order to determine suitable locations for the cones in the pressure tunnels. Hydraulic jacking consists of isolating a certain section of a bore hole and gradually pressurizing this part with water until a fracture is initiated in the surrounding rock. The shut-in pressure ( $P_s$ ) can be measured in several cycles. If the drill hole direction is in a principle stress direction, estimates on the in-situ rock stresses can be made. The shut-in pressure will then be an estimate on  $\sigma_3$ .  $\sigma_1$  and the drill hole rupture strength of the rock ( $T$ ) can also be estimated by recording the water pressure and flow (Nilsen and Palmström, 2000).

For the test results at SmiSto, the safety factor at each measure location has been calculated with the following formula:

$$FS = \frac{\bar{P}_s}{P_w} = \frac{\bar{P}_s}{\rho_w \cdot g \cdot h} \quad (5.1)$$

Where  $\bar{P}_s$  is the mean value of  $P_s$  in three cycles. The mean safety factor for different locations along the bore holes has been calculated, and is indicated in Figure 5.7 and 5.8.

The rock stress measurements are presented for both of the main head race tunnels in the following.

### *Smibelg*

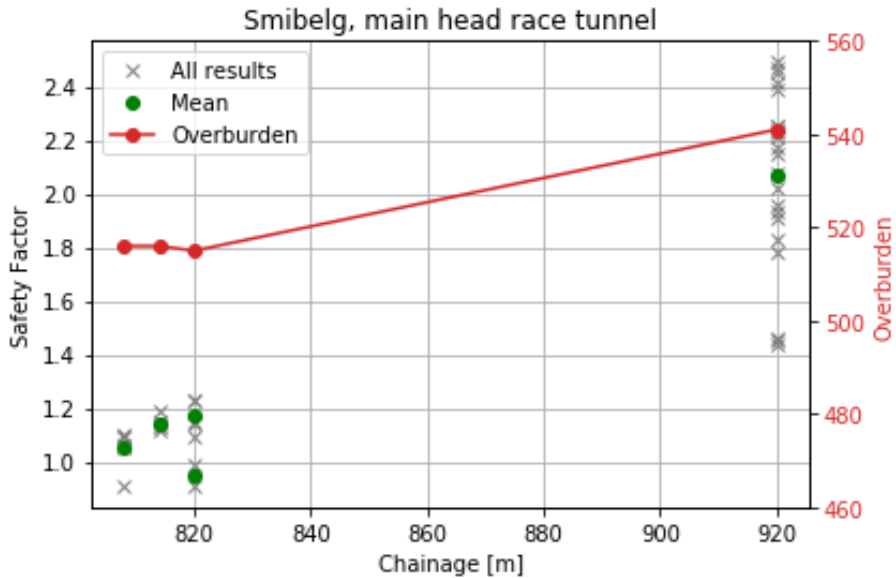


**Figure 5.7:** Results from hydraulic jacking tests with chainage numbers in the Smibelg head race tunnel. The overburden is roughly sketched.

### *Storåvatn*

As mentioned in Section 5.1, Storåvatn HPP consists of two turbines. Consequently, stress measurements for cone placement at the Storåvatn branch tunnel and the main head race tunnel have been performed. The rock stress measurements conducted in the branch tunnel to the Storåvatn lake are presented in Chapter 7. Thus, only the results from the main head race tunnel shown in Figure 5.8 are presented in this section.

Results from the measurements indicate that there is a general increase in safety factor with increasing overburden. However, there are relatively large variations at measurement locations and also between nearby measurement areas.

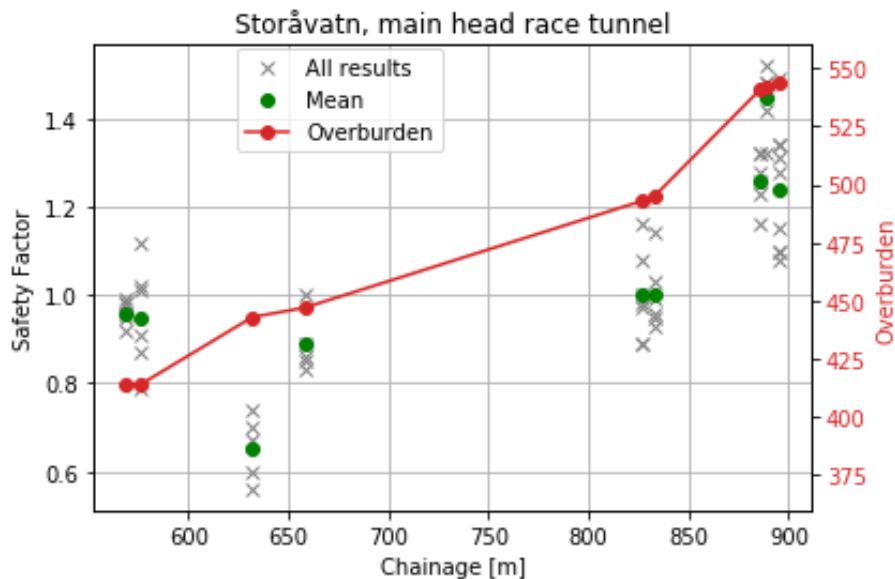


**Figure 5.8:** Safety factor from hydraulic jacking tests related to cone placement in the main head race tunnel of Storåvatn. Overburden is roughly sketched. Results from SINTEF (2016).

## 5.4 Expected conditions in the pre-liminary phase

### 5.4.1 Rock mass quality

Distribution of the expected rock mass quality in the tunnel systems are shown in Figure 5.9 and 5.10. The rock mass quality has here been divided in five categories ranging from Q1 to Q5, where Q1 indicates the best quality of rock mass. Table 5.2 explains the division of the categories.

#### *Smibelg HPP*

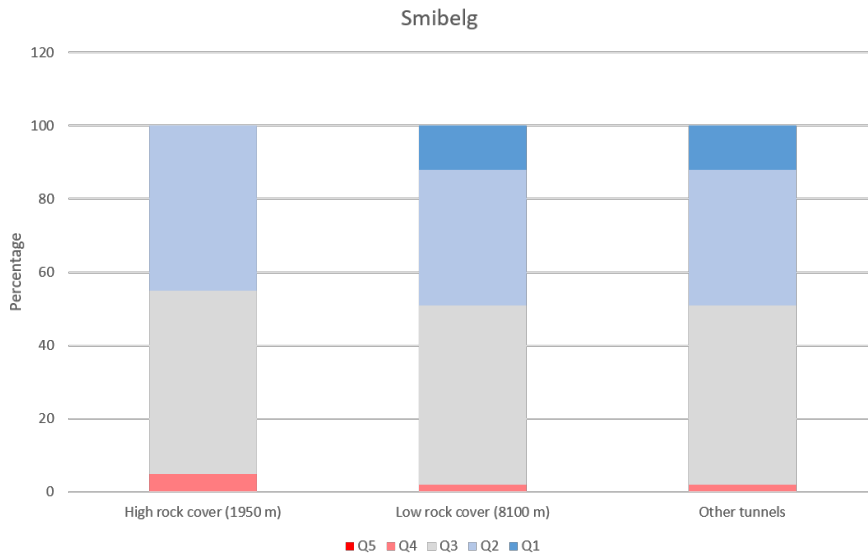
For Smibelg HPP around 95 % of the tunnel system is expected to be located in rock mass of good to fair quality (Q2 and Q3). In parts of the tunnel with high rock cover, poor rock conditions might be encountered with spalling due to increased rock stresses. Zones of weathered rock and clay-filled discontinuities can also be encountered. Sections of the tunnel system with lower rock overburden are considered to likely be associated with higher rock mass quality.

#### *Storåvatn HPP*

The expected rock mass quality for Storåvatn HPP share similarities with Smibelg HPP. Typically better conditions with respect to rock mass quality are expected in areas with lower rock

**Table 5.2:** Explanation of the rock mass classification used in the pre-liminary phase of the project (Lunde and Lie, 2013).

Category	Quality	Characteristics
Q1	Very good	Massive rock, $J_v < 5$ , rough joints without coating and no weathering.
Q2	Good	Fresh rock, $5 < J_v < 10$ , planar and rough joints, Some of these have coating and some are weathered.
Q3	Fair	$10 < J_v < 20$ , planar and thin joints with smooth coating or surface-weathered joints. Moderate intensity of stress induced spalling in class Q1 and Q2.
Q4	Poor	Partly weathered rock, $J_v > 20$ , rock mass with pronounced clay gouge zones and general presence of clay on joint surfaces. Intense spalling in class Q1 and Q2.
Q5	Very poor	Fractured, altered and clay-containing rock mass. Low resistance to deformations. Elastoplastic behavior at low stresses.

**Figure 5.9:** Anticipated rock mass quality in the Smibelg HPP.

cover. However, the percentage of poor rock conditions (Q4) expected are close to doubled compared to Smibelg. This is partly due to the thrust zone that the main head race tunnel will have to cross.

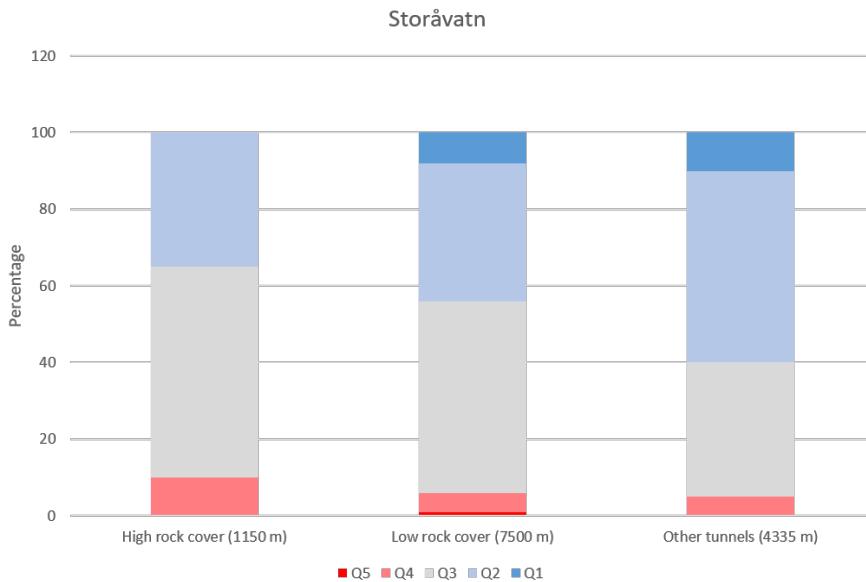


**Figure 5.10:** Anticipated rock mass quality in the Storåvatn HPP.

## 5.4.2 Groundwater inflow

### *Smibelg HPP*

In the pre-liminary phase of the project it was commented that joints crossing the foliation could be water-conducting. Foliation joints in gneissic rock are generally tight, and was not considered to be a source of higher water inflows. Connection between discontinuities and water sources on the surfaces was considered possible, but mainly local water sources within the bedrock were expected to cause the water inflows. A more jointed rock mass near the tunnel portals due to exfoliation joints was considered to increase the likelihood of water inflow in these areas (Lunde and Lie, 2013).

### *Storåvatn HPP*

In the pre-liminary phase of the project, no leakage was expected in areas of the tunnel system located in the gneissic rock. There was assumed to be an increased likelihood of water inflow in the vicinity of the thrust boundary to the schistose, sedimentary rocks around chainage 2+000 m to 2+500 m above the tunnel. From geological maps (see Qvale et al. (2012)), zones of marble/limestone had been observed in this area that can have open channels for groundwater flow. It was not excluded that water inflow could occur near the transitions between gneiss and the metamorphosed sedimentary rocks (Lunde and Lie, 2013).

### 5.4.3 Grout consumption

Rough estimates of grout consumptions for the D&B 20 m<sup>2</sup> tunnels were given to both the Smibelg and Storåvatn tunnel system. These are summarized in Table 5.3. It was commented that these estimates could deviate by  $\pm 100\%$ . Additionally, it was expected that there would be a consumption of microfine cement around 8400 kg.

**Table 5.3:** *Expected grout consumption in the SmiSto project. The total grout take is equally distributed among the two hydro power plants.*

Number of pre-grouting rounds	Number holes per round	Grout take per hole (21 m)	Total grout take	Total work hours
10	40	630 kg	252 000 kg	420

## 5.5 Conditions encountered during project construction

As of December 2019, excavation of the Smibelg tunnel system is finalized and excavation of the Storåvatn tunnel system is approaching finalization. Consequently, several of the unknowns during the pre-liminary stage of the project have now become more revealed. Considering the topic of this thesis being water inflow and rock mass grouting works in the project, the conditions with respect to these factors were not all as expected. According to Johansen (2019), the magnitude of encountered groundwater inflows and the consumption of rock mass grout in the project stands out compared to other hydro power projects constructed in Norway.

### 5.5.1 Rock mass conditions

The Q-system developed by NGI has been used for categorizing the rock mass quality during engineering geological mapping. Generally, segments of 40 m have been assigned a Q-value. In cases where the condition of the rock mass is significantly different within the 40 m interval, smaller sections are used. In addition to assigning a rock mass quality, joint structures, water inflows and other comments related to the rock mass properties have been noted. Appendix B.2 shows an example of typical mapping sheet used in the project.

Below, the distribution of rock mass quality (Q-values) along the two main head race tunnels is presented. The final Q-values are dependent on six parameters related to the condition of the rock mass and the presented plots in Figure 5.11 and 5.12 and they give limited information as to the general condition of the rock mass. However, they may be useful in the comparison to the expected conditions described in Section 5.4.

*Smibelg HPP*

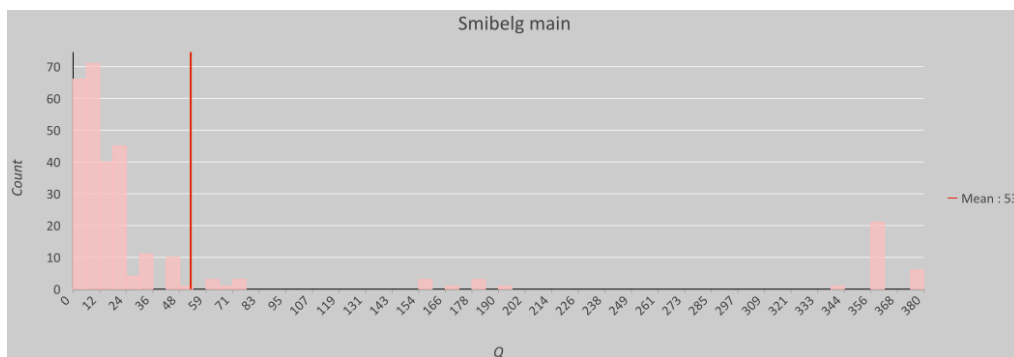


**Figure 5.11:** Histogram of rock mass quality (*Q*-value) between chainage 0+000 m and 8+300 m for the head race tunnel of Smibelg.

Table 5.4 shows the accumulated percentages for the *Q*-values compared to the respective quality term.

**Table 5.4:** Percentages of *Q*-values below certain upper limits regarding quality for the main head race tunnel of Smibelg. Based on NGI (2015).

Upper <i>Q</i> limit	Accumulated percentage	Quality of upper limit
6	22	Poor to Fair
10	40	Fair
40	78	Good
100	84	Very good

The results show that around 6 % of the total number of mapped sections are within rock mass of very good quality. Further, 60 % of the tunnel sections have a quality from good to exceptionally good. About 10 % of the sections denote rock mass of extremely good quality (*Q* > 100). In the lower range, 22 % of the rock mass has a *Q*-value below 6.

*Storåvatn HPP*

Figure 5.12 shows the distribution of rock mass quality along the Storåvatn main head race tunnel between chainage 0+000 m and 7+200 m.

The histogram shows that the majority of rock mass quality is in the range between 0 and 11. Considering rock mass quality from mapped tunnel sections, there is a tendency towards lower quality of the rock mass in the main head race tunnel of Storåvatn HPP. Similar to Table 5.4,



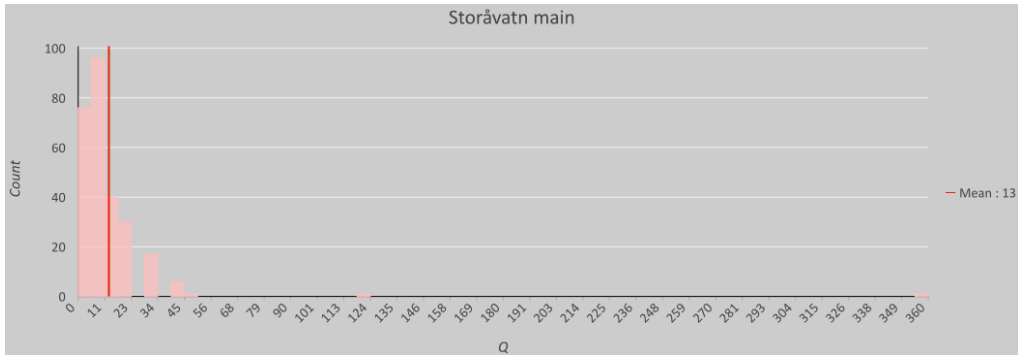


**Figure 5.12:** Histogram of rock mass quality (*Q*-value) between chainage 0+000 m and 7+200 m for the Storåvatn main head race tunnel.

Table 5.5 shows the distribution of *Q*-values for this tunnel.

**Table 5.5:** Percentages of *Q*-value below certain upper quality limits for the Storåvatn head race tunnel. Based on NGI (2015).

Upper <i>Q</i> limit	Accumulated percentage	Quality of upper limit
6	27	Poor to Fair
10	60	Fair
40	94	Good
100	96	Very good

Around 60% of the mapped sections have  $Q \leq 10$ , corresponding to quality from fair to very poor. Some 34 % of the sections have a *Q*-value between 10 and 40, indicating good rock mass quality.

### 5.5.2 Groundwater inflow

The conditions with respect to groundwater inflow will be presented in more detail for two tunnel sections in the Storåvatn tunnel system in Chapter 7. Some of the experiences with groundwater inflow conditions will therefore briefly be mentioned in the following.

#### *Smibelg HPP*

As commented in Section 5.4, the foliation joints have generally been related to only small amounts of groundwater inflow. The groundwater inflows of significance have been related to steep joints ( $>60^\circ$ ) intersecting the foliations. From chainage 3+000 m to Kvansskardvatn at around 10+000 m in the main head race tunnel, probe drilling results indicate that no considerable water inflow occurred. Up to chainage 3+000 m, certain sections gave relatively high

inflows, up to 500 l/min in one bore hole. Water inflows up to 800 l/min were encountered during drilling for the branch tunnel to Smibelgvatn. The results for Mannåga branch tunnel has not been immediately available for the author, and the conditions for this tunnel regarding inflow of water is not known. Only small inflows were encountered in the other, shorter tunnels of the tunnel system.

#### *Storåvatn HPP*

The conditions with respect to water inflow during drill and blast operations of the Storåvatn HPP must be regarded as exceptionally challenging. The maximum groundwater inflow experienced in the project occurred in the main head race tunnel near chainage 3+000 m. This was an area considered to have an increased likelihood of water inflow (see Section 5.4). At this locations, the water pressures were measured to around 30 bar. Estimations suggest inflow rates of well above 1000 l/min. The difficulties resulted in a down-time of tunnel excavation for one month in order to grout the conductive discontinuities. Between chainage 3+031 m and 3+090 m, at least 15 rounds of post-grouting were needed to seal the inflows behind the tunnel face. Segments of higher water inflows have also been met, both at lower and higher chainages.

Similar to the situation at Smibelg HPP, only small groundwater inflows seem to be caused by the foliation joints. The most water-bearing discontinuities are mainly observed to have a steep dip.

### **5.5.3 Rock mass grouting**

The bar plot in Figure 5.13 evidences the actual grout consumption in the project, based on data gathered up till August 2019. One can observe the significant surpassing of the expected grout consumption at SmiSto.

The most striking result is the consumption of industrial cement used at the Storåvatn main head race tunnel. The total cement consumption in this tunnel was some 2400 tonnes of cement alone. Compared to the rough estimate given in the pre-liminary phase, this amount is about 19 times higher than the early estimate. For the Smibelg main head race tunnel the total cement take of about 606 tonnes is around five times greater than the initial suggestions. From these numbers it is clear that there have been considerable challenges related to sealing the groundwater inflows. For Storåvatn HPP, the final amount of grout is expected to increase even further until project completion. Table 5.6 shows the results presented in Figure 5.13 in table format.

As of December 2019, the main head race tunnel of Smibelg has had break-through to Kvannskardvatn and excavation of the Smibelg tunnel system is consequently complete. From the gathered

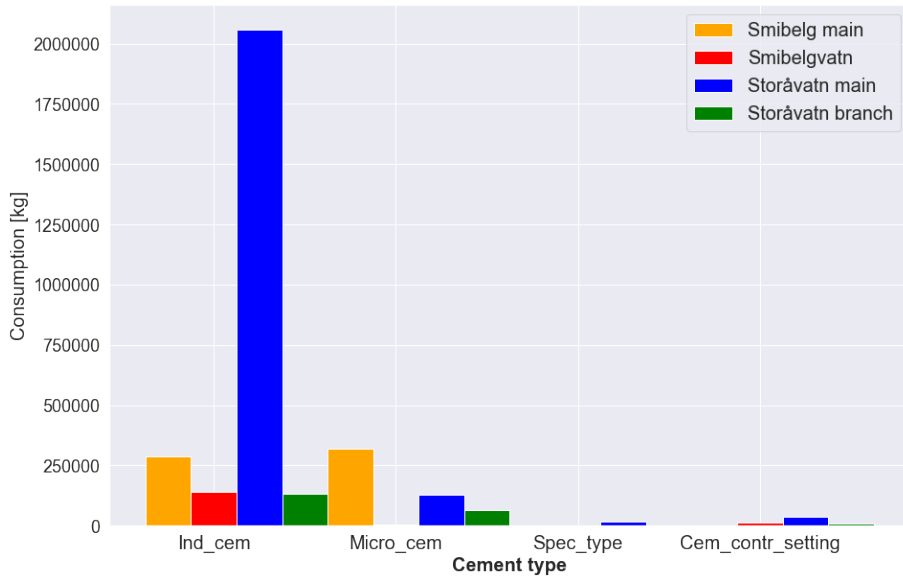


**Figure 5.13:** Distribution of the consumption for the different cement types used during construction of the SmiSto hydro power project. For explanation of the cement types, see Appendix E.1.

**Table 5.6:** Detailed overview of the results from Figure 5.13. The cement consumptions are in tonnes.

Tunnel	Ind_cem	Micro_cem	Spec_type	Cem_contr_setting	Total
<i>Smibelg main</i>	288	318	0.35	0.02	606
<i>Smibelgvatn</i>	141	7	0.05	12	160
<i>Storåvatn main</i>	2060	127	15	36	2238
<i>Storåvatn branch</i>	133	66	1	9.6	210
<b>Total</b>	2622	518	16	58	<b>3214</b>

data, no grouting has been performed from chainage 2+700 m up to the break-through around chainage 10+000 m.

For the Storåvatn HPP, grouting has still been continuously applied for chainage 6+900 m to 7+400 m. From chainage 7+400 m up to the face location at 7+560 m by 09 December 2019, no grouting has been required (Johansen, 2019).

## 5.6 Methodology of grouting and water inflow measurement

This Section reviews the strategies for grouting, as well as methodologies of measuring ground-water inflow in bore holes in the SmiSto project. The information presented is based on oral communication with Ernst Ove Johansen in Hæhre (Johansen, 2019).

### **Grouting strategy**

The criteria for when there is a necessity for pre-grouting ahead of the tunnel face has been dependent on the inflow rate in bore holes, location of the tunnel face, pumping capacity and how much water the roadway can manage without suffering damage. Generally, two to four probe holes are drilled ahead of the tunnel face, in areas where groundwater inflows are expected. In cases where the maximum inflow rate in a single holes is below around 30-50 l/min, pre-grouting is normally not considered to be necessary.

In cases where grouting is found necessary, six to eight new bore holes are drilled for the grout curtain. For these holes, the drill rate ( $\frac{m}{min}$ ), amount of water inflow ( $\frac{l}{min}$ ), color of the bored material and weaker zones in the rock have been recorded.

In the early stages of tunnel construction, micro-cement was the principal cement type used in the project (see Figure 5.13). However, the use of fine-grained cement failed to give a satisfactory grouting result. With time, industry cement has been the main cement type used. Based on the collected data, around 16.5 tonnes of coarse grained cement (Spec\_type) has been used for the entire project. This cement material has maximum grains of around 4 mm and has been used to seal larger inflows at the tunnel face. In certain cases it has been necessary to perform post-grouting. In these situations grouting by controlled setting have been performed, often with an unsatisfying result due to the low temperature of the groundwater. It was found that reducing the water/cement-ratio was the most efficient method to achieve an acceptable post-grouting result.

The applied pressure for the grouting works in the project is determined by the water pressure experienced in bore holes and the overburden of rock above the tunnel. The mean pressure used in the project has been around 50 bar. The minimum and maximum pressure applied have been 10 bar and 85 bar respectively. The stop criterion has been controlled by the reached counter-pressure of grouting. The grouting process in holes are consequently stopped when the desired pressure is reached. There have been attempts to set the stop criteria based on the grout take. In the lower parts of the Storåvatn tunnel system, this did not give a satisfactory grouting result. In chainages above 7+000 m, however, the application of a stop criteria based on grout consumption has worked with satisfying results.

### **Water inflow measurement**

The water inflows in probe drilling holes ahead of tunnel phase have been measured by using a stop watch and a bucket. With time, the tunnel workers have set approximate values of the water inflow based on experience with comparable inflow rates.

# Methodology

This chapter presents the methodologies that has been used for gathering, systematizing and preparing the available data for analysis in Chapter 8. An explanation of how the methods used in the analysis have been applied will also follow.

## 6.1 Data gathering

Data from engineering geological mapping, probe drilling ahead of the tunnel face and documentation of rock mass grouting has been given to the author by engineers in Multiconsult. Work and documentation of probe drilling rounds and grouting rounds have been performed by the contractor in the project, Hæhre. Engineering geological mapping has routinely been executed by engineering geologists in Multiconsult.

The author visited the project site in May and August 2019. At both occasions, more documentation and information from the contractors and consultants were collected. The documentation has been available to the author in PDF-format. Appendix B.1, B.2 and B.3 shows typical PDF-documents of probe drilling, engineering geological mapping and rock mass grouting in the tunnels respectively.

## 6.2 Data systematization

The data has mainly been systematized using Excel spreadsheets. Parameter names in the spreadsheets have been standardized to enable efficient processing of the data with Python 3.7 open-source software. The spreadsheets have later been imported in ArcGIS Pro to include the data in a geographic information system (GIS).

### 6.2.1 Probe drilling results

Information that typically has been recorded in probe drilling rounds are location of the tunnel face, length of the drill hole, penetration rate, color of the bored material, particular weak zones in the rock mass and groundwater occurrences. In many cases, occurrences of groundwater inflow has been commented, but no quantitative estimates are given. Thus, the actual amounts of groundwater inflow that occurred is often not known.

Quantitative measures are without doubt more valuable than qualitative comments in cases of groundwater inflow. The qualitative comments are however still valuable in that they give indications to how much water inflow that was experienced. In the project report that was written prior to this master thesis, the author concluded that it was preferential to divide the inflow estimates, both qualitative and quantitative, in categories (Haugerud, 2019). An effort has been put to relate quantitative estimates with the comments from probe drilling results. The division shown in Figure 6.1 below shows typical inflow magnitudes for the respective comments in cases where both estimates have been available. This division has also been used in the ArcGIS Pro model (see Appendix C). Using both quantitative and qualitative estimates involves much uncertainty, but has been necessary to provide an overview of the conditions.

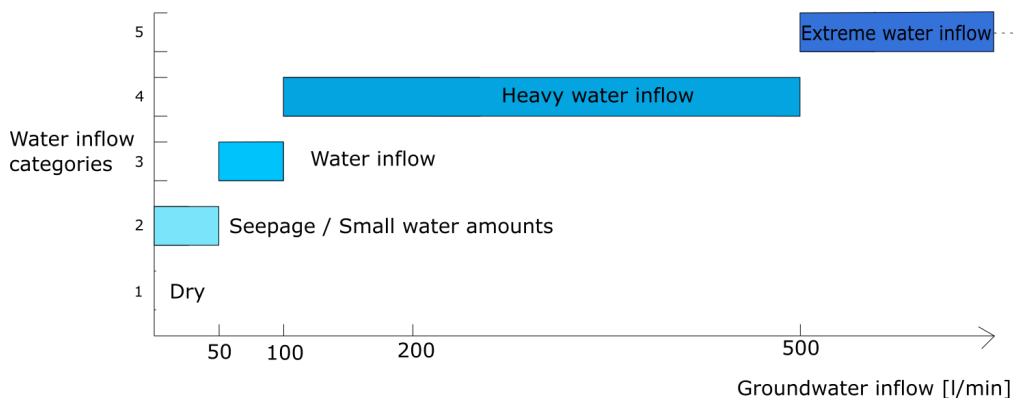


**Figure 6.1:** Water inflow categories based on quantitative estimates and qualitative comments.

Another challenge was to make the probe drilling results comparable to the rock mass conditions at the drill hole location, relevant for the work in Chapter 8. The probe drill holes will often cross chainage intervals with different rock mass quality (Q-values). The rock mass quality between two adjacent chainage intervals can be very different, e.g. near weakness zones. A natural question that arises is what Q-value that should be used along the bore hole length. Figure 6.2 illustrates this problem.

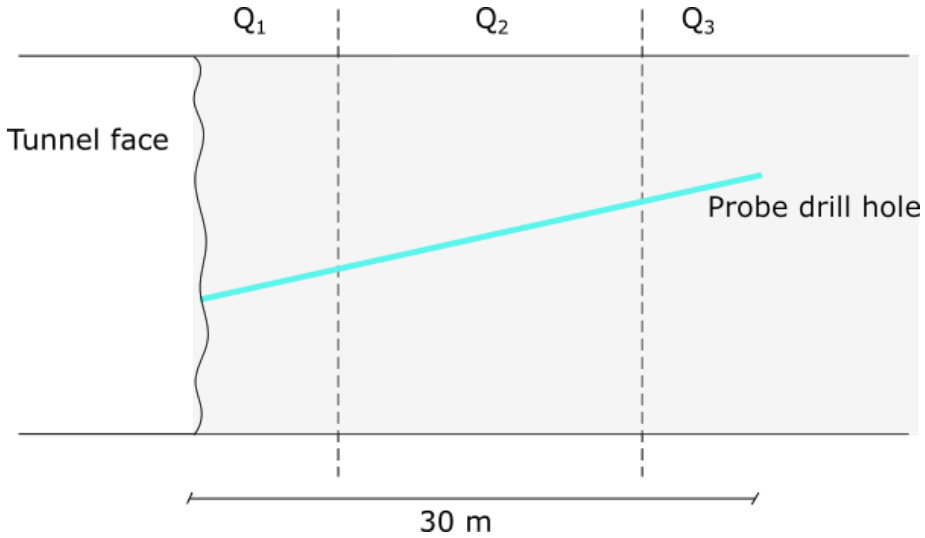


**Figure 6.2:** A probe drill hole crossing multiple chainage intervals ( $Q_1 \neq Q_2 \neq Q_3$ ). Illustrating the problem of selecting Q-values for the probe drill hole results.

Holmøy (2008) encountered a similar problem in her doctoral thesis work. This was solved by selecting the minimum Q-value of the chainage intervals that the probe drill hole crossed.

$$Q_{elements} = \min \{Q_i\}_{i=1}^n, \quad \text{for } i = 1, 2, 3, \dots, n \text{ elements} \quad (6.1)$$

The author chose this approach in his project work, and continues to use this methodology for the data analysis presented in Chapter 8.

## 6.2.2 Rock mass grouting

The results from pre-grouting are separated from post-grouting. The reason for this is that rock grouting is analyzed with respect to water inflow amounts from probe drilling results. At the same tunnel face location, probe drill holes and rock grouting holes often coincide. Post-grouting results have been gathered, but function more as an indicator for locations where it was particularly difficult to seal the water inflows.

The pre-grouting results from the contractor in the project give information on the number of bore holes ( $n_h$ ) drilled for grouting and the total bore meter length ( $l_{bm}$ ). The length of each bore hole is therefore not known, but the bore holes in a pre-grouting curtain tend to have similar

lengths. The length of the pre-grouting curtain ( $l_c$ ) is consequently estimated as:

$$l_c = \frac{l_{bm}}{n_h} \quad (6.2)$$

Similar to water inflow categories in probe drilling, the amount of rock mass grouting used in a pre-grouting round has also been categorized. These categories have been divided dependent on the total cement consumption ( $C_{tot}$ ) in a pre-grouting round. Equation 6.3 is used for calculation of  $C_{tot}$ .

$$C_{tot} = \sum_{j=a}^d C_j \quad (6.3)$$

$C$  indicates the cement amount and the letters  $a$  to  $d$  indicate different cement types. Industry cement, micro cement, special type cement (e.g. with coarser grains or saw dust) and cement with accelerating additive have often been used interchangeably.

Figure 6.3 shows the division of rock mass grout consumption in categories from 1 to 5.

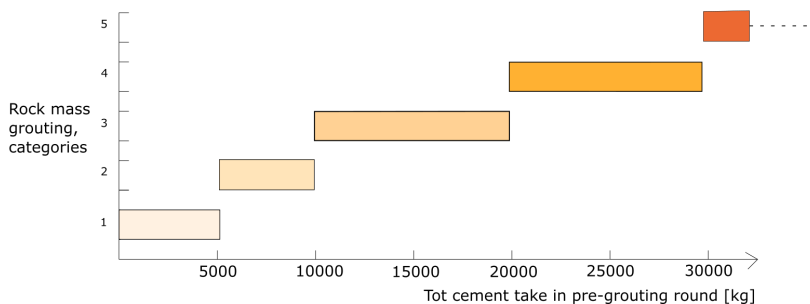


**Figure 6.3:** Division of pre-grouting rounds in categories based on total grout consumption.

This division has also been used for the model in ArcGIS Pro (see Appendix C).

### 6.2.3 Tunnel mapping

Results from rock mass quality estimation for tunnel chainage intervals have also been systematized in Excel spreadsheets. In addition to state a Q-value of the rock mass, the tunnel mapping schemes include valuable information regarding orientation of joints and discontinuities. Conditions of the structures and comments on the joint conditions are also given (see Appendix B.2). Joint mapping from the investigations have been used to produce stereonet for tunnel sections in Chapter 8. The orientations of the discontinuities have occasionally been estimated based on








strike and dip symbols in tunnel mapping and the known orientation of the tunnel at the respective location.

Generally, the rock mass has been assigned one specific Q-value for a section ranging from typically 10 to 40 m. In some cases, however, an interval for the Q-value has been given. In these situations, the author has used to lowest Q-value when comparing the results with grouting and water inflow in bore holes.

The Q-values of the rock mass in mapped tunnel sections have been categorized and assigned colors along the tunnel alignments. The categories are based on the Q-system and are shown in Table 6.1 below.

**Table 6.1:** *Division of rock mass quality categories. The division is based on NGI (2015).*

Quality	Upper Q-value limit	Color of line
Extremely good	400	
Very good	100	
Good	40	
Fair	10	
Poor	4	

Strike and dip measurements from tunnel mapping has been gathered and presented in stereonet for sections of the Storåvatn tunnel system that is analyzed in Chapter 7. In some cases both strike / dip direction and dip have been indicated in the tunnel mapping. Generally, only a strike and dip symbol with an estimate of the dip has been reported. In these cases, quantitative values of strike and dip have been estimated based on the orientation of the tunnel for the respective location. Some of the work related to processing of the strike and dip data is attached in Appendix E.4.

## 6.3 ArcGIS Pro

As previously stated, ESRI's ArcGIS Pro has been used to make a geographic model of the results from probe drilling, grouting and tunnel mapping. Additionally, geologic features such as fault zones have been included and ortophotos have been used to reveal discontinuities on the surface.

To be able to present the information geographically in ArcGIS Pro, the data has first been gathered and systematized with Excel spreadsheets. Then, data processing with Python 3.7 has prepared the spreadsheets for implementation in ArcGIS Pro and for the statistical analysis. Ap-

pendix E gives a list of relevant scripts that have been used to accomplish this. Categories of water inflow amounts and cement take have been illustrated with categories in the model with the methodology presented in Section 6.2. The categorical lines follow the tunnel alignments and their lengths on the map have been adapted to the actual length described in documentations by the contractor. For pre-grouting rounds, the length of the respective lines are the same as the length of the pre-grouting curtains ( $l_c$ ).

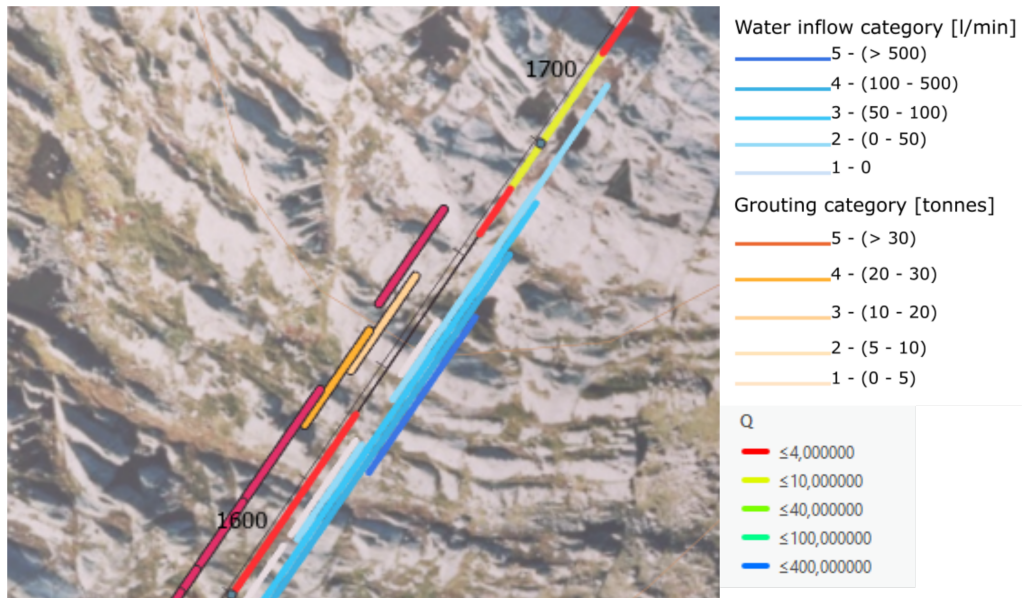


**Figure 6.4:** Ortophoto illustrating the rock mass quality, groundwater inflow and rock mass grouting categories. The photo shows the conditions between chainage 1+600 m to around 1+700 m of the Storåvatn main head race tunnel. See chainage numbers for image scale.

## 6.4 Statistical analysis

This section describes the methodology used in the statistical analysis of the data gathered in this thesis. One part of the analysis regards paired plots of rock mass parameters and the groundwater inflow in probe drilling holes. Another part is related to the application of the approach proposed by Panthi (2006) for estimation of specific leakage in probe drilling holes. The last part of the analysis regards results of the grout takes in the project, where a multivariate linear regression (MLR) model is used.

### 6.4.1 Semi-analytical approach for estimating specific leakage

The approach introduced by Panthi (2006) is used in Chapter 8 for calculation of the specific leakage. The methodology used in this part of the analysis is summarized in the following:

- Estimation of  $f_a$  for each probe drill hole.
  - The depth factor ( $D$ ) was estimated for every 200 m along the head race tunnel with longitudinal profiles along the Storåvatn main head race tunnel (see Appendix D.2). The depth factor at each probe drill hole was chosen depending on the  $D$ -value located the closest to the bore hole location.
  - The values of  $J_s$  and  $J_p$  were determined based on the joint conditions in the Storåvatn main head race tunnel.
  - Equation 3.7 was then used to estimate  $f_a$ .
- Estimation of the specific leakage  $q_t$  by Equation 3.6. Procedure for the estimations are shown in Appendix E.7.
- Comparison of the average of the actual inflow rates at the respective tunnel face location with the average of the estimations for the same tunnel face location with Equation 3.6. The Python script used in the calculations for this analysis is shown in Appendix E.7.

### 6.4.2 Multiple linear regression (MLR) model

Multivariate linear regression is a statistical technique where explanatory variables are used to predict the outcome of a response variable (Ross, 2004). In Chapter 8, the method has been applied between the grout take in pre-grouting rounds and seven parameters of the rock mass. The aim of this analysis is to investigate possible relationships between the response variable and the covariates. Further, with a MLR model, it is tested if a linear combination of the covariates can give adequate estimates to the grout takes. Similar to the analysis of groundwater inflow, the minimum Q-value have been chosen in cases where the bore holes cross more than one interval that has been assigned a Q-value (see Figure 6.2).

The analyzed data is gathered from four head race tunnels, included in both the Smibelg and Storåvatn tunnel system. The analysis is limited to the total grout takes in pre-grouting rounds ahead of the tunnel face (see Equation 6.3). It is considered that  $C_{tot}$  will depend on the total length of bore holes drilled ahead of the tunnel face for the pre-grouting curtain. Longer drill holes will penetrate a greater volume of the rock mass and potentially perforate more discontinuities. Consequently, with more bored meters ahead of the tunnel face ( $l_{bm}$ ), a greater grout take is expected for principally similar rock mass conditions. To account for this dependence,

the response variable for grout take is defined as the ratio between the total cement consumption and the sum of bored meters for the pre-grouting curtain. This parameter is named  $\bar{C}_{tot}$ .

$$\bar{C}_{tot} = \frac{C_{tot}}{l_{bm}} \quad (6.4)$$

Python 3.7 has been utilized to develop the multivariate linear regression model for the response variables and the covariates. The Statsmodels module in the open-source software has been used for this purpose (see Perktold et al. (2009)). The different parameters and the MLR model will be further described in Chapter 8.

### Theory

In order to use a MLR model to predict future responses of an outcome variable given a number of input variables, several assumptions should be fulfilled;

- The outcome variable can be expressed in terms of a linear relationship between the explanatory variables.
- The mean of the errors,  $E[e]$ , is equal to zero.
- The error variances,  $Var(\underline{Y}) = Var(\underline{e}) = \sigma^2$ , are constant (i.e. homoscedasticity is fulfilled).
- The errors are uncorrelated and normally distributed.

(Epifani, 2016)

When the validity of the multiple linear regression model is justified, the input variables  $x_i$ , where  $i = 1, 2, \dots, k$  are related to the output variable by:

$$Y = \beta_0 + \beta_1 x_1 + \beta_2 x_2 + \dots + \beta_k x_k + e \quad (6.5)$$

Where  $e$  is the random error and is assumed to be normally distributed with mean 0 and (constant) variance  $\sigma^2$ . The parameters  $\beta_0, \dots, \beta_k$  are unknown and must be estimated from the data. Thus, the estimators  $B_0, \dots, B_k$  are introduced and the least squares estimators are those that minimize:

$$\sum_{i=1}^n (Y_i - B_0 - B_1 x_{i1} - B_2 x_{i2} - \dots - B_k x_{ik})^2 \quad (6.6)$$

From Equation 6.6 it is seen that one can have a set of  $i = 1, 2, \dots, n$  data. Matrix notation becomes advantageous:

$$\underline{Y} = \begin{bmatrix} Y_1 \\ Y_2 \\ \vdots \\ Y_n \end{bmatrix} \quad \underline{X} = \begin{bmatrix} 1 & x_{11} & x_{12} & \cdot & x_{1k} \\ 1 & x_{21} & x_{22} & \cdot & x_{2k} \\ \vdots & \cdot & \cdot & \ddots & \vdots \\ 1 & x_{n1} & x_{n2} & \cdot & x_{nk} \end{bmatrix}$$

$$\underline{\beta} = \begin{bmatrix} \beta_0 \\ \beta_1 \\ \vdots \\ \beta_k \end{bmatrix} \quad \underline{B} = \begin{bmatrix} B_0 \\ B_1 \\ \vdots \\ B_k \end{bmatrix} \quad \underline{e} = \begin{bmatrix} e_1 \\ e_2 \\ \vdots \\ e_n \end{bmatrix}$$

The multiple regression model (see Equation 6.5) for n data points can then be written as:

$$\underline{Y} = \underline{X} \underline{\beta} + \underline{e}$$

The least square estimators in Equation 6.6 are partial derivated with respect to the estimators of  $\beta$ , i.e.  $B_0, B_1, \dots, B_k$ , and set equal to zero to determine the best fit for the data. In matrix form, the least squares estimators can be found by the equation:

$$\underline{B} = (\underline{X}^T \underline{X})^{-1} \underline{X}^T \underline{Y} \quad (6.7)$$

Where  $\underline{X}^T$  is the transpose matrix of  $\underline{X}$  (Ross, 2004).

### Diagnosics of the MLR model

The assumptions mentioned introductorily should be checked for the MLR model. Several tools developed for model diagnostics are available and in use today. Some of the conditions that should be checked are explained below.

#### *Normality of the residuals*

A MLR model assumes that the residuals follow a normal distribution, have mean equal to zero and a constant, but unknown variance. This condition can be checked with the Shapiro-Wilk

test for normality. A significance level of  $\alpha = 0.05$  is common. In cases where the p-value of the test is lower than  $\alpha$ , there is a statistical discrepancy, and the assumption of normality for the residuals are likely not valid (D'Agostino and Stephens, 1986). Olive (2010) argues that plots of the residuals and response plots between the fitted and the actual values are valuable for checking the adequacy of a MLR model.

#### *Collinearity - Variation Inflation Factor (VIF)*

A high degree of collinearity indicates a strong linear relationship between two covariates. The term multicollinearity is used when there is a strong linear relationship between more than three covariates (Nia et al., 2016). The variance Inflation Factor (VIF) can be used to check for multicollinearity in a data set. This is valuable to check the validity of the assumption that the predictor variables are independent of one another. However, this technique does not give indication as to which of the other predictor variables are causing the high VIF of the other covariate. Craney and Surlles (2002) mentions that a VIF above 5 or 10 can be a reasonable limit for when a predictor variable should be removed from the data set.

#### *P-value of covariates and backwards elimination*

The Statsmodels module give p-values for each covariate used in the MLR model. A higher p-value gives an indication that the covariate does not have a high influence on the outcome of the response variable.

Backwards elimination is a form of stepwise regression where the covariate with the highest p-value (often above a certain significance level,  $\alpha$ ) is removed from the model and a new model is made without this covariate. This process continues until all covariates with a p-value greater than  $\alpha$  are removed (Olive, 2010).

#### *Coefficient of determination ( $R^2$ )*

The coefficient of determination is a parameter that indicates how well the input variables in the linear model explains the variation of the response data.  $R^2$  is in the range of 0 to 1 where a value closer to 1 denotes a good fit to a linear model. The parameter is defined as:

$$R^2 = 1 - \frac{\sum e_i^2}{\sum (Y_i - \bar{Y})^2} \quad (6.8)$$

Where  $e_i$  is the difference between the observed and fitted value of the response variable.  $\bar{Y}$  is the mean of the response variable (Ross, 2004).

# Analysis of tunnel segments

## 7.1 Introduction

In this analysis, two segments of the Storåvatn HPP tunnel system are considered. In both areas, higher water inflows and grout consumption were experienced. For each segment, geologic parameters that are known to control groundwater inflow and grout take are described for the respective locations. One segment regards an area of the branch tunnel to Storåvatn, and the other a section of the main head race of Storåvatn HPP. The segments are shown in Table 7.1 below.

A brief discussion will follow after engineering geological factors assumed to influence the water inflow and grout take in each segment have been presented. In Chapter 9 the two tunnel segments are discussed together.

**Table 7.1:** *Overview of the analysis areas.*

Segment name	Tunnel	Chainage interval		Inclination [%]
		From	To	
Segment A	Storåvatn branch tunnel	0+000 m	0+800 m	17.5
Segment B	Storåvatn main tunnel	1+200 m	1+650 m	10.0

Figure 7.1 shows a map overview of the analyzed segments.

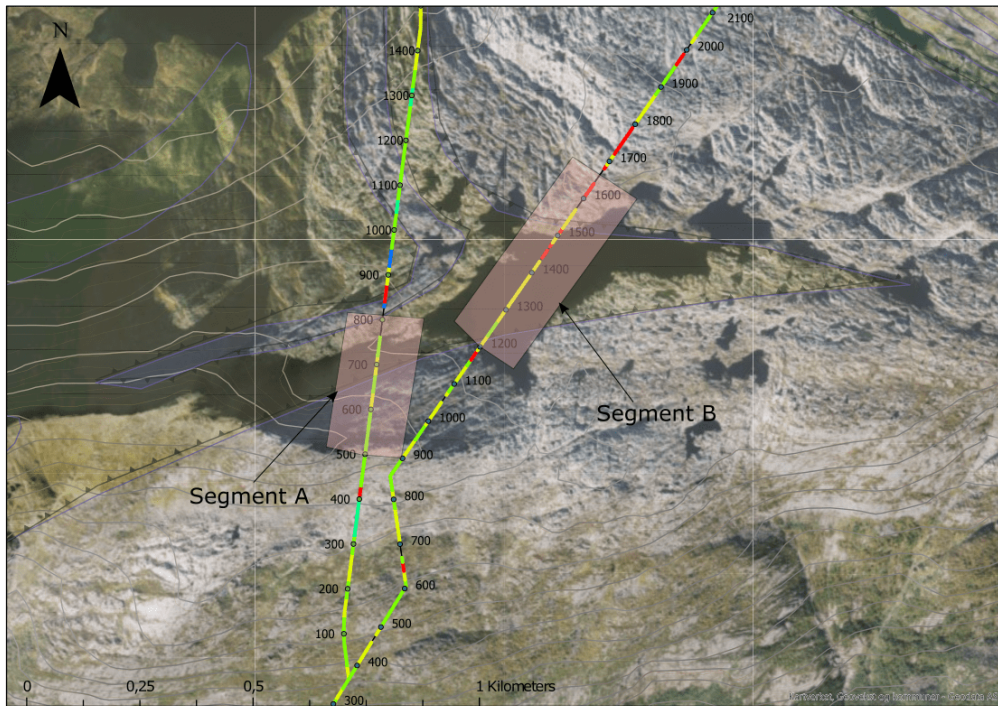


**Figure 7.1:** The analysis areas shown in an orthophoto with elevation lines. The contour interval is 50 m on the map.

## 7.2 Tunnel segment A

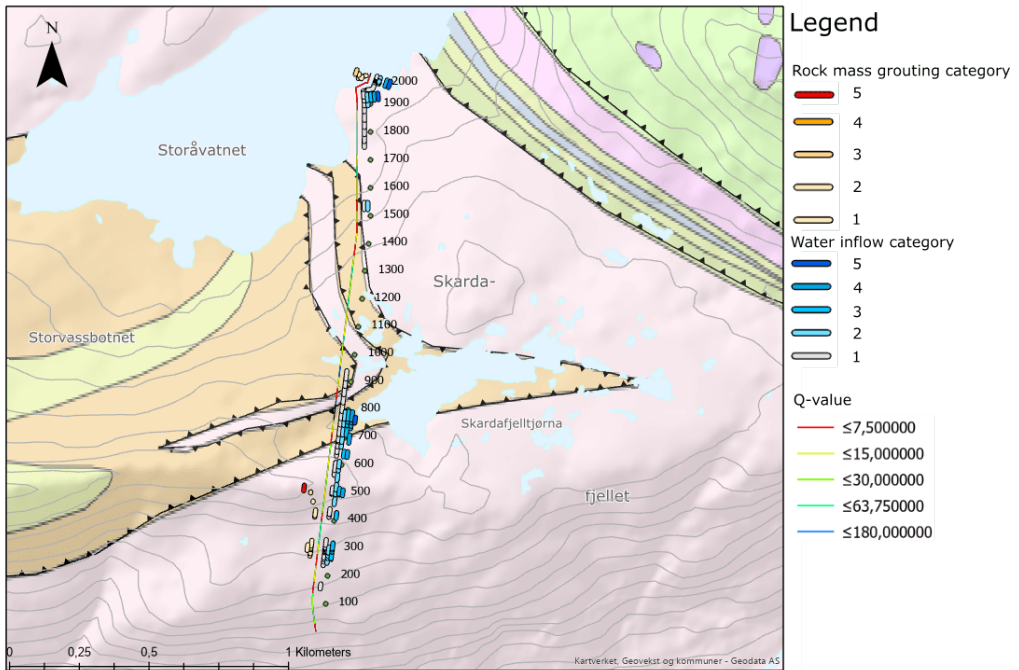
### 7.2.1 Introduction

Figure 7.2 shows a topographic map of the Storåvatn branch tunnel with water inflow categories and grouting categories along the tunnel. The categoric lines show the actual length of the probe drill holes and the average length of bore holes for grouting at the tunnel face location.

For a more detailed overview of the distribution of water inflow categories and water inflow categories along the branch tunnel, the reader is referred to Figure 8.3b.

Figure 7.2 suggests that the most substantial groundwater inflows occurred between chainage 0+500 m and 0+800 m. Higher water leakage was also encountered towards the Storåvatn lake (chainage 1+800 m to 2+030 m). Here, relatively large amounts of rock grouting was used. However, much of the grouting works in this area was performed as a routine towards lake piercing of Storåvatn and was specified at an early stage. The grouting works performed in the





**Figure 7.2:** Topographic map of the Storåvatn branch tunnel with water inflow and grouting categories. Contour interval = 50 m.

vicinity of the the Storåvatn lake will therefore not be given much attention here. It is noticeable that no significant water inflow was encountered between chainage 0+800 m and 1+800 m. The focus area in the part of Storåvatn branch tunnel is consequently for the section between 0+000 m and 0+800 m. The maximum water inflow was measured in the order of 500 l/min near chainage 0+750 m and the maximum grout take in a pre-grouting round was around 43 000 kg where the tunnel face location was around 0+500 m.

## 7.2.2 Conditions on the surface

### Rock types

From the geological map in Figure 5.4, the tunnel segment is expected to mainly be located in the pre-Cambrian gneiss. The boundary to the mica-rich gneiss is located within the tunnel interval on the surface. Considering a general gentle dip of this layer to the north east, the rock type is not expected to be present in the tunnel segment.

## Large-scale discontinuities

The aerial photograph in Figure 7.3 suggest that for chainages up to around 0+700 m, one set of discontinuities dominates. These discontinuities seem to be striking ENE-WSW and can be observed with distances of several kilometers from the fault zone separating the pre-Cambrian gneiss and the Straumbotn and Tjörnrastra nappes. They are likely to have a steep dip ( $>60^\circ$ ) due to their relatively straight appearance in variable topographic conditions. However, a slight curvature towards south in decreasing elevation might suggest a dip towards the south-east. This discontinuity set is hereby denoted DS 1. Discontinuities are indicated with red lines on the orthophoto in Figure 7.3. The foliation joints of the gneiss are difficult to observe in surface images of this tunnel interval.

When the tunnel is approaching the thrust fault and towards the mica-rich gneiss, the system of discontinuities on the surface becomes more complex. Discontinuities striking NNW-SSE become noticeable. Similar to DS 1, these are also likely to have a steep dip due to their straight appearance on the surface. This set of discontinuities is denoted DS 3. From chainage 0+800 m and onward, discontinuities related to the foliation are also identifiable on the surface. These have strike NW-SE with a seemingly gentle dip towards NE.

East of the tunnel segment another discontinuity set is visible on the surface. This is named DS 2 and from interpretations on the surface it seems to have a strike towards N-S. This set of discontinuities is also interpreted to be have a steep dip ( $> 60^\circ$ ).

The observed sets of discontinuities in the vicinity of the branch tunnel are summarized in Table 7.2 below. Documents of the ArcGIS model are attached in Appendix C and display orthophotos for the higher chainages of the branch tunnel.

**Table 7.2:** Summary of discontinuity sets observed on surface imagery for Storåvatn branch tunnel.

Name discontinuity set	Apparent strike	Dip	Comment
Foliation	NW-SE	Shallow ( $<45^\circ$ )	Particularly present from 0+800 m and onwards.
DS 1	ENE-WSW	Steep ( $>60^\circ$ )	Possibly dipping steeply towards SSE.
DS 2	N-S	Steep ( $>60^\circ$ )	More conspicuous 400 m east of the tunnel segment. Might not dominate as a joint set in the tunnel.
DS 3	NNW-SSE	Steep ( $>60^\circ$ )	Pronounced from chainage 0+800 m and onwards.

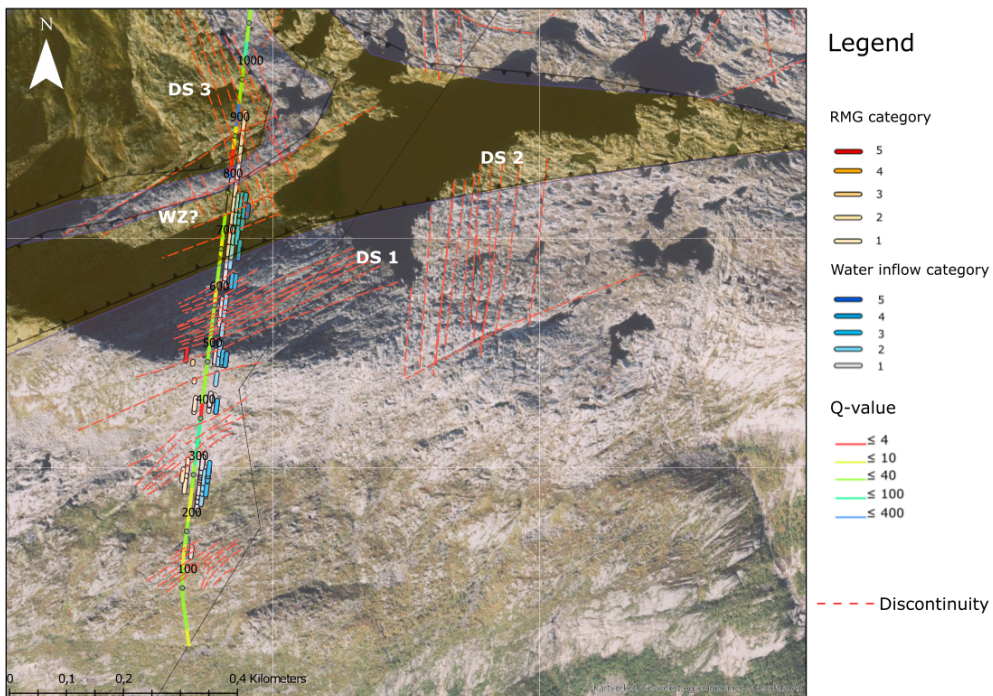


**Figure 7.3:** Aerial photograph of the Storåvatn branch tunnel with overview of rock mass grouting and water inflow in probe drilling rounds. The image also shows distribution of rock mass quality ( $Q$ -values) along the tunnel.

### Weakness zones

Around chainage 0+750 m, the tunnel is located below a zone interpreted as heavily fractured rock mass from orthophotos. The terrain shows a depression at this location, and the segment could possibly be a weakness zone with persistence towards depth in the rock massif. From aerial photographs it can be seen that the spacing of DS 1 decreases towards the assumed weakness zone. When passing this area, discontinuities related to DS 3 become more pronounced. Further, it is seen that the width of the zone on the surface is around 100 m. Given an overburden of around 400 m at this location, it is however questioned if the zone would reach the tunnel level. In the longitudinal profile along the tunnel in Figure 7.5, the weak zone is drawn to a profound level to show where the zone could reach the tunnel. Its propagation is based on an interval of the tunnel observed to be heavily fractured. Based on a general impression of the topographic profile, it could however be reasonable to expect a dip towards the south, since a weak zone observed on the surface tends to dip towards the steepest ridge of the depression (Nilsen, 2016). It is emphasized that the orientation of the potential zone could be oriented differently and is likely to have a much narrower propagation with depth. Figure 7.4 shows an excerpt of

the area with the weakness zone from Figure 7.3. Skardafjelltjørna water source (633 m.a.s.l.) is located some 100 m northeast of the tunnel around this location.

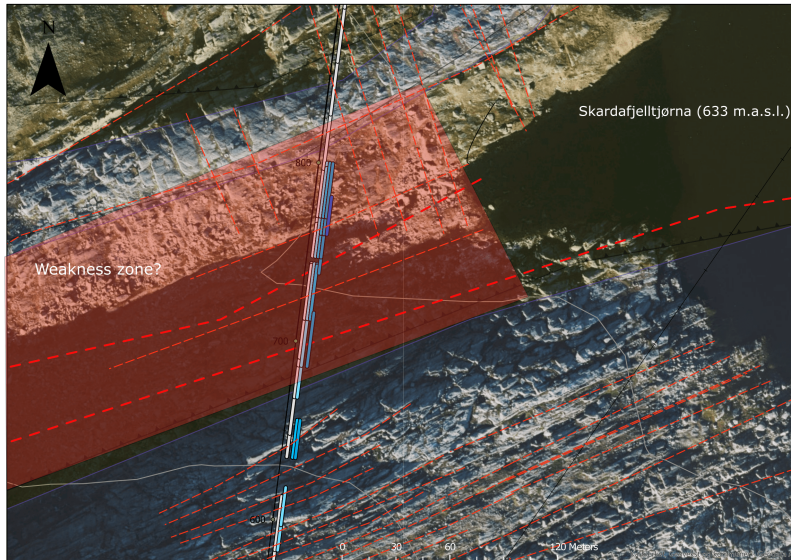


**Figure 7.4:** Aerial photograph of the weakness zone crossing the branch tunnel to Storåvatn lake. See chainage numbers for scale.

Figure 7.5 shows a longitudinal geologic profile along the head race tunnel. The DS 1 structures are indicated as well as more fractured zones on the surface. Sections inside the tunnel with more fractured rock mass are indicated with lines along the tunnel alignment (see the figure legend). The geology is interpreted by the author based on mapping on the surface described by Qvale et al. (2012) and observations from engineering geological mapping in the tunnel.

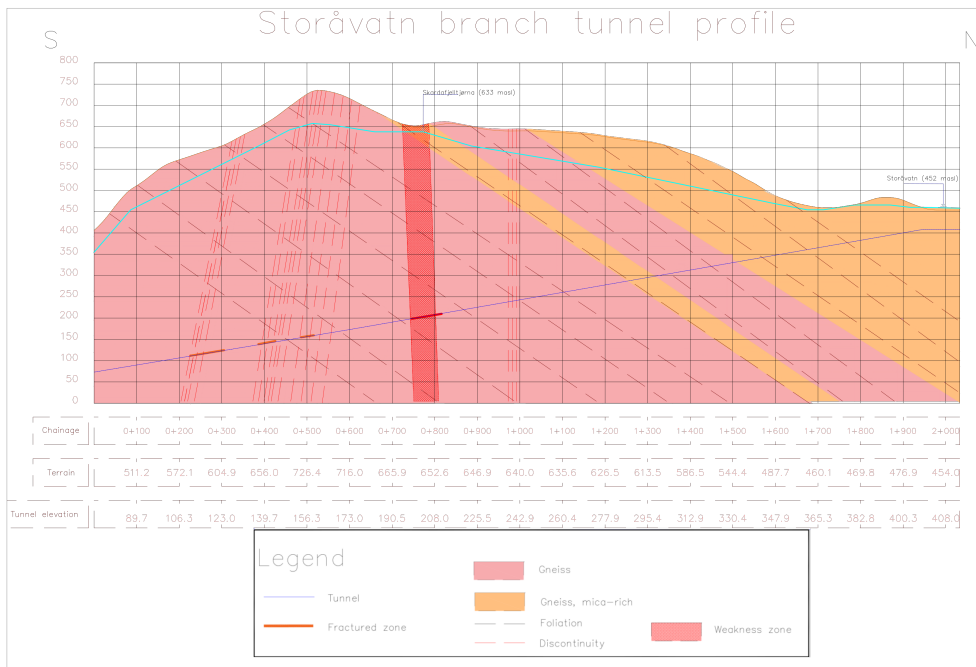


**Figure 7.5:** Geological profile sketch along the Storåvatn branch tunnel. The blue dashed line indicates a rough sketch of the groundwater table level based on water sources on the surface and an assumption of a high groundwater table. An enlarged image of the geologic profile is included in Appendix D.1. Made with Autodesk's Civil 3D.

### 7.2.3 Conditions in the tunnel

#### Rock types

There seem to be no clear transitions between rock types in the tunnel segment. The rock type in the tunnel segment is interpreted as the gneiss of pre-Cambrian age.

#### Joint systems and discontinuities

Joints and discontinuities along the Storåvatn branch tunnel have been measured and noted in engineering geological mapping inside the tunnel. The measurements between 0+000 m and 1+000 m have been gathered in a stereonet presented in Figure 7.6. It was observed that the joint conditions were similar for this tunnel interval, which is the reason for a larger chainage interval compared to that of segment A. In total,  $n = 72$  entries have been included.

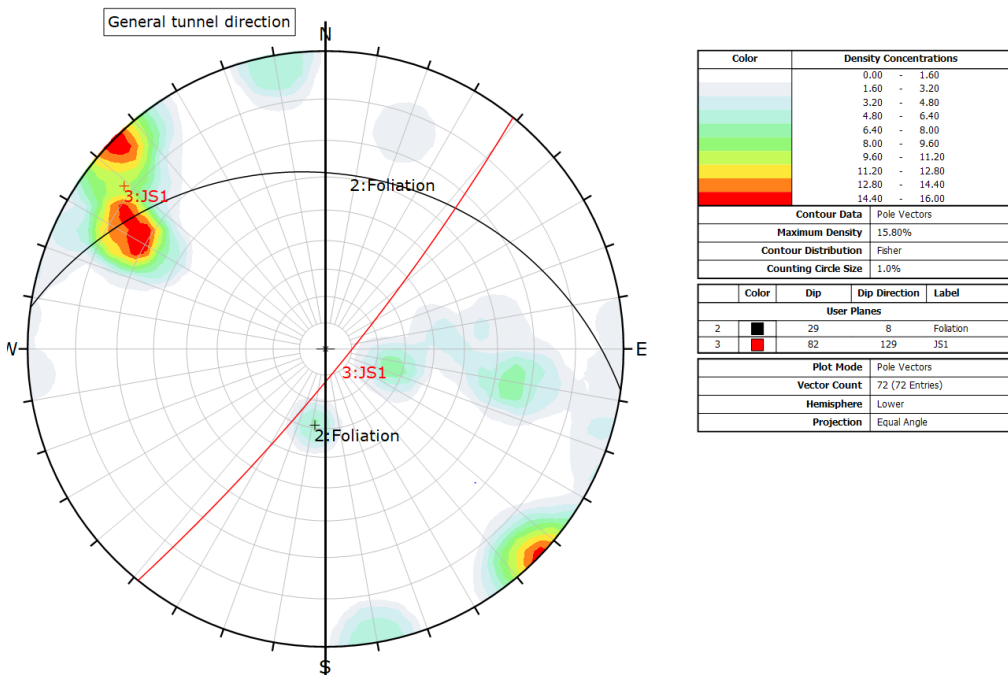


**Figure 7.6:** Stereonet contour plot with interpreted joint set and foliation. Chainage interval of Storåvatn branch tunnel: 0+000 m to 1+000 m. Made with Dips by Rocscience.

The contour plot evidences a grouping for joints striking NE-SW with a steep dip (around  $80^\circ$ ) towards the SE. This joint set is denoted  $JS_A 1$ . A grouping of poles denoting a similar strike as  $JS_A 1$ , but a steep dip towards NW indicates that these joints show some variation in dip

**Table 7.3:** Table showing the approximate orientations of the foliation and JS<sub>A</sub> 1.

Joint set	Strike	Dip
Foliation	N100°E	30° NE
JS <sub>A</sub> 1	N040°E	80° SE

direction. Discontinuities related to the foliation dominate in some parts of the tunnel section, generally at higher chainages towards 1+000 m. The orientation of the branch tunnel varies between NNW-SSE and NNE-SSW. A general tunnel direction (around N000°E) is indicated in Figure 7.6. The joint set, JS<sub>A</sub> 1, is consequently oriented with a mean angle to the general tunnel alignment.

#### *Characteristics of JS<sub>A</sub> 1*

The bullet points below sum up some observed characteristics of the joints related to JS<sub>A</sub> 1. Small amounts of information have been available with respect to the aperture of the joints.

- The joint set is water-leading. Particularly from 0+240 m to 0+340 m, an area of the tunnel which was grouted.
- Generally, the discontinuities are continuous in the entire tunnel contour (i.e. observable from wall to wall).
- The joint spacing varies. In more fractured areas, results from tunnel mapping indicate that the joint spacing can be below 0.5 m.
- The joint alteration has value  $J_a = 2$  in areas where JS<sub>A</sub> 1 dominates. This indicates slightly altered joint walls with non-softening mineral coatings. From the tunnel mapping it has been commented that the joints can have a white coating and occasionally rust on the joint surfaces.
- The joint roughness ( $J_r$ ) is 1.5 in areas where the joint set dominates. This indicates that the joints are rough, irregular and planar.

#### *Foliation*

The discontinuities related to the foliation are generally not water-leading, but the tunnel is commented to be moist in locations where the foliation joint set is the principal joint set in the tunnel. The aperture of the joints has not been commented in tunnel mapping, but is assumed not to be of significance with respect to groundwater inflows. Zones with thickness 0.5-1.5 m of weak layers and weaker zones are occasionally encountered along the tunnel and have orientation parallel to the foliation.

### Weakness zones

From around chainage 0+760 m to around 0+820 m, engineering geological mapping in the tunnel indicates a weathered and significantly fractured zone. Shotcrete and bolting was used in this section of the tunnel for rock support and reinforcement. The rock mass was observed to be "earthy" and could be scraped off and dug with a geologic hammer. Though being remarkably fractured, no dripping or inflow of significance was reported in this area from the engineering geological mapping. From Figure 7.3 it is however seen that the inflows in probe drilling holes ahead of the tunnel face were relatively large in this area with inflows greater than 500 l/min. Figure 8.3b gives a more detailed overview of the groundwater inflows.

### Overburden and rock stress measurements

For tunnel segment A, the lowest rock overburden is around 350 m in the lower chainages. The area with the highest overburden is located near Skardafjelltjørna where it is close to 600 m for chainages around 0+550 m (see Figure 7.5).

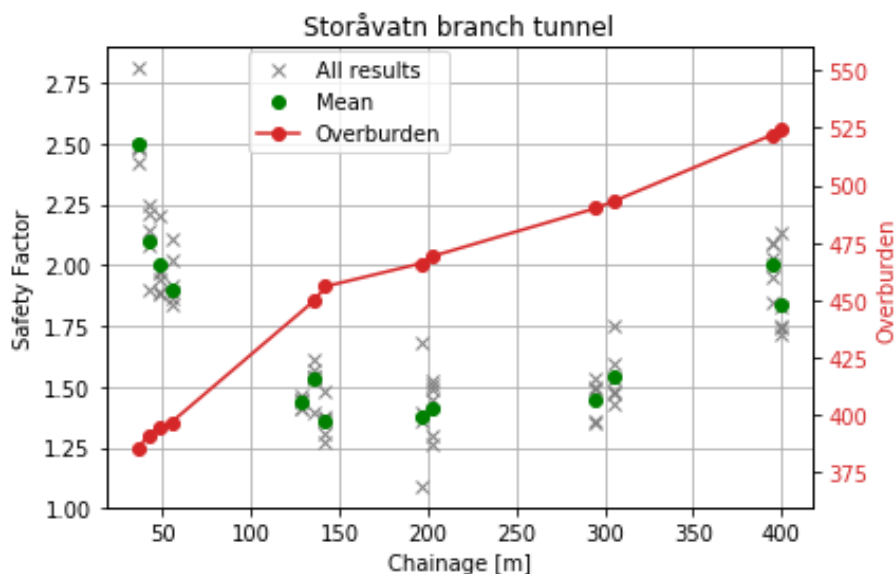


**Figure 7.7:** Safety factor estimated from hydraulic jacking results for Storåvatn branch tunnel. Overburden is roughly sketched. Results from SINTEF (2016).

Rock stress measurements by hydraulic jacking have been performed for chainages between around 0+000 m and 0+400 m. The measurements were made related to determining an adequate location for the transition to the penstock in the head race tunnel. Measurements of the minimum principle stress at the locations shown in Figure 7.7 gives valuable information for



evaluating the stress situation at these locations. In the figure below, the overburden is roughly sketched for each measurement location. For the first 50 m, the safety factor was found to be relatively high. Further testing revealed a section with lower  $\sigma_3$  from 0+150 m to around 0+300 m. An increased safety factor was again observed around 0+400 m.

It is uncertain in what direction  $\sigma_3$  acts. In cases where the test hole is drilled parallel to a principal stress direction, this can be determined (Nilsen and Palmström, 2000). The direction of  $\sigma_1$ ,  $\sigma_2$  and  $\sigma_3$  is however unknown.

## 7.2.4 Rock mass grouting

Figure 7.8 shows the distribution of the total grout take in pre-grouting rounds for different tunnel face locations along the Storåvatn branch tunnel. For segment A, documentation of the rock mass grouting up to chainage 0+500 m is available. As mentioned in Section 7.2.1, the highest water inflow in a probe drilling hole for the segment was encountered around chainage 0+750 m. Documentation of rock mass grouting is available between chainage 1+900 m to 2+033. However, this segment was grouted as part of a routine procedure and specified by consultants when approaching the lake piercing to Storåvatn.

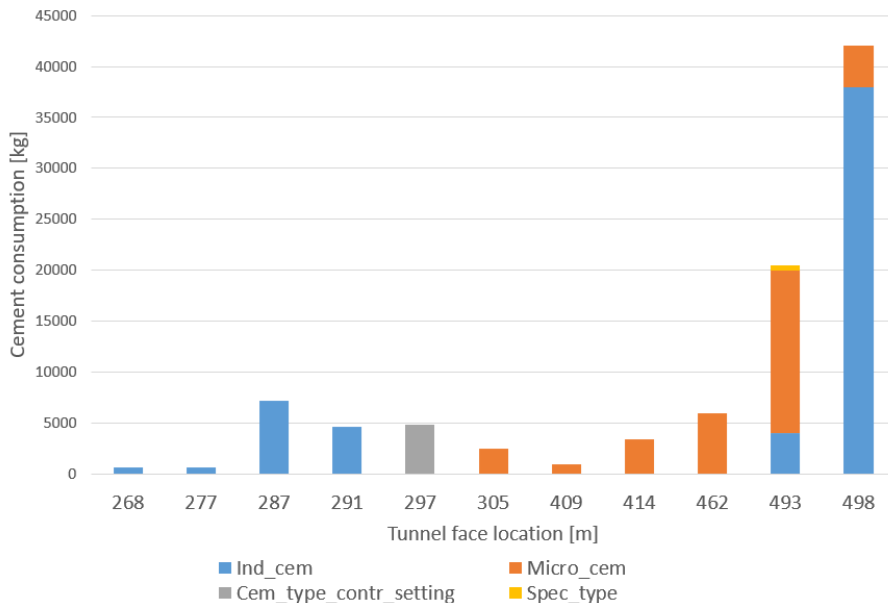


**Figure 7.8:** Distribution of different cement types along the branch tunnel to Storåvatn lake. For explanation of the cement types in Figure 7.8, see Appendix E.1.

From the plot, the following remarks are made:

- The greatest grout take from the gathered data was around 42 tonnes at tunnel face location 0+498 m.
- Cement with an accelerating additive was only used for the pre-grouting round at face location 0+297 m.
- The special type cement with coarser particles was only used at face location 0+493 m in a section of the tunnel with a relatively large grout consumption.
- Micro cement was the main cement type used between 0+300 m and 0+493 m.

For the pre-grouting rounds associated with the highest grout takes in Figure 7.8, the roof and right wall of the tunnel was shotcreted between 0+496 m and 0+508 m. This interval of the tunnel was also commented to be a more fractured zone with a reduced spacing of JS<sub>A</sub> 1 and discontinuities having a shallow dip westwards. Conditions of the joints with respect to alteration and infilling material was not given, but based on  $J_a = 2$ , there seem to be a tendency that the discontinuities have a thin coating on the surfaces. The shotcreted segment of the tunnel was also commented to give water inflow in the tunnel in the engineering geological mapping.

## 7.2.5 Discussion

In the following, the engineering geological conditions characterizing tunnel segment A are discussed related to the encountered groundwater inflows and the performed rock mass grouting.

### Groundwater inflow

The branch tunnel is located in variations of gneissic rock. A rock type associated with high strength and stiffness that can consist of discontinuities with significant persistence. According to the rock mass categories described by Klüver and Kveen (2004), this rock mass shares similarities with rock mass class B. Particularly one joint set (JS<sub>A</sub> 1) was related to the water inflows in the analyzed area, and engineering geological mapping indicates that these discontinuities were likely to cause the larger water inflows. Further, this joint set shares similar orientation as the observed discontinuity set, DS 1, from surface imagery. The joints related to JS<sub>A</sub> 1 were noted to be slightly altered ( $J_a = 2$ ), which again is a favorable characteristic with respect to water flow. The joints are steeply dipping ( $\sim 80^\circ$  SE), a property known to favor water inflow in tunnels (Selmer-Olsen, 1981, Zarei et al., 2011). Figure 7.3 shows that the area where rock stress measurements were performed (0+000 m to 0+400 m) was related to moderate water inflow (50 - 100  $\frac{l}{min}$ ) during probe drilling. However, water inflows associated with water inflow category 5 were also encountered. The stress measurements by hydraulic fracturing suggest a section with reduced  $\sigma_3$  between chainage 0+150 m and 0+320 m in the tunnel. Such local reductions in the in-situ stresses can originate from the in-homogeneous mechanical properties

of the rock mass (Myrvang, 2001). Variations could for instance be due to differences in rock type or in zones with increased fracturing.

Descriptions from engineering geological mapping shows that the rock mass is significantly more fractured in the area of the tunnel observed with a lower  $\sigma_3$ . Discontinuities related to JS<sub>A</sub> 1 are mainly responsible for the increased fracturing in this area. The reduced in-situ stresses could be caused by the concentration of discontinuities. Similarly, due to higher stiffness, competent rock outside of this zone would be subjected to higher rock stresses. A "de-stressed" segment in the tunnel could increase the hydraulic conductivity since a higher rock stress normal to the discontinuities would contribute to a reduced joint aperture.

The orientation of the in-situ principal stresses are also considered to influence the discontinuities' ability to conduct water. If one assumes that the topographic effects control the principal rock stress orientations near the tunnel section, the direction and plunge of  $\sigma_1$  could be close to coincide with the joints in JS<sub>A</sub> 1. Having the maximum principal stress in-plane with the strike of JS<sub>A</sub> 1 would facilitate the aperture of the discontinuities and could therefore increase the hydraulic conductivity of the rock mass in areas where this joint set dominates. A groundwater table located close to the surface would give high water pressures, driving the water flow, assuming a good hydraulic connection between joints from the tunnel level and towards the surface. Figure 7.9 gives an illustration of this possible situation.

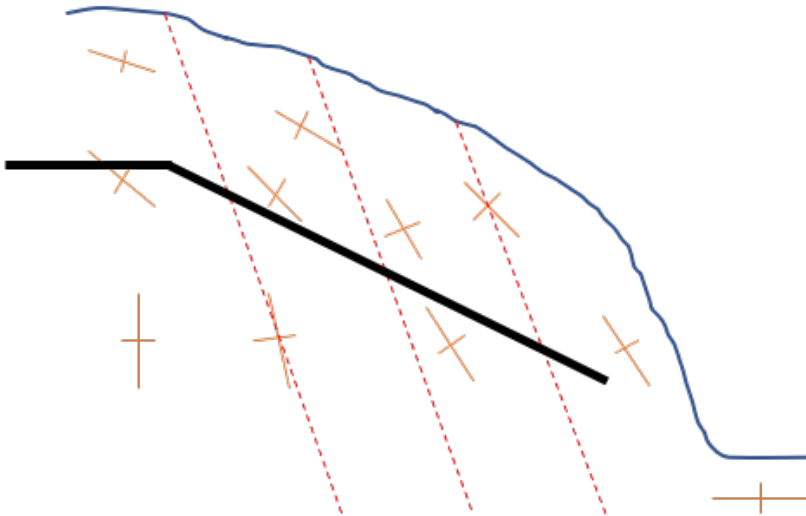


**Figure 7.9:** Sketch of a possible situation at Storåvatn where the maximum principal stress is oriented nearly in-plane to the main joint set within the rock massif for some locations. This presupposes the assumption that topographic effects control the stress orientations near the tunnel. Red lines indicates the joint system, the black line indicates the tunnel and the orange crosses the directions of  $\sigma_1$  and  $\sigma_3$ .

The explained interaction between rock type, joint characteristics, rock stress and groundwater conditions supports previous comprehensions (summarized in Chapter 3). However, the rock stress conditions will depend of more factors than just the topographic effects. Structurally dependent stresses can distort the expected stress situation considerably.

### **Grout consumption and grouting strategy**

The joint set related to the highest water inflow and joint aperture in the tunnel segment is JS<sub>A</sub> 1. Joints related to this joint set normally have a steep dip and are oriented in mean angles to the tunnel direction. This orientation is considered to be fair with respect to pre-grouting the rock mass. A strike normal to the tunnel axis is regarded as optimal. Considering that the tunnel is located in the pre-Cambrian gneiss with discontinuities generally having slightly altered surfaces with non-softening mineral coating, the rock mass type is assumed to be between category A to B according to the classes introduced by Klüver and Kveen (2004). From experience, a satisfactory grouting results is normally achieved in this rock mass class without significant effort.

As indicated in Section 7.2.4, the grout consumption was particularly large for the pre-grouting round at tunnel face location 0+493 m and 0+498 m. In this area of the tunnel a more fractured zone of width around 12 m was encountered. Further, this was an area associated with high water inflows in probe drill holes (category 4), which continued to give inflow into the tunnel also after the grouting works. The conditions indicate particularly open joints with high hydraulic conductivity. The concentration of the discontinuities in this area will reduce the competence of the rock mass. A local reduction in stiffness could cause the groundwater pressure to be relatively high compared to the rock stresses (mainly  $\sigma_3$ ). This could in turn facilitate a higher hydraulic conductivity and also cause an increased grout consumption.

The strategy applied for sealing the water-inflows is also a controlling factor for the final grout take. The pre-grouting rounds performed up to chainage 0+493 m showed that micro-cement was the main cement type used. When encountering water inflows at tunnel face location 0+493 m, it is likely that the initial grouting strategy involved the use of micro-cement for the respective pre-grouting round. Utilization of this cement material was associated with a large grout take (around 16 tonnes) compared to a consumption of 4 tonnes using industry cement. At tunnel face location 0+498 m, it seems likely that micro-cement was initially used also for this pre-grouting curtain before using industry cement. However, a relatively high grout take was also experienced with industry cement (38 tonnes) before a satisfactory pressure was reached.

There are several uncertainties and limitations regarding information on the performed grouting in tunnel segment A. It seems likely that the documentation from rock mass grouting gathered

by the author does not include all data of the rock mass grouting. This is due to an interval of the tunnel from around 0+520 m to 0+800 m where water inflows up to 500 l/min were encountered, but no documentation of rock mass grouting has been found.

## **7.3 Tunnel segment B**

### **7.3.1 Introduction**

For the main head race tunnel of Storåvatn there have been several segments of high groundwater inflows. As a result, more than one area of this tunnel could have been included in the analysis. For an overview of the rock mass quality (Q-value), grouting and water inflows along the tunnel, see Appendix C.4. To limit the extent of the analysis, one section for this head race tunnel has been chosen. Namely, the interval of the tunnel between chainage 1+200 m and 1+650 m.

In this interval, water inflows up to 600 l/min were measured in one bore hole. The greatest amount of total cement consumption was 84 tonnes in a single pre-grouting round. Figure 7.10 shows a geological map of the area around tunnel section B with distribution of rock mass quality along the tunnel. Figure 7.11 shows the distribution of water inflows in the respective tunnel segment.

The section is located near the fault zone between the gneissic bedrock and the Tjörnrastra nappe near Skardafjelljtjørna. Considering the geologic profile in Figure 7.5, this boundary is expected to have dip around 30° to the NE. Compared to tunnel segment A, it is situated closer to the fault boundary between the pre-Cambrian gneiss and the Straumbotn nappe to the north-east (see Figure 5.2).

### **7.3.2 Conditions on the surface**

Figure 7.12 shows an ortophoto of the area around tunnel segment B where interpreted discontinuities and results from geologic mapping are displayed (see Qvale et al. (2012)). Results of rock mass quality (Q-value), water inflow and grout takes are also shown in order to give an overview of the relevant conditions along the tunnel segment.

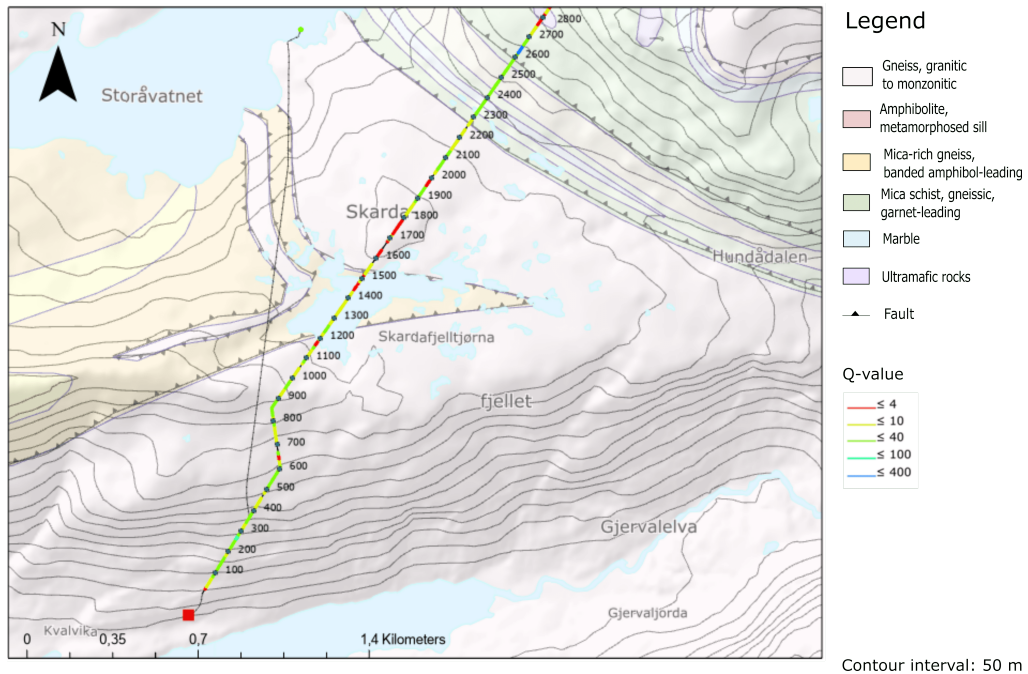


**Figure 7.10:** Geological map showing the main head race tunnel of Storåvatn with distribution of  $Q$ -values.

### Rock types

From geological mapping presented in Qvale et al. (2012), the boundary to the mica-rich gneiss is located at around chainage 1+200 m on the surface. The transition to the pre-Cambrian gneiss is indicated at around chainage 1+550 m. The tectonic boundary to the Straumbotn nappe on the surface is located some 700 m away from tunnel segment B, following the tunnel alignment.

### Large-scale discontinuities

Larger and smaller water sources related to Skardadjelljørna are located above the tunnel segment. As a result, observations on the surface are limited in this area. However it can be seen that the discontinuity sets, DS 1 and DS 2 observed near tunnel segment A, are also pronounced in the second tunnel segment. For information on the assumed attitudes of these discontinuity sets, it is referred to Section 7.2.

DS 2 has a relatively continuous presence along the tunnel alignment and towards the metamorphosed sedimentary strata, which is located above the tunnel around chainage 2+300 m. Discontinuity set 1 is also present along the tunnel segment, but becomes more pronounced towards 2+200 m. It is seen that both DS 1 and DS 2 are oriented in mean angles ( $45 \pm 15^\circ$ ) to

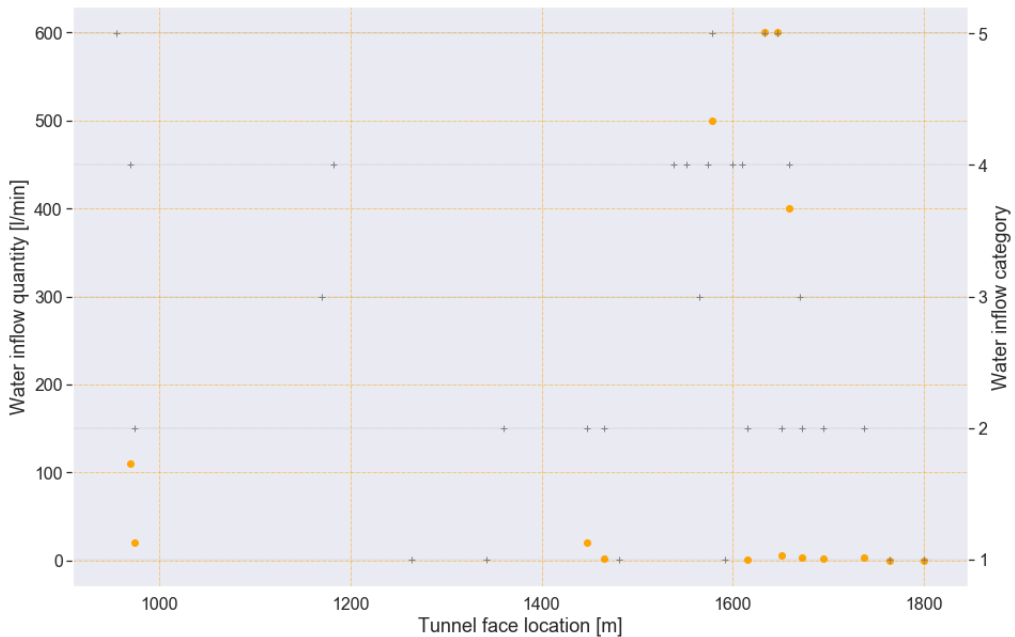


**Figure 7.11:** Distribution of water inflow categories and estimates in tunnel segment B. The circles denote quantitative estimates and the crosses categories of the encountered groundwater inflows.

the north-eastern fault zone and are persisting of distances well above 1 km.

### Weakness zones

In tunnel segment A, a fractured zone in the rock mass was observed to the south west of Skardafjelltjørna water source. The zone was commented to possibly be a weakness zone that could show persistence with depth. Discontinuities related to DS 1 were observed to be more densely spaced towards this zone. These discontinuities follow the length axis of Skardafjelltjørna. Further, Qvale et al. (2012) have interpreted that a principal portion of the water source is located in the gneiss of Neoproterozoic to Cambro-Silurian age. This is a rock type associated with a lower strength and resistance to erosion than the pre-Cambrian gneiss. Considering these factors, the zone of more fractured rock could extend towards the location of tunnel segment B on the surface. Again, the persistence of this zone with depth is uncertain.

## 7.3.3 Conditions in the tunnel

### Rock types

Based on descriptions from tunnel mapping it has been challenging to point out the transitions between the pre-Cambrian gneiss and the gneiss of Neoproterozoic to Cambro-Silurian age.

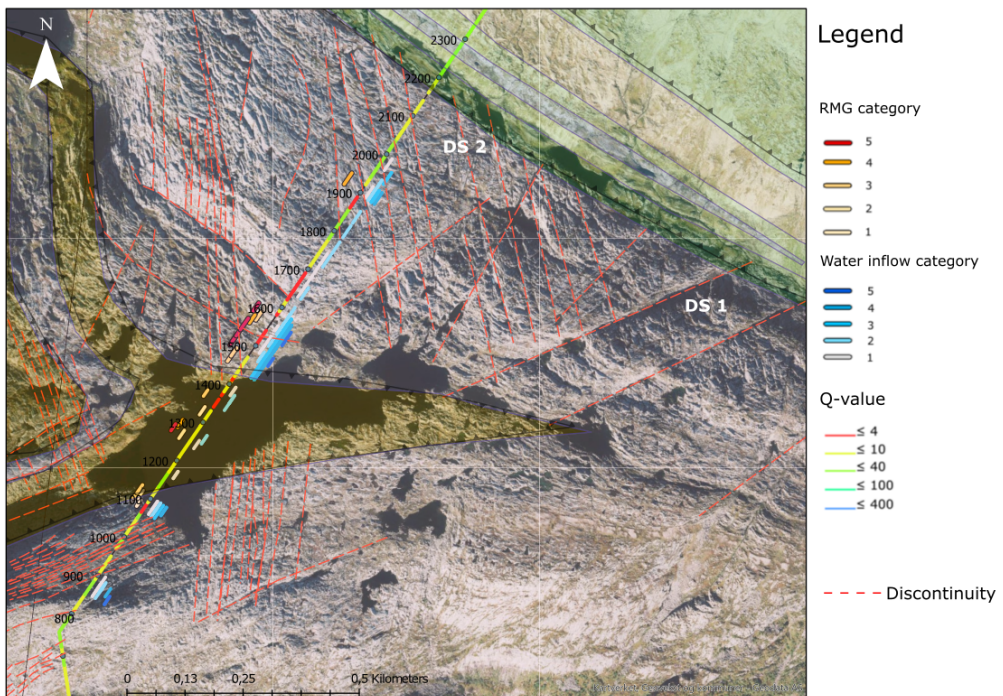


**Figure 7.12:** Aerial photograph with the section for analysis (chainage 1+200 m to 1+650 m). For legend regarding the rock types, see Figure 7.10.

Considering strike and dip measurements of the foliation near the rock boundaries on the surface ( $\sim 30^\circ$  NE), the rock boundaries may be located at chainage numbers above that of tunnel segment B.

### Joint systems and discontinuities

Similarly as for tunnel segment A, strike and dip attitudes of discontinuities have been gathered in the segment between chainage 1+100 m and 1+650 m. The results are presented in a stereonet shown in Figure 7.13. In total, 42 entries have been included.

Interpretations from the stereonet concludes that two joint sets ( $JS_B$  1 and  $JS_B$  2) dominate along the tunnel segment. Measurements of joints related to the foliation in the tunnel indicate a similar orientation as for tunnel segment A. However, the foliation structures are seldom drawn or indicated in tunnel mapping for the respective tunnel interval. Further, they do not seem to play any significant role related to the groundwater inflows.

Table 7.4 gives an overview of the joint sets and their respective orientations.



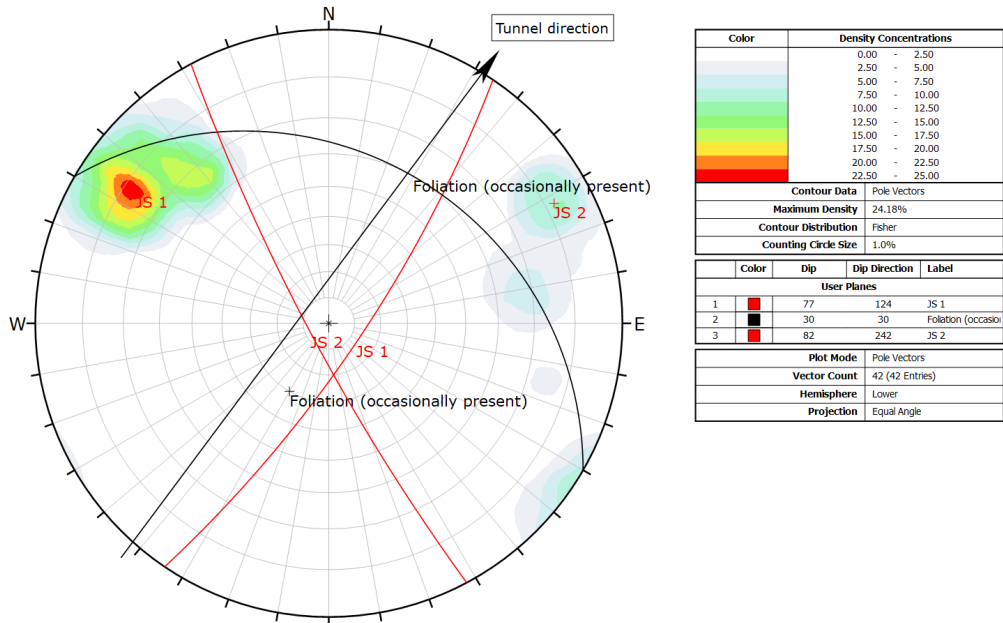


Figure 7.13: Contour stereonet for the distribution of joints in tunnel segment B.

Table 7.4: Joint sets present in tunnel segment B.

Joint set	Strike	Dip
Foliation	N120°E	30° NE
$JS_B 1$	N034°E	77° SE
$JS_B 2$	N152°E	82° SW

The table indicates two joint sets,  $JS_B 1$  and  $JS_B 2$ , in addition to the less pronounced foliation joints in the tunnel. The conditions of the joint sets are presented in the following.

#### Condition of $JS_B 1$

Observed characteristics of  $JS_B 1$  are summarized below.

- The joint set is water-conducting. Mapping of the tunnel indicates that the joint set regularly causes minor inflows and dripping in the tunnel. In grouted sections, the inflows are lower.
- The discontinuities are normally persisting and can often be followed in the entire tunnel contour.

- There is a variable joint spacing. In fractured zones, the spacing between JS<sub>B</sub> 1 can be lower than 1 m.
- The typical aperture of the joints is not known.
- In areas where JS<sub>B</sub> 1 dominates, the joints are commented to be smooth and planar, but the discontinuities can also be observed with a wavy attitude.
- The discontinuities tend to have oxidized surfaces of rust. In cases of infilled material, only small amounts of finer particles are present.

#### *Condition of JS<sub>B</sub> 2*

Observed characteristics of JS<sub>B</sub> 2 are summarized below.

- Discontinuities belonging to JS<sub>B</sub> 2 are water-leading. Intense dripping occurs in some sections of the tunnel segment.
- The majority of the discontinuities can be followed in the entire tunnel contour. They have a persisting appearance.
- Similar to JS<sub>B</sub> 1, the joint spacing of JS<sub>B</sub> 2 varies. In more fractured zones, the joint spacing can be around 2 m. Otherwise, the joints occur more or less sporadically in the tunnel.
- The typical aperture of the joints has not been commented. Similar to JS<sub>B</sub> 1, the joint set conducts water and the discontinuities' aperture facilitate inflow to the tunnel.
- Occasionally, the joint set is commented to have a thin coating. What material the infillings consist of is not known.
- The joints seem to be smooth and planar. Sporadically, they express a more wavy appearance.

Figure 7.14 shows a geologic profile along tunnel segment B. The tunnel alignment and elevations are also shown. Additionally, an in-plane view of the tunnel is given to the left of the profile. This illustration shows what joint sets are present in the tunnel and which of these give rise to the water inflows in the tunnel segment. Grouted areas along the tunnel are also shown.

#### **Weakness zones**

A fractured zone is observed from chainage 1+600 m to around 1+670 m. Shotcrete was applied to an extensive part of the roof and walls in the tunnel near this interval. The majority of the discontinuities at this location seems to have strike from around N030°E to N045°E. Weathered material that could be scraped with a hammer was also commented in the tunnel.

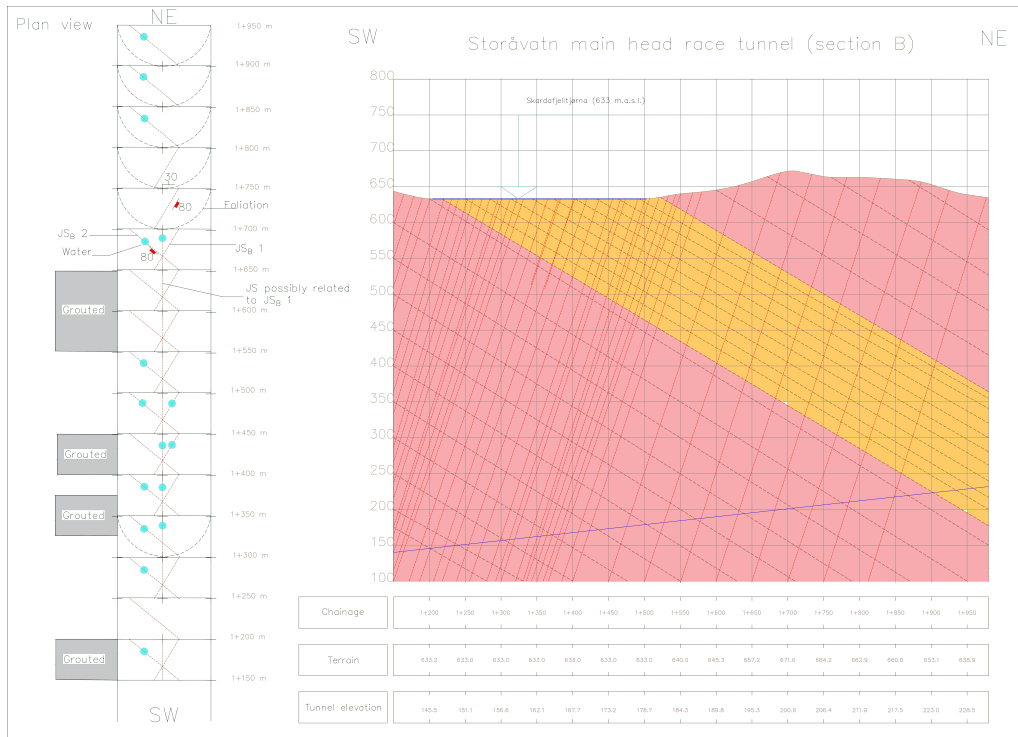


**Figure 7.14:** Longitudinal, geologic profile of tunnel segment B. Symbology is similar to that of Figure 7.5. Joint sets observed in the tunnel with water inflows are shown for plan view illustration of the tunnel. An enlarged image of this figure is found in Appendix D.1. Made with Autodesk's Civil 3D.

### Rock stress conditions

The rock stress measurements in the main head race tunnel of Storåvatn were performed in chainages prior to the tunnel segment of interest. The hydraulic jacking tests for determining adequate cone location were executed up to chainage 0+895 m. The rock stress conditions can vary significantly between the test locations and the area of the tunnel segment. The results are consequently considered to be of limited use for evaluating the stress conditions in the chainage interval of tunnel segment B.

Compared to tunnel segment A, the second tunnel segment is located further away from the valley side towards the Gjervalen fjord. The rock overburden varies from around 500 m near the lower chainages to around 400 m near chainage 1+650 m. In chainages around 1+100 to 1+200 m some spalling in the rock with discontinuities parallel to the tunnel were observed. These were not associated with water inflow.

### 7.3.4 Rock mass grouting

Figure 7.15 gives an overview of the consumption of different cement materials for each tunnel face location in the tunnel segment.

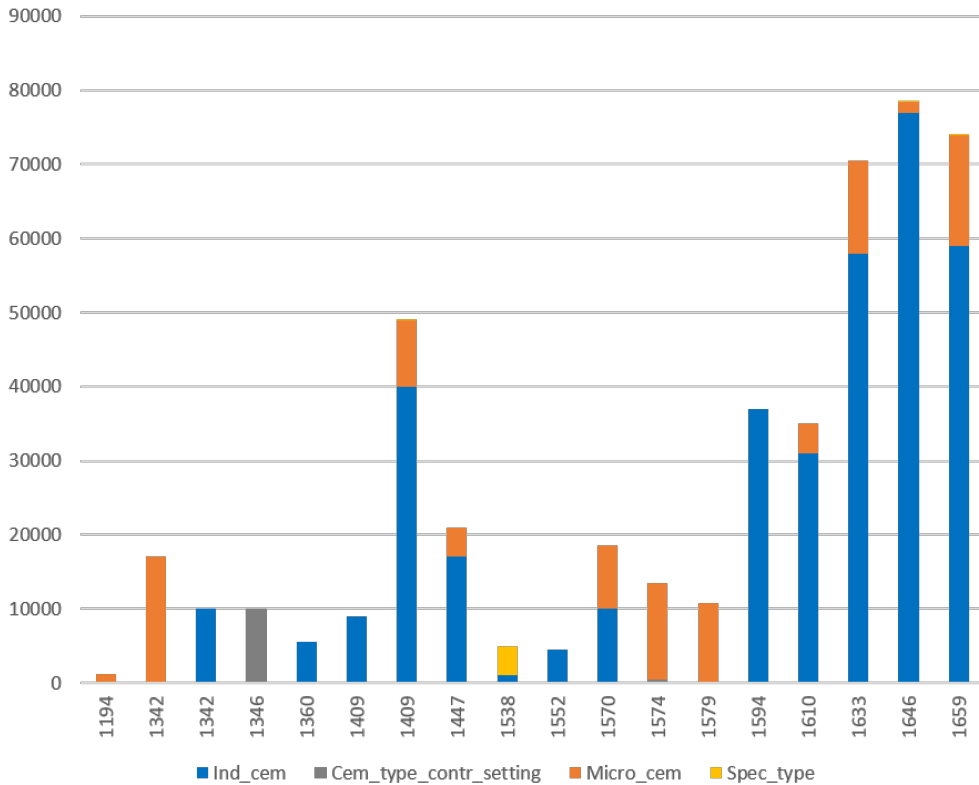


**Figure 7.15:** Distribution of different cement types in tunnel segment B. For explanation of the cement types, see Appendix E.1. Cement consumptions are in kg.

From the figure, the following remarks are made:

- The grouting strategy has mainly consisted of industry cement as the cement material.
- A significant grout consumption with grout takes up to above 80 tonnes were experienced from chainage 1+570 m to 1+659 m.
- Cement with coarser grains (Spec\_type) was the principal cement type used at face location 1+538 m.
- Grouting by controlling the setting time was not performed except at tunnel face location 1+346 m.

### 7.3.5 Discussion

In the following, the engineering geological conditions characterizing tunnel segment B are discussed related to the encountered groundwater inflows and grout consumption.

#### Groundwater inflow

The tunnel segment in the Storåvatn head race tunnel experienced water inflows up to 600 l/min in probe drilling holes. The inflows were greatest around tunnel face location 1+600 m. In the tunnel, two joint sets ( $JS_B$  1 and  $JS_B$  2) are water-leading. These can also be observed as large-scale discontinuities on the surface. Further, the Skardafjelltjørna water source is located above the tunnel for a relatively long distance ( $\sim 300$  m). In the case where the discontinuity sets are persistent with depth, vertical fractures will potentially give a short drainage path to the tunnel.

As one regard the joint systems in the tunnel related to the water inflows in addition to the geological conditions on the surface, certain characteristics are noticed. The Straumbotn nappe is located north-east of the tunnel segment and is separated from the pre-Cambrian gneiss by a fault zone. Joints conducting water in the tunnel are oriented in mean angles ( $45^\circ \pm 15^\circ$ ) to the fault boundary. These are persisting on the surface and have a steep dip. The above-mentioned conditions turn the thoughts to similar observations made by Selmer-Olsen (1981) discussed in Section 3.4. The resemblances to the considerations and the theory proposed by Selmer-Olsen are striking. This with respect to the rock type, discontinuities and the geologic boundaries. Consequently, there are indications that the problems with water inflows in tunnel segment B is a case that can be added to the examples studied by Selmer-Olsen.

The orientation and magnitude of the in-situ stresses are unknown factors. Spalling with joints parallel to the tunnel was observed in the lower chainages of the tunnel segment. This could indicate relatively high vertical rock stresses compared to horizontal stresses at the tunnel level. If  $\sigma_v = \sigma_1$ , this would be an orientation favoring water flow in the two joint sets dominating in the tunnel.

#### Grout consumption and grouting strategy

The distribution of performed rock mass grouting works show that there was a considerable higher grout consumption from around chainage 1+600 m to 1+660 m. The main cement type used for this area of the tunnel was industry cement without accelerators or the use of coarser particles.

The rock mass class is considered to be class A or B, according to the categories introduced by Klüver and Kveen (2004). From experience, a satisfactory grouting result is achieved fairly

easy in this rock mass category. However, the conditions can vary and make the grouting process challenging. The orientation of the joints in the rock mass is one of these factors.

The strike of  $JS_B 1$  is oriented close to parallel to the tunnel direction in tunnel segment B, while  $JS_B 2$  has strike nearly perpendicular to the tunnel. Intersecting  $JS_B 1$  with drill holes for pre-grouting can therefore be challenging. However, communication with  $JS_B 2$  can make the grout material penetrate  $JS_B 1$  where the joint sets are intersecting. The joint sets seem to generally have a low amount of infill material. Further,  $JS_B 1$  and  $JS_B 2$  have potential to conduct considerable amounts of water into the tunnel. The grout mixture should in this case have a low w/c-ratio and industry cement or coarser cement types adapted to the aperture of the discontinuities should be used. From around chainage 1+600 m it was challenging to seal the joints and the grout take with industry cement was high (up to 80 tonnes). Other than the consumption of different cement types, limited information has been available regarding factors such as the w/c-ratio.

# Statistical analysis

This chapter regards the statistical analysis of results gathered of water inflow, rock mass grouting and rock mass quality in the project. The chapter is divided in two. In the first part, rock mass parameters and water inflow quantities are compared to investigate possible relationships between the parameters. Further, a semi-analytical approach has been used to estimate water inflow quantities for given rock mass conditions and compare the results to the experienced quantities. Finally, a multivariate linear regression for grout take has been made using covariates describing the condition of the rock mass.

## 8.1 Groundwater inflow

### 8.1.1 Overview of the results

The maximum water inflow category for a probe drilling round has been used for the analysis in this chapter, as described in Chapter 6. The analyzed data have been gathered from four of the tunnels in the SmiSto project; the main head race tunnel of Smibelg and Storåvatn and the branch tunnels to Smibelgvatn and Storåvatn lakes. For the other tunnels which have not been included, the amount of available data is scarce and the tunnels are generally shorter in length. Figure 8.1 shows the distribution of groundwater inflow categories in probe bore holes.

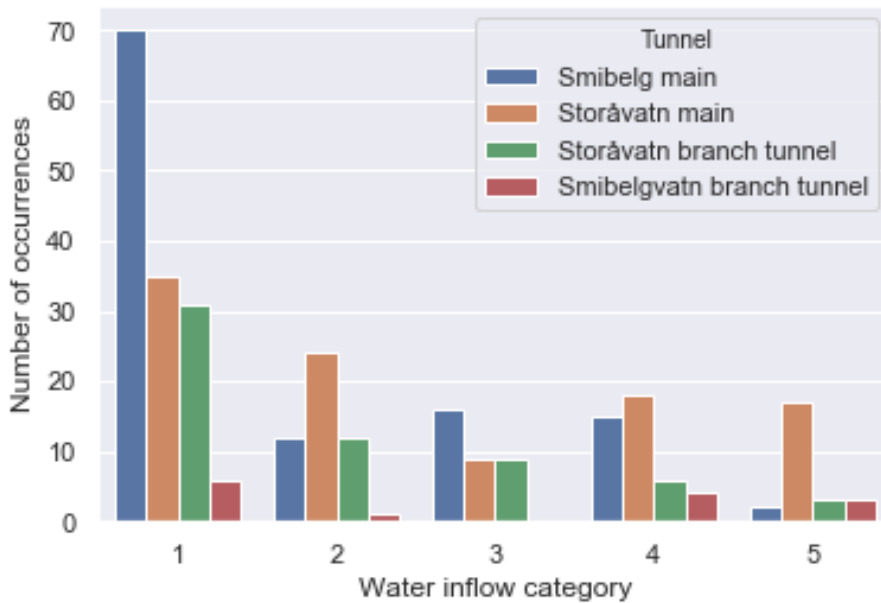


**Figure 8.1:** Distribution of water inflow categories from the four analyzed tunnels. In total,  $n = 293$  data points are included.

The plot shows that the majority of the results belongs to category 1, equivalent to no water inflow in the bore holes. It also evidences the number of data points for each of the tunnels. The available data amounts are naturally lower for the branch tunnels, as these are shorter than the main head race tunnels in length.

The increased water inflows that have occurred in the Storåvatn main head race tunnel are noticeable from the plot. For instance, the total number of data points from the Smibelg main head race tunnel are 115, but only 1.7 % of the results are within category 5. For the main head race tunnel of Storåvatn, the total of number of data points are 103, but here 16.5 % denote the highest water inflow category. Further, it is seen that a relatively large portion of the inflow measurements in Smibelgvatn branch tunnel also belongs to category 5.



Table 8.1 summarizes the number of probe drilling rounds and the portion of the data that belongs to water inflow category 5.

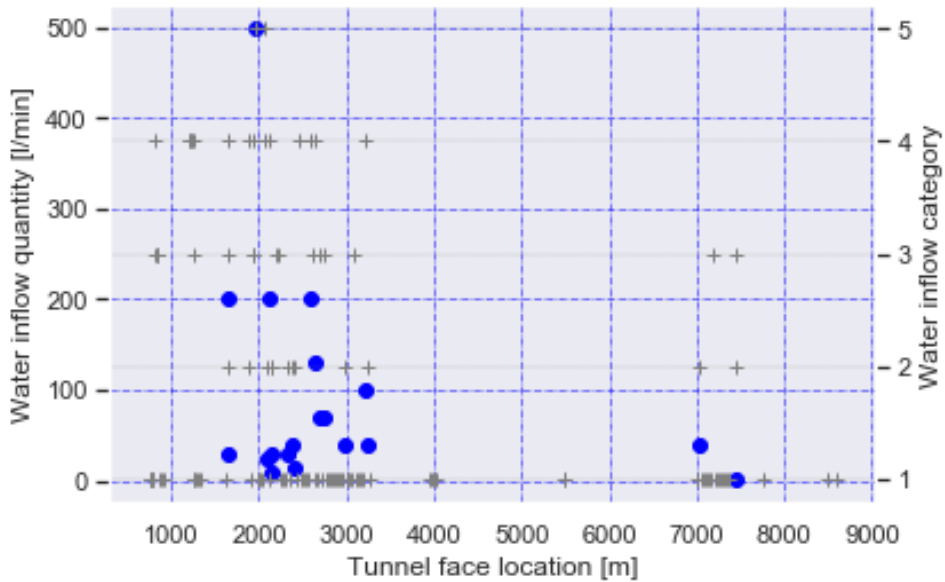
**Table 8.1:** *Overview of highest category in the analyzed tunnel sections.*

Tunnel	Count in cat. 5	Total count	Percentage
Smibelg main	2	115	1.7
Storåvatn main	17	103	16.5
Storåvatn branch	3	61	4.9
Smibelgvatn branch	3	14	21.4

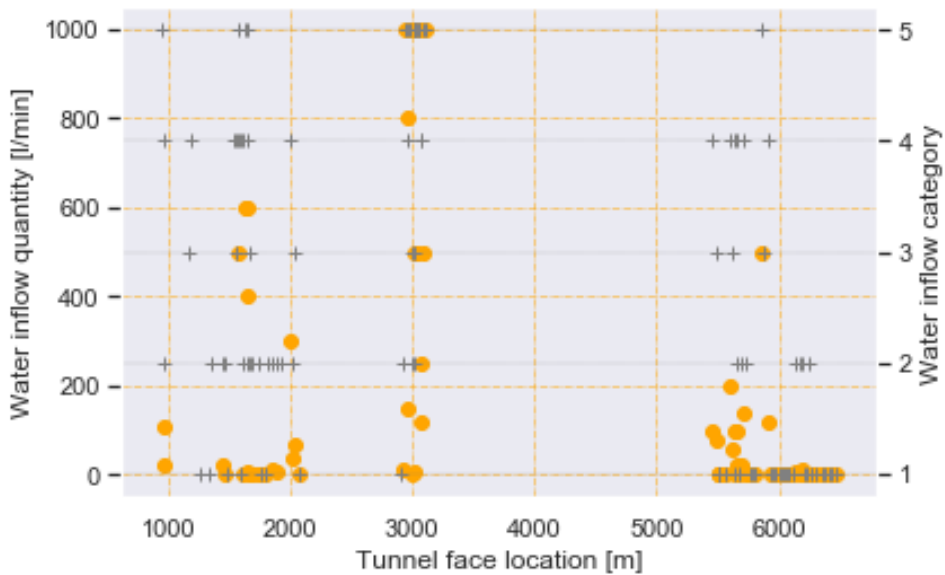
Figure 8.2 and 8.3 show the distribution of water inflow categories and quantitative inflow estimates for the four tunnels. These plots give a more detailed description of where along the head race tunnels the water inflow problems were the greatest.

Figure 8.2 evidences the increased water inflow problems in the main head race tunnel of Storåvatn compared to that of Smibelg. Extensive water inflow amounts were encountered between chainage 1+000 m to 2+000 m at Storåvatn main head race tunnel. The greatest groundwater inflow occurred between chainage 2+900 m to 3+100 m, with pressures above 30 bar and around 1000 l/min or more in several bore holes. For the Smibelg main head race tunnel, the problems related to water inflow were the greatest between chainage 0+700 m and 3+300 m with inflow quantities up to 500 l/min in a bore hole.

With respect to the distribution of water inflow amounts and categories shown in Figure 8.3, the water inflows in the Smibelgvatn branch tunnel were the greatest at chainages towards the lake piercing, i.e. from chainage 0+150 m to 0+300 m. Here, the inflow amounts up to 800 l/min in one bore hole were measured. In the Storåvatn branch tunnel, water inflow quantities reached at least 500 l/min in some bore holes. The water inflow difficulties in this tunnel seems to have been most challenging between chainage 0+100 m to 0+750 m.

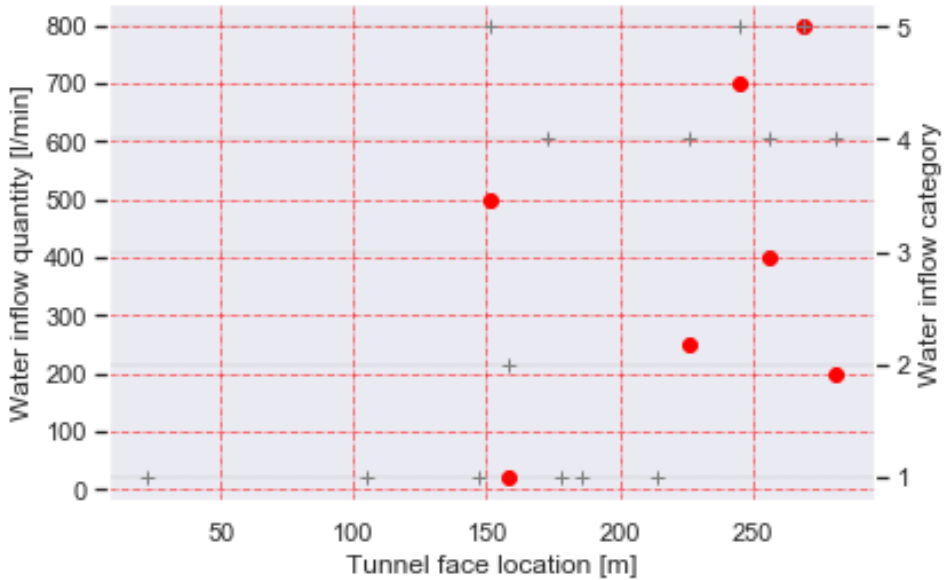
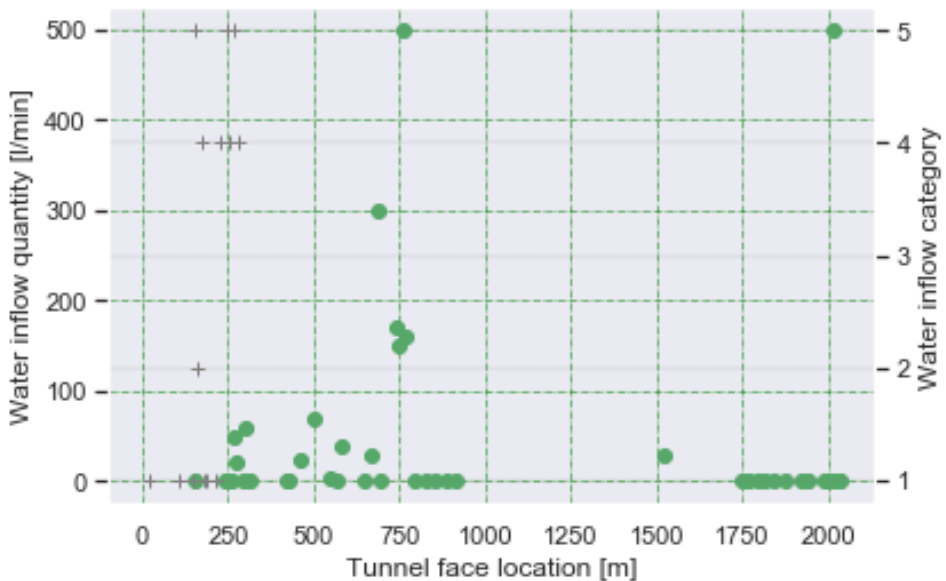


(a) Smibelg main head race tunnel.



(b) Storåvatn main head race tunnel.

**Figure 8.2:** Distribution of the maximum encountered groundwater inflow by category and quantitative estimate for the main head race tunnels. Circles denote quantitative estimates and crosses water inflow categories.

(a) *Smibelvatn branch tunnel.*(b) *Storåvatn branch tunnel.*

**Figure 8.3:** Distribution of the maximum encountered groundwater inflow by category and quantitative estimate in the branch tunnels to Storåvatn and Smibelvatn lakes. Circles denote quantitative estimates and crosses water inflow categories.

## 8.1.2 Statistical analysis

The results presented in Section 8.1.1 are analyzed further in the following. As a result, the water inflows considered still regard the highest encountered water inflow in a bore hole during a probe drilling round. Effort has been put to compare the water inflow amounts (quantitative estimates) to the different rock mass quality parameters in the Q-system and estimates of the rock overburden. Figure 8.4 shows scatter-plots between these parameters. The relationship between the parameters and the water inflow quantities are commented for each of the plots below.

Due to scattering, there seem to be no clear trend in the results of  $RQD$  with inflow amount in Figure 8.4a.

Most of the larger water inflows seem to be located in section with  $J_n = 6$  (see Figure 8.4b). However, scattering of the data indicates no systematic relationship between the inflows and this joint parameter.

The results of the joint roughness coefficient in Figure 8.4c are limited in that only two categories are present ( $J_r = 1.0$  and  $J_r = 1.5$ ). The inflow amounts of both categories can vary from 0 to 1000 l/min. There seem to be no clear relationship between the water inflows and the  $J_r$ -value.

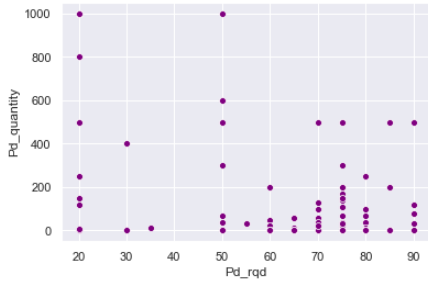
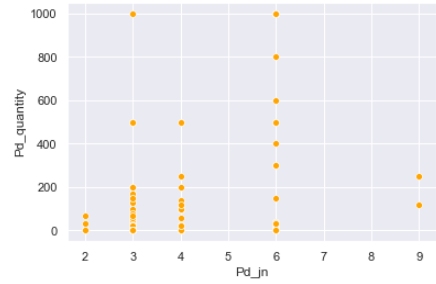
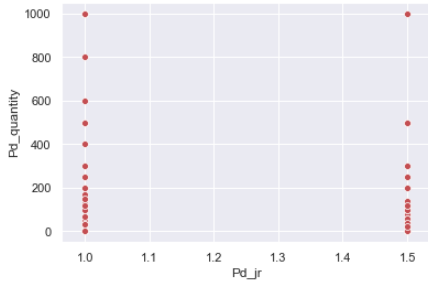
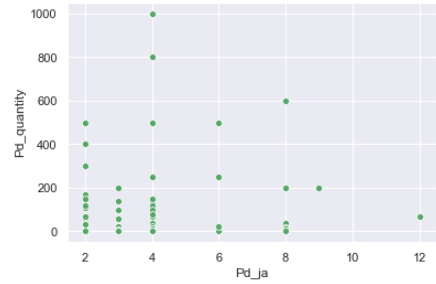
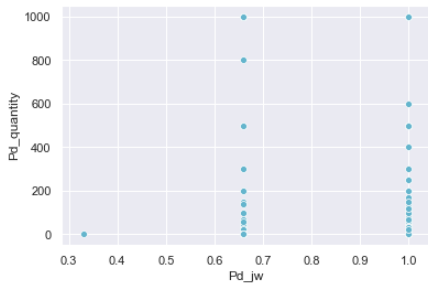
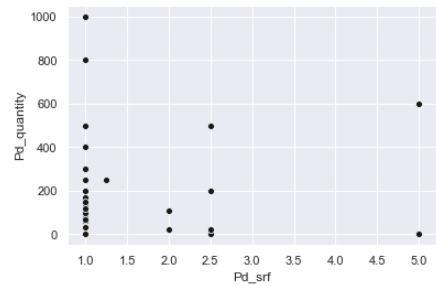
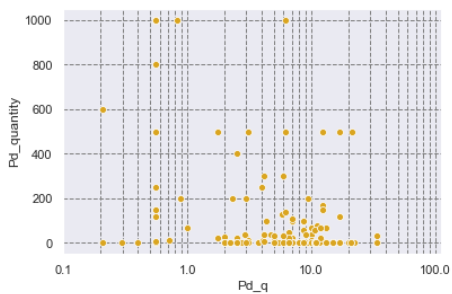
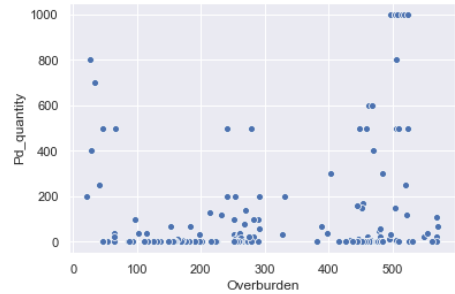
From Figure 8.4d there seem to be a weak correlation between the joint alteration number ( $J_a$ ) and water inflow quantities. The greatest water inflows were encountered where  $J_a = 4$ , but relatively large inflows also occurred in sections with both lower and higher  $J_a$ -values.

The plot between water inflow estimates and the  $J_w$ -parameter in Figure 8.4e shows that the water inflows are relatively well-distributed for  $J_w = 0.66$  and  $J_w = 1.0$ .

From Figure 8.4f, most of the data belong to  $SRF = 1$ , and is relatively well-distributed for this category. No clear trend in the data is observed.

The plot in Figure 8.4g is dominated by that most of the  $Q$ -values were in the range between 1 and 10. The results have a relatively large degree of scattering. No clear increase nor decrease of water inflow with different  $Q$ -values is seen.

There is a tendency from the plot in Figure 8.4h that the greatest water inflows occur in sections where the tunnel has a relatively high overburden ( $> 400$  m).

(a) Water inflow quantity [l/min] vs  $RQD$ .(b) Water inflow quantity [l/min] vs  $J_n$ .(c) Water inflow quantity [l/min] vs  $J_r$ .(d) Water inflow quantity [l/min] vs  $J_a$ .(e) Water inflow quantity [l/min] vs  $J_w$ .(f) Water inflow quantity [l/min] vs  $SRF$ .(g) Water inflow quantity [l/min] vs  $Q$ -value.

(h) Water inflow quantity [l/min] vs overburden.

**Figure 8.4:** Plots of predictor variables against the response variable.

### 8.1.3 Comparison of water inflow quantities and rock mass parameters

The semi-analytical approximation to specific leakage in probe drilling holes by Panthi (2006) is applied in this section. The methodology used in this analysis have been presented previously, and the reader is referred to Section 6.4.1 for information. The estimates by Equation 3.6, presented in Section 3.6.2, are compared with the actual inflow rates [l/min/m] in probe drilling holes. The analysis is only performed for the main head race tunnel of Storåvatn to limit the analysis.

#### Estimation of the permeability factor ( $f_a$ )

The calculation of the depth factor ( $D$ ) was described in Section 6.4.1. For the parameters regarding the discontinuities,  $J_s = 5$  m and  $J_p = 20$  m are chosen. This is based on a general observed spacing of the discontinuities in the tunnel. The discontinuities are persisting and can generally be followed in the entire tunnel contour, also in cases where they have relatively sharp angles to the tunnel alignment. Given a typically 20 m<sup>2</sup> cross-sectional area of the tunnel, the value of joint persistence is set to 20 m. From these estimates, the permeability factor has been estimated for each probe drilling result.

The estimated values of specific inflow by Equation 3.6 are compared to the actual inflow rates in bore holes for both head race tunnels. Figure 8.5 shows the resulting average values at each tunnel face location for both the estimates and the actual encountered specific inflows. Lines indicate the overall mean of the results.

From the plot it can be observed that, generally, the approximated values of specific leakage overestimate the mean of the actual encountered inflow at each probe drill round. However, from chainage 3+000 m to 3+100 this does not seem to be the case, where considerably higher water inflows were encountered. The lines indicating the overall mean shows the tendency for the overestimation of specific water leakage.

## 8.2 Rock mass grouting - Multiple Linear Regression (MLR)

A multivariate linear regression (MLR) model has been developed in an attempt to make a fit between the grout take (response variable) and covariates related to rock mass parameters. The aim of the MLR model is to analyze which of the rock mass parameters have a significant influence on the cement consumption in rock mass grouting. Additionally, with a MLR model it is investigated if the grout take can be adequately expressed by a linear combination of the covariates.

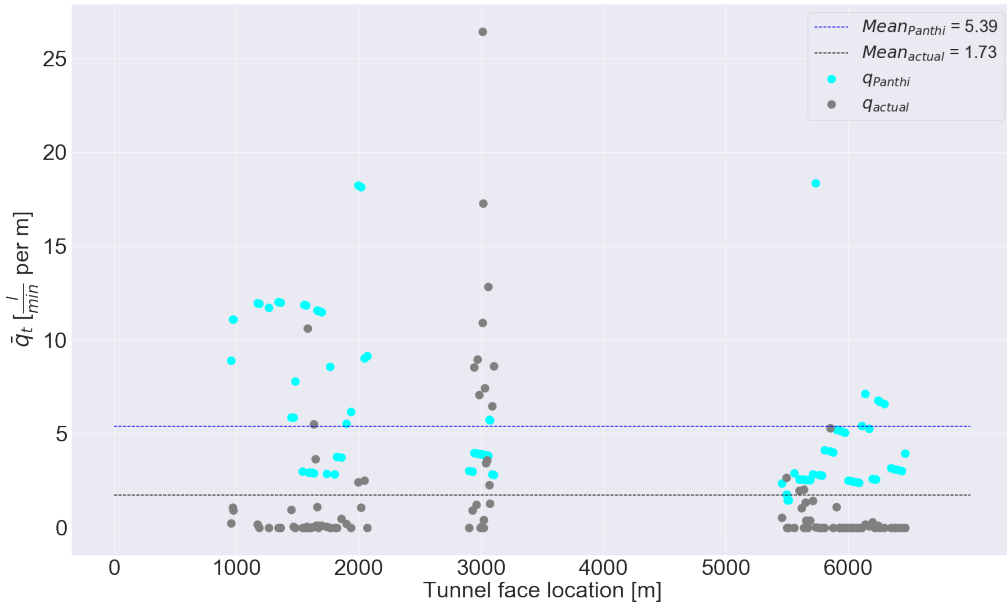


**Figure 8.5:** Distribution of estimated and actual inflow rates in probe drilling holes along the tunnel face locations in the Storåvatn main head race tunnel.

### 8.2.1 Description of the data set

The data set that has been used for the MLR model in this analysis includes data from the four head race tunnels presented in Section 8.1.1. Table 8.2 shows the response variable (grout take) and the covariates used in the model.

**Table 8.2:** Covariates and the response variable in the model. The  $Q$ -value is dependent on the other RMG-parameters and was therefore not included.

Response variable	Covariates
$\bar{C}_{tot} [\frac{kg}{m}]$	RMG_rqd RMG_jn RMG_jr RMG_ja RMG_jw RMG_srf Overburden [m]

The covariates are mainly related to rock mass quality parameters, but overburden of rock above the tunnel has also been included. The response variable is defined as the ratio between the total cement take in a pre-grouting round and the average length bore holes in the grout curtain (see

Equation 8.1). The parameter ( $\bar{C}_{tot}$ ) is named Cem\_per\_m in Appendix E.1.

$$\bar{C}_{tot} = \frac{C_{tot}}{l_c} \quad (8.1)$$

In total,  $n = 87$  data points have been included in the model. Figure 8.6 shows a distribution plot and a box plot of the grout take variable.

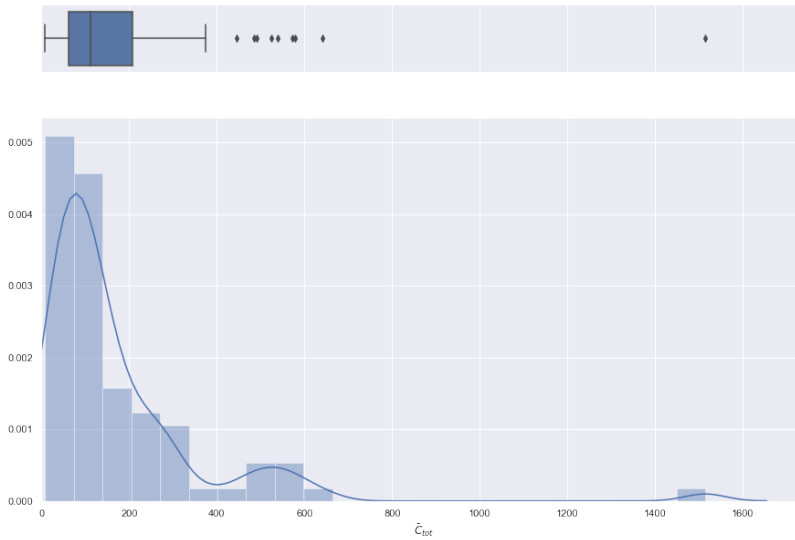


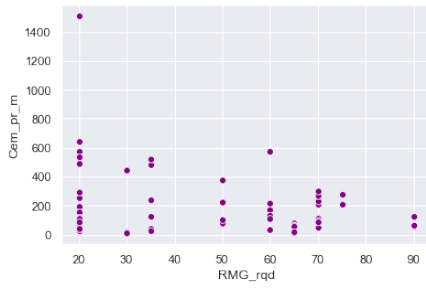
**Figure 8.6:** Distribution and box plot of the response variable ( $\bar{C}_{tot}$ ) in  $\frac{kg}{m}$ .

The plot shows that the 75 % of the data are below  $Q_{75} \approx 200 \frac{kg}{m}$ . The median is located around  $\bar{C}_{tot} = 100 \frac{kg}{m}$ . The highest grout take per bored meter was around  $1500 \frac{kg}{m}$ . The distribution of the response variable does not seem to fit well with a normal distribution.

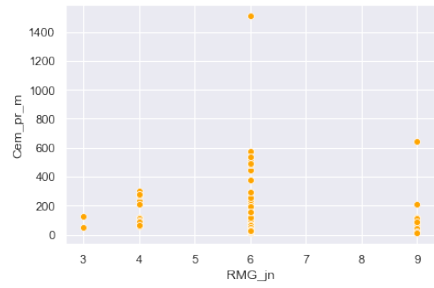
Figure 8.7 shows pair plots between the response variable and the input variables.



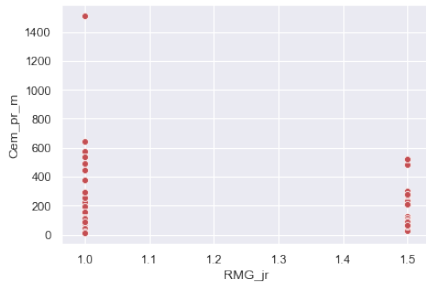
## 8.2 Rock mass grouting - Multiple Linear Regression (MLR)



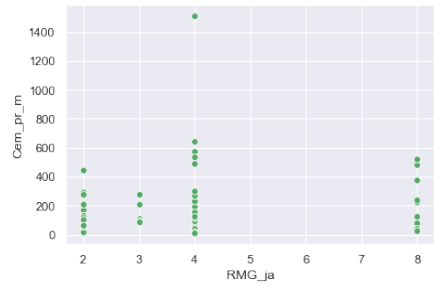
(a) *Cem per m vs RQD.*



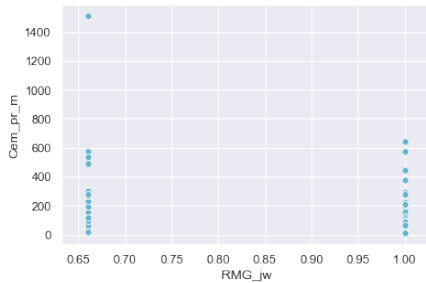
(b) *Cem per m vs  $J_n$ .*



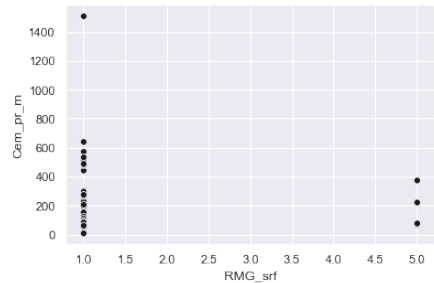
(c) *Cem per m vs  $J_r$ .*



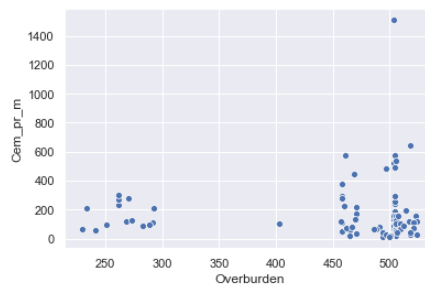
(d) *Cem per m vs  $J_a$ .*



(e) *Cem per m vs  $J_w$ .*



(f) *Cem per m vs SRF.*



(g) *Cem per m vs overburden.*

**Figure 8.7:** *Plots of predictor variables against the response variable.*

## 8.2.2 Stepwise regression analysis

Initially, a MLR model was attempted to fit the grout take with the above-mentioned covariates, but the normality assumption (described in Chapter 6) of residuals was violated. As commented in Section 4.4, Nia et al. (2016) encountered a similar normality problem in a MLR analysis of grout take. By log-transforming the response variable, a new MLR model was made which satisfied the normality assumption. This transformation was also made in this MLR analysis of grout take. The other assumptions described in Section 6.4 were tested. The procedure and results are summarized below.

- The normality assumption of the residuals was fulfilled after testing with the Shapiro-Wilk test. A p-value = 0.72 was well above the  $\alpha = .05$  significance level for the test. A plot showing the distribution of the normalized residuals is shown in Figure 8.8.
- The assumption of homoscedasticity was fulfilled with a significance level of  $\alpha = .05$ , tested with Bartlett's test. For information on this test, see Keating and Leung (2010).
- Collinearity between covariates was checked by the variation inflation factor (VIF). A threshold of 5 was used to assess collinearity between the predictor variables during stepwise regression (see Table 8.3).

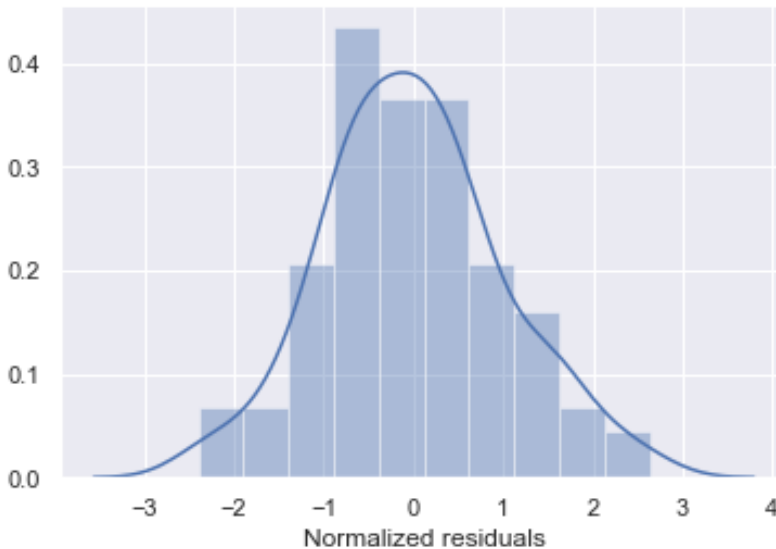


**Figure 8.8:** Distribution of the normalized residuals after log-transforming the response variable ( $\bar{C}_{tot}$ ).

In the stepwise regression, covariates with a high p-value and a high variation inflation factor were removed one by one. The resulting models for each step are shown in Table 8.3.

**Table 8.3:** Models in stepwise regression using backward elimination of covariates.

Parameters	Model 1			Model 2			Model 3			Model 4			Model 5		
	p-value	VIF	$R^2$	p-value	VIF	$R^2$	p-value	VIF	$R^2$	p-value	VIF	$R^2$	p-value	VIF	$R^2$
RMG_ja	0.605	7.6	0.090	0.186	1.7	0.090	0.157	1.7	0.089	0.148	1.7	0.089	0.254	1.1	0.080
RMG_jw	0.134	1.7		0.134	1.7		0.080	1.3		0.049	1.1		0.072	1	
Overburden	0.306	9.9		0.164	6.3		0.155	5.4		0.093	4.3		0.071	1.1	
RMG_jr	0.680	11.1		0.400	4.2		0.384	4.2		0.369	4.1				
RMG_jn	0.819	2.1		0.831	2.1		0.878	1.8							
RMG_rqd	0.812	4.7		0.842	3.8										
RMG_srf	0.893	4.7													

It is seen that if one assumes the validity of a multivariate log-linear model between the response variable and the predictor variables, the covariates that are most likely to affect the grout take are  $J_w$ ,  $J_a$  and the rock overburden. The table below shows the coefficients for each covariate.

**Table 8.4:** Results for the coefficients of covariates in the model with standard error and 95% confidence interval.

Name	Coefficient	Std error	Confidence interval (95 %)	
			Lower	Upper
Constant	6.3083	0.811	4.696	7.921
RMG_ja	0.0731	0.064	-0.053	0.200
RMG_jw	-1.1172	0.613	-2.337	0.102
Overburden	-0.0022	0.001	-0.005	0.000

The model suggests that a lower value of RMG\_jw increases the grout take, while a higher value of RMG\_ja increases the grout take. A lower overburden gives a slight increase in the cement consumption, but the influence on cement take is barely noticed. The confidence intervals and standard errors of the coefficients evidence a relatively large uncertainty in the results.



## Discussion

### 9.1 Analysis in areas of interest

Chapter 7 included a separate discussion for each of the analyzed tunnel segments. In this chapter, the areas will be discussed together with respect to general characteristics and resemblances related to the rock mass conditions relevant for the water inflows and the rock mass grouting. Some aspects of the applied grouting strategy are also discussed.

#### 9.1.1 Groundwater inflow

A joint set striking NE-SW and having a steep dip was present in both tunnel segment A and tunnel segment B ( $JS_A$  1 and  $JS_B$  1 respectively). This joint set shared orientation with a set of large-scale discontinuities observable on the surface (DS 1). The joint sets both gave water inflows into the tunnel. Relative to the thrust zone near the Straumbotn mappe, the joints have orientation in mean angles to the fault structure. This characteristic has been observed in previous tunneling projects to possibly be related to discontinuities with a high potential for water inflow in tunnels (Selmer-Olsen, 1981). A joint set striking NW-SE ( $JS_B$  2) in tunnel segment B also had an orientation in mean angles to the fault. However, these discontinuities did not dominate in tunnel segment A. The discontinuities observed on the surface and the steep, water-conducting joints in the tunnel could have originated from processes that generate pinnate fissures, observed in previous tunneling projects. It seems that a common characteristic of the water-leading joints is that they have a steep dip and have a low amount of infill material. The main rock type in both tunnel segments is the pre-Cambrian gneiss, associated with both high strength and stiffness. These properties are known to facilitate persistent discontinuities which can have a significant aperture, allowing fluid flow.

Stress measurements by hydraulic jacking were performed for an area within tunnel segment A. For tunnel segment B, the test locations were outside the area of interest. In the branch tunnel to Storåvatn lake, an area characterized by a reduced  $\sigma_3$  was associated with high water inflows (category 5). A reduction in the rock stresses could give an increased hydraulic conductivity in this area. Both the analyzed areas are located at great depth within the rock mass (> 100 m). If one considers the rock stresses induced from topographic effects, the major principal stress could be oriented with sharp angles to the water-conducting joint sets. This will be a direction favorable for the conductivity of the joints, with  $\sigma_3$  possibly being oriented normal to the discontinuities. Rock stresses are however a complex phenomenon that depend on the origin of the rock stresses as well as the mechanical properties of the rock mass. Other than topographic effects, the stress situation will for instance also be controlled by tectonic forces.

### 9.1.2 Rock mass grouting

Based on the rock mass condition and the orientation of the joints in the analyzed tunnel segments, a satisfactory grouting result was expected to be achieved fairly easy based on experience with similar conditions. This is reflected in the expected rock mass grout consumption described in the pre-liminary phase of the project, as well as general comprehensions acquired from experience with similar projects (Klüver and Kveen, 2004). However, this has in many cases not been the situation for Storåvatn HPP. The discontinuities that need to be grouted in order to seal the water inflows seem to have a considerable persistence and aperture. Similarly as for the groundwater flow discussed above, the stress situation could also favor a high grout take in the rock mass.

There is a tendency that micro cement types were used initially in the grouting process. However, a high grout consumption was generally observed using this cement type. With respect to the rock mass type dominating in the tunnel segments, both industry and micro cements are considered to be appropriate for the grouting works (Klüver and Kveen, 2004). However, as indicated by Hognestad et al. (2011), micro cements are intended for discontinuities having a smaller aperture. There has been an alternating use of micro and industry cement in a majority of the pre-grouting rounds in the tunnel segments. There are also indications toward that micro cement have initially been used for rock mass grouting in these situations, before using industry cement. The grout take with micro cement has surpassed 10 tonnes for pre-grouting rounds in both tunnel segments. Despite the consumption of industry cement also being large (up to 70 tonnes) at some locations, this cement material seems to be more adapted to the water-leading discontinuities. According to Johansen (2019), there has also been a tendency to avoid the use of micro cement due to poor grouting results in the initial stages of the project.

There have been limited information to the author regarding other aspects of the grouting strategy applied at the relevant tunnel locations. A lower w/c-ratio is known to reduce the flow properties of the grout. In the case of grouting water-filled discontinuities, an improved flow of the grout can be experienced during the grouting process. The w/c-ratio has been determined by workers in the tunnel depending on the conditions of the tunnel face at the relevant location and can consequently vary at different locations, and even during the grouting process. Applying a relatively low amount of water compared to cement is considered to be favourable for achieving a good grouting result in the observed rock mass conditions. Further, results indicate a generally sparse use of accelerators in the grout mix for the pre-grouting rounds, even in cases of industry cement consumption surpassing 50 tonnes at more than one pre-grouting round. According to Hognestad et al. (2011) the use of accelerators can have a reducing effect on the grout take. Though its potential effect on the grout consumption is unknown for the analyzed areas, it could have contributed in reducing both the time and cement consumption in the grouting works. However, rock mass grouting is an experience-based field and must continuously be adapted to the rock mass conditions. A general rule regarding the grouting procedure does not exist.

## 9.2 Statistical analysis

### 9.2.1 Groundwater inflow

#### Estimates of inflow using a semi-analytical approach

The semi-analytical approach proposed by Panthi (2006) was used to estimate groundwater inflows in the main head race tunnel of Storåvatn and compare these to the actual inflows.

There is a tendency that the approach overestimates the groundwater inflows in the tunnel. At certain chainages, the estimates correlate fairly well with the encountered water leakages, e.g. where the tunnel face was located around 5+500 m. However, the overall mean of the estimates is around three times higher than the mean of the measured data. Between chainage 3+000 m and 3+100 m, an area associated with high water pressures and large inflows, the encountered leakages are in some cases observed to be greater than the estimated values.

The semi-analytical approach used in this analysis was developed by Panthi (2006) with the intention to assess groundwater flow *out* of the head race tunnel during operation. The equation is based on experiments where water was pumped in bore holes with a pressure exceeding the expected operating pressure in the tunnel. In this analysis, however, the equation has been used to evaluate groundwater flow *into* the head race tunnel. The nearest water source on the surface was used to evaluate the hydrostatic water pressure for a given probe drill hole in this

analysis. The approximation, however, was developed considering a specific water source on the surface, certain to be related to the flow of water. Since the groundwater flow in the rock mass is complex and highly depends on the conditions of the discontinuities, the water sources which were considered in this analysis might not affect the actual driving pressures for the water inflows experienced. Instead, local groundwater tables within the rock mass could be the source of the inflows. Thus, water sources not relevant for the encountered inflows will give incorrect estimates of the hydrostatic water pressures and erroneous calculations of the water inflows.

While applying the approach another limitation was observed. When estimating the groundwater inflow, the hydrostatic pressure will always be greater than zero. This is because the nearest water source on the surface with respect to the tunnel condition is considered. Further, the rock mass parameters used for input variables will also be greater than zero. The same regards the permeability factor,  $f_a$ , which similarly is estimated from parameters related to the rock mass. Consequently, the estimates of groundwater inflow in bore holes will always surpass zero. However, several situations have been observed where probe drill rounds ahead of the tunnel face have not given any inflow of water. It is likely that these properties of the equation contributes to the general overestimation of water leakage. Other, general limitations are associated with the choice of rock mass parameters for probe drill holes. These will be discussed in the next section.

### **Comparison of groundwater inflow quantities and rock mass parameters**

Parameters regarding rock mass quality (Q-value) appear scattered for different water inflow quantities. Generally, there seem to be no clear correlation between the considered rock mass parameters and the water inflows. This is rather surprising since certain discontinuity parameters are considered to have an influence on the inflow of water. For instance, a higher value of  $J_a$  indicates more weathered joint surfaces and more infill material. Joints that are more weathered and have more infill material are by several authors regarded to reduce the potential for water inflows (Holmøy, 2008, Panthi and Nilsen, 2010, Singhal, 2010). A lower value of  $RQD$  and a higher  $J_n$ -value indicates more extensive jointing and fracturing of the rock mass. Since the flow of groundwater mainly is limited to the discontinuities, one could be of the impression that this would be associated with higher inflows. From the results in Chapter 8, this does not seem to be the case. Panthi and Nilsen (2010) observed a similar result, but discussed that the  $RQD$ -value only covers a small range of the possible block size in the rock volume. However, it was found that  $J_n$  could be related to the water leakage and was proportional to the leakage amount in bore holes. Observations in the tunnels show that higher water inflows can occur in zones of heavier fracturing. However, situations with higher inflows have also been observed where the rock mass has generally been of good quality with few, but persisting discontinuities.



In this case, even a single open joint has been observed to be the source of the high inrush of groundwater. This might give some explanation to the observed result.

Regarding the joint roughness, authors have different opinions on its effect on the groundwater flow. Singhal (2010) reviews its dependence on the stress situation, but argues that a higher roughness of the joints generally tend to reduce the hydraulic conductivity. Panthi and Nilsen (2010) found that the  $J_r$  parameter, similar to  $J_n$ , was proportional to the leakage amount. Small variations of the joint roughness in the project could contribute to the result achieved in this analysis, where no clear correlation to the water inflows was found.

There is a tendency that larger inflows occur in areas having greater rock overburden. In one way this is logical since the water pressures will increase with depth from the groundwater table, and pressure differences are the driving forces for groundwater flow. However, some empirical relations have proposed negative correlations between the hydraulic conductivity and the rock overburden and suggest that the inflows should generally be lower with higher rock cover. Then again, severe water inrushes at great depths is not a new problem in tunnelling.

The results in the statistical analysis of rock mass parameters show the complexity regarding water inflow in rock tunnels. No clear relationship was found between rock mass parameters of the Q-system and the water inrushes during tunnel excavation. There are several limitations that can influence the results. Firstly, the measured water inflows have in many cases been given visual estimates by workers in the tunnel. If the estimates have strong deviations from the actual values, this will reduce the quality of the analysis. Other limitations are discussed further in the following.

#### *The influence of grouting on the results from probe drilling*

The encountered water inflow in probe drilling rounds can be influenced in areas where pre-grouting ahead of the tunnel face has been performed. In cases where the probe drill holes intersect the grouted rock mass, the hydraulic conductivity of the rock volume will be lower than the fresh, un-grouted rock. Consequently, it is assumed that also the groundwater inflows in these areas will be lower. A previously performed pre-grouting curtain can extend further than a recently excavated zone. Bore holes drilled for a probe drilling round at the new tunnel face location will then cross a zone of grouted rock mass having an unknown extent. However, it has been challenging to identify probe bore holes which have been drilled in grouted rock.

Since a probe bore hole drilled in a grouted rock mass generally is assumed to give lower water inflow, the maximum inflow of water in a probe drilling round was considered in the statistical analysis. This was then an indication of the maximum potential for water inflow at the relevant

tunnel location. To limit the data only to the maximum inflow, caused the number of data points to reduce considerably. However, some measures were necessary to consider the probe drill holes likely to not be affected by pre-grouted zones in the rock mass. Holmøy (2008) also called attention to this problem and used a more sophisticated method to analyze results in her doctoral thesis. It was unfortunately not found time for applying this methodology or developing a similar method for the analysis in this thesis. If a similar method had been applied, the analysis could potentially include more of the gathered data. The model of the project in ArcGIS Pro includes all results of groundwater inflow with categories shown along the tunnel alignments (see Appendix C).

#### *Assigning Q-values to the probe drilling results*

Probe drill holes can cross several intervals associated with different Q-values. In cases where the bore hole crosses more than one interval, the smallest Q-value has been chosen. In her doctoral thesis, Holmøy (2008) followed a similar approach arguing that the smallest Q-value should be chosen to prevent more fractured zones in the rock mass to be neglected.

This approach has limitations in that it favors a low Q-value for the results of the bore hole. The actual position along the bore hole where the main source of the higher inflow of water is located may be in an area of the rock mass with a higher Q-value. In many cases it has been difficult to identify exactly where along the bore hole the main source of the water inflow was located. An improved approach might consist of giving weights to the rock mass quality for different locations dependent on their respective contribution to the inflow. For such an approach to be feasible, the conditions along the bore hole should be logged with more detailed results.

One should not disregard the limitation to the Q-system itself. The rock mass classification system is intended to be used for the stability of underground constructions. Its applicability for statistical analysis of groundwater inflow is therefore questioned. Finally, the categorization of the rock mass with a Q-value is subjective and depends on the perception of the person investigating the rock mass.

## **9.2.2 MLR model of grout take and rock mass parameters**

The results from the MLR model show that the fit of the data does not explain the variation of the response variable well. The coefficient of determination is 0.08, and is consequently well below 1. Further, the coefficients of the covariates have a high standard deviation. This indicates the relatively large uncertainty related to how the covariates influence the response variable. Within a 95 % confidence interval,  $J_w$  and  $J_a$  can both have a positive or a negative effect on the grout take. From these observations, the multiple linear regression model does not seem to be a suit-

able approach for explaining the grout take.

The diagnostics of the model put limitations to the credibility of the information one can extract from the regression. Considering the backward regression, it seems that the  $SRF$ ,  $RQD$  and  $J_n$  have a small influence on the grout take. From the model it was found that the joint roughness had a relatively low significance to the model with a p-value of 0.369. Since the grout material penetrates discontinuities it could be thought that a more fractured rock mass would be associated with higher grout takes. However joint conditions such as aperture and roughness can also influence the grout consumption. For instance, many discontinuities with small aperture can give a lower grout take than a single joint with a significant aperture.

The results show that the alteration of the joints,  $J_w$  and the overburden have the highest p-value based on this data set. Of these covariates,  $J_a$  is most likely to have an influence on the model. The positive correlation between  $J_a$  and the grout take indicates that higher values of joint alteration gives a higher grout take. This was also an observation by Strømsvik (2019) in her studies of grout take in selected Norwegian tunnelling projects. Since weathering of the joint surfaces and infill material in the void space tend to seal the discontinuities, this is regarded as a somewhat surprising result. However, the resistance to the flow of grout in discontinuities is assumed to also be dependent on the type of infill material.

A lower value of  $J_w$  indicates a higher amount of water dripping or flowing into the structure after excavation. It is natural that locations having a lower joint water reduction factor and higher inflows can be locations where it has been necessary to grout the rock mass.

### **Limitations to the model**

When describing the data set it was found that the distribution of grout takes deviated from a normal distribution and the residuals of the model failed to fulfill the Shapiro-Wilk test for normality. The response variable was then log-transformed, an approach also followed by Nia et al. (2016) in a similar analysis. However, Changyong et al. (2014) have indicated the shortcomings that this approach can have. They argue that log-transforming the response variable should be avoided since the approach in some cases will not make the data more normal. The influence on log-transforming the variable to the model is not discussed in depth here, but must be regarded as a possible limitation to the analysis.

Though the presented model fulfills the normality assumption of the residuals and homoscedasticity, the model is without poor in respect to expressing a relation between the covariates and the grout take. A coefficient of determination of 0.08 indicates a weak correlation. Further, the

covariates generally have a high p-value (above 0.05) and their influence on the model can therefore also be challenged. Other parameters not considered in this model can have a greater effect on the grout take. The applied grout pressure drives the grout penetration in discontinuities and is consequently considered as a parameter that should have been included. Unfortunately, the final grouting pressure has only been available for some pre-grouting rounds. The parameters was consequently not included. Finally, other statistical model could be more appropriate for analysing this data set. For instance, non-linear regression models are available and could possibly have been used.

# Conclusions and recommendations

## 10.1 Conclusions

This master thesis has included an analysis using empirical methods for two tunnel segments of the Storåvatn HPP. Statistical methods have also been applied to compare certain rock mass parameters to the experienced groundwater inflows in both Smibelg and Storåvatn hydro power project. The statistical analysis related to the groundwater inflows also included the application of a semi-analytical approach. To investigate potential dependencies between the rock mass parameters and the experienced grout consumptions in the project, a model using multiple linear regression was developed. Further, the master thesis has also consisted of systematic data gathering from the project and presenting the results in a model using ArcGIS Pro.

- The analysis shows that the discontinuities related to the high water inflows in the tunnel have a steep dip and could originate from processes generating pinnate fissures in the rock mass.
- Unexpectedly high grout takes have been observed in the project. The analysis indicates that the orientation and character of discontinuities make the grouting process challenging. Industry cement seems to be the most adequate cement type for grouting with respect to the rock mass conditions in two analyzed tunnel segments. An increased use of accelerating additives is a measure that could potentially have reduced the grout takes.
- Application of a semi-analytical approach proposed by Panthi (2006) generally seems to overestimate the water inflows. At certain locations of the Storåvatn head race tunnel, the estimates correspond fairly well with the actual inflow rates.
- In a statistical comparison between rock mass parameters and groundwater inflow quan-

---

tities, a weak correlation is observed for parameters regarding rock mass quality by the Q-system. There is a tendency that the water inflow quantities increase with increasing rock overburden.

- A multiple linear regression model between grout takes in pre-grouting rounds and different rock mass parameters indicate that  $J_a$ ,  $J_w$  and the rock overburden have the greatest influence to the model. However, the MLR model does not give a satisfactory fit to the data. Other statistical models and/or other parameters could be used to give a better prediction of the grout consumption.

## 10.2 Recommendations for further work/research

This thesis has focused on which parameters, relevant for the rock mass, control the amount of water inflow and the grout takes experienced in the SmiSto hydro power project. Uncertainties are associated with the methodologies that have been used. An improvement for the analysis could consist of applying a methodology where the rock mass quality for different segments of a bore hole is weighted depending on the amount of water inflow experienced. A similar approach would not be possible for the analysis regarding grout take, since it is generally unknown how the grout propagates in the rock mass.

For further research on the topic it could be interesting to apply similar statistical methods to other tunneling projects. Methods related to the dependency between similar measurement locations (e.g. by geostatistics) could also be of interest. Since the grout take depends on factors related to the grouting process itself, a similar analysis should include measurements of the applied grout pressure and the applied w/c-ratio if available. The dependency of grout take and different cement materials could also be an interesting relationship to analyze.

Finally the results from the study indicates that discontinuities oriented in mean angles to nearby tectonic faults, have been related to joints with significant potential for water inflow in the tunnel. The water-conducting discontinuities are steep, persistent and are located in rocks with high strength and stiffness. In future tunneling projects where similar observations are made, considerable water inflows may be encountered. In these cases, the characteristics should be analyzed to investigate the hold of this theory, proposed almost 40 years ago.

# Bibliography

- Aasen, O. and Lunde, M. (2017) Optimised Design and Construction of Norwegian Underground Hydro Schemes: a case study of the Smisto Hydropower Project.
- Babiker, M. and Gudmundsson, A. (2004) The effects of dykes and faults on groundwater flow in an arid land: the Red Sea Hills, Sudan. *Journal of Hydrology* 297(1), pp. 256–273. ISSN: 0022-1694. DOI: <https://doi.org/10.1016/j.jhydrol.2004.04.018>.
- Bane NOR (2019) *Teknisk Regelverk - Tunneler, Portaler og vannsikring*. URL: [https://trv.banenor.no/wiki/Tunneler/Prosjektering\\_og\\_bygging/Portaler\\_og\\_vannsikring](https://trv.banenor.no/wiki/Tunneler/Prosjektering_og_bygging/Portaler_og_vannsikring).
- BASF (2011) *Pre-Excavation Grouting in Rock Tunneling*.
- Black, J. H. (1987) Flow and flow mechanisms in crystalline rock. *Geological Society, London, Special Publications* 34(1), pp. 185–200. ISSN: 0305-8719. DOI: 10.1144/GSL.SP.1987.034.01.13.
- Blindheim, O. T. and Øvstedal, E. (n.d.) Design Principles And Construction Methods For Water Control In Subsea Road Tunnels In Rock. In: *Publication 12*.
- Braathen, A. and Gabrielsen, R. (2000) Bruddsoner i fjell - oppbygning og definisjoner. *Gråsteinen* 7.
- Brekkhuis, A. (2015) *Hæhre med stor kraftjobb i Nordland*. Visited: 16.09.19. URL: <http://www.bygg.no/article/1238600>.
- Carlsson, A. and Olsson, T. (1977) Variations of hydraulic conductivity in some Swedish rock types. In: *Proceedings of International Symposium Rockstore*, pp. 257-263.
- Changyong, F., Hongyue, W., Naiji, L., Tian, C., Hua, H., Ying, L., et al. (2014) Log-transformation and its implications for data analysis. *Shanghai archives of psychiatry* 26(2), p. 105.

- 
- Craney, T. and Surles, J. (2002) Model-dependent variance inflation factor cutoff values. English. *Quality Engineering* 14(3), pp. 391–403. ISSN: 0898-2112.
- D'Agostino, R. and Stephens, M. (1986) *Tests for Normal Distribution in Goodness-Of-Fit Techniques*.
- Davik, K. I., Kveen, A., Aasen, O., Åndal, T., Kjølberg, R., and Heimli, P. (2002) *Berginjeksjon, Håndbok nr. 1*.
- El Tani, M. (2003) Circular tunnel in a semi-infinite aquifer. *Tunnelling and Underground Space Technology* 18(1), pp. 49–55. ISSN: 0886-7798. DOI: [https://doi.org/10.1016/S0886-7798\(02\)00102-5](https://doi.org/10.1016/S0886-7798(02)00102-5).
- Epifani, I. (2016) Multiple Linear Regression. Presentation slides. *Politecnico di Milano*. Milan, Italy.
- Muskat, M. (1937) *Flow of homogeneous fluids through porous media*. English. R. Muskat M.; Wyckoff (red.). New York, NY, United States.
- Fossen, H., Pedersen, R.-B., Bergh, S., and Andresen, A. (2013) *Landet blir til: Norges geologi*. nor. In: 2. utg. Trondheim: Norsk geologisk forening. Chap. 6 En fjellkjede blir til, pp. 182–233. ISBN: 9788292394830.
- Ganerød, G. V., Braathen, A., and Willemoes-Wissing, B. (2008) Predictive permeability model of extensional faults in crystalline and metamorphic rocks; verification by pre-grouting in two sub-sea tunnels, Norway. *Journal of Structural Geology* 30(8), pp. 993 - 1004. ISSN: 0191-8141. DOI: <https://doi.org/10.1016/j.jsg.2008.04.001>.
- Gong, B., Jiang, Y., Okatsu, K., Wu, X., Teduka, J., and Aoki, K. (2018) The Seepage Control of the Tunnel Excavated in High-Pressure Water Condition Using Multiple Times Grouting Method. *Processes* 6(9), p. 159.
- Goodman, R. E., Moye, D. G., VanSchalkwyk, A., and Javandel, I. (1965) Ground water inflows during tunnel driving. English. *Engineering Geology (Sacramento, Calif.)* 2(1), pp. 39–56. ISSN: 0094-923X.
- Gustafson, G. (2009) *Hydrogeologi för bergbyggare*. swe. Stockholm.
- Hadi, F. and Homayoon, K. (2017) New empirical model to evaluate groundwater flow into circular tunnel using multiple regression analysis. *International Journal of Mining science and Technology*.
- Hassani, A., Katibeh, H., and Farhadian, H. (2016) Numerical analysis of steady-state groundwater inflow into Tabriz line 2 metro tunnel, northwestern Iran, with special consideration



- 
- of model dimensions. English. *Bulletin of Engineering Geology and the Environment* 75(4), pp. 1617–27. ISSN: 1435-9529.
- Haugerud, H. (2019) Evaluation of geologic conditions and groundwater inflow in tunnels near Gjervalen, Nordland. English.
- Hognestad, H. O., Fagerbo, J. I., Kveen, A., Backer, L., Grøv, E., Frogner, E., and Aarset, A. (2010) *Håndbok nr. 06: Praktisk berginjeksjon for underjordsanlegg*.
- Hognestad, H. O., Fagermo, J. I., Kveen, A., Backer, L., Grøv, E., Frogner, E., and Aarset, A. (2011) *Rock Mass Grouting*. Norsk Forening for Fjellsprengningsteknikk.
- Holmøy, K. (2008) *Significance of Geological Parameters for Predicting Water Leakage in Hard Rock Tunnels*. PhD thesis. Norwegian University of Science and Technology.
- Hudson, J. A. and Harrison, J. P. (2000) *Engineering rock mechanics: an introduction to the principles*. Elsevier.
- Johansen, E. O. (2019) *Oral communication*.
- Karlsrud, K. (2001) Control of water leakage when tunnelling under urban areas in the Oslo region. In: *NFF Publication 12: Water control*.
- Keating, J. and Leung, M. (2010) Bartlett's Test. In: pp. 61–64. ISBN: 1412961270.
- Klüver, B. H. (2000) *Berginjeksjon*. 2151, p. 23.
- Klüver, B. H. and Kveen, A. (2004) *SVV Publikasjon nr 104: Berginjeksjon i praksis*.
- Kolymbas, D. and Wagner, P. (2007) Groundwater ingress to tunnels – The exact analytical solution. *Tunnelling and Underground Space Technology* 22(1), pp. 23–27. ISSN: 0886-7798. DOI: <https://doi.org/10.1016/j.tust.2006.02.001>.
- Kveen, A. and Lindstrøm, M. (2005) Publication no. 107: Tunnel investigation and groundwater control.
- Lien, J. E., Lillevik, S., Mehlum, A., and Soknes, S. (2000) Frøytatunnelen - Fra geologisk kartlegging til ferdig tunnel. *Fjellsprengningsdagen*.
- Lindholm, C. (2019) Earthquakes in Norway. *Fjellsprengningskonferansen 2019*, pp. 8.1–8.13.
- Løset, F. (1981) Geological engineering experience from the sewage tunnel Lysaker - Slemmestad. Norwegian. *Rock Blasting Conference, Norwegian Tunnelling Association*, pp. 31.1–31.11.
- Lunde, M. and Lie, V. (2013) *Report: Smibelg HPP and Storåvatn HPP*. Tech. rep. Multiconsult.
-

- 
- Moon, J. and Fernandez, G. (2010) Effect of Excavation-Induced Groundwater Level Drawdown on Tunnel Inflow in a Jointed Rock Mass. *Engineering Geology* 110(3), pp. 33–42. ISSN: 0013-7952. DOI: <https://doi.org/10.1016/j.enggeo.2009.09.002>.
- Multiconsult (n.d.) *Smisto hydro power project*. Online. Available at <https://www.multiconsult.no/prosjekter/smisto-kraftverk/>. Visited: 05.03.19.
- Myrvang, A. (2001) *Rock Mechanics, University Compendium*. Norwegian University of Science and Technology.
- Nelson, S. A. (2012) Chapter 5 - Minerals. In: *Physical Geology, Lecture Notes*.
- NGU (n.d.) *Geological map*. Online. Downloaded from: [www.ngu.no](http://www.ngu.no). Visited at: 27.04.19.
- Nia, A. R., Lashkaripour, G. R., and Ghafoori, M. (2016) Prediction of grout take using rock mass properties. *Bulletin of Engineering Geology and the Environment* 76(4), pp. 1643–1654. DOI: 10.1007/s10064-016-0956-5.
- Nilsen, B. (2016) *Ingeniørgeologi Berg, Grunnkurskompendium*.
- Nilsen, B. and Palmström, A. (2000) *Engineering Geology and Rock Engineering*. 2nd ed. Norwegian Group for Rock Mechanics (NBG). ISBN: 82-91341-33-8.
- Norwegian Geotechnical Institute (2015) *Bruk av Q-systemet: bergmasseklassifisering og bergforsterkning*.
- Olive, D. J. (2010) Multiple linear and 1D regression. Available on <http://www.math.siu.edu/olive/regbk.htm>.
- Palmström, A. (1995) *RMi - a rock mass characterization system for rock engineering purposes*. PhD thesis. University of Oslo.
- Palmstrom, A. and Broch, E. (2006) Use and misuse of rock mass classification systems with particular reference to the Q-system. *Tunnelling and Underground Space Technology* 21(6), pp. 575–593. ISSN: 0886-7798. DOI: <https://doi.org/10.1016/j.tust.2005.10.005>.
- Panthi, K. (2006) *Analysis of Engineering Geological Uncertainties Related to Tunnelling in Himalayan Rock Mass Conditions*. PhD thesis.
- Panthi, K. (2010) *Note on specific leakage using Panthi's approach*.
- Panthi, K. (2013) Pre-injection versus post-injection grouting - A review of a case from the Himalaya. In: vol. 4.
- Panthi, K. and Basnet, C. (2019) Leakage potential through a shotcrete lined high-pressure head-race tunnel - An analysis on a case from Nepal. In:
-

- 
- Panthi, K. and Nilsen, B. (2010) Uncertainty Analysis for Assessing Leakage Through Water Tunnels: A Case from Nepal Himalaya. *Rock Mechanics and Rock Engineering* 43, pp. 629–639. DOI: 10.1007/s00603-009-0075-8.
- Perktold, J., Seabold, S., and Taylor, J. (2009) *Statsmodels - Statistics in Python*. Visited: 07.12.2019. URL: <https://www.statsmodels.org/stable/index.html>.
- Pratt, H., Swolfs, H., Brace, W., Black, A., and Handin, J. (1977) Elastic and transport properties of an in situ jointed granite. *International Journal of Rock Mechanics and Mining Sciences & Geomechanics Abstracts* 14(1), pp. 35–45. ISSN: 0148-9062. DOI: [https://doi.org/10.1016/0148-9062\(77\)90560-5](https://doi.org/10.1016/0148-9062(77)90560-5).
- Qvale, H., Qvale, G., and Gjelle, S. (2012) *Bedrock map of Sjøna 1927 IV, M 1:50 000*.
- Rafi, J. Y. and Stille, H. (2014) Control of rock jacking considering spread of grout and grouting pressure. *Tunnelling and Underground Space Technology* 40, pp. 1–15. ISSN: 0886-7798. DOI: <https://doi.org/10.1016/j.tust.2013.09.005>.
- Rohr-Torp, E. (1994) Present uplift rates and groundwater potential in Norwegian hard rocks. *Geological Survey of Norway*.
- Ross, S. M. (2004) *Introduction to probability and statistics for engineers and scientists*. Elsevier Academic Press. ISBN: 0-12-598057-4.
- Selmer-Olsen, R. (1981) Considerations of large water leakages in deep-seated tunnels. *Rock Blasting Conference 1981*, pp. 173-187.
- Singhal, B. (2010) *Applied Hydrogeology of Fractured Rocks: Second Edition*. Springer. ISBN: 978-90-481-8799-7.
- SINTEF (2016) *Rock stress measurements at SmiSto. Hydraulic jacking test results*.
- Statens Vegvesen (2016) *N500 - Vegtunneler*.
- Stille, H. (2015) *Rock Grouting - Theories and Applications*. Vulkan Förlag. ISBN: 978-91-637-7638-0.
- Strømsvik, H. (2019) The significance of hydraulic jacking for grout consumption during high pressure pre-grouting in Norwegian tunnelling. *Tunnelling and Underground Space Technology* 90, pp. 357–368. ISSN: 0886-7798. DOI: <https://doi.org/10.1016/j.tust.2019.05.014>.
- Thomas, D., Mendez, H., Kripal, C., and Ataollah, R. (2016) Advanced seismic investigations during construction of hydro tunnels. In: *Recent Advances in Rock Engineering (RARE 2016)*. Atlantis Press. ISBN: 978-94-6252-260-2. DOI: <https://doi.org/10.2991/rare-16.2016.24>.
-

---

Zarei, H., Uromeihy, A., and Sharifzadeh, M. (2011) Evaluation of high local groundwater inflow to a rock tunnel by characterization of geological features. *Tunnelling and Underground Space Technology* 26(2), pp. 364 - 373. ISSN: 0886-7798. DOI: <https://doi.org/10.1016/j.tust.2010.11.007>.

---

# Appendices



Appendix **A**

## The Q-system (NGI, 2015)

Table 1 RQD-values and volumetric jointing.

1 RQD (Rock Quality Designation)			RQD
A	Very poor	(> 27 joints per m <sup>3</sup> )	0-25
B	Poor	(20-27 joints per m <sup>3</sup> )	25-50
C	Fair	(13-19 joints per m <sup>3</sup> )	50-75
D	Good	(8-12 joints per m <sup>3</sup> )	75-90
E	Excellent	(0-7 joints per m <sup>3</sup> )	90-100
Note: i) Where RQD is reported or measured as ≤ 10 (including 0) the value 10 is used to evaluate the Q-value ii) RQD-intervals of 5, i.e. 100, 95, 90, etc., are sufficiently accurate			

 Table 2 J<sub>n</sub> – values.

2 Joint set number		J <sub>n</sub>
A	Massive, no or few joints	0,5-1.0
B	One joint set	2
C	One joint set plus random joints	3
D	Two joint sets	4
E	Two joint sets plus random joints	6
F	Three joint sets	9
G	Three joint sets plus random joints	12
H	Four or more joint sets, random heavily jointed "sugar cube", etc	15
J	Crushed rock, earth like	20
Note: i) For tunnel intersections, use 3 x J <sub>n</sub> ii) For portals, use 2 x J <sub>n</sub>		



Table 3  $J_r$  – values.

3 Joint Roughness Number		$J_r$
<b>a) Rock-wall contact, and</b>		
<b>b) Rock-wall contact before 10 cm of shear movement</b>		
A	Discontinuous joints	4
B	Rough or irregular, undulating	3
C	Smooth, undulating	2
D	Slickensided, undulating	1,5
E	Rough, irregular, planar	1,5
F	Smooth, planar	1
G	Slickensided, planar	0,5
Note: i) Description refers to small scale features and intermediate scale features, in that order		
<b>c) No rock-wall contact when sheared</b>		
H	Zone containing clay minerals thick enough to prevent rock-wall contact when sheared	1
Note: ii) Add 1 if the mean spacing of the relevant joint set is greater than 3 m (dependent on the size of the underground opening)		
iii) $J_r = 0,5$ can be used for planar slickensided joints having lineations, provided the lineations are oriented in the estimated sliding direction		

Table 4  $J_a$  – values.

4 Joint Alteration Number		$\Phi_r$ approx.	$J_a$
<b>a) Rock-wall contact (no mineral fillings, only coatings)</b>			
A	Tightly healed, hard, non-softening, impermeable filling, i.e., quartz or epidote.		0.75
B	Unaltered joint walls, surface staining only.	25-35°	1
C	Slightly altered joint walls. Non-softening mineral coatings; sandy particles, clay-free disintegrated rock, etc.	25-30°	2
D	Silty or sandy clay coatings, small clay fraction (non-softening).	20-25°	3
E	Softening or low friction clay mineral coatings, i.e., kaolinite or mica. Also chlorite, talc gypsum, graphite, etc., and small quantities of swelling clays.	8-16°	4
<b>b) Rock-wall contact before 10 cm shear (thin mineral fillings)</b>			
F	Sandy particles, clay-free disintegrated rock, etc.	25-30°	4
G	Strongly over-consolidated, non-softening, clay mineral fillings (continuous, but <5 mm thickness).	16-24°	6
H	Medium or low over-consolidation, softening, clay mineral fillings (continuous, but <5 mm thickness).	12-16°	8
J	Swelling-clay fillings, i.e., montmorillonite (continuous, but <5 mm thickness). Value of $J_a$ depends on percent of swelling clay-size particles.	6-12°	8-12
<b>c) No rock-wall contact when sheared (thick mineral fillings)</b>			
K	Zones or bands of disintegrated or crushed rock. Strongly over-consolidated.	16-24°	6
L	Zones or bands of clay, disintegrated or crushed rock. Medium or low over-consolidation or softening fillings.	12-16°	8
M	Zones or bands of clay, disintegrated or crushed rock. Swelling clay. $J_a$ depends on percent of swelling clay-size particles.	6-12°	8-12
N	Thick continuous zones or bands of clay. Strongly over-consolidated.	12-16°	10
O	Thick, continuous zones or bands of clay. Medium to low over-consolidation.	12-16°	13
P	Thick, continuous zones or bands with clay. Swelling clay. $J_a$ depends on percent of swelling clay-size particles.	6-12°	13-20

Table 5  $J_w$  – values.

5 Joint Water Reduction Factor		$J_w$
A	Dry excavations or minor inflow ( humid or a few drips)	1.0
B	Medium inflow, occasional outwash of joint fillings (many drips/“rain”)	0,66
C	Jet inflow or high pressure in competent rock with unfilled joints	0.5
D	Large inflow or high pressure, considerable outwash of joint fillings	0,33
E	Exceptionally high inflow or water pressure decaying with time. Causes outwash of material and perhaps cave in	0.2-0.1
F	Exceptionally high inflow or water pressure continuing without noticeable decay. Causes outwash of material and perhaps cave in	0,1-0,05
Note: i) Factors C to F are crude estimates. Increase $J_w$ if the rock is drained or grouting is carried out ii) Special problems caused by ice formation are not considered		

Table 6 SRF-values.

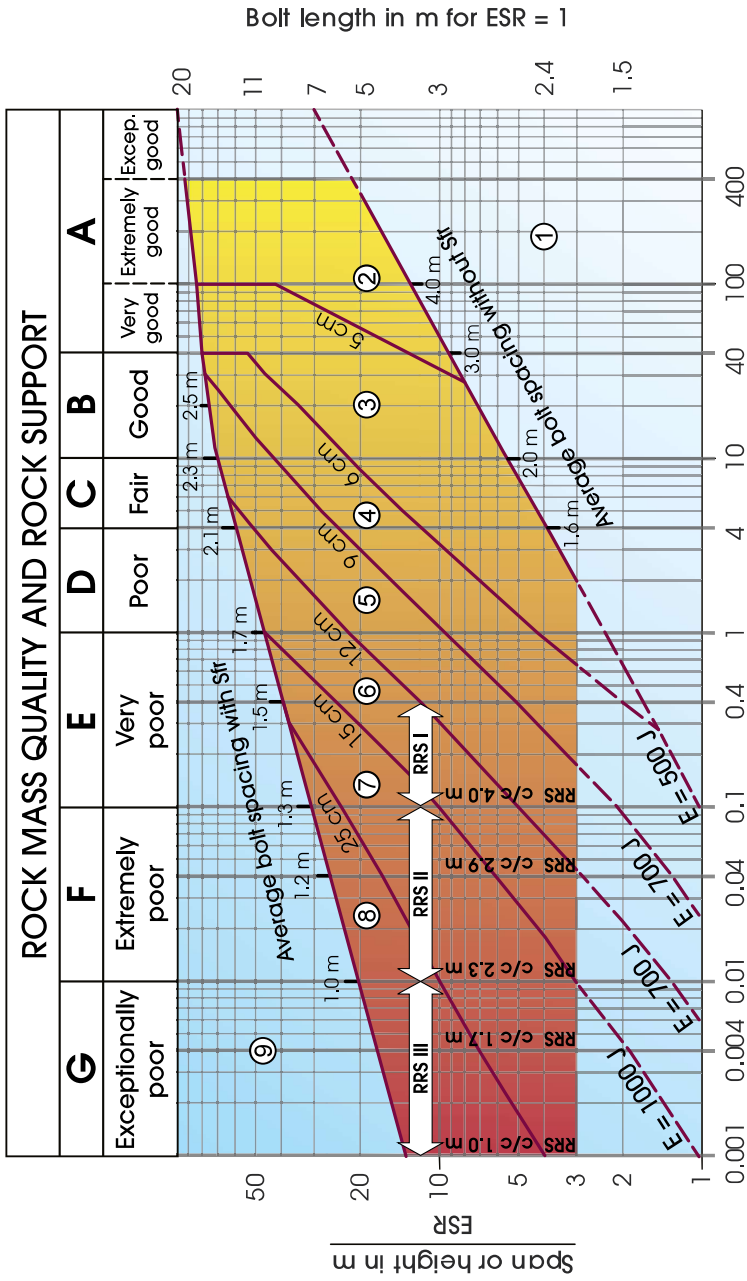
6 Stress Reduction Factor		SRF		
<b>a) Weak zones intersecting the underground opening, which may cause loosening of rock mass</b>				
A	Multiple occurrences of weak zones within a short section containing clay or chemically disintegrated, very loose surrounding rock (any depth), or long sections with incompetent (weak) rock (any depth). For squeezing, see 6L and 6M	10		
B	Multiple shear zones within a short section in competent clay-free rock with loose surrounding rock (any depth)	7.5		
C	Single weak zones with or without clay or chemical disintegrated rock (depth $\leq$ 50m)	5		
D	Loose, open joints, heavily jointed or "sugar cube", etc. (any depth)	5		
E	Single weak zones with or without clay or chemical disintegrated rock (depth $>$ 50m)	2.5		
Note: i) Reduce these values of SRF by 25-50% if the weak zones only influence but do not intersect the underground opening				
<b>b) Competent, mainly massive rock, stress problems</b>		$\sigma_c / \sigma_1$	$\sigma_0 / \sigma_c$	<b>SRF</b>
F	Low stress, near surface, open joints	$>200$	$<0.01$	2.5
G	Medium stress, favourable stress condition	200-10	0.01-0.3	1
H	High stress, very tight structure. Usually favourable to stability. May also be unfavourable to stability dependent on the orientation of stresses compared to jointing/weakness planes*	10-5	0.3-0.4	0.5-2 2-5*
J	Moderate spalling and/or slabbing after $>$ 1 hour in massive rock	5-3	0.5-0.65	5-50
K	Spalling or rock burst after a few minutes in massive rock	3-2	0.65-1	50-200
L	Heavy rock burst and immediate dynamic deformation in massive rock	$<2$	$>1$	200-400
Note: ii) For strongly anisotropic virgin stress field (if measured): when $5 \leq \sigma_1 / \sigma_3 \leq 10$ , reduce $\sigma_c$ to $0.75 \sigma_c$ . When $\sigma_1 / \sigma_3 > 10$ , reduce $\sigma_c$ to $0.5 \sigma_c$ , where $\sigma_c$ = unconfined compression strength, $\sigma_1$ and $\sigma_3$ are the major and minor principal stresses, and $\sigma_0$ = maximum tangential stress (estimated from elastic theory)				
iii) When the depth of the crown below the surface is less than the span; suggest SRF increase from 2.5 to 5 for such cases (see F)				
<b>c) Squeezing rock: plastic deformation in incompetent rock under the influence of high pressure</b>		$\sigma_0 / \sigma_c$	<b>SRF</b>	
M	Mild squeezing rock pressure	1-5	5-10	
N	Heavy squeezing rock pressure	$>5$	10-20	
Note: iv) Determination of squeezing rock conditions must be made according to relevant literature (i.e. Singh et al., 1992 and Bhasin and Grimstad, 1996)				
<b>d) Swelling rock: chemical swelling activity depending on the presence of water</b>		<b>SRF</b>		
O	Mild swelling rock pressure	5-10		
P	Heavy swelling rock pressure	10-15		

Table 7 ESR-values.

7 Type of excavation		ESR
A	Temporary mine openings, etc.	ca. 3-5
B	Vertical shafts*: i) circular sections ii) rectangular/square section * Dependant of purpose. May be lower than given values.	ca. 2,5 ca. 2,0
C	Permanent mine openings, water tunnels for hydro power (exclude high pressure penstocks) water supply tunnels, pilot tunnels, drifts and headings for large openings.	1,6
D	Minor road and railway tunnels, surge chambers, access tunnels, sewage tunnels, etc.	1,3
E	Power houses, storage rooms, water treatment plants, major road and railway tunnels, civil defence chambers, portals, intersections, etc.	1,0
F	Underground nuclear power stations, railways stations, sports and public facilities, factories, etc.	0,8
G	Very important caverns and underground openings with a long lifetime, $\approx$ 100 years, or without access for maintenance.	0,5

Table 8 Conversion from actual Q-values to adjusted Q-values for design of wall support.

In rock masses of good quality	$Q > 10$	Multiply Q-values by a factor of 5.
For rock masses of intermediate quality	$0.1 < Q < 10$	Multiply Q-values by a factor of 2.5. In cases of high rock stresses, use the actual Q-value.
For rock masses of poor quality	$Q < 0.1$	Use actual Q-value.



$$\text{Rock mass quality } Q = \frac{RQD}{J_n} \times \frac{J_r}{J_a} \times \frac{J_w}{SRF}$$

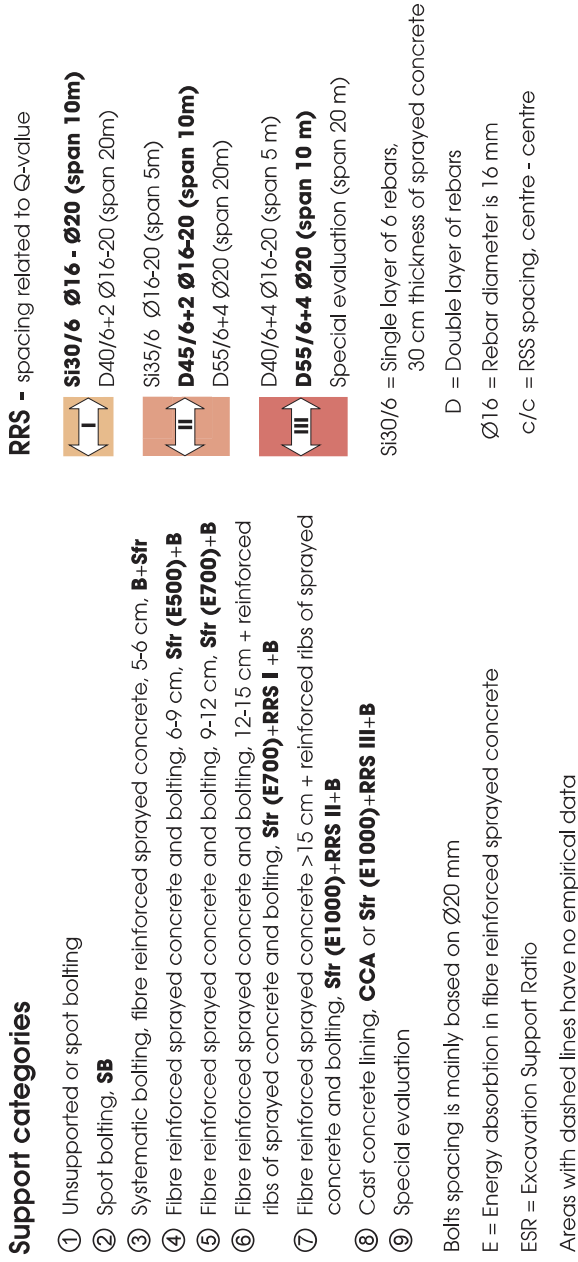


Figure 7 Permanent support recommendations based on Q-values and span/ESR.






Appendix **B**

## Typical documentation

# B.1 Probe drilling results



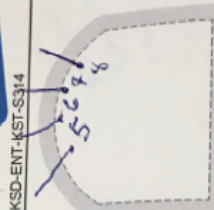
Dok nr. FSC3-KSD-ENT-KST-S314

Siste rev. 02.02.2017    Ansv. RSL

Prosjekt | Stuff:

Sonderborring nr.	
Peil nr	1/9
Lengde	3013
Antall hull	24
Hulldiameter	64
Start ki:	
Stopp ki:	

Anmerking



Hull nr	0 - 3 m	3 - 6 m	6 - 9 m	9 - 12 m	12 - 15 m	15 - 18 m	18 - 21 m	21 - 24 m	24 - 27 m	27 - 30 m
Hull 5										
Farge	G	G/B	B	G/B	G/B	G	G	G		
Borsynk	2,3	2,4	2,7	1,3	1,7	1,7	1,6	1,5		
Vann		ca 20L								
Spesielle forhold		ca 4M	SLEPPE ca 7,5M							
Hull 6										
Farge	G	G/B	G/B	G	G	G				
Borsynk	2,4	2,5	1,7	1,7	1,7					
Vann		VANN								
Spesielle forhold		SLEPPE ca 4,5M	HÆHRE VANN							
Hull 7										
Farge	G	G/B	G/B	G/B	G/B	G/B	G/B	G/B		
Borsynk	2,2	2,0	1,6	1,7	1,6	1,6	1,7	1,9		
Vann		Vann								
Spesielle forhold		ca 4,5m	Flere brønsløper innover						totalt ca 30L	
Hull 8										
Farge	G	G/B	G/B	G/B	G/B	G/B	G/B	G/B		
Borsynk	2,0	1,8	1,7	1,7	1,8	1,8	1,8	1,8		
Vann										
Spesielle forhold			Flere brønsløper innover						totalt ca 10L	

Sign. byggherre:

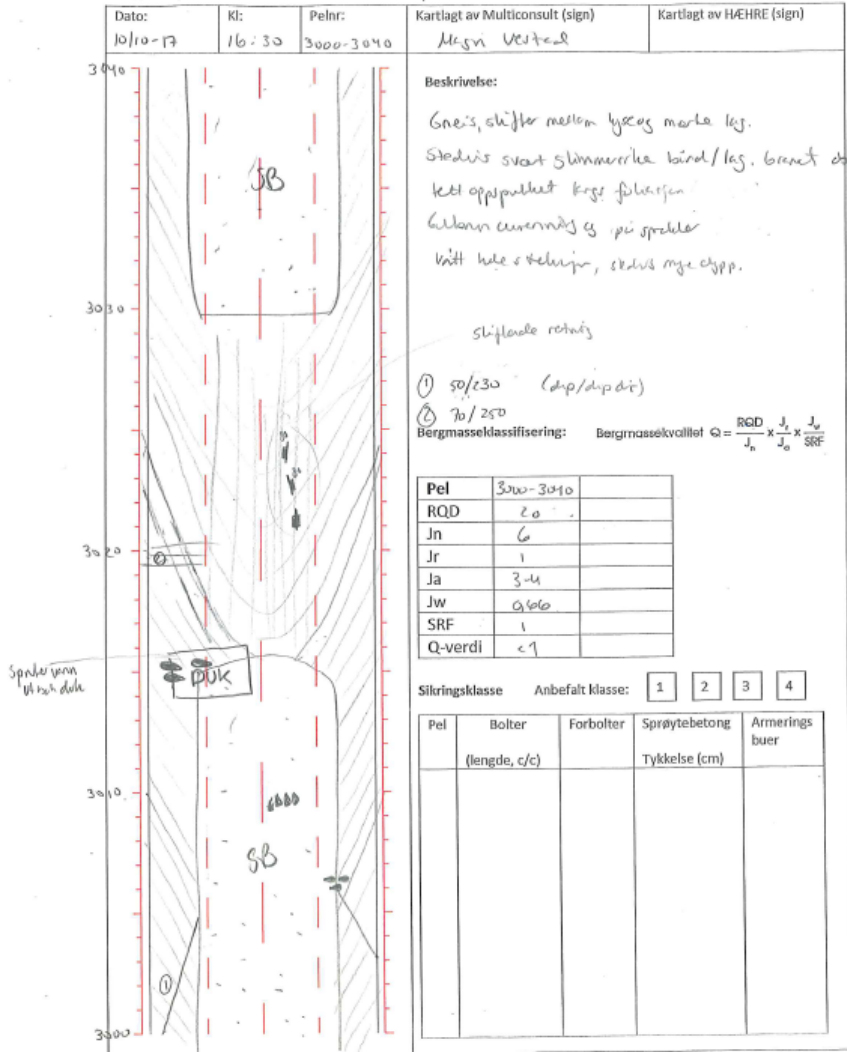
Sign. entreprenør:

## B.2 Engineering geological mapping

### GEOLOGISK KARTLEGGING OG KLASSIFISERING

Smisto Kraftverk

Tunneldel/stuff: *Sandstikkveien tilleg*



## B.3 Rock mass grouting

Forøtaksystem FS-System Kvalitet i prosjekt			<b>HÆHRE</b>		
Injeksjonsapparat			DOK. Nr FS03-KSD-ENT-KST-5312		
Osikjenner:	Faglig ansvarlig:	Utarbeidet dato	Side 1 av 1		
Gystein Birkeland	Rune S. Lien	08.11.11			
Adm. og publisering:	Oppdatert av	Rev. Dato	Ref. ISO-ent		
MR/AG	MR/EH	02.02.2017			

Prosjekt:	Stoa i vater	Stuff:	Hovedkyp
-----------	--------------	--------	----------

Injeksjon nr.	Start		Slutt		Pel nr.:
	Dato	Kl.	Dato	Kl.	
	09.08	0000	09.08.	1200	8013

Ant. hull:	5	Borelengde [m]:	12-18m	Hulldiam. [mm]:	64	Tverrsnitt [m <sup>2</sup> ]:	20
------------	---	-----------------	--------	-----------------	----	-------------------------------	----

Prosess	Beskrivelse	Mengde	Enh.	Prosess	Beskrivelse	Mengde	Enh.
	Bormeter	78m	[m]		Spesial type Mauring.		[kg]
	Opp/nedlegg	16	[stk]		Polystyren		[kg]
	Pakkeplassering	5	[stk]		Silikaslurry (Groutech)		[kg]
	Ekstra pakker plasseringer	3	[stk]		Dynamon SX-N		[kg]
	Industriemønt	12000	[kg]		Pumpetid	12t	[time]
	Inj sømønt type Styrt herding.		[kg]		Ekstra leredetid	6t	[time]

Anmerkninger:

Hull nr.	1	2	3	4	5	6	7	8	9	10
Kg:	500	4000	500	500	6500					

Dato:	13.08.	Sign.:	<i>[Signature]</i>
-------	--------	--------	--------------------

2017 C:\Users\2288\AppData\Local\Microsoft\Windows\Temporary Internet Files\Content.Outlook\5UFP42ZE\F803-KSD-ENT-KST-5312\Injeksjonsapparat\mssheet.docx

Side 1 av 1

Appendix **C**

## SmiSto - ArcGIS Pro model

---

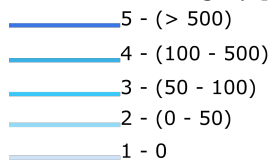
## C.1 Legend

### Results

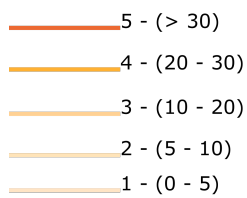
#### Rock mass quality (Q-value)



#### Water inflow category [l/min]

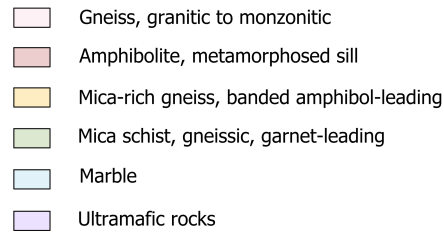


#### Grouting category [tonnes]



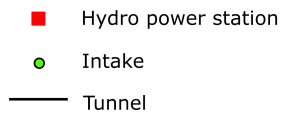
### Geology

#### Main rock types



—▲— Fault

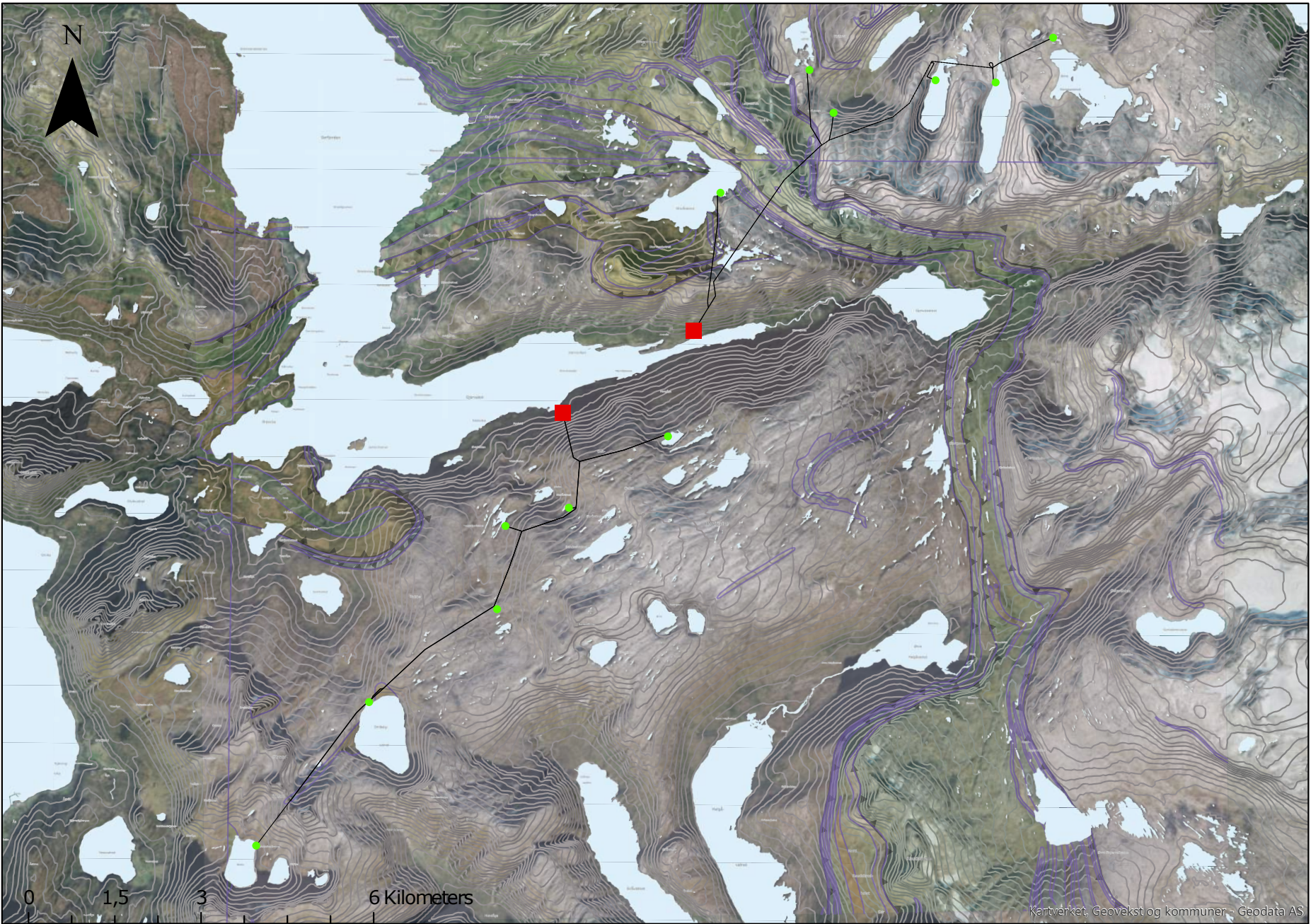
#### Tunnel system



Contour interval on maps= 5m

---

## **C.2 SmiSto overview**



N

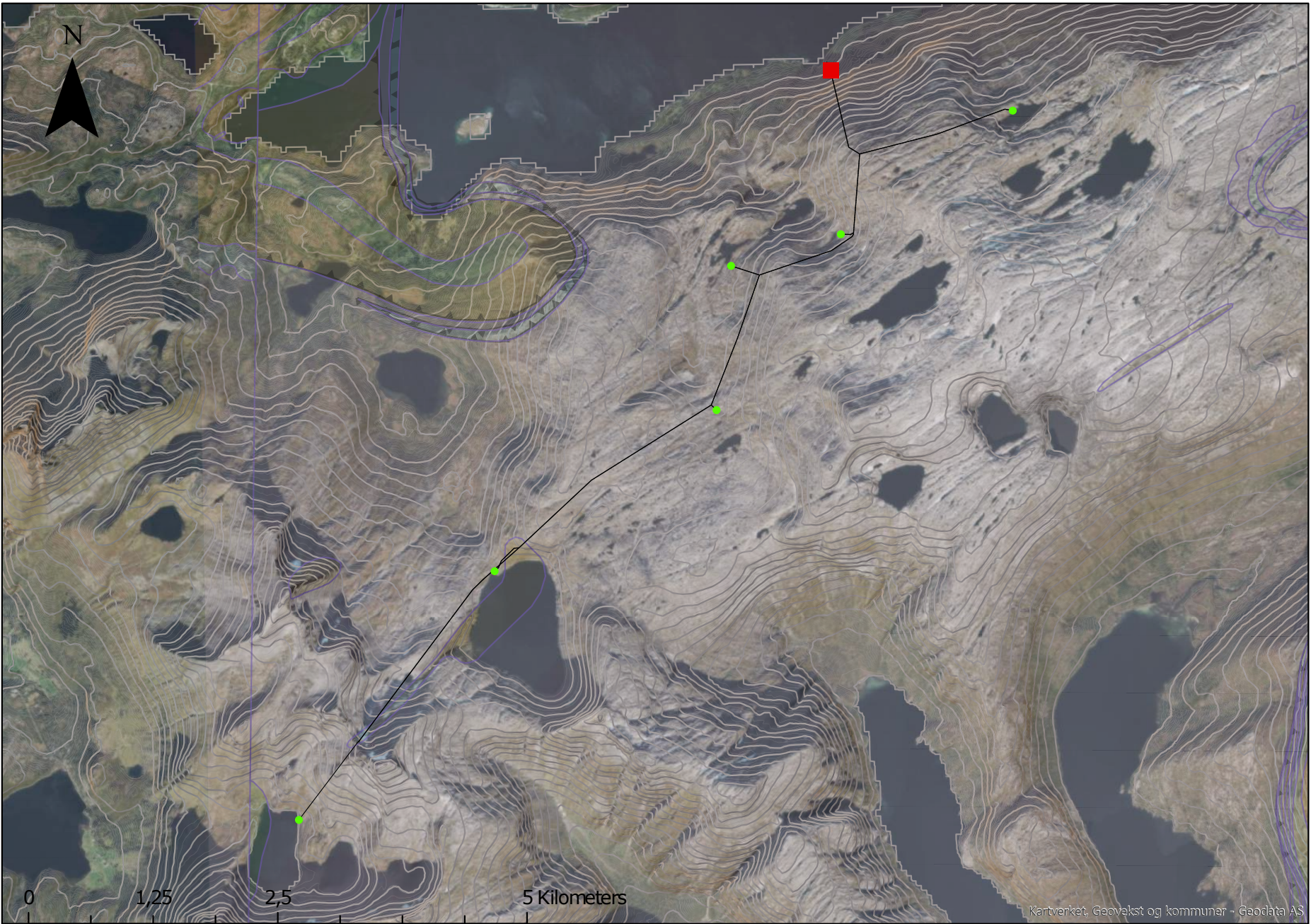


0 1,5 3 6 Kilometers



---

### **C.3 Smibelg HPP**

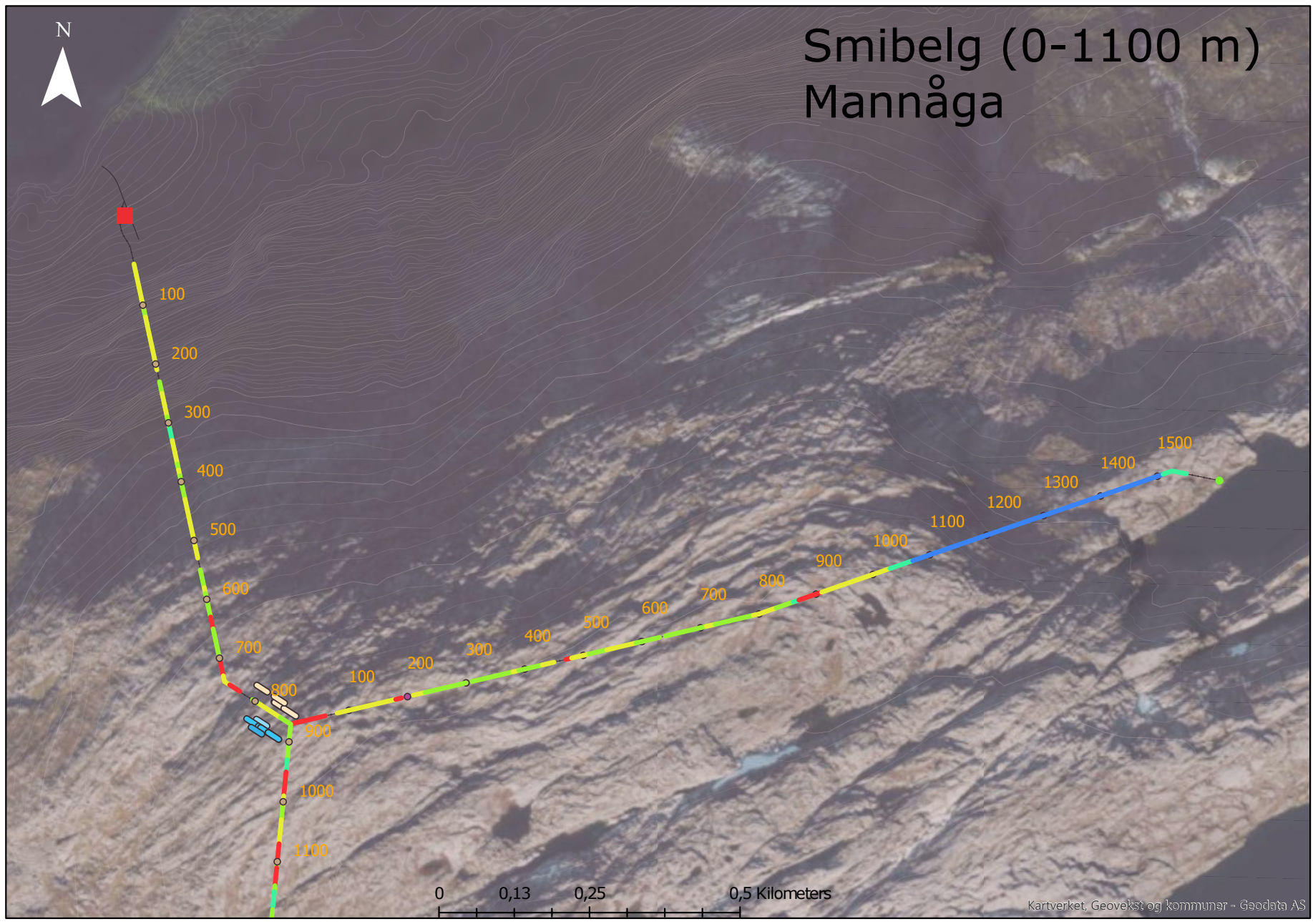


N

0 1,25 2,5 5 Kilometers



# Smibelg (0-1100 m) Mannåga



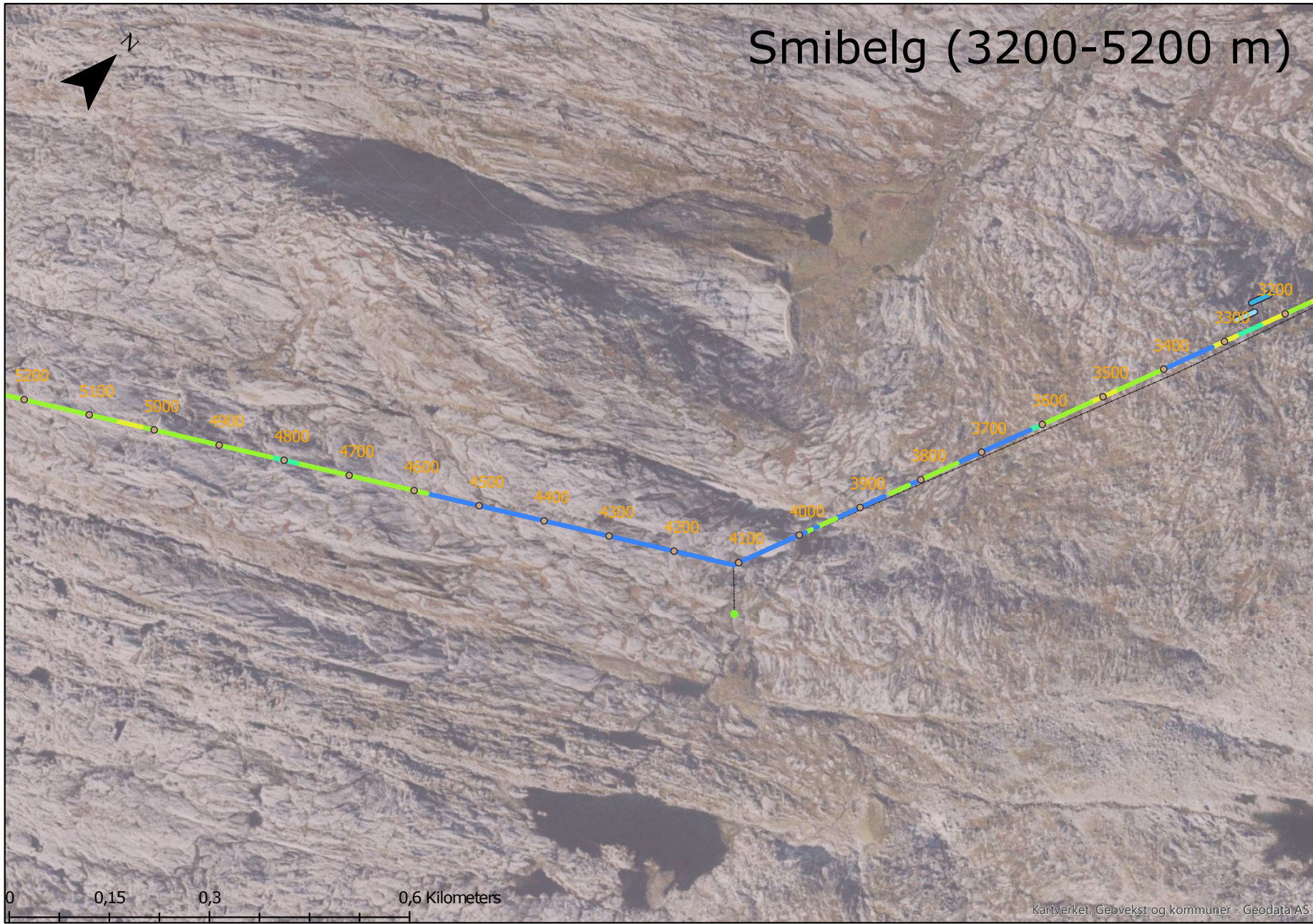
0 0,13 0,25 0,5 Kilometers

# Smibelg (1000-3200 m) Vakkerjordvatn



0 0,15 0,3 0,6 Kilometers

# Smibelg (3200-5200 m)



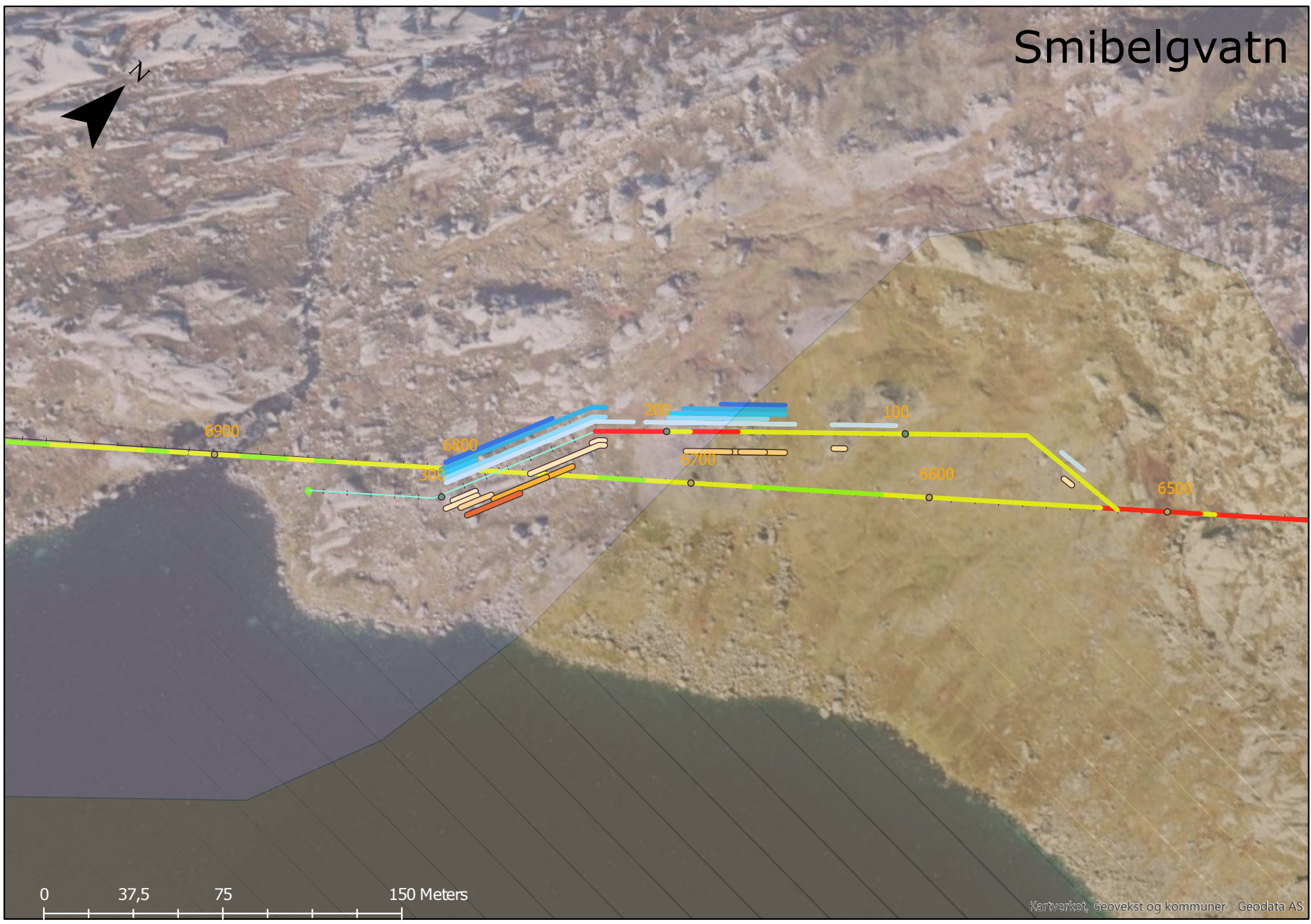
0 0,15 0,3 0,6 Kilometers

# Smibelg (5200-7100 m)



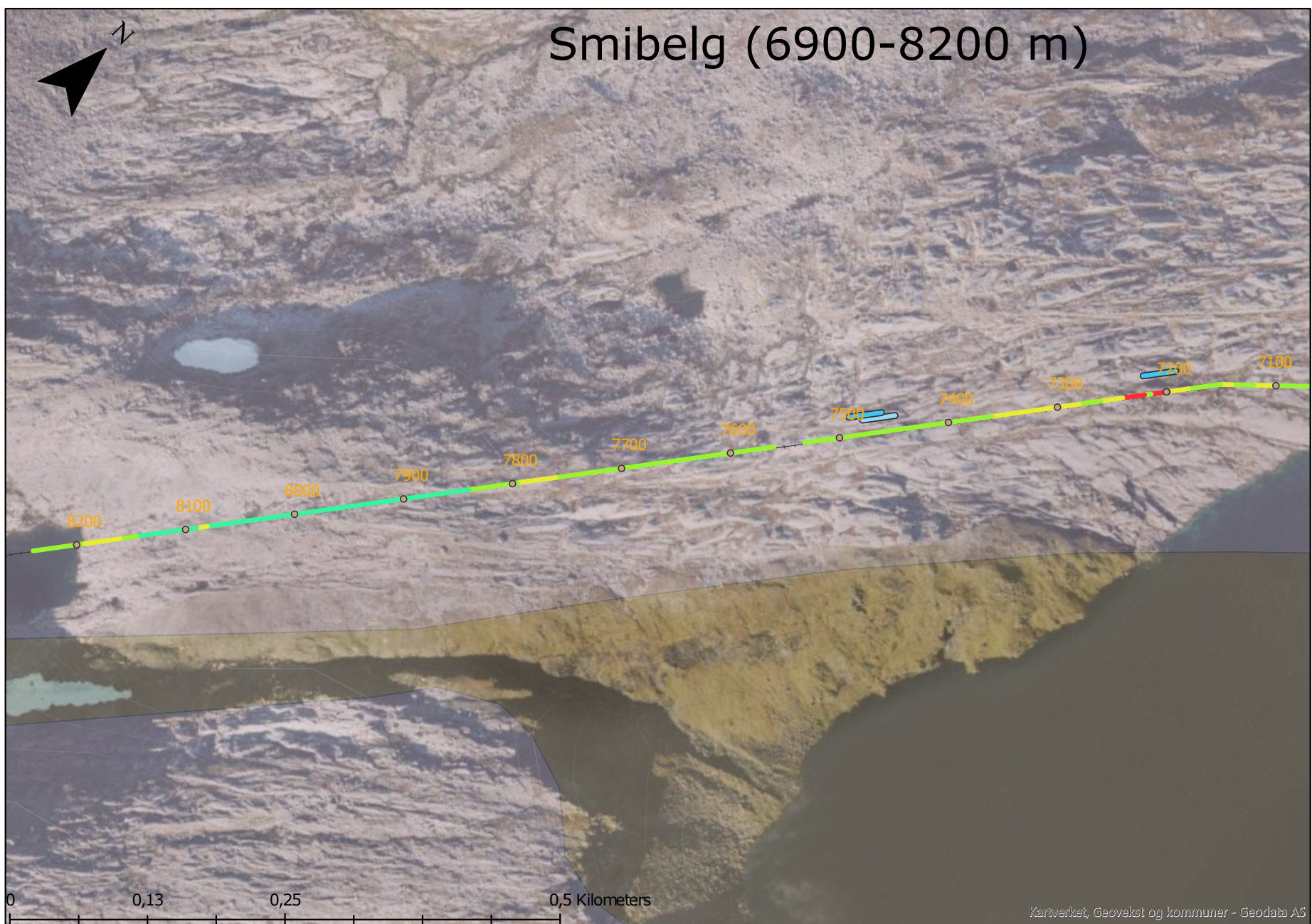
0 0,15 0,3 0,6 Kilometers

# Smibelgvatn



0 37,5 75 150 Meters

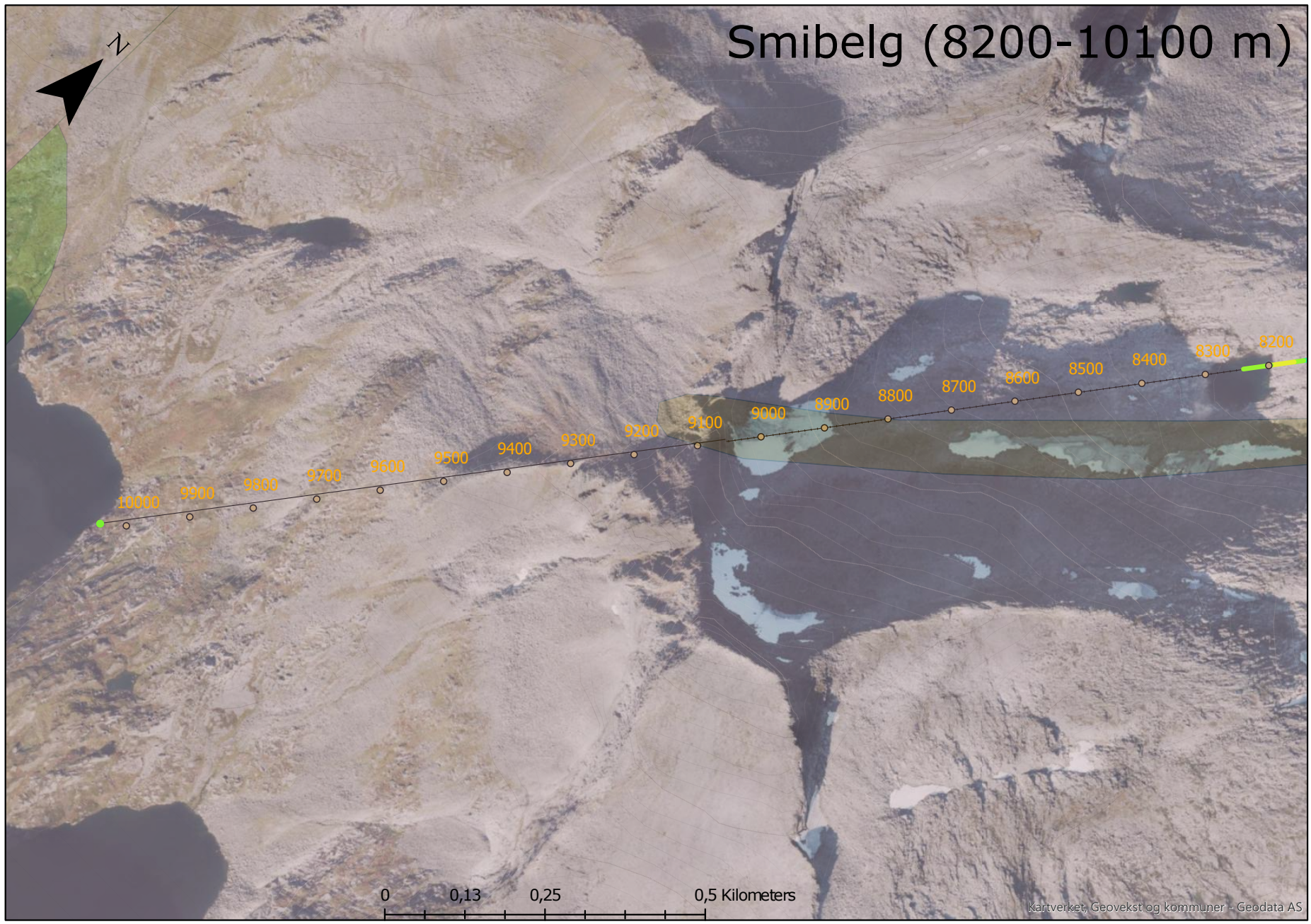
# Smibelg (6900-8200 m)



0 0,13 0,25 0,5 Kilometers



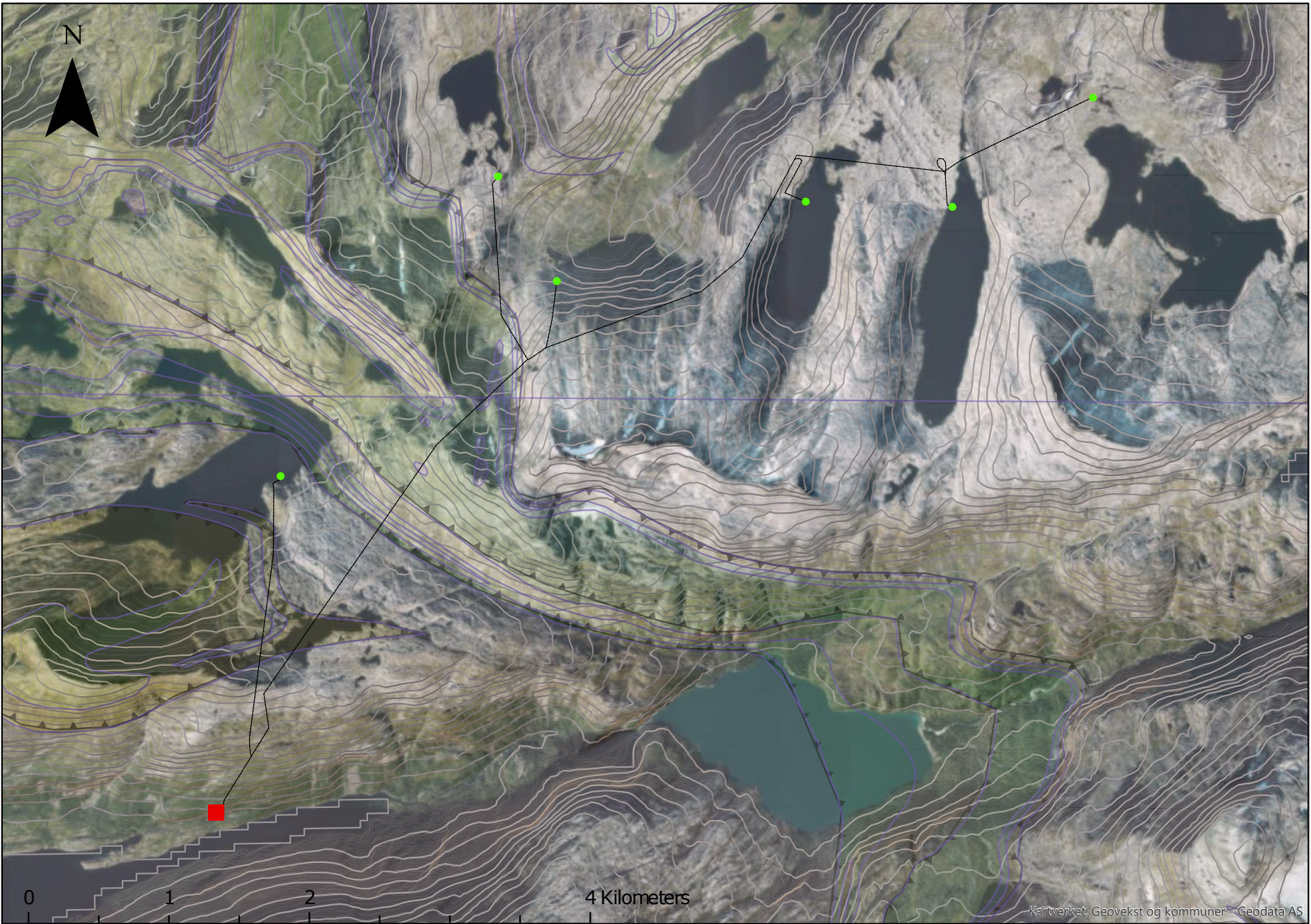
# Smibelg (8200-10100 m)



0 0,13 0,25 0,5 Kilometers

---

## **C.4 Storåvatn HPP**



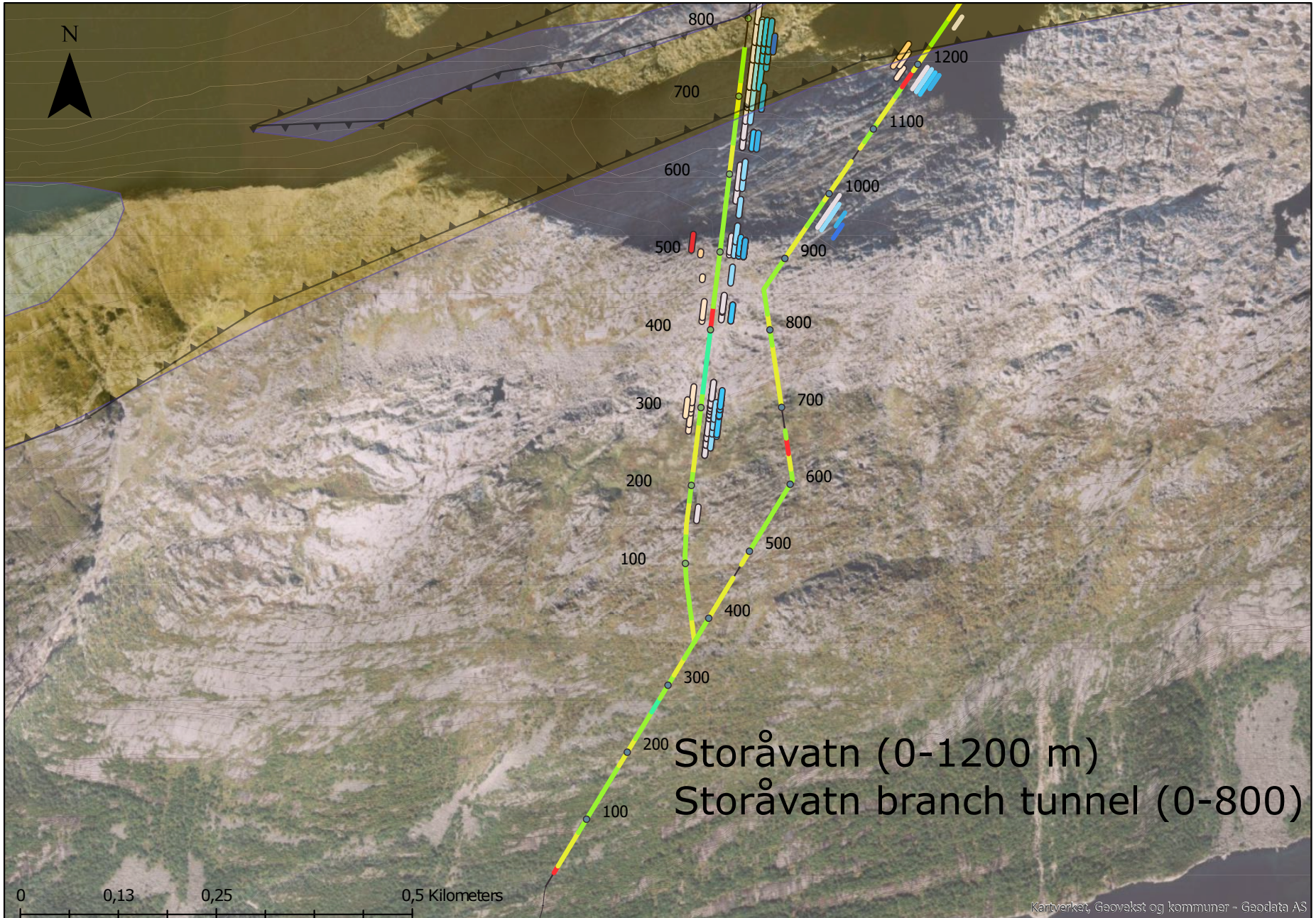
N

0

1

2

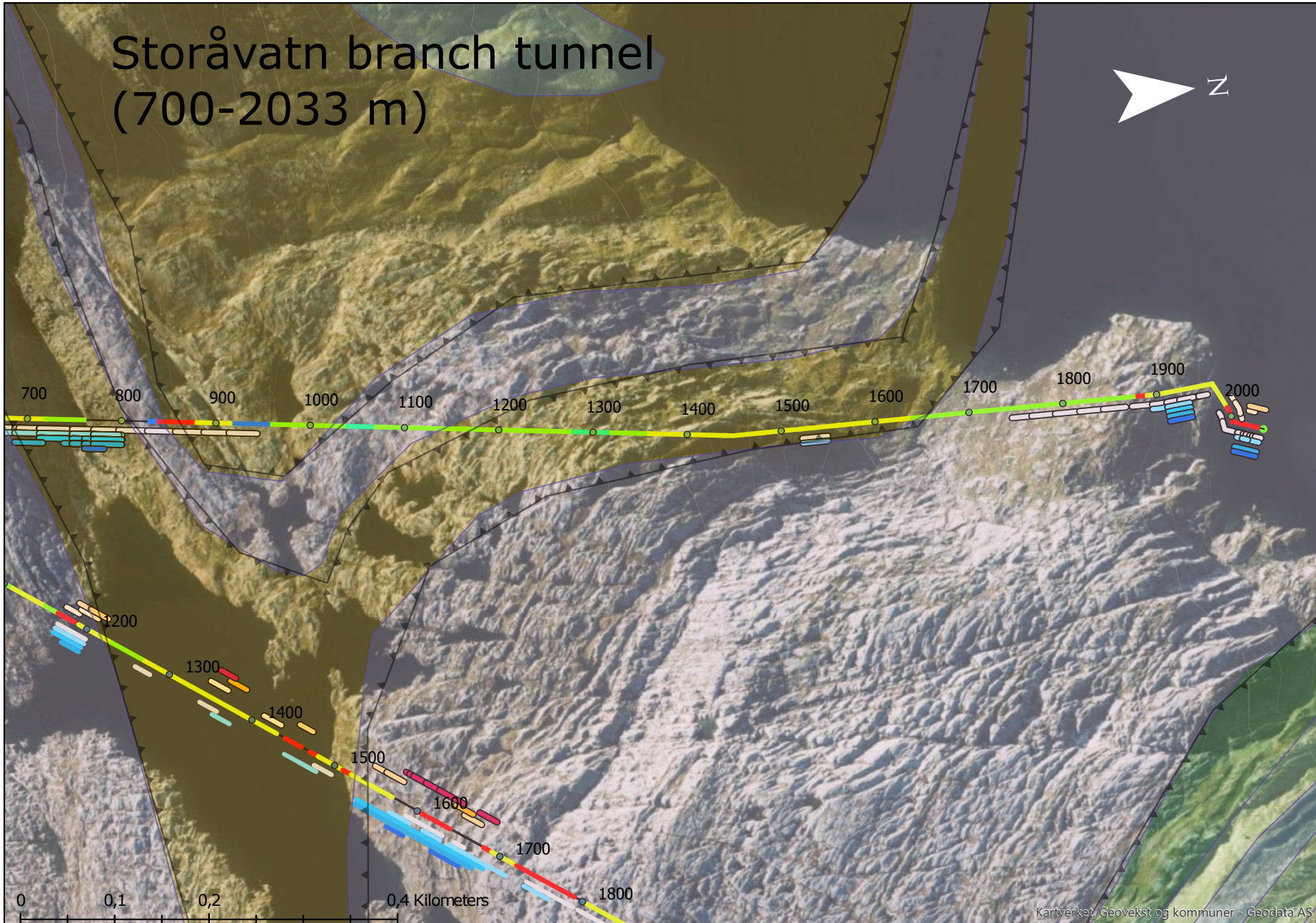
4 Kilometers



Storåvatn (0-1200 m)  
Storåvatn branch tunnel (0-800)

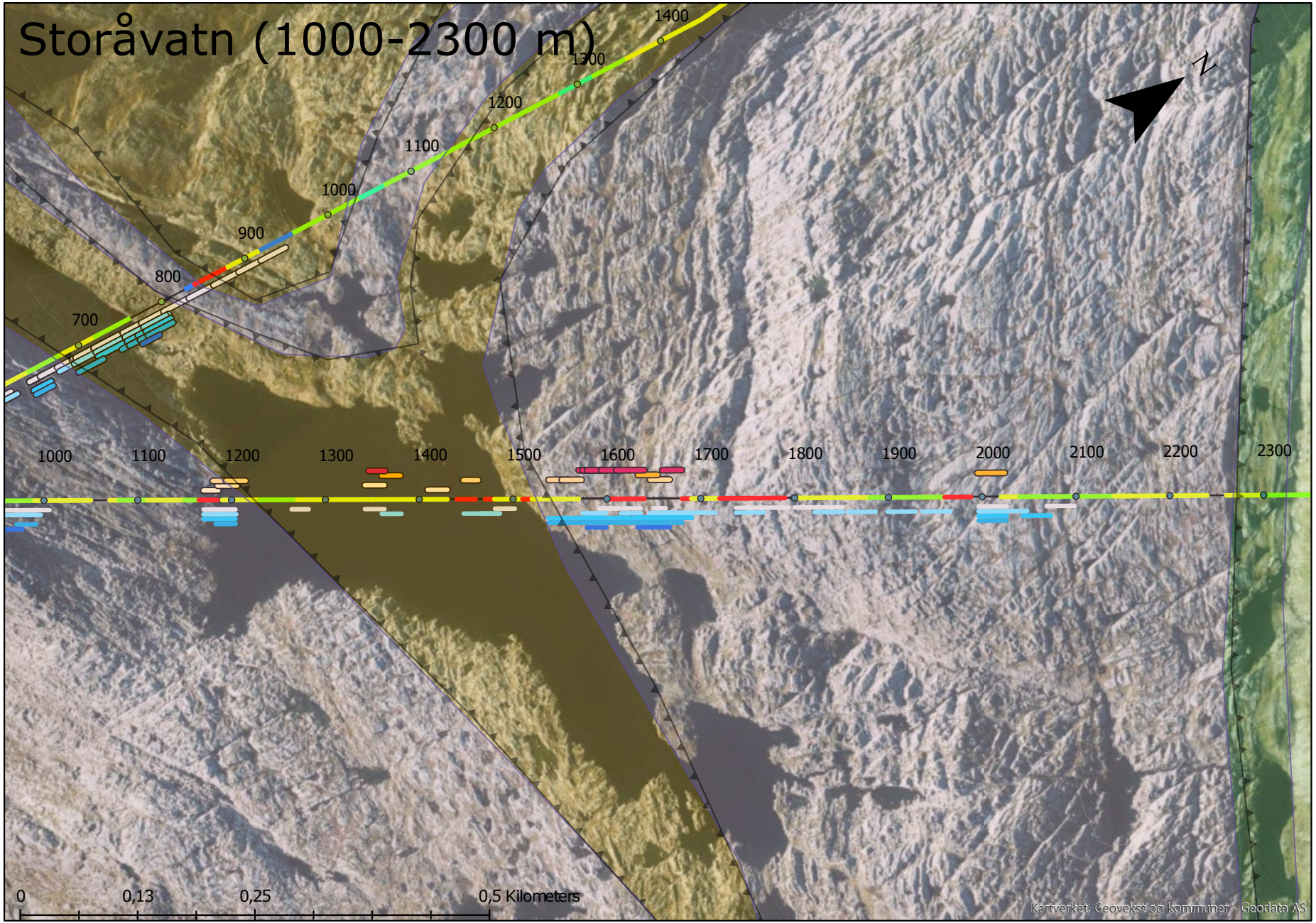


# Storåvatn branch tunnel (700-2033 m)



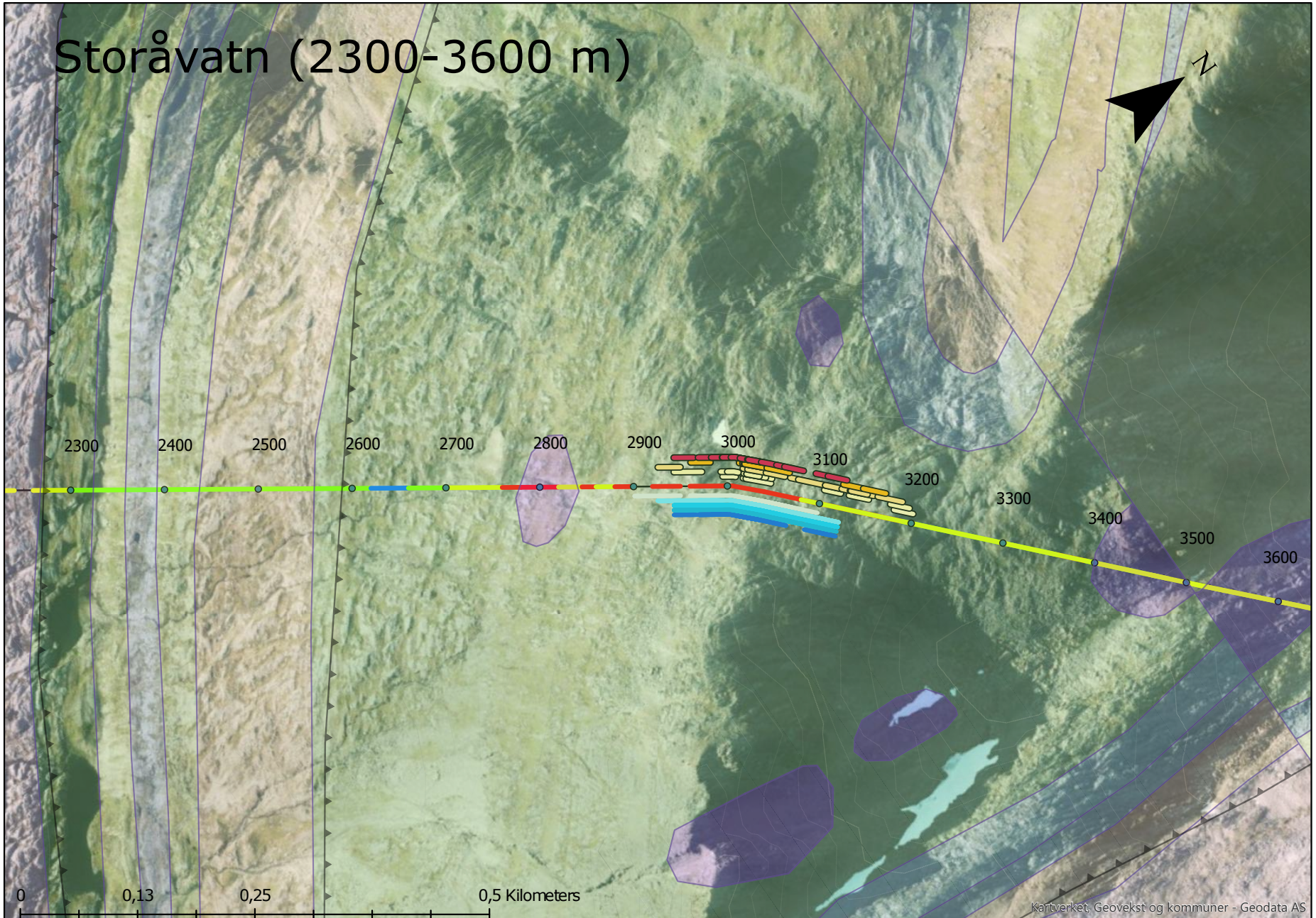
0 0,1 0,2 0,4 Kilometers

# Storåvatn (1000-2300 m)



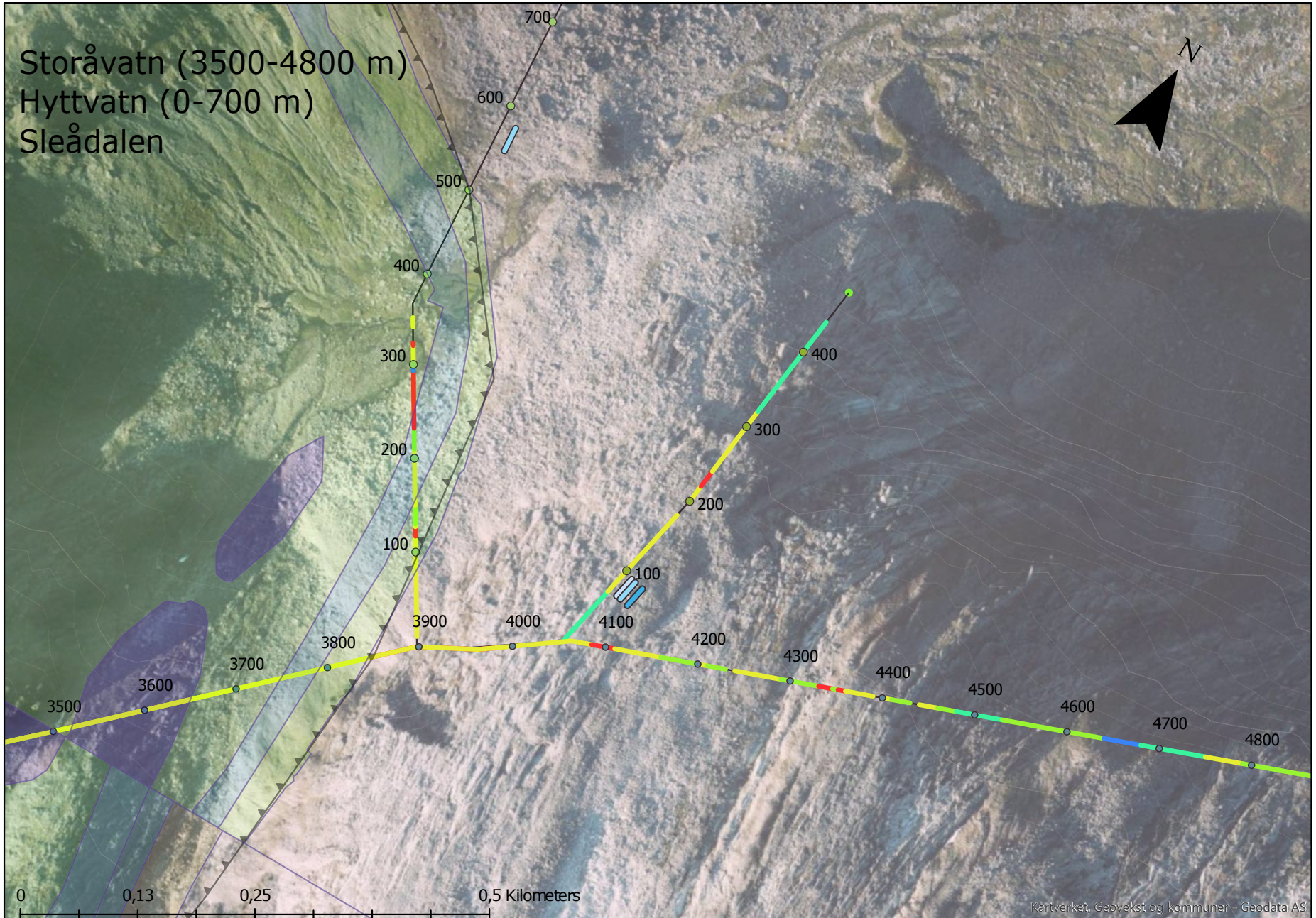
0 0,13 0,25 0,5 Kilometers

# Storåvatn (2300-3600 m)



0 0,13 0,25 0,5 Kilometers

Storåvatn (3500-4800 m)  
Hyttvatn (0-700 m)  
Sleådalen



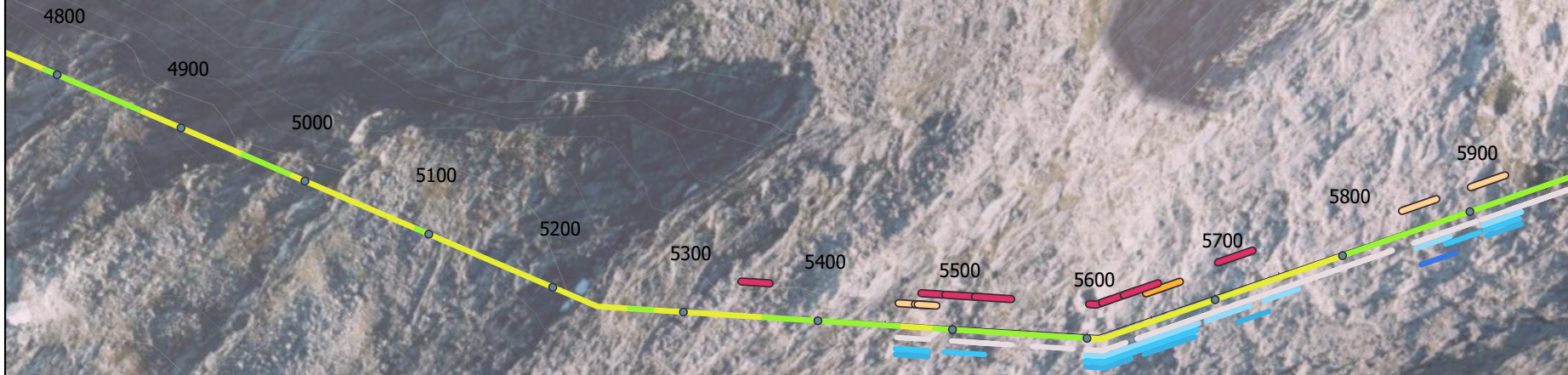
0 0,13 0,25 0,5 Kilometers



# Hyttvatn (400-1400 m)

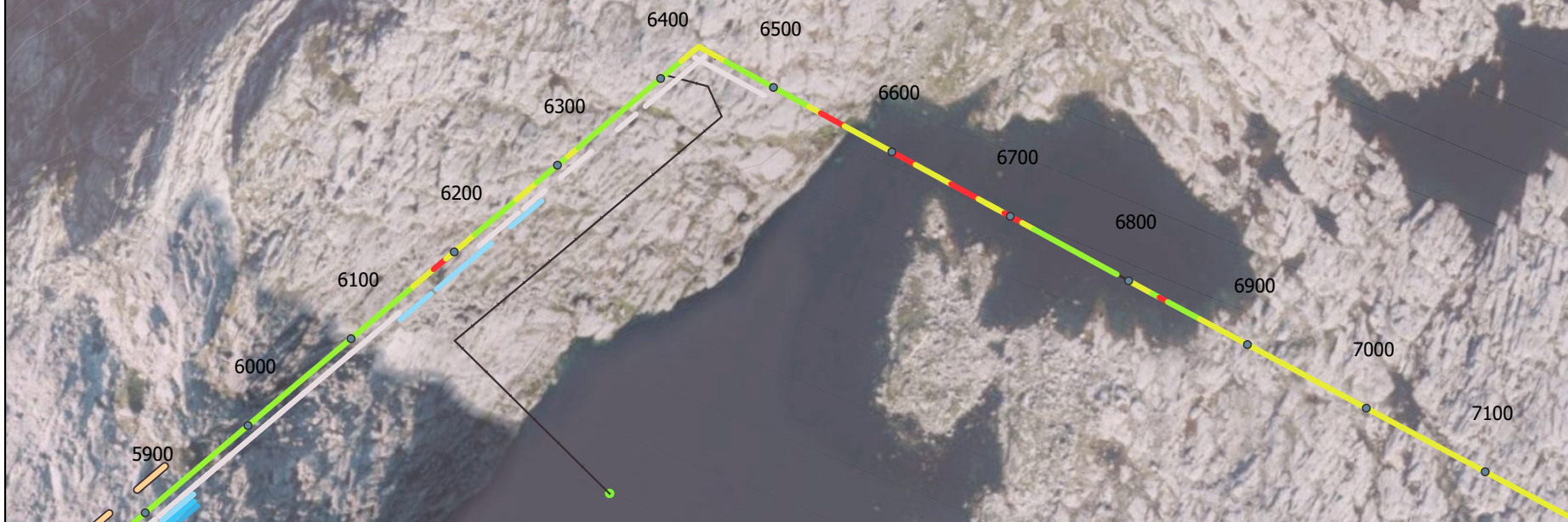


# Storåvatn (4800-5900 m)



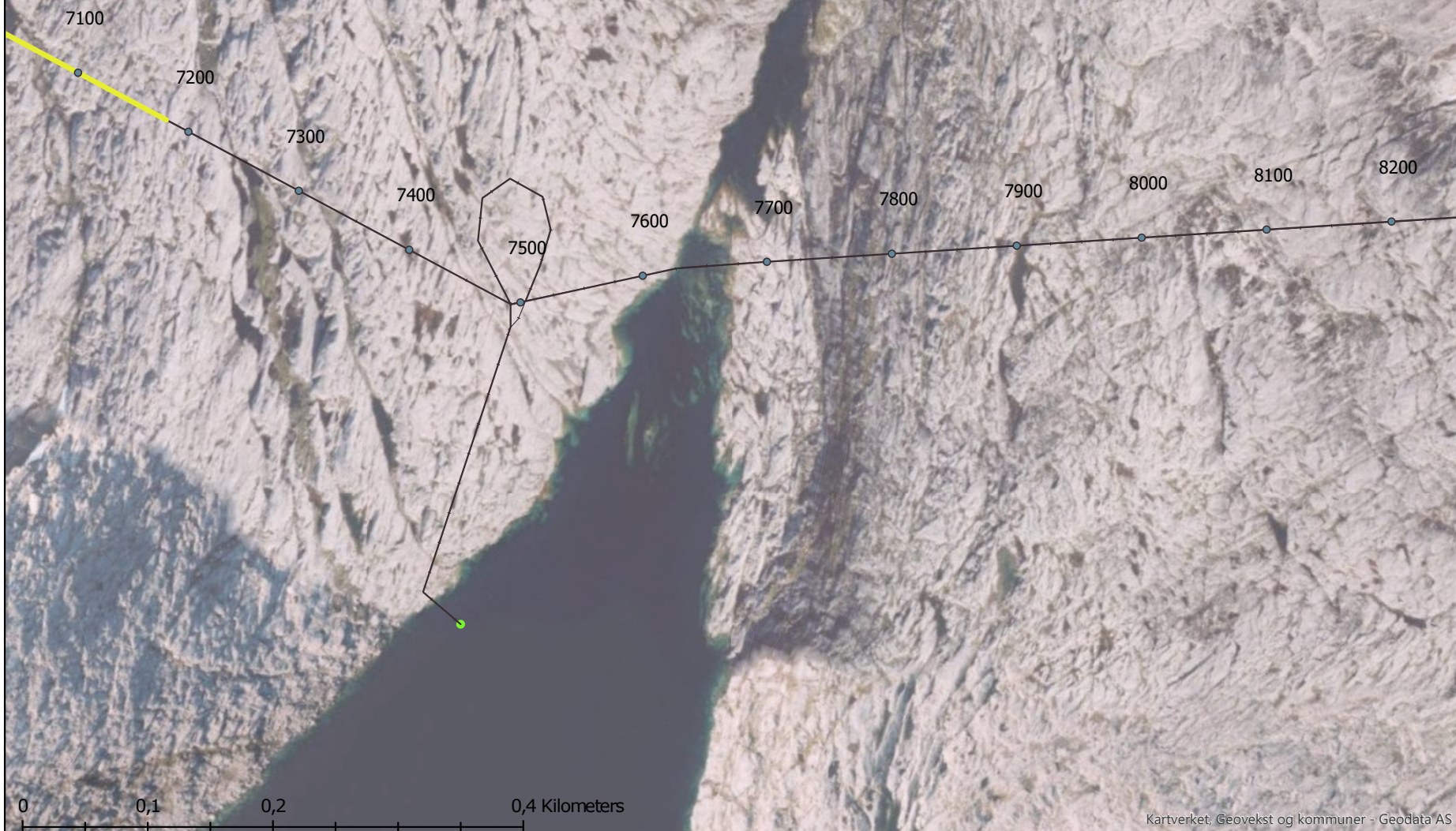
0 0,1 0,2 0,4 Kilometers

# Storåvatn (5800-7100 m) W. Sandvikvatn



0 0,1 0,2 0,4 Kilometers

# Storåvatn (7100-8200 m)



0 0,1 0,2 0,4 Kilometers

# Storåvatn (8000-8600 m)



8000

8100

8200

8300

8400

8500

8600

0

0,1

0,2

0,4 Kilometers



# Appendix **D**

## Longitudinal profiles

---

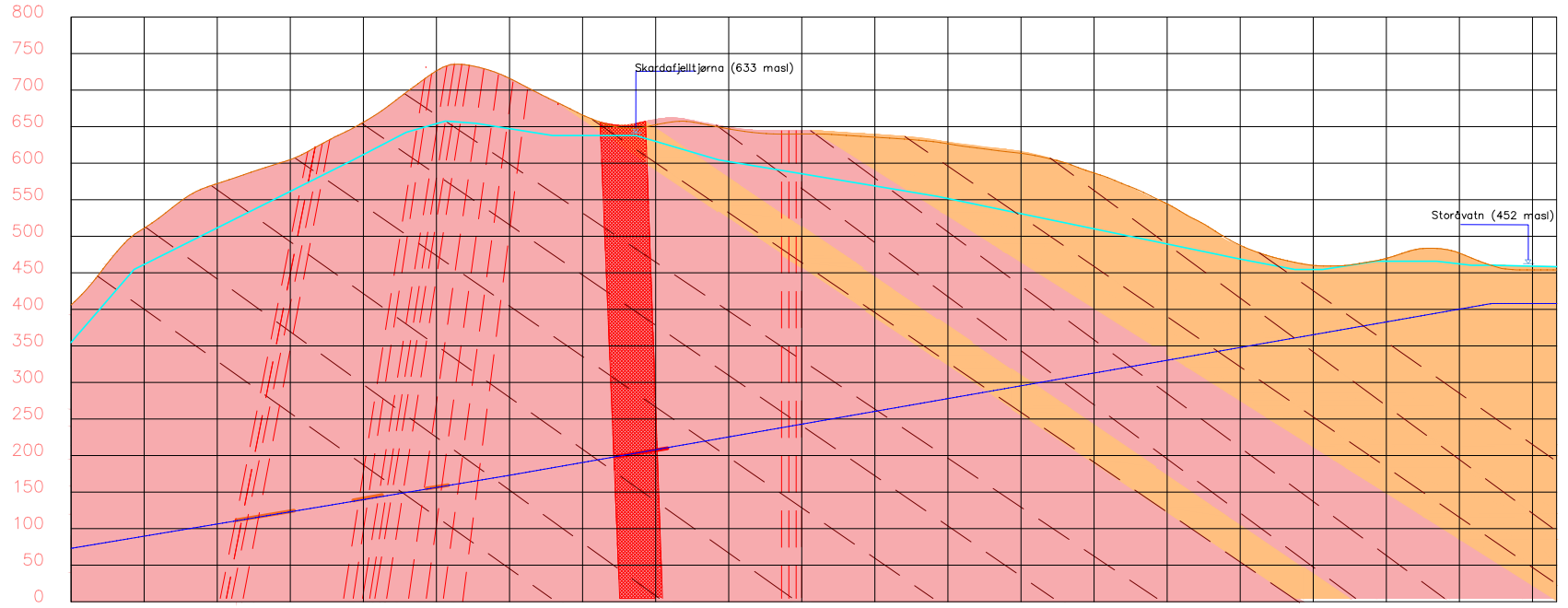
## **D.1 Longitudinal, geologic profiles from Chapter 7**



# Storávatn branch tunnel profile

S

N



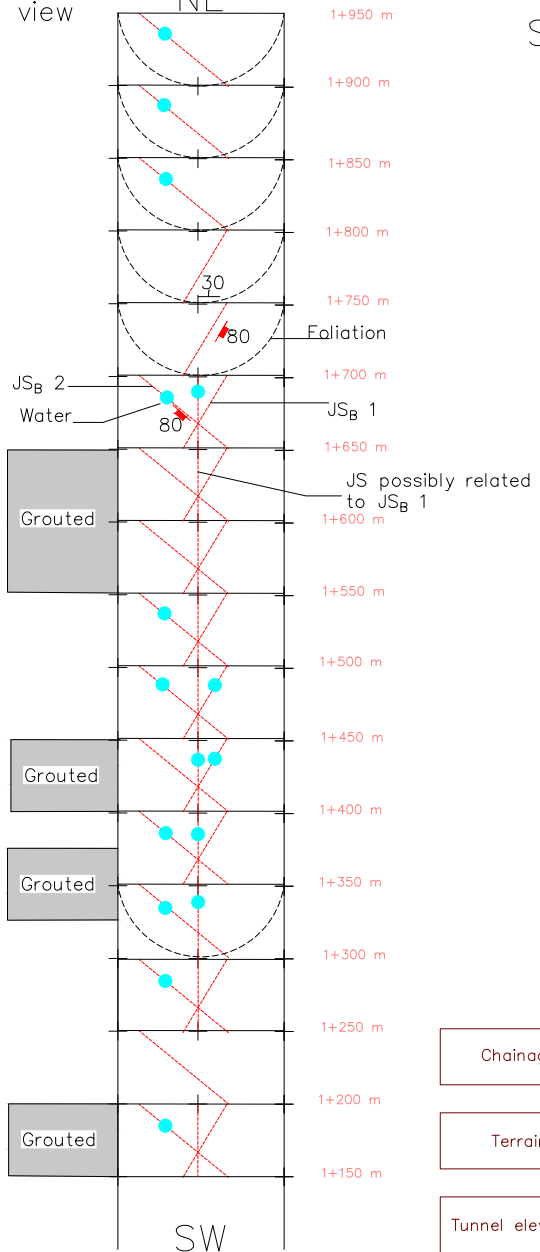
Chainage	0+100	0+200	0+300	0+400	0+500	0+600	0+700	0+800	0+900	1+000	1+100	1+200	1+300	1+400	1+500	1+600	1+700	1+800	1+900	2+000
Terrain	511.2	572.1	604.9	656.0	726.4	716.0	665.9	652.6	646.9	640.0	635.6	626.5	613.5	586.5	544.4	487.7	460.1	469.8	476.9	454.0
Tunnel elevation	89.7	106.3	123.0	139.7	156.3	173.0	190.5	208.0	225.5	242.9	260.4	277.9	295.4	312.9	330.4	347.9	365.3	382.8	400.3	408.0

### Legend

- Tunnel
- Fractured zone
- Gneiss
- Gneiss, mica-rich
- Foliation
- Discontinuity
- Weakness zone

Plan view

NE

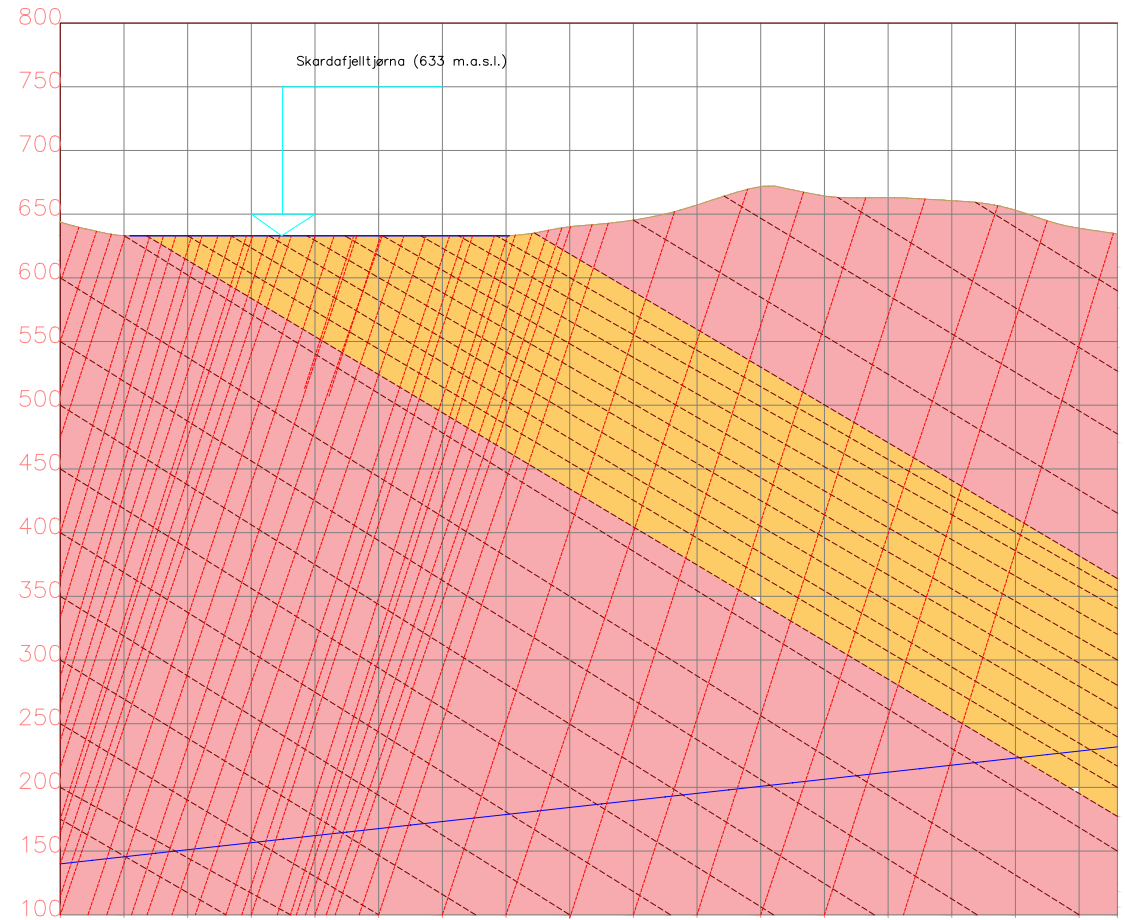


SW

SW

Storåvatn main head race tunnel (section B)

NE

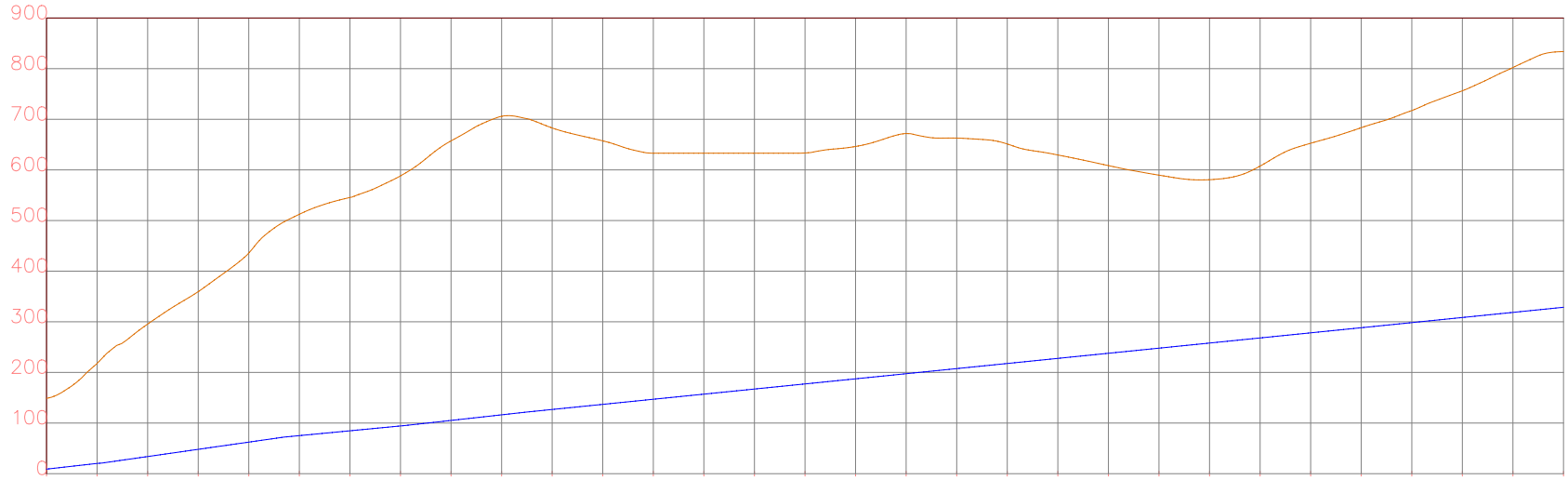


Chainage	1+200	1+250	1+300	1+350	1+400	1+450	1+500	1+550	1+600	1+650	1+700	1+750	1+800	1+850	1+900	1+950
Terrain	633.2	633.0	633.0	633.0	633.0	633.0	633.0	640.0	645.3	657.2	671.6	664.2	662.9	660.6	653.1	638.9
Tunnel elevation	145.5	151.1	156.6	162.1	167.7	173.2	178.7	184.3	189.8	195.3	200.9	206.4	211.9	217.5	223.0	228.5

---

## **D.2 Longitudinal profiles Storavatn main head race tunnel**

## Storåvatn Main Head Race Tunnel (0+000 m to 3+000 m)

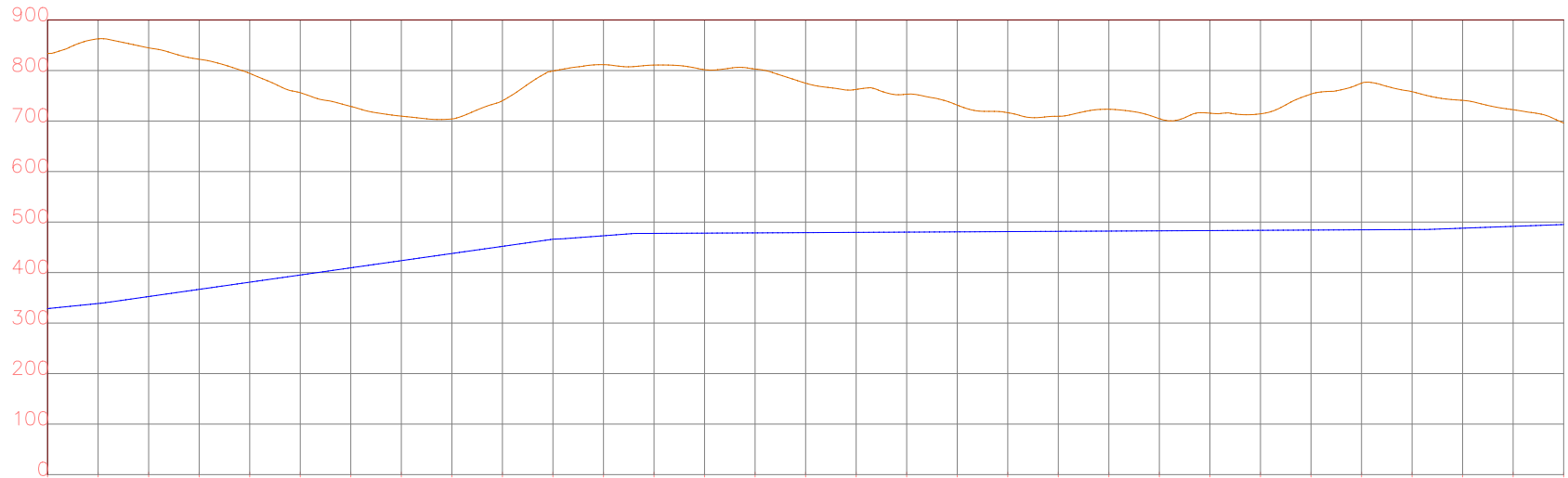


<b>Chainage</b>	0+100 0+200 0+300 0+400 0+500 0+600 0+700 0+800 0+900 1+000 1+100 1+200 1+300 1+400 1+500 1+600 1+700 1+800 1+900 2+000 2+100 2+200 2+300 2+400 2+500 2+600 2+700 2+800 2+900
-----------------	---

<b>Terrain</b>	217.8 295.5 359.6 435.9 512.3 545.5 588.2 657.3 705.8 682.8 657.4 633.0 633.0 633.0 633.5 646.3 671.9 662.8 651.2 629.5 608.5 589.6 580.7 607.6 652.7 683.4 717.2 756.2 802.3
----------------	---

<b>Tunnel elevation</b>	20.2 33.8 48.1 62.3 75.1 84.7 94.2 105.1 116.2 126.8 136.9 147.0 157.1 167.2 177.3 187.3 197.4 207.5 217.6 227.7 237.8 247.9 258.0 268.1 278.2 288.3 298.4 308.5 318.6
-------------------------	--

## Storávatn Main Head Race Tunnel (3+000 m to 6+000 m)



Chainage

3+100 3+200 3+300 3+400 3+500 3+600 3+700 3+800 3+900 4+000 4+100 4+200 4+300 4+400 4+500 4+600 4+700 4+800 4+900 5+000 5+100 5+200 5+300 5+400 5+500 5+600 5+700 5+800 5+900

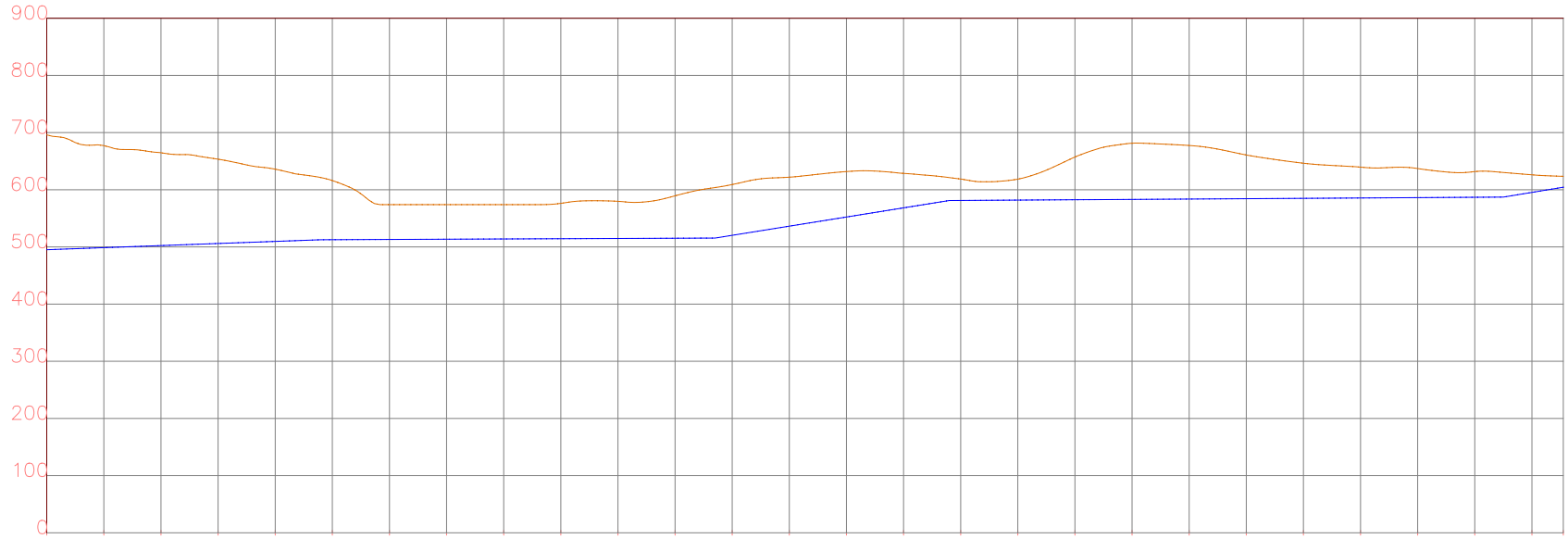
Terrain

862.7 844.8 822.3 794.3 756.2 729.0 709.7 704.1 740.2 798.9 811.6 810.8 801.7 802.9 774.9 762.5 753.1 731.5 716.5 709.4 723.3 704.7 715.6 714.3 753.3 774.9 758.1 740.9 722.4

Tunnel elevation

338.7 352.5 366.8 381.0 395.2 409.4 423.6 437.7 451.9 466.0 472.9 477.5 478.1 478.6 479.1 479.6 480.1 480.6 481.1 481.6 482.1 482.6 483.1 483.6 484.1 484.6 485.1 487.8 491.5

## Storåvatn Main Head Race Tunnel (6+000 m to 8+700 m)



<b>Chainage</b>	6+100	6+200	6+300	6+400	6+500	6+600	6+700	6+800	6+900	7+000	7+100	7+200	7+300	7+400	7+500	7+600	7+700	7+800	7+900	8+000	8+100	8+200	8+300	8+400	8+500	8+600
<b>Terrain</b>	677.2	664.7	653.5	636.0	616.0	574.0	574.0	574.0	576.2	579.8	589.4	609.1	622.0	631.8	628.7	618.8	618.5	657.3	681.4	677.5	660.8	646.4	639.6	637.1	631.8	626.2
<b>Tunnel elevation</b>	498.7	502.4	506.0	509.6	512.6	513.1	513.5	513.9	514.4	514.8	515.2	520.3	536.3	552.3	568.4	581.3	581.9	582.5	583.1	583.8	584.4	585.0	585.6	586.2	586.8	595.4

Appendix **E**

# Python scripts for data processing

---

## E.1 Standard formatting names

data.txt

Standard names used in excel-files

-----  
Sheet names

-----  
"All" = Sheet with PD, RMG and Tunnel mapping  
"Q" = Sheet with Q values from tunnel mapping  
"RMG" = Sheet with data from Rock Mass Grouting  
"PD" = Sheet with data from Probe Drilling Results  
"Elev" = SHEet with data regarding terrain and tunnel elevation  
  
"Pd\_after" = Probe drilling holes drilled after a pre-grouting round  
-----

-----  
Tunnel mapping

-----  
"Start" = Start of Q value interval [m]  
"Mid" = Mid-point of Q value interval [m]  
"End" = End of Q value interval [m]  
"RQD" = RQD-value  
"Jn" = Jn-value  
"Jr" = Jr-value  
"Ja" = Ja-value  
"Jw" = Jw-value  
"SRF" = SRF-value  
"Q" = Q-value  
-----

-----  
Probe drilling

-----  
"Face\_loc" = Location of tunnel face [m]  
"Delta\_face" = Change in location of tunnel face [m]  
"Pd\_len" = Length of probe drill hole [m]  
"Pd\_end" = End of probe drill hole [m]  
"Pd\_cat" = Category of water inflow amount in PD  
"Pd\_com" = Comment to the probe drill hole  
"Pd\_quantity" = Water inflow quantity measured in [l/min]  
-----



---

"Pd\_rqd" = RQD-value for PD interval  
"Pd\_jn" = Jn-value for PD interval  
"Pd\_jr" = Jr-value for PD interval  
"Pd\_ja" = Ja-value for PD interval  
"Pd\_jw" = Jw-value for PD interval  
"Pd\_srf" = SRF-value for PD interval  
"Pd\_q" = Q-value for PD interval

Additional columns for Smibelg and Storåvatn main head race tunnel:

"W\_source" = Name of water source used in eq\_Panthi  
"W\_level" = Elevation of water table for water source  
"H\_static" = Height of water column above the tunnel level  
"Qt" = Inflow [l/min] per m in a probe drill hole  
"Eq\_Panthi" = Equation for water flux in bore holes by Panthi and Nilsen 2010

---

#### Rock Mass Grouting

---

"Face\_loc" = Location of tunnel face [m]  
"Date" = Date of grouting [dd.mm.yyyy]  
"Nr\_hol" = Number of grout holes at tunnel face  
"Av\_hol\_len" = Average length of grout holes [m]  
"End\_avg" = Average end of bore hole length [m]  
"Bore\_m" = Total bore meter of grout holes [m]  
"Nr\_packs" = Total number of packers used  
"Nr\_ex\_packs" = Number of extra packers used  
"Ind\_cem" = Total amount industrial cement used at face [kg]  
"Micro\_cem" = Total amount micro cement used at face [kg]  
"Cem\_type\_contr\_setting" = Total amount of cement with accelerator additive [kg]  
"Spec\_type" = Total amount of cement with coarser material grains [kg]  
"Cem\_tot" = Total cement used [kg] sum of Ind, Mic, Contr, Spec  
"Cem\_pr\_m" = Ratio of "Cem\_tot" and "Bore\_m"  
"Bolt\_mort" = Total amount of bolt mortar used [kg]  
"Poly\_ue" = Total amount of Polyuretan used at face [kg]  
"Si\_sl" = Total amount of Silica Slurry used at face [kg]  
"Dyn\_sxn" = Total amount of Dynamon SXN used at face [kg]  
"Pres" = Pressure in bore holes at stop of grout process [bar]  
"Pump\_t" = Total RMG pumping time [hours]  
"Ex\_t" = Extra time needed after pumping for RMG hardening [hours]  
"Cat" = Rock mass grouting category

---

---

## E.2 Identify standard formatted columns in Excel

```
#!/usr/bin/env python3
# -*- coding: utf-8 -*-
"""
Created on Sun Sep 22 11:36:30 2019

This script includes a function named find_col.

find_col opens an Excel sheet with results of probe drilling and tunnel mapping.
Based on standard formatted column names, it identifies the column for where the
parameters are located. The results are saved in a data dictionary to be imported
in the script namd "Assign_Q_val231019.py".

@author: Haakon Jørlo Haugerud
"""

def find_col():
    import openpyxl as pxl
    import os

    dataDict = {}

    path = input('Type the path name for the excel file \n')
    filename = input('Type the name of the file, without .xlsx \n')
    filename = filename + '.xlsx'

    os.chdir(path)

    wb = pxl.load_workbook(filename, data_only=True)
    sheet_q_string = input('Write the name of the sheet where the Q values are saved \n')
    sheet_alle_string = input('Write the name of the sheet where all results are saved \n')
    input('Remember to follow standard names for columns in the sheets, see textfile \n')

    sheet_q = wb[sheet_q_string]
    sheet_alle = wb[sheet_alle_string]
    dataDict['wb'] = wb
    dataDict['sheet_q'] = sheet_q
    dataDict['sheet_alle'] = sheet_alle

    for col_alle in range(1, sheet_alle.max_column+1):
        for row_alle in range(1, sheet_alle.max_row+1):
            if sheet_alle.cell(row_alle, col_alle).value == 'Face_loc':
                dataDict['col_face_loc'] = col_alle
            elif sheet_alle.cell(row_alle, col_alle).value == 'Pd_len':
                dataDict['col_pd_len'] = col_alle
            elif sheet_alle.cell(row_alle, col_alle).value == 'Pd_end':
                dataDict['col_pd_end'] = col_alle
            elif sheet_alle.cell(row_alle, col_alle).value == 'Pd_rqrd':
                dataDict['col_alle_rqrd'] = col_alle
            elif sheet_alle.cell(row_alle, col_alle).value == 'Pd_jn':
                dataDict['col_alle_jn'] = col_alle
            elif sheet_alle.cell(row_alle, col_alle).value == 'Pd_jr':
                dataDict['col_alle_jr'] = col_alle
            elif sheet_alle.cell(row_alle, col_alle).value == 'Pd_ja':
                dataDict['col_alle_ja'] = col_alle
            elif sheet_alle.cell(row_alle, col_alle).value == 'Pd_jw':
                dataDict['col_alle_jw'] = col_alle
            elif sheet_alle.cell(row_alle, col_alle).value == 'Pd_srf':
                dataDict['col_alle_srf'] = col_alle
            elif sheet_alle.cell(row_alle, col_alle).value == 'Pd_q':
                dataDict['col_alle_q'] = col_alle

    for col_q in range(1, sheet_q.max_column+1):
        for row_q in range(1, sheet_q.max_row+1):
            if sheet_q.cell(row_q, col_q).value == 'Start':
                dataDict['col_q_start'] = col_q
            elif sheet_q.cell(row_q, col_q).value == 'Mid':
                dataDict['col_q_mid'] = col_q
            elif sheet_q.cell(row_q, col_q).value == 'End':
                dataDict['col_q_end'] = col_q
            elif sheet_q.cell(row_q, col_q).value == 'RQD':
```

---

```
        dataDict['col_q_rqd'] = col_q
    elif sheet_q.cell(row_q,col_q).value == 'Jn':
        dataDict['col_q_jn'] = col_q
    elif sheet_q.cell(row_q,col_q).value == 'Jr':
        dataDict['col_q_jr'] = col_q
    elif sheet_q.cell(row_q,col_q).value == 'Ja':
        dataDict['col_q_ja'] = col_q
    elif sheet_q.cell(row_q,col_q).value == 'Jw':
        dataDict['col_q_jw'] = col_q
    elif sheet_q.cell(row_q,col_q).value == 'SRF':
        dataDict['col_q_srf'] = col_q
    elif sheet_q.cell(row_q,col_q).value == 'Q':
        dataDict['col_q_q'] = col_q
```

```
    return(dataDict)
```

---

## E.3 Assign Q-values to bore holes

```
#!/usr/bin/env python3
# -*- coding: utf-8 -*-
"""
Created on Sun Sep 22 11:14:39 2019

This script uses Q-value results from tunnel mapping and probe drilling data
to assign the Q-parameters related to the lowest Q-value to the water inflow results.

The script presupposes that the find_col function in find_col_final.py is imported.

@author: Haakon Jørlo Haugerud

"""
import pandas as pd
import openpyxl as pxl
import os
from operator import itemgetter

#os.chdir('C:\Users\hj\OneDrive - NTNU\Skole\5. år\MASTEROPPGAVER\EXCEL for ArcGIS Pro\Spyder')

from find_col_final import find_col #import find location of column function
dataDict = find_col() #Runs the function

# unpacking dict
wb, sheet_q, sheet_alle, col_face_loc, col_pd_len, col_pd_end, col_alle_rqd,\
    col_alle_jn, col_alle_jr, col_alle_ja, col_alle_jw, col_alle_srf, col_alle_g,\
    col_q_start, col_q_mid, col_q_end, col_q_rqd, col_q_jn, col_q_jr, col_q_ja,\
    col_q_jw, col_q_srf, col_q_q = itemgetter(*dataDict.keys())(dataDict)

for row_alle in range(2, sheet_alle.max_row+1):
    face_loc_ref = sheet_alle.cell(row_alle, col_face_loc) #Get tunnel face location
    face_loc = face_loc_ref.value

    pd_end_ref = sheet_alle.cell(row_alle, col_pd_end) #end of probe drill hole
    pd_end = pd_end_ref.value

    if pd_end == None:
        pass
    else:

        for row_q in range(2, sheet_q.max_row): #Iterate rows in Q sheet

            if row_q < sheet_q.max_row+1 and row_alle < sheet_alle.max_row+1: #Check if not past last row

                if sheet_q.cell(row_q+1, col_q_start).value != None: #Check if you're not comparing with last row with None elements of Q Start

                    if face_loc >= sheet_q.cell(row_q, col_q_start).value and face_loc < sheet_q.cell(row_q+1, col_q_start).value:

                        #Check if probe drill length is in entire q value interval
                        if face_loc >= sheet_q.cell(row_q, col_q_start).value and pd_end <= sheet_q.cell(row_q, col_q_end).value:
                            if sheet_q.cell(row_q, col_q_q).value == None: # If that interval has no Q-value. Dont do anything
                                pass
                            else: #If that interval has Q values. Implement those
                                sheet_alle.cell(row_alle, col_alle_rqd).value = sheet_q.cell(row_q, col_q_rqd).value
                                sheet_alle.cell(row_alle, col_alle_jn).value = sheet_q.cell(row_q, col_q_jn).value
                                sheet_alle.cell(row_alle, col_alle_jr).value = sheet_q.cell(row_q, col_q_jr).value
                                sheet_alle.cell(row_alle, col_alle_ja).value = sheet_q.cell(row_q, col_q_ja).value
                                sheet_alle.cell(row_alle, col_alle_jw).value = sheet_q.cell(row_q, col_q_jw).value
                                sheet_alle.cell(row_alle, col_alle_srf).value = sheet_q.cell(row_q, col_q_srf).value
                                sheet_alle.cell(row_alle, col_alle_g).value = sheet_q.cell(row_q, col_q_g).value

                        #Check if probe drill length is crossing q value intervals
                        elif face_loc >= sheet_q.cell(row_q, col_q_start).value and pd_end > sheet_q.cell(row_q, col_q_end).value:
                            teller = 0 # Setter teller lik 0
                            nonNone = [] # Definerer liste med ikke None elementer
                            if sheet_q.cell(row_q, col_q_q).value != None:
                                nonNone.append(teller) # Hvis denne current rad Q-verdi ikke er None, append til nonNone
                            else:
```

---

```

pass

while pd_end > sheet_q.cell(row_q+teller,col_q_end).value and row_q+teller <= sheet_q.max_row:
    teller = teller + 1 #Find how many q intervals the bore hole is crossing
    if sheet_q.cell(row_q+teller,col_q_q).value != None:
        nonNone.append(teller) #Append alle nonNone verdier av q som PD-boret krysser
    else:
        pass

    #Set start values
if nonNone == []:
    rqd = None
    jn = None
    jr = None
    ja = None
    jw = None
    srf = None
    q = None
else:
    rqd = sheet_q.cell(row_q+nonNone[0],col_q_rqd).value
    jn = sheet_q.cell(row_q+nonNone[0],col_q_jn).value
    jr = sheet_q.cell(row_q+nonNone[0],col_q_jr).value
    ja = sheet_q.cell(row_q+nonNone[0],col_q_ja).value
    jw = sheet_q.cell(row_q+nonNone[0],col_q_jw).value
    srf = sheet_q.cell(row_q+nonNone[0],col_q_srf).value
    q = sheet_q.cell(row_q+nonNone[0],col_q_q).value

for i in nonNone: #Compare and find minimum Q values in intervals that string crosses
    #if row_q + nonNone[i] != sheet_q.max_row:
    if sheet_q.cell(row_q+nonNone[i],col_q_q).value <= q:#If next Q-value is lower than previous, update parameters
        rqd = sheet_q.cell(row_q+nonNone[i],col_q_rqd).value
        jn = sheet_q.cell(row_q+nonNone[i],col_q_jn).value
        jr = sheet_q.cell(row_q+nonNone[i],col_q_jr).value
        ja = sheet_q.cell(row_q+nonNone[i],col_q_ja).value
        jw = sheet_q.cell(row_q+nonNone[i],col_q_jw).value
        srf = sheet_q.cell(row_q+nonNone[i],col_q_srf).value
        q = sheet_q.cell(row_q+nonNone[i],col_q_q).value

        #Assign verdier til cellene i PD
        sheet_alle.cell(row_alle,col_alle_rqd).value = rqd
        sheet_alle.cell(row_alle,col_alle_jn).value = jn
        sheet_alle.cell(row_alle,col_alle_jr).value = jr
        sheet_alle.cell(row_alle,col_alle_ja).value = ja
        sheet_alle.cell(row_alle,col_alle_jw).value = jw
        sheet_alle.cell(row_alle,col_alle_srf).value = srf
        sheet_alle.cell(row_alle,col_alle_q).value = q

    else:
        pass

elif sheet_q.cell(row_q+1,col_q_start).value == None:
    #Check if probe drill length is in entire q value interval
    if face_loc >= sheet_q.cell(row_q,col_q_start).value and face_loc < sheet_q.cell(row_q,col_q_end).value and pd_end <= sheet_q.c
        if sheet_q.cell(row_q,col_q_q).value == None: # If that interval has no Q-value. Dont do anything
            pass
        else: #If that interval has Q values. Implement those

            rqd = sheet_q.cell(row_q,col_q_rqd).value
            jn = sheet_q.cell(row_q,col_q_jn).value
            jr = sheet_q.cell(row_q,col_q_jr).value
            ja = sheet_q.cell(row_q,col_q_ja).value
            jw = sheet_q.cell(row_q,col_q_jw).value
            srf = sheet_q.cell(row_q,col_q_srf).value
            q = sheet_q.cell(row_q,col_q_q).value

            #Assign verdier til cellene i PD
            sheet_alle.cell(row_alle,col_alle_rqd).value = rqd
            sheet_alle.cell(row_alle,col_alle_jn).value = jn
            sheet_alle.cell(row_alle,col_alle_jr).value = jr
            sheet_alle.cell(row_alle,col_alle_ja).value = ja
            sheet_alle.cell(row_alle,col_alle_jw).value = jw
            sheet_alle.cell(row_alle,col_alle_srf).value = srf
            sheet_alle.cell(row_alle,col_alle_q).value = q

```

---

---

```
    else:  
        pass
```

```
new_filename = input('Name the new saved file \n')  
new_filename = new_filename + '.xlsx'  
wb.save(new_filename)
```

---

## E.4 Processing of strike and dip results

```
# -*- coding: cp1252 -*-
#strike and dip treatment
def strike_dip_complete():
    # -*- coding: utf-8 -*-
    """
    Created on Wed Oct 30 13:38:50 2019

    This function open an Excel sheet with info on the orientation of discontinuities
    in eng. geol. mapping. It fills in dip direction and strike of a joint given
    that either strike, dip and dip direction is given or that the dip direction
    and dip is given.

    It then saves the results to a new Excel file at a file location and name for the
    choice of the user.

    @author: Haakon Jrlo Haugerud
    """
    import openpyxl as pxl
    import os

    path = input("Type path for excel file \n")
    os.chdir(path)

    filename = input("Type name of the excel file \n")
    filename = filename + ".xlsx"

    wb = pxl.load_workbook(filename)

    sheet = input("Type name of excel sheet \n")
    sheet_data = wb[sheet]

    max_row = sheet_data.max_row
    max_col = sheet_data.max_column

    for rows in range(1,max_row+1):
        for cols in range(1,max_col+1):
            if sheet_data.cell(rows,cols).value == "Chainage":
                col_ch = cols
                row_ch = rows
            elif sheet_data.cell(rows,cols).value == "Dip dir":
                col_dd = cols
                row_dd = rows
            elif sheet_data.cell(rows,cols).value == "Strike":
                col_strike = cols
                row_strike = rows
            elif sheet_data.cell(rows,cols).value == "Dip":
                col_dip = cols
                row_dip = rows
            elif sheet_data.cell(rows,cols).value == "Dir":
                row_dir = rows
                col_dir = cols

    strikes = []
    dip_dirs = []

    for rows in range(2,max_row+1):
        chainage = sheet_data.cell(rows,col_ch).value
        dip_dir = sheet_data.cell(rows,col_dd).value
        strike = sheet_data.cell(rows,col_strike).value
        dip = sheet_data.cell(rows,col_dip).value
        direction = sheet_data.cell(rows,col_dir).value

    if dip_dir == None: #Calculate dip dir value
        if dip == 90:
            if strike <= 90:
                sheet_data.cell(rows,col_dd).value = strike + 90
            else:
                sheet_data.cell(rows,col_dd).value = strike - 90
        elif dip < 90:
            if strike >= 0 and strike <= 90:
                if direction == "NW" or direction == "W" or direction == "N":
```

---

```

        if strike + 270 == 360:
            sheet_data.cell(rows,col_dd).value = 0
        else:
            sheet_data.cell(rows,col_dd).value = strike + 270
    elif direction == "SE" or direction == "E" or direction == "S":
        sheet_data.cell(rows,col_dd).value = strike + 90
elif strike > 90 and strike <= 180:
    if direction == "SW" or direction == "S" or direction == "W":
        sheet_data.cell(rows,col_dd).value = strike + 90
    elif direction == "NE" or direction == "N" or direction == "E":
        sheet_data.cell(rows,col_dd).value = strike -90

if strike == None: #For calculating strike, when dip_dir
    if dip_dir >= 90 and dip_dir < 270:
        if dip_dir - 90 == 180:
            sheet_data.cell(rows,col_strike).value = 0
        else:
            sheet_data.cell(rows,col_strike).value = dip_dir - 90
    elif dip_dir >= 270 and dip_dir < 360:
        sheet_data.cell(rows,col_strike).value = 360 - (dip_dir + 90)

strikes.append(sheet_data.cell(rows,col_strike).value)
dip_dirs.append(sheet_data.cell(rows,col_dd).value)

new_file = input("Type name of new file \n")
new_file = new_file + ".xlsx"
wb.save(new_file)

```



---

## E.5 Overburden calculation

```
# -*- coding: utf-8 -*-
"""
Created on Fri Oct 25 09:34:29 2019

This script takes in an Excel spreadsheet, tunnel inclination and surface elevation
data and calculates the overburden above the tunnel

The script presupposes that columns in sheets uses standard names as indicated in
attached .txt file in thesis.

The script estimates the terrain level at the face location and uses this to calculate
overburden independent on the length of the probe drill hole

It searches for the nearest known terrain point at face location. This makes it very
dependent on the Digital Elevation Data points' density.

@author: Haakon Jørlo Haugerud
"""

import openpyxl as pxl
import os

new_dir = input('Write directory \n')
os.chdir(new_dir)

filename = input('Write name of excel file \n')
filename = filename+'.xlsx'

sheet_elv = input('Write name of elevation sheet \n')

sheet_pd = input('Write name of sheet for which you want to calculate overburden values \n')

wb = pxl.load_workbook(filename,data_only=True)

sheet_elv = wb[sheet_elv]
sheet_pd = wb[sheet_pd]

tunnel_elev_list = []

overburden_list = []

for rows_pd in range(1,sheet_pd.max_row+1):
    for cols_pd in range(1,sheet_pd.max_column+1):
        if sheet_pd.cell(rows_pd,cols_pd).value == "Terrain":
            col_terrain = cols_pd
            row_terrain = rows_pd
        elif sheet_pd.cell(rows_pd,cols_pd).value == "Tunnel_elev":
            col_t_elev = cols_pd
            row_t_elev = rows_pd
        elif sheet_pd.cell(rows_pd,cols_pd).value == "Overburden":
            col_ob = cols_pd
            row_ob = rows_pd
        elif sheet_pd.cell(rows_pd,cols_pd).value == "Face_loc":
            col_floc = cols_pd
            row_floc = rows_pd

for rows_elev in range(1,sheet_elv.max_row+1):
    for cols_elev in range(1,sheet_elv.max_column+1):
        if sheet_elv.cell(rows_elev,cols_elev).value == "X":
            col_X = cols_elev
            row_X = rows_elev
        elif sheet_elv.cell(rows_elev,cols_elev).value == "Z":
            col_Z = cols_elev
            row_Z = rows_elev
        elif sheet_elv.cell(rows_elev,cols_elev).value == "Incl":
            col_incl = cols_elev
            row_incl = rows_elev
        elif sheet_elv.cell(rows_elev,cols_elev).value == "hor":
            col_hor = cols_elev
            row_hor = rows_elev
        elif sheet_elv.cell(rows_elev,cols_elev).value == "vert":
```

---

```

col_vert = cols_elev
row_vert = rows_elev

incl = []
hlims = []
vlims = []

j = 1
while sheet_elev.cell(row_hor+(j),col_hor).value != None:
    hlims.append(sheet_elev.cell(row_hor+(j),col_hor).value)
    vlims.append(sheet_elev.cell(row_vert+(j),col_vert).value)
    incl.append(sheet_elev.cell(row_incl+j,col_incl).value)
    j = j + 1

# hlims is a list with horizontal distance where the tunnel changes inclination
# incl is a list of inclination between hlims

for i in range(0,len(hlims)):

    for row_pd in range(row_floc+1, sheet_pd.max_row+1): #Iterates on the face locations
        face_loc = sheet_pd.cell(row_pd,col_floc).value

        if i <= (len(hlims)-2) and face_loc > hlims[i] and face_loc < hlims[i+1]:
            tunnel_elev = vlims[i] + (face_loc - hlims[i]) * incl[i+1]

            tunnel_elev_list.append(tunnel_elev)

            diff_x_list = []
            vert_list = []
            horz_list = []

            for row_terrain in range(row_X+1, sheet_elev.max_row+1):
                horz = sheet_elev.cell(row_terrain,col_X).value
                vert = sheet_elev.cell(row_terrain,col_Z).value

                vert_list.append(vert)
                horz_list.append(horz) #Import all terrain points

                diff_x = abs(face_loc - horz)

                diff_x_list.append(diff_x)

            min_diff = min(diff_x_list)
            diff_min_index = diff_x_list.index(min_diff)

            overburden = round(vert_list[diff_min_index] - tunnel_elev)

            overburden_list.append(overburden)

            sheet_pd.cell(row_pd,col_terrain).value = vert_list[diff_min_index] #Assign terrain values
            sheet_pd.cell(row_pd,col_ob).value = overburden #Assign overburden values
            sheet_pd.cell(row_pd,col_t_elev).value = tunnel_elev #Assign tunnel elev

        else:
            pass

new_filename = input('Name the new saved file \n')
new_filename = new_filename + '.xlsx'
wb.save(new_filename)

```

---

---

## E.6 Export maximum inflow in probe drilling round to new Excel file

```
# -*- coding: utf-8 -*-
"""
Created on Thu Nov 14 12:05:53 2019

This script reads standard formatted excel files with probe drilling results and
extracts the row with maximum inflow category to a new excel sheet.
The user is then asked the location and name for the resulting file with the results.

@author: Haakon Jørlo Haugerud
"""

import pandas as pd
import os

#Reads excel files with probe drilling and rock mass grouting results

dir_Smvatn = r'C:\Users\hjh\OneDrive - NTNU\Skole\5. år\MASTEROPPGAVER\EXCEL for ArcGIS Pro\Smibelg\Smibelgvatn'
os.chdir(dir_Smvatn)
filename = r'Alle_resultater_Smibelgvatn'
filename = filename + '.xlsx'
sheet_RMG = 'RMG'
sheet_PD = 'PD'
sheet_RMG1 = pd.read_excel(filename, sheet_name=sheet_RMG)
sheet_PD1 = pd.read_excel(filename, sheet_name=sheet_PD)

dir_Smhov = r'C:\Users\hjh\OneDrive - NTNU\Skole\5. år\MASTEROPPGAVER\EXCEL for ArcGIS Pro\Smibelg\Hovedlop'
os.chdir(dir_Smhov)
filename = r'Alle_resultater_Smhov'
filename = filename + '.xlsx'
sheet_RMG2 = pd.read_excel(filename, sheet_name=sheet_RMG)
sheet_PD2 = pd.read_excel(filename, sheet_name=sheet_PD)

dir_Sthov = r'C:\Users\hjh\OneDrive - NTNU\Skole\5. år\MASTEROPPGAVER\EXCEL for ArcGIS Pro\Storåvatn\Hovedlop'
os.chdir(dir_Sthov)
filename = r'Alle_resultater_Sthov'
filename = filename + '.xlsx'
sheet_RMG3 = pd.read_excel(filename, sheet_name=sheet_RMG)
sheet_PD3 = pd.read_excel(filename, sheet_name=sheet_PD)

dir_Stgren = r'C:\Users\hjh\OneDrive - NTNU\Skole\5. år\MASTEROPPGAVER\EXCEL for ArcGIS Pro\Storåvatn\Grentunnel'
os.chdir(dir_Stgren)
filename = r'Alle_resultater_gren'
filename = filename + '.xlsx'
sheet_RMG4 = pd.read_excel(filename, sheet_name=sheet_RMG)
sheet_PD4 = pd.read_excel(filename, sheet_name=sheet_PD)

#Gathers rock mass grouting results in one dataframe
sheets_RMG = pd.concat([sheet_RMG1, sheet_RMG2, sheet_RMG3, sheet_RMG4])
#sheets_PD = pd.concat([sheet_PD1, sheet_PD2, sheet_PD3, sheet_PD4])

# Creates new excel file with maximum results from each probe drilling round in the tunnel
input("The new file name will be 'max_PD_excel2', press any key to continue \n")
new_filename = "max_PD_excel2.xlsx"

new_sheet_names = ["SM Vatn", "SM Hov", "ST Hov", "ST Gren"]

#Creates data dictionary with the Probe drilling results
Pd_sheets_dict = {}
Pd_sheets_dict["sheet_PD1"] = sheet_PD1
Pd_sheets_dict["sheet_PD2"] = sheet_PD2
Pd_sheets_dict["sheet_PD3"] = sheet_PD3
Pd_sheets_dict["sheet_PD4"] = sheet_PD4

#Goes through each probe drilling results excel file and looks for the maximum value of water inflow category
```

---

```

for k in new_sheet_names:

    writer = pd.ExcelWriter(new_filename, sheet_name=k)

    if k == "SM Vatn":
        sheetPD = Pd_sheets_dict["sheet_PD1"]
        os.chdir(dir_Smvatn)

        #Kopieres nedover
    elif k == "SM Hov":
        sheetPD = Pd_sheets_dict["sheet_PD2"]
        os.chdir(dir_Smhov)

    elif k == "ST Hov":
        sheetPD = Pd_sheets_dict["sheet_PD3"]
        os.chdir(dir_Sthov)

    else:
        sheetPD = Pd_sheets_dict["sheet_PD4"]
        os.chdir(dir_Stgren)

    ps_fc = sheetPD.columns.tolist().index("Face_loc") #Column position face location
    ps_cat = sheetPD.columns.tolist().index("Pd_cat") #Column position pd category

    face_locs = []

    rows_pd = 0
    count = 0
    while rows_pd < sheetPD.shape[0]: # Check that you are not in the last row

        face_loc = sheetPD.iloc[rows_pd, ps_fc]
        face_locs.append(face_loc)

        Pd_cat = []
        i = 0
        while sheetPD.iloc[rows_pd+i, ps_fc] == face_loc: #Make list with pd categories for same face location
            Pd_cat.append(sheetPD.iloc[rows_pd + i , ps_cat])
            i=i+1
            if (rows_pd+i >= sheetPD.shape[0]):
                break

        i_max = rows_pd + Pd_cat.index(max(Pd_cat)) #Index in rows for max category for current face location

        row_series = sheetPD.iloc[i_max, :]

        # Creates a dataframe including the row with the maximum inflow category in the probe drilling round
        df = pd.DataFrame(row_series)
        df = df.transpose()

        if count == 0:

            df.to_excel(writer, startrow=count, startcol=0)
            count = count + 2
        else:
            df.to_excel(writer, startrow=count, startcol=0, header=False)
            count = count + 1

        rows_pd = rows_pd + i #+1? #Oppdater til neste rad under

    writer.save() #Saves the file with maximum inflow category at the same folder as the read excel file

    # dataframe from each newly saved file with maximum inflow categories
    if k == "SM Vatn":
        df_SmVatn = pd.read_excel(new_filename)
    elif k == "SM Hov":
        df_SmHov = pd.read_excel(new_filename)
    elif k == "ST Hov":
        df_StHov = pd.read_excel(new_filename)
    else:
        df_StGren = pd.read_excel(new_filename)

    # Merge all dataframes together and save to new excel file where user specifies path and filename

```

---

---

```
df = pd.concat([df_SmHov,df_StHov,df_StGren,df_SmVatn])
dir_final = input("Type the path where you want the file with all results saved \n")
filename = input("Type the name of the file with all results \n")

os.chdir(dir_final)
df.to_excel(filename+".xlsx")
```

---

## E.7 Semi-analytical water leakage analysis with approach proposed by Panthi (2006)

```
# -*- coding: utf-8 -*-
"""
Created on Wed Dec 18 14:21:01 2019

This script consists of two parts:

1. Estimation of fa and calculation of specific leakage [l/min/m] by Panthi's equation.
   - The following parameters are used:
       * D has been estimated for every 200 m interval along the tunnel.
       * Js = 5 m
       * Jp = 20 m

       * h_static is the height of the water column above tunnel
         level of the nearest water source to the tunnel

2. Calculation of mean values of specific leakage
   - Calculation of mean values of specific leakage from Panthi's estimate
     for same tunnel face locations.

   - Calculation of mean values of actual specific leakage in the probe drill holes.

@author: Haakon Jørlo Haugerud
"""

import pandas as pd
import os
import numpy as np
import matplotlib.pyplot as plt

#-----
#Part 1
#-----

#Importing the data
directory = r'C:\Users\hjh\OneDrive - NTNU\Skole\5. år\MASTEROPPGAVER\EXCEL for ArcGIS Pro\Storåvatn\Hovedlop'
filename = r'Alle_resultater_StHov.xlsx'

sheet_PD = 'PD'
sheet_elev = 'Elev'

os.chdir(directory)

sheet_PD = pd.read_excel(filename, sheet_name=sheet_PD)
sheet_PD = sheet_PD[["Face_loc", "Pd_quantity", "Qt", "H_static", "Pd_jr", "Pd_jn", "Pd_ja"]]

sheet_elev = pd.read_excel(filename, sheet_name=sheet_elev)

# Setting Jp and Js parameters
Jp = 20
Js = 5

# Make array of unique tunnel face locations
f_locs = sheet_PD["Face_loc"].drop_duplicates()

# This for loop estimates the specific leakage by Panthi's equation
for row_pd in range(0, len(sheet_PD["Face_loc"])):
    diff_list = [] #Minimum distance between f_loc and H_dist
    D_list = []
    f_loc = sheet_PD.iloc[row_pd, 0]
    for row_elev in range(0, len(sheet_elev["D"].dropna())):
        D = sheet_elev.loc[row_elev, "D"]
        H_dist = sheet_elev.loc[row_elev, "H_dist"]

        diff_list.append(abs(f_loc-H_dist))
```

---

```

        D_list.append(D)

min_pos = np.argmin(diff_list)
D_export = D_list[min_pos]

sheet_PD.loc[row_pd,"D"] = D_export

#Panthi params
fa = Jp/(Js*D_list[min_pos])
sheet_PD.loc[row_pd,"fa"] = fa

h_static = sheet_PD.loc[row_pd,"H_static"]
panthi_jr = sheet_PD.loc[row_pd,"Pd_jr"]
panthi_ja = sheet_PD.loc[row_pd,"Pd_ja"]
panthi_jn = sheet_PD.loc[row_pd,"Pd_jn"]

eq_panthi = fa * h_static * panthi_jr * panthi_jn / panthi_ja

sheet_PD.loc[row_pd,"Eq_Panthi"] = eq_panthi

#-----
# Part 2 - Calculating mean values of specific leakage at tunnel face location
#-----

qt_mean_list = []
panthi_mean_list = []
i = 0

for f_pos in f_locs:
    qt_list = []
    panthi_list = []

    if i < len(sheet_PD["Face_loc"]):

        f_loc_pd = sheet_PD.loc[i,"Face_loc"]

        while f_loc_pd == f_pos:

            q_panthi = sheet_PD.loc[i,"Eq_Panthi"]
            qt = sheet_PD.loc[i,"Qt"]

            if np.isnan(qt) == True:
                pass
            else:
                qt_list.append(qt)

            if np.isnan(q_panthi) == True:
                pass
            else:
                panthi_list.append(q_panthi)

            i = i + 1
            if i == len(sheet_PD["Face_loc"]):
                break

        else:
            f_loc_pd = sheet_PD.loc[i,"Face_loc"] #Update the face_loc

    qt_mean = np.mean(qt_list)
    qt_mean_list.append(qt_mean)

    panthi_mean = np.mean(panthi_list)
    panthi_mean_list.append(panthi_mean)

else:
    pass

```

---





---

## E.8 Multivariate linear regression in Python

```
"""
Created on Thu Dec 5 10:34:29 2019

This script shows the process of developing the MLR model and running
diagnostics tools to check the validity and adequacy of the model.

@author: Haakon Jrlo Haugerud
"""

#Importing modules
import os
import pandas as pd
import matplotlib.pyplot as plt
import matplotlib as mpl
import seaborn as sns
import math
from sklearn import linear_model
get_ipython().run_line_magic('matplotlib', 'inline')
from statsmodels.stats.outliers_influence import variance_inflation_factor
import pingouin as png

sns.set(style='darkgrid')

# Loading the data from Excel-sheets

dir_Smvatn = r'C:\Users\hjh\OneDrive - NTNU\Skole\5. r\MASTEROPPGAVERN\EXCEL for ArcGIS Pro\Smibelg\Smibelgvatn'
os.chdir(dir_Smvatn)
filename = r'Alle_resultater_Smibelgvatn'
filename = filename + '.xlsx'
sheet_RMG = 'RMG'
sheet_PD = 'PD'
sheet_RMG1 = pd.read_excel(filename, sheet_name=sheet_RMG)
sheet_PD1 = pd.read_excel(filename, sheet_name=sheet_PD)

dir_Smhov = r'C:\Users\hjh\OneDrive - NTNU\Skole\5. r\MASTEROPPGAVERN\EXCEL for ArcGIS Pro\Smibelg\Hovedlop'
os.chdir(dir_Smhov)
filename = r'Alle_resultater_Smhov'
filename = filename + '.xlsx'
sheet_RMG2 = pd.read_excel(filename, sheet_name=sheet_RMG)
sheet_PD2 = pd.read_excel(filename, sheet_name=sheet_PD)

dir_Sthov = r'C:\Users\hjh\OneDrive - NTNU\Skole\5. r\MASTEROPPGAVERN\EXCEL for ArcGIS Pro\Storvatn\Hovedlop'
os.chdir(dir_Sthov)
filename = r'Alle_resultater_StHov'
filename = filename + '.xlsx'
sheet_RMG3 = pd.read_excel(filename, sheet_name=sheet_RMG)
sheet_PD3 = pd.read_excel(filename, sheet_name=sheet_PD)

dir_Stgren = r'C:\Users\hjh\OneDrive - NTNU\Skole\5. r\MASTEROPPGAVERN\EXCEL for ArcGIS Pro\Storvatn\Grentunnel'
os.chdir(dir_Stgren)
filename = r'Alle_resultater_gren'
filename = filename + '.xlsx'
sheet_RMG4 = pd.read_excel(filename, sheet_name=sheet_RMG)
sheet_PD4 = pd.read_excel(filename, sheet_name=sheet_PD)

sheets_RMG = pd.concat([sheet_RMG1, sheet_RMG2, sheet_RMG3, sheet_RMG4])
sheets_PD = pd.concat([sheet_PD1, sheet_PD2, sheet_PD3, sheet_PD4])

# Removing NaN-elements in the dataframe and defining response variable

df = sheets_RMG[["Cem_pr_m", "RMG_rq", "RMG_jn", "RMG_jw", "RMG_jr", "RMG_ja", "RMG_srf", "Overburden"]]
df_removedNAN = df.dropna()

in_vars = df_removedNAN[["RMG_rq", "RMG_jn", "RMG_jw", "RMG_jr", "RMG_ja", "RMG_srf", "Overburden"]]
out_var = df_removedNAN["Cem_pr_m"]
log_out_var = [math.log(x) for x in df_removedNAN["Cem_pr_m"]]
```

---

```

# Defining the dataframe of covariates and the response variable
# for final implementation in MLR model

X = df_removedNAN.ix[:,1:]
#y = log_out_var    #Use when comparing non-log values of grout take to covariates
y = log_out_var    #Use when comparing log values of grout take to covariates
X

# Import the Statsmodels module

import statsmodels.api as sm
import statsmodels.formula.api as smf

# Creating the MLR model

Xc = sm.add_constant(X)
linear_regression = sm.OLS(y,Xc)
fitted_model = linear_regression.fit()

# Gives summary of the first model

fitted_model.summary()

# Shows a heat map of the correlation between covariates

corr = X.corr()
sns.heatmap(corr,xticklabels=corr.columns,yticklabels=corr.columns,cmap="RdBu")

# Shows distribution of the residuals and tests for normality

model_norm_residuals = fitted_model.get_influence().resid_studentized_internal
plt_x = pd.Series(model_norm_residuals,name="Normalized residuals")
fig=sns.distplot(plt_x)
from scipy.stats import shapiro
shapiro(model_norm_residuals)

# Checks for multicollinearity in the covariate dataframe

#Multicollinearity by VIF
#gather features
Xc_rem = Xc.ix[1:,:]
features = "+".join(Xc_rem.columns)

# get y and X dataframes based on this regression:
#y, X = dmatrices('Cem_pr_m ~' + features, df_removedNAN, return_type='dataframe')

vif = pd.DataFrame()
vif["VIF Factor"] = [variance_inflation_factor(Xc_rem.values, i) for i in range(Xc_rem.shape[1])]
vif["features"] = Xc_rem.columns

vif.round(1)

# Removing SRF

Xc2 = Xc[["const", "RMG_jn", "RMG_jw", "RMG_rq", "RMG_ja", "RMG_jr", "Overburden"]]

# Checks for multicollinearity in the covariate dataframe

```

---

---

```

#Multicollinearity by VIF
#gather features
Xc_rem = Xc2.ix[1, :]
features = "+".join(Xc_rem.columns)

# get y and X dataframes based on this regression:
#y, X = dmatrices('Cem_pr_m ~' + features, df_removedNAN, return_type='dataframe')

vif = pd.DataFrame()
vif["VIF Factor"] = [variance_inflation_factor(Xc_rem.values, i) for i in range(Xc_rem.shape[1])]
vif["features"] = Xc_rem.columns

vif.round(1)

# Creates the second MLR model

linear_regression = sm.OLS(y, Xc2)
fitted_model = linear_regression.fit()
fitted_model.summary()

# Removes RQD

Xc3 = Xc[["const", "RMG_jn", "RMG_jw", "RMG_ja", "RMG_jr", "Overburden"]]
linear_regression = sm.OLS(y, Xc3)
fitted_model = linear_regression.fit()
fitted_model.summary()

# Checks for multicollinearity in the covariate dataframe

#Multicollinearity by VIF
#gather features
Xc_rem = Xc3.ix[1, :]
features = "+".join(Xc_rem.columns)

# get y and X dataframes based on this regression:
#y, X = dmatrices('Cem_pr_m ~' + features, df_removedNAN, return_type='dataframe')

vif = pd.DataFrame()
vif["VIF Factor"] = [variance_inflation_factor(Xc_rem.values, i) for i in range(Xc_rem.shape[1])]
vif["features"] = Xc_rem.columns

vif.round(1)

#Removes Jn

Xc4 = Xc[["const", "RMG_jw", "RMG_ja", "RMG_jr", "Overburden"]]
linear_regression = sm.OLS(y, Xc4)
fitted_model = linear_regression.fit()
fitted_model.summary()

# Checks for multicollinearity in the covariate dataframe

#Multicollinearity by VIF
#gather features
Xc_rem = Xc4.ix[1, :]
features = "+".join(Xc_rem.columns)

# get y and X dataframes based on this regression:
#y, X = dmatrices('Cem_pr_m ~' + features, df_removedNAN, return_type='dataframe')

vif = pd.DataFrame()
vif["VIF Factor"] = [variance_inflation_factor(Xc_rem.values, i) for i in range(Xc_rem.shape[1])]
vif["features"] = Xc_rem.columns

```

---

---

```

vif.round(1)

# Removes Jr

Xc4 = Xc[["const", "RMG_ja", "RMG_jw", "Overburden"]]
linear_regression = sm.OLS(y, Xc4)
fitted_model = linear_regression.fit()
fitted_model.summary()

# Tests for homoscedasticity

png.homoscedasticity(Xc, method="bartlett", alpha=0.05)

# Checks for multicollinearity in the covariate dataframe

#Multicollinearity by VIF
#gather features
Xc_rem = Xc4.ix[1:, :]
features = "+".join(Xc_rem.columns)

# get y and X dataframes based on this regression:
#y, X = dmatrices('Cem_pr_m ~' + features, df_removedNAN, return_type='dataframe')

vif = pd.DataFrame()
vif["VIF Factor"] = [variance_inflation_factor(Xc_rem.values, i) for i in range(Xc_rem.shape[1])]
vif["features"] = Xc_rem.columns

vif.round(1)

# Removes Ja

Xc5 = Xc[["const", "RMG_jw", "Overburden"]]
linear_regression = sm.OLS(y, Xc5)
fitted_model = linear_regression.fit()
fitted_model.summary()

# Checks for multicollinearity in the covariate dataframe

#Multicollinearity by VIF
#gather features
Xc_rem = Xc5.ix[1:, :]
features = "+".join(Xc_rem.columns)

# get y and X dataframes based on this regression:
#y, X = dmatrices('Cem_pr_m ~' + features, df_removedNAN, return_type='dataframe')

vif = pd.DataFrame()
vif["VIF Factor"] = [variance_inflation_factor(Xc_rem.values, i) for i in range(Xc_rem.shape[1])]
vif["features"] = Xc_rem.columns

vif.round(1)

# Creates the last MLR model

Xc5 = Xc[["const", "RMG_jw", "Overburden"]]
linear_regression = sm.OLS(y, Xc5)
fitted_model = linear_regression.fit()
fitted_model.summary()

```

---

